The Role of CD4+ T cells in Periodontal Disease

Lauren Dee Campbell
(BSc Hons)

Submitted in fulfillment of the requirements for the
Degree of Doctor of Philosophy

School of Medicine, Dentistry and Nursing
College of Medical, Veterinary and Life Sciences
University of Glasgow

May 2017

Abstract

Introduction: Periodontal disease (PD) is the most common bone destructive chronic inflammatory disease in humans. Severe PD affects 8-15% of the population and impacts on the ability to chew and appearance, reduces quality of life, and is responsible for a substantial proportion of dental care costs. A dysbiotic oral biofilm is necessary but insufficient for development of PD. Rather, a dysregulated immune response to the disease-associated biofilm results in destruction of tooth supporting structures and eventual tooth loss. Despite the apparent involvement of the immune system in PD, clinical management focuses solely on the mechanical removal of the oral biofilm – with partial success and frequent recurrence. Therefore, a better understanding of the immune response in PD could highlight potential novel preventative and therapeutic strategies. T cells are present at sites of PD; however, there remains ambiguity regarding whether these T cells are protective or destructive in PD. The aim of these studies was to characterize CD4+ T cells in a *P. gingivalis*-induced murine model of PD.

Results: *P. gingivalis*-infected mice displayed subtle changes in their CD4+ T cell compartment, predominantly in the draining lymph nodes (dLNs). Such changes included a suggested increase in T follicular helper cells, a trend towards a decrease in regulatory T cells and a trend towards increased production of IFN-γ. Elevated levels of IFN-γ were also noted in gingival CD8+ T cells and splenocytes, with similar trends in CD8+ T cells from dLNs. The transcriptome of CD4+ T cells isolated from gingivae and dLNs of *P. gingivalis*–infected suggested minimal changes in gene expression following infection; however, identified a profile of the mucosal oral CD4+ T cell compared with CD4+ T cells of the dLN. To investigate the response of CD4+ T cells specific for *P. gingivalis*, the bacteria were genetically manipulated to express ovalubumin (OVA) peptide 323-339. However, these OVA peptide expressing *P. gingivalis* failed to induce a response in OVA-specific T cells, both *in vitro* and *in vivo*.

Conclusion: These data imply that CD4+ T cells do not substantially change upon *P. gingivalis* infection in a murine model. IFN-γ production, however, was elevated both locally and systemically. Together, the data presented in this thesis and data previously published warrant further investigations into the role of IFN-γ in PD and may point to IFN-γ as a biomarker or biological target for adjunctive PD therapy.

Author's declaration

I declare that, except where explicit reference is made to the contribution of others, that this dissertation is the result of my own work and has not been submitted for any other degree at the University of Glasgow or any other institution.

Lauren Campbell

Table of Contents

List of tables

List of figures

Acknowledgements

I have been extremely lucky to work with so many talented and supportive people at the Institute of Infection, Immunity and Inflammation and the Glasgow Dental School. Without the help and support that was given to me throughout my PhD, I would definitely not have been able to complete this thesis.

I would firstly like to acknowledge my supervisors Professor Iain McInnes and Dr Shauna Culshaw for their support and encouragement. In particular, I owe my greatest thanks to Shauna. I did not expect to have such an encouraging and dedicated supervisor who would always be at hand for advice – even when not in the same building! If it wasn't for Shauna I don't think that I would have made it through my PhD.

I would next like to thank the members of the Glasgow Oral Immunology Group – otherwise known as 'Team Tooth' – especially Ana Adrados Planell, Dr Jennifer Malcom, Dr John Butcher and Jason Brown for their help with the planning and execution of experiments. Jennifer was my mentor in the lab, always so full of knowledge and ready to offer advice and help. Above this, Jennifer was a great friend who made working in the lab enjoyable. Thanks go to John for travelling to and from UWS to help out with many of my experiments – even at ridiculous times in the morning. Last but certainly not least; I would like to give a huge thanks to Ana. Not only did she help out in just about every experiment that I ever conducted, she was a great friend who appreciated my long stories and always made me laugh.

I would also like to thank the members of the GBM group for their support in lab meetings and also in the lab. This was very much appreciated. I also owe thanks to Dr Owain Millington for his help with the fluorescent images presented in this thesis, as well as his encouragement in me undertaking a PhD in the first place. I would like to thank Diane Vaughan for her help with all of the cell sorts and all of the JRF staff for their constant support, no matter how big the experiment – particularly Colin Chapman. I would also like to thank Dr David Lappin for his help

to understand statistics. Also, I would like to thank The Sir Jules Thorn Charitable Trust (Grant Agreement Number 13/JTPhD) for funding my project.

I would also like to thank all of the friends that I made throughout my PhD, especially Dr Ruth McCartney. Time spent in the lab was definitely more fun when Ruth was around, as she would always have me laughing. Ruth was always there for support, whenever it was needed. Dr Suleman Sabir and Shafqat Ahrar Jaigirdar were also supportive friends that were willing to share their immunology knowledge and are people that I am happy to have met.

Finally I would like to thank my friends and family. Thanks go to all the uni girls who have always encouraged me and made science fun. A special thanks go to my Mum and Dad who are always there to support and encourage me, and this was as evident as ever throughout my PhD. They always believe in me and push me in the right direction. My sister, Robyn, for not only making a fabulous summer student but for her constant support and motivation. Robyn always makes me laugh, even in the final and stressful stages of the preparation of this thesis. Additional thanks go to Marco, for his encouragement throughout my PhD and his enthusiasm to understand my research, despite being an accountant with no immunology knowledge whatsoever! Without the support of all of my family I would not have been able to complete my thesis, and I hope I have made you all proud.

Definitions/Abbreviations

ABC	Alveolar bone crest
AHR	Aryl hydrocarbon receptor
AIDS	Acquired immunodeficiency syndrome
ANOVA	Analysis of variance
APC	Antigen presenting cell
BACS	Bouyancy-activated cell sorting
Bcl-6	B cell lymphoma 6 protein
BOP	Bleeding on probing
BSA	Bovine serum albumin
CD	Cluster of differentiation
cDNA	Complementary deoxyribonucleic acid
CEJ	Cemento-enamel junction
CFA	Complete Freud's adjuvant
CFU	Colony-forming units
CMC	Carboxymethyl cellulose
CO_2	Carbon dioxide
CR1	Complement receptor 1
CTLA4	Cytotoxic T-lymphocyte-associated protein 4
CVD	Cardiovascular disease
CXCR5	CXC chemokine receptor 5
DAF	Decay accelerating factor
DAS28	Disease activity score 28
DC	Dendritic cells
dH_2O	Distilled water
dLN	Draining lymph node
DMARD	Disease modifying anti-rheumatic drug
DN	Double negative
DNA	Deoxyribonucleic acid
DNase	Deoxyribonuclease
dNTPs	Deoxynucleotide triphosphates
DP	Double positive

ECM	Extracellular matrix
EDTA	Ethylene diamine tetra-acetic acid
ELISA	Enzyme-linked immunosorbent assay
EOP	Early-onset periodontitis
EU	ELISA units
FACS	Fluorescence-activated cell sorting
FcR	Fc receptor
FITC	Fluorescein isothiocyanate
FOXP3	Forkhead box P3
G	Gingiva
GC	Gingival crevice
GCF	Gingival crevicular fluid
gDNA	Genomic deoxyribonucleic acid
GEC	Gingival epithelial cell
GF	Germ free
GFP	Green fluorescent protein
GITR	Glucocorticoid-induced TNFR-related protein
GM	Gingival margin
GWAS	Genome-wide association study
H&E	Haematoxylin and Eosin
H_2O_2	Hydrogen peroxide
HI-FCS	Heat-inactivated fetal calf serum
HIV	Human immunodeficiency virus
HK	Heat killed
HRP	Horse radish peroxidase
ICAM	Intracellular adhesion molecule
IFN	Interferon
IgG/M/A/E	Immunoglobulin G/M/A/E
IHC	Immunnohistochemistry
IL	Interleukin
ILC	Innate lymphoid cell
JRF	Joint research facility
kDa	Kilodalton

KO	Knockout
LAD	Leukocyte adhesion deficiency
LFA	Lymphocyte function-associated antigen
LN	Lymph node
LOA	Loss of attachment
LPS	Lipopolysaccharide
M	Molar
MACS®	Magnetic-activated cell sorting
MAPK	Mitogen-activated protein kinase
mDC	Myeloid dendritic cell
$MgCl_2$	Magnesium chloride
MHC	Major histocompatibility complex
Micro-CT	Micro-computed tomography
mRNA	Messenger ribonucleic acid
N.D.	Not detected
N/A	Not applicable
NaN_3	Sodium azide
NFAT	Nuclear factor of activated T cells
NGS	Next generation sequencing
NK	Natural killer
NK-κB	Nuclear factor κ-light-chain-enhancer of activated B
nM	Nanomolar
NO	Nitric Oxide
OD	Optical density
OHI	Oral hygiene instructions
OVA	Ovalbumin
P. gingivalis	*Porphyromonas gingivalis*
PACS	PCR-activated cell sorting
PAMP	Pathogen-associated molecular pattern
PBS	Phosphate buffered saline
PBS-T	PBS with tween
PCA	Principle component analysis
PCR	Polymerase chain reaction

PD	Periodontitis
PE	Phycoerythrin
PFA	Paraformaldehyde
PMA	Phorbol 12-myristate 13-acetate
PPD	Periodontal pocket depth
qRT-PCR	Quantitative real time PCR
RA	Rheumatoid arthritis
RANKL	Receptor activator of NF-κB ligand
RBC	Red blood cell
RIN	RNA integrity number
RNA	Ribonucleic acid
RNAi	RNA interference
RNase	Ribonuclease
RORγT	RAR-related orphan receptor gamma T
RPMI	Roswell Park Memorial Insitute media
rRNA	Ribosomal RNA
SA	Streptavidin
SD	Standard deviation
SDS	Sodium dodecyl sulfate
SEM	Standard error of the mean
siRNA	Small interfering RNA
SPF	Specific pathogen free
STAT	Signal transducer and activator of transcription
TCM	Central memory T cell
TCR	Tcell receptor
TEM	Effector memory T cell
TG	Tris/glycine
TGF	Tranforming growth factor
TGS	Tris/glycine/SDS
Th	T helper
TI-1/2	T-independent type 1/2
TLR	Toll-like receptor
TMB	Tetramethylbenzidine

TNF	Tumour necrosis factor
TRM	Tissue-resident memory T cell
U	Enzyme activity units
WT	Wild type

1 General Introduction

1.1 Periodontal Disease

1.1.1 Clinical Classification of Periodontal Disease

Periodontal diseases include gingivitis and periodontitis (PD). Gingivitis is inflammation of the gingiva predominantly resulting from accumulation of dental plaque. As the removal of the dental plaque permits resolution of gingival inflammation, gingivitis is reversible. Conversely, PD is a chronic inflammatory disease that is characterized by the irreversible destruction of gingiva, periodontal ligament and alveolar bone, which ultimately results in tooth loss (Armitage, 2004). Whilst gingivitis precedes PD, all gingivitis cases do not progress to PD, with the manifestation of gingivitis offering only 30% of predictive value to PD (Listgarten et al., 1985).

PD can be diagnosed based on clinical assessment of gingival inflammation and tissue destruction, which can be measured by assessing bleeding on probing (BOP) and loss of attachment (LOA) measurements, respectively. LOA is the distance between the cementoenamel junction (CEJ) and the gingival crevice (GC) and is measured by a periodontal probe. The periodontal pocket depth (PPD), which is the distance between the gingival margin (GM) and GC, is also increased in PD (**figure 1.1**). Radiographs may be used to confirm the degree of alveolar bone loss (Armitage, 2004). PD can be generally categorized as chronic or aggressive (**figure 1.2**). Chronic PD has a slow progression rate and is the most common type of PD, usually affecting those over the age of 35 (Armitage and Cullinan, 2010). By contrast, aggressive PD is less common, typically affects younger individuals and is differentiated by rapid loss of attachment and bone destruction (Albandar, 2014). The PD can be further described as mild, moderate or severe based on the amount of LOA (**table 1.1**). Finally, PD can be termed as localized if less than 30% of teeth are involved, or generalized if more than 30% of teeth are implicated (Armitage, 2004).

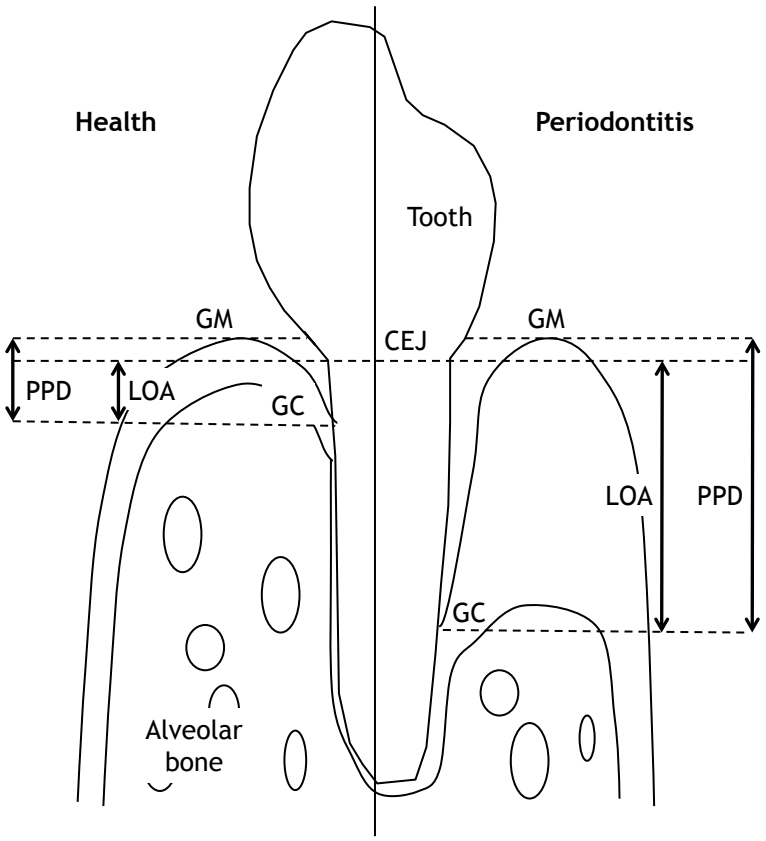

Figure 1.1. Clinical assessment of periodontitis.
Loss of attachment (LOA) determines the presence and severity of periodontitis. LOA is the distance from the cementoenamel junction (CEJ) to the gingival crevice (GC) and is measured using a periodontal probe. The periodontal pocket depth (PPD) is the distance between the gingival margin (GM) and the GC. Greater LOA and PPD are found in periodontitis compared to health.

Table 1.1. Loss of attachment determines severity of PD.

Severity of PD	Loss of attachment (mm)	No. of affected sites
Mild	≥ 3	≥ 2
Moderate	≥ 4	≥ 2
Severe	≥ 6	≥ 2

Figure 1.2. Advanced and aggressive forms of periodontitis.
Clinical photographs demonstrating advanced and aggressive forms of periodontitis in patients attending Glasgow Dental Hospital. The patients show gingival inflammation and recession, tooth loss, drifting teeth. All patients were unhappy with their appearance and all required extensive treatment, and require ongoing additional dental care throughout life. All patients maintained reasonable oral hygiene. Patient B suffered from Type 1 diabetes; patients A and C are healthy. All photos were reproduced with patient consent.

1.1.2 Prevalence and treatment

PD is the most common chronic inflammatory disease in humans. Its high worldwide prevalence qualifies PD as a global health concern. The global economic burden of dental diseases – contributed to significantly by PD – was $442 billion in 2010 and currently is likely to be greater (Listl et al., 2015). In the UK, approximately 45% of the total population will experience some form of PD; moreover, PD affects 60% of individuals over the age of 65 (White et al., 2012). PD is typically diagnosed and treated years after the initial onset, branding it a 'silent' disease. Severe PD, that affects 8-15% of the population, will compromise quality of life, affecting a

patient's appearance, speech, mastication and subsequently nutritional status (Chapple, 2014). The disease is not limited to the oral cavity; rather it is associated with systemic diseases including cardiovascular disease (CVD) (Dietrich et al., 2013), rheumatoid arthritis (RA) (de Pablo et al., 2009) and type II diabetes (Chapple and Genco, 2013). The links between PD and systemic diseases are not fully described; however, each of these diseases is typified by chronic inflammation and results from a complex mix of genetic and environmental risk factors.

The current treatment for PD is focused on the physical removal of dental plaque, in a non-specific manner. The therapy involves the non-surgical removal of supragingival and subgingival plaque by dentists or dental hygienists, through mechanical debridement, together with dental education and oral hygiene instructions (OHI) (Herrera et al., 2002, Needleman et al., 2005). PD progression can be halted by non-surgical plaque removal in patients exhibiting shallow to moderate PPDs; however, its success in patients with deep PPDs is variable (Tomasi et al., 2008, Nordland et al., 1987). Surgery can be indicated where non-surgical debridement has failed, with an aim of achieving shallower PPDs. As patients cannot remove plaque from deep periodontal pockets themselves, reducing the PPD allows maintenance of good oral hygiene and prevents disease progression (Wang and Greenwell, 2001).

Antimicrobials and antibiotics have been used as adjuncts to mechanical debridement to promote elimination of pathogenic organisms in difficult-to-access sites (e.g. root furcations and deep pockets). The efficacies of various systemic antibiotics including amoxicillin, azithromycin, clindamycin, doxycycline, metronidazole, spiramycin and tetracycline for adjunctive therapy have been assessed in clinical trials (Jepsen and Jepsen, 2016). Together the studies implied that adjunctive antibiotic treatment tended to improve PD outcome – particularly in aggressive PD and patients with deep pockets – however, there was a high level of heterogeneity between studies (Herrera et al., 2002, Haffajee et al., 2003, Sanz et al., 2008, Keestra et al., 2015a, Keestra et al., 2015b). Therefore, it was suggested that due to systemic side effects, adverse side effects and prevalence of

bacterial resistance, dentists should assign therapy based on individual patients considering the balance of benefits and risks (Jepsen and Jepsen, 2016).

Current PD treatment strategies frequently permit short-term improvements in PD state; however, the long-term stability is lacking (Mdala et al., 2013). Consequently, recurrence and progression of disease in patients with previous improvement is common – even in patients with strict compliance with OHI (Galindo et al., 2015). Therefore, it is fundamental to understand the host immune response that precedes and ensues in the progression of PD, to prevent disease and to identify novel targets for treatment

1.1.3 Risk factors for PD

The presence of a dental plaque biofilm is necessary for the initiation of PD, but is insufficient for the development of this disease. This was first described by Loe et al (1986), whereby Sri Lankan tea workers developed a range of severities of PD, despite exposure to the same environmental stimuli and presenting with similarly large dental plaque deposits (Löe et al., 1986). Thus, an individual's susceptibility is not simply a reflection of their oral hygiene.

Studies of twins have provided evidence that susceptibility to PD is around 50% attributed to genetic variation (Michalowicz et al., 2000, Torres de Heens et al., 2010). Genome wide associations studies (GWAS) recognized PD risk to be associated with alterations in genetic factors involved in nervous system, cellular immunity, cytokine signaling and epithelial barrier function (Divaris et al., 2013, Offenbacher et al., 2016).

The incidence of PD largely increases with age. Whilst juvenile PD does exist, the manifestation of disease typically occurs in adults with worsening of severity in increased patient age (Norderyd and Hugoson, 1998, Norderyd et al., 1999, Renvert et al., 2013). There is no definitive explanation for the association between age and PD, but this is believed to represent an accumulation of risk factor exposure over

time (Löe et al., 1986), and the concomitant impaired efficiency of tissue damage repair (Ashcroft et al., 2002).

Gender has been implicated as a risk factor for PD, with some studies finding greater prevalence in men (Slade and Spencer, 1995, Albandar and Kingman, 1994). However, the correlation between sex and PD is not consistent between studies. Rather, the greater periodontal destruction observed in some studies has been linked with gender-related behaviour, for example reduced access to dental care and less stringent oral hygiene practice by men (AlJehani, 2014).

A plethora of environmental and systemic factors deem an individual to be at an increased risk of developing of PD. These include, but are not limited to, smoking, diabetes, CVD, stress, obesity, osteoporosis and pregnancy (AlJehani, 2014).

1.2 Microbiology of Periodontal Disease

1.2.1 Composition of dental plaque biofilm

As aforementioned, the presence of a dental plaque biofilm is required for the initiation of PD. Therefore dental plaque is the primary etiological agent of PD and has been the focus of myriad studies investigating the disease.

The evolution of new technologies has been a powerful tool for the study of the human microbiome. Conventional cultural methods prevented complete analysis of the bacterial diversity within the oral cavity, as many species are uncultivatable. This limitation was overcome by 16S ribosomal RNA (rRNA) profiling, particularly with the development of next generation sequencing (NGS) (Kilian et al., 2016). It has been estimated that over 700 species of bacteria reside within the oral cavity. Specifically, the periodontal pocket may harbour approximately 400 of these bacterial species and in general dental plaque is composed of around 100 different species (Paster et al., 2006).

The development of an oral biofilm is initiated by the adherence of *Streptococci* and *Actinomycetes* species to salivary proteins covering the tooth surface, including

glycoproteins and mucins, through outer membrane proteins and pili (van Houte, 1982). Subsequently, bacteria of the same or different genera adhere and aggregate to the early colonizers of the tooth surface, leading to eventual colonization of bacteria including *Prevotella*, *Proprionibacteria* and *Veillonella*. Whilst species within early colonizers would not typically aggregate with bacteria of the late colonizers, the adherence of intermediate colonisers, such as *Fusobacterium nucleatum*, acts as a link between members of the biofilm (Kolenbrander, 2000).

The microbiome within the oral cavity is heterogeneous. Distinct microbial biofilms associate with different niches within the mouth, including teeth, supragingival surfaces, subgingival surfaces, tongue, soft and hard palate (Xu et al., 2015, Dewhirst et al., 2010). Likewise, different biofilms associate with health and disease. Socransky initially identified three 'red complex' bacterial species residing in subgingival plaque that most commonly associated with PD. The 'red complex' included *Porphyromomas gingivalis* (*P. gingivalis*), *Tannerella forsythia* (*T. forsythia*) and *Treponema denticola* (*T. denticola*) (Socransky et al., 1998). *P. gingivalis* was isolated from 25% of individuals displaying periodontal health but 79% of PD patients (Griffen et al., 1998). Not strictly complying with Koch's postulates, *P. gingivalis* and the other 'red complex' bacteria were isolated from healthy individuals in low numbers, but were below the detectable limit post PD treatment and were found to increase upon PD regression (Costalonga and Herzberg, 2014). With the emergence of 16S rRNA NGS, 123 bacterial species were found in greater abundance in PD. These included previously described *Spirochaetes* and *Bacterioidetes* species, and *Sinergistes*. In healthy subgingival biofilms, 53 bacterial species – including *Proteobacteriae* – were found in greater numbers (Griffen et al., 2012). The association of PD with a plethora of bacterial species implied that inflammation resulted from a polymicrobial infection.

As specific bacteria could not be solely attributed to the development of PD, the dysbiosis hypothesis emerged. Hajishengalis et al (2011) illustrated that *P. gingivalis* present in small numbers within a biofilm mediated changes in the composition and abundance of commensal bacteria. The shift from a health-associated biofilm to a dysbiotic PD-associated biofilm altered crosstalk with the

host, in a manner that was sufficient to induce inflammation and ultimately alveolar bone destruction (Hajishengallis et al., 2011b). Since *P. gingivalis* thrived at low frequencies, but had the capacity to modulate members of the biofilm, it was entitled a 'keystone pathogen' (Darveau et al., 2012). Interestingly, in an animal model lacking commensal bacteria, *P. gingivalis* was unable to induce bone loss, despite its maintained ability to colonize the mouth. The phrase, 'polymicrobial synergy and dysbiosis' has been used to describe the changes in the oral biofilm that associate with disease (Hajishengallis et al., 2011).

Animal models of PD have demonstrated that *P. gingivalis* does not directly destroy host alveolar bone, but rather alters the proportion and composition of commensal bacteria, disrupting homeostatic host-biofilm crosstalk, thereby leading to alveolar bone loss. Nonetheless, the presence of *P. gingivalis* in periodontal health indicated that the keystone pathogen does not consistently lead to disease. However, it is likely that genetic and environmental factors make an individual susceptible to PD. PD may now defined as a dysregulated immune response to a dysbiotic oral biofilm.

1.2.2 *Porphyromonas gingivalis*

Although clearly not in isolation causative of PD, *P. gingivalis* remains the most studied PD-associated bacteria and is commonly used in animal models. *P. gingivalis* is a non-motile, rod shaped, gram-negative anaerobe belonging to the phylum *Bacteroidetes* (Holt and Ebersole, 2005). Whilst the pathogenicity of different strains varies (**table 1.2**), *P. gingivalis* exerts a wide array of virulence factors that permit its establishment and survival within a host.

Table 1.2. Features of different strains of *P. gingivalis* isolated from humans.

Strain of *P. gingivalis*	FimA type	Capsular serotype	Virulence
W83	IV	K1	High
W50	IV	K1	High
HG184	II	K2	High
A7A1-28 (ATCC 53977)	II	K3	High
ATCC 49417	II	K4	High
HG1690	II	K5	High
HG1691	Ib	K6	High
381	I	No capsule	Low
ATCC 33277	I	No capsule	Low

1.2.2.1 *P. gingivalis* virulence factors

(i) Adherence

In order for *P. gingivalis* to colonize the oral cavity, it must first adhere to the surface. The fimbriae, and precisely the major fimbrial component (FimA), are required for the adherence of the bacteria to the saliva-coated surfaces within the oral cavity (Malek et al., 1994). Inactivation of the *fimA* gene generated a *P. gingivalis* mutant incapable of fibrillin production and hence the mutant displayed incomplete fimbriae. Whilst this mutant was able to coaggreagte with *Streptococcus gordonii* G9B almost as efficiently as wildtype (WT) *P. gingivalis* 381, its capacity to bind to saliva-coated hydroxyapatite was significantly reduced along with an impaired ability to cause bone loss in a rat model of PD (Malek et al., 1994). Additionally, the hemagglutinin domains of gingipains function in the adherence and colonization of *P. gingivalis* through direct adhesion to extracellular matrix (ECM) proteins and indirectly through the ability to process the fimbrillin subunit of fimbriae (Chen et al., 2001). The genes *hagB* and *hagC* encode two highly homologous hemagglutinins. *P. gingivalis* W83 mutants of either *hagB* or *hagC* showed less adherence to oral epithelial cells than WT bacteria. Surprisingly, a double mutant lacking expression of both genes displayed a reduction in capacity to adhere to cells than WT *P. gingivalis*, but increased adherence compared to single

mutants. This was explained by an increase in gingipain RgpA and Kgp gene expression (Connolly et al., 2017).

(ii) Gingipains

Gingipains are membrane bound cysteine proteases, which exert their functions upon secretion (Chen et al., 2001). Gingipains are either arginine-specific (RgpA or RgpB) or lysine-specific (Kgp) proteases (Wilensky et al., 2013), and their activity is directly responsible for host tissue damage that promotes *P. gingivalis* colonization within the oral cavity. Major components of the periodontal connective tissue (type I and IV collagen) and ECM ptoteins, including laminin and fibrinogen, are subjected to gingipain-mediated tissue destruction (Holt et al., 1999). Furthermore, gingipains enhance survival of *P. gingivalis* in the gingival pocket through the capacity to attach to other bacteria and to host cells (Sheets et al., 2006), as well as providing a source of nutrition by cleavage of host proteins (Holt et al., 1999). As will be discussed below, gingipains are a key factor in host immune evasion strategies employed by *P. gingivalis*.

(iii) Capsule Barrier

Persistence of *P. gingivalis* within the host is aided by its capsule (Grenier and Mayrand, 1987). Primarily, the capsule acts as a barrier, preventing access of destructive host effectors to the bacterium (Singh et al., 2011). Furthermore, the increased hydrophobicity of the capsule is thought to reduce complement activation, thereby opsonization and subsequent phagocytosis are evaded (Schifferle et al., 1993a). Contributing to the inability to activate complement, the capsule can also conceal lipopolysaccharides (LPS) and other bacterial structures that are capable of inducing the host's immune response (Schifferle et al., 1993b). Additionally, the hidden immune-inducing structures of *P. gingivalis* present implications for dendritic cell (DC) maturation. To mature, the immature DC must encounter antigen and subsequently upregulate CD11c, CD40, CD86 and major histocompatibility complex (MHC) class II expression on the surface of the cell. Using flow cytometry to determine the presence of these markers, it was demonstrated that a non-encapsulated mutant *P. gingivalis* strain triggered faster

DC maturation than that by the encapsulated W50 strain (Singh et al., 2011). Furthermore, presence of a capsule has been shown to modulate pro-inflammatory cytokine secretion by human fibrobasts *in vitro* (Brunner et al., 2010). The capsule therefore enhances *P. gingivalis* survival, promoting a prolonged infection and low-grade chronic inflammation.

1.2.2.2 *P. gingivalis* and immune system evasion

(i) Gingipains and complement

The activation of complement by the classical, alternative or mannose-binding lectin pathways forms part of the innate response (Song, 2012). C3 is an important complement component as its cleavage produces C3a and C3b. C3b opsonizes a pathogen to enhance phagocytosis, whilst C3a functions as an anaphylatoxin, thereby recruiting phagocytes. *P. gingivalis* is able to evade complement through heterodimeric high-molecular-mass RgpA (HRgpA), which cleaves C3 resulting in the production of C3b. This active fragment is then degraded, and hence becomes inactive (Popadiak et al., 2007). Thus, gingipains are again shown to be crucial for the survival of *P. gingivalis*.

Toll-like receptors (TLRs) are structurally related, pattern recognition receptors expressed on the cell surface, which respond to microbial pathogens (Song, 2012). Cross talk between complement and TLRs is essential to coordinate an appropriate early innate immune response, and therefore provides a target for which invading pathogens can manipulate to enhance their survival (**figure 1.3**). Whilst *P. gingivalis* has been shown to generally inhibit the complement casacade, the bacterium has been shown to generate C5a through its C5 convertase-like enzyme. The production of C5a inhibited intracellular killing and enhanced the ability of the bacteria to survive within macrophages, an observation also noted in interferon gamma (IFN-γ) primed macrophages (Wang et al., 2010a). Further studies of these observations demonstrated that C5a together with *P. gingivalis* – in an intracellular Ca^{2+} dependent manner – synergistically increased intracellular cyclic adenosine monophosphate (cAMP) levels within macrophages, over three fold greater than that induced by *P. gingivalis* alone (Wang et al., 2010a). This has important

implications in the survival of *P. gingivalis* as cAMP can trigger immunosuppressive signaling (Parry and Mackman, 1997). The increase in cAMP levels was also dependent on TLR2, with confocal microscopy illustrating that in *P. gingivalis*-infected macrophages, C5a receptor (C5aR), TLR2 and *P. gingivalis* all locate within close proximity of each other. *P. gingivalis* therefore induces subversive cross talk between complement and TLR2 in order to suppress cytokine signaling (Wang et al., 2010a). Furthermore, TLR2 is fundamental for immune evasion by *P. gingivalis* as TLR2 deficient mice and TLR2 deficient macrophages are able to rapidly clear infection (Liang et al., 2011).

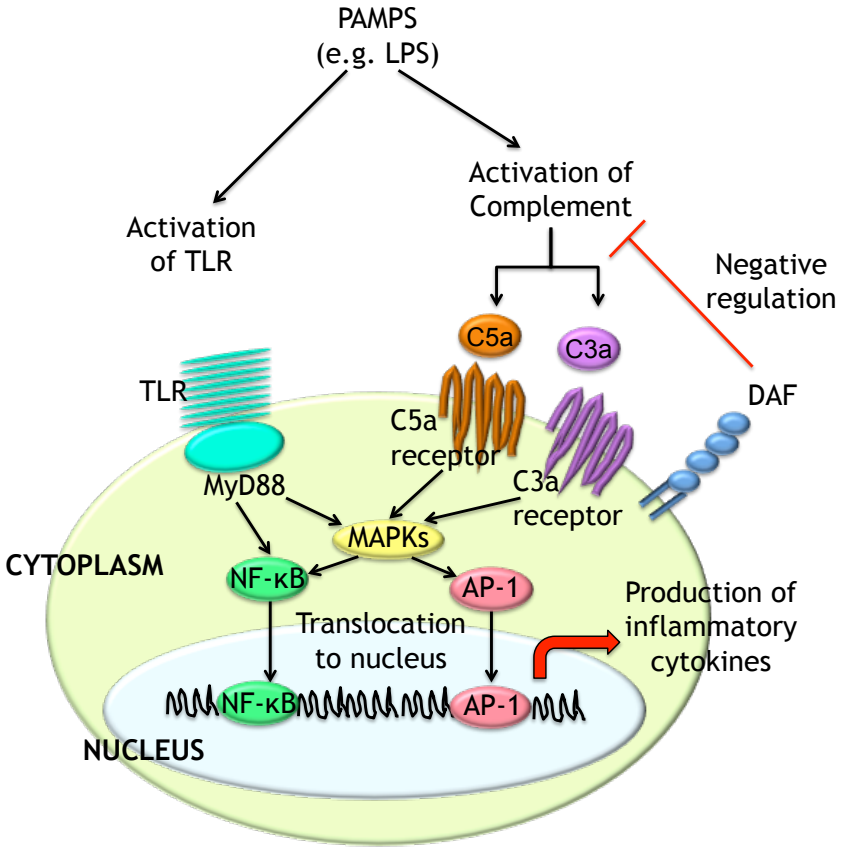

Figure 1.3. The cross talk between toll-like receptors and complement. Pathogen-associated molecular patterns (PAMPS) can activate both Toll-like receptors (TLRs) and complement. The activation of complement, through the functions of G protein-coupled C5a and C3a receptors, regulates TLR signaling. Thus, complement activation regulates intracellular signaling molecules such as mitogen-activated protein kinase (MAPK) and therefore transcription factors such as nulear factor-kappa B (NF-κB), highlighting the importance of crosstalk between TLRs and complement. Decay-accelerating factor (DAF) is a negative regulator of complement hence its absence results in amplified complement activation and TLR signaling (adapted from (Zhang et al., 2007)).

Additionally, binding of C5a to its receptor can also prevent the expression of *Il12p35*, *Il12*, *Il23p40* and *Il23p19* messenger RNA (mRNA), along with inhibiting IL-12p70 and IL-23 protein expression through inhibition of TLR4 (Hawlisch et al., 2005). This function is required to prevent T helper (Th) 1 and Th17 subset-mediated tissue damage in health. The binding of C5a to C5aR also inhibits nitric oxide (NO) production in activated macrophages, a process exploited by various pathogens. Therefore, unregulated production of C5a by *P. gingivalis* can interfere with the initiation of T cell polarization and production of NO – ultimately restricting the induction of a protective immune response (Wang et al., 2010a).

The ability of *P. gingivalis* to exert many of its pathogenic effects and alter the commensal abundance of an oral biofilm is complement dependent (Liang et al., 2011, Hajishengallis et al., 2011b). In a *P. gingivalis*-induced PD model, the burden of *P. gingivalis* was reduced by 99% following inhibition of C5aR and concomitantly, a reduction in total oral anaerobic bacterial load was observed – to numbers present prior to *P. gingivalis* infection. The C5aR inhibition had no impact on the number of bacteria in the mouths of uninfected mice, demonstrating that blockade of C5aR does not directly effect commensal oral bacteria but rather the effect is mediated through *P. gingivalis* (Hajishengallis et al., 2011b).

(ii) Antagonism of TLR4

Upon recognition of the lipid A component of gram negative bacterial LPS by TLR4, a strong innate immune response is initiated through downstream signaling (**figure 1.4**). TLR4 undergoes oligomerization following recognition of LPS, and through binding with Toll-interleukin-1 receptor (TIR), adaptor proteins are recruited. TLR4 is able to recruit and signal through each of the five known TIR-containing adaptors – MyD88, TIRAP, TRIF, TRAM and SARM – a unique feature of this TLR. The signal transduction pathway of TLR4 can therefore be categorized into MyD88-dependent or MyD88-independent pathways, whereby the dependent pathway mediates pro-inflammatory cytokine production and the independent pathway mediates the expression of Type I interferons (reviewed by(Lu et al., 2008). *P. gingivalis*, however, is able to evade and potently antagonise the TLR4 receptor, inhibiting the induction of this immune response. Endogenous lipid A 1- and 4'-phosphatases

function to alter *P. gingivalis* lipid A to its non-phosphorylated form, which is immunologically 'silent' and permits evasion of TLR4 activation. Still, in microenvironmental conditions where the concentration of hemin is high, lipid A 1- and 4'-phosphatase activities are inhibited, generating mono-phosphorylated tetra-acylated lipid A that antagonizes TLR4, thereby actively suppressing immunity. Whilst the presence of lipid A TLR4 agonists were evident in *P. gingivalis* LPS isolates, strong TLR4 activation did not occur, suggesting that presence of immune evading or suppressing lipid A exerted dominance over the agonistic functions (Coats et al., 2009).

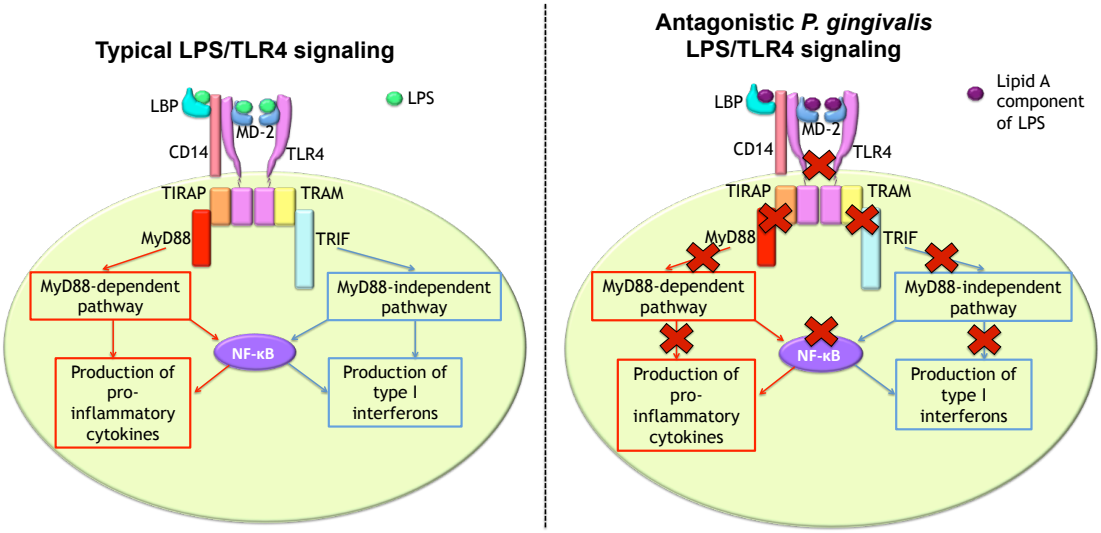

Figure 1.4. Typical LPS/TLR4 signaling compared to *P. gingivalis* LPS antagonism of TLR4.
LPS directly binds to LPS binding protein (LBP), which is the bridge between the association of CD14 and LPS. LPS is then transferred to the TLR4/MD2 receptor complex by CD14 and TLR4 undergoes oligomerization. Adaptor proteins are then recruited, resulting in either MyD88 dependent or independent signaling leading to the production of proinflammatory cytokines or type I interferons, respectively. In contrast, the lipid A component of *P. gingivalis* LPS is a potent antagonist of TLR4, hence the downstream signaling does not occur, preventing the production of inflammatory cytokines and interferons (Adapted from Lu et al., 2008).

(iii) Surface molecule modulation

Membrane-bound TLR co-receptor CD14 on macrophages is a receptor for LPS. CD14, in its soluble and biologically active form, interacts with cells that do not typically express the receptor itself, including epithelial and endothelial cells. This interaction enables endothelial or epithelial cells to become activated and induce

an inflammatory response that prevents bacterial colonization. Again, gingipains can interfere with this process by cleaving membrane-bound CD14 of macrophages. The cleavage of CD14 was concomitant with a reduction in TNF-α production and phagocytosis, in both human and murine macrophages (Duncan et al., 2004, Wilensky et al., 2015).

T cells are crucial components of adaptive immunity (discussed later) and like other constituents of the immune response; T cells can be targeted by *P. gingivalis*. Gingipains have the capacity to manipulate T cells, through the binding of RgpA and Kgp gingipains to CD4 and CD2. In the gingipain bound state, CD4 and CD2 are cleaved, preventing anti-CD4 and anti-CD2 antibody labeling for flow cytometry. Further still, as CD4 is required for the binding of a T cell to its cognate antigen presented within MHC-II and CD2 is required for cell-cell interactions, RgpA and Kgp have the potential to reduce the ability of T cells to elicit an appropriate immune response (Yun et al., 2005).

(iv) Interference with cytokines and chemokines

A number of cytokines and chemokines are expressed in healthy periodontal tissues. IL-8 is expressed by epithelial cells at the interface with bacterial cells, thereby creating a gradient of expression directing neutrophil migration to the area of bacterial colonization whilst preventing damage to the periodontal tissues (Darveau et al., 1998). Neutrophils are important in initial protection against plaque bacteria – highlighted by the fact that patients with low neutrophil numbers or reduced neutrophil function often suffer from severe periodontitis (Madianos et al., 1997). Interestingly, it has been shown that neutrophil migration is not stimulated by *P. gingivalis* and in fact migration triggered by microbial stimuli is blocked by *P. gingivalis*. This phenomenon is linked with the ability of *P. gingivalis* to adhere to and invade epithelial cells, leading to reduction of IL-8 and intracellular adhesion molecule (ICAM)-1 expression (Madianos et al., 1997, Darveau et al., 1998). It was later found to be SerB, a haloacid dehydrogenase family phosphoserine phosphatase enzyme, located on the outer membrane of *P. gingivalis* that was responsible for the IL-8 inhibition, known as chemokine paralysis (Bainbridge et al., 2010). SerB is released from the membrane upon contact with gingival epithelial cells (Zhang et

al., 2005), however in both its membrane bound and released states, it can interfere with signaling pathways of the host cell which are responsible for cytoskeletal regulation. This causes rearrangements of actin microfilaments and tubulin microtubules, allowing invasion of the cell and inhibition of IL-8 secretion (Tribble and Lamont, 2010). SerB was imperative for the intracellular survival of *P. gingivalis* (Hasegawa et al., 2008) and for optimal bone loss in a rat model of PD (Bainbridge et al., 2010).

Furthermore, *P. gingivalis* FimA mediated TLR2 signaling induced production of IL-10 by naïve CD4+ T cells in a murine systemic infection model. This IL-10 subsequently inhibited the production of IFN-γ by T cells, a response that is thought to help control early *P. gingivalis* infection (Gaddis et al., 2013).

Not only is *P. gingivalis* able to inhibit cytokine production but it can also degrade cytokines that have been translated by human gingival epithelial cells (GEC). Whilst IL-8 was found to be downregulated by *P. gingivalis,* gene expression of *Il6* and *Il8* by GECs stimulated with *P. gingivalis* was significantly increased by comparison to non-challenged GECs. Therefore, cytokine reduction by *P. gingivalis* is not consistently controlled at the transcriptional level. Kgp has the capacity to degrade IL-6, IL-8 and IL-1ß, whilst RgpA and RgpB contribute only to the destruction of IL-8 and IL-1ß (Stathopoulou et al., 2009a). Arginine-specific gingipains have been shown to decrease the accumulation of IL-2 in Jurkat T cells co-cultured with *P. gingivalis*, despite the initial increase in Ca^{2+} concentration and reactive oxygen species (ROS) production. As IL-2 is fundamental for proliferation and communication of T cells, *P. gingivalis* may have the ability to downregulate and evade the adaptive immune response (Khalaf and Bengtsson, 2012).

In addition to inhibition and degradation of cytokines, *P. gingivalis* can influence specific T cell cytokine production. Owing to differences in sugar composition and structure of the different capsular serotypes, which are determined by locus PG0106 – PG0120 variations, DC maturation may be influenced by specific strains of *P. gingivalis*. Thereby, the induction of a Th immune response is dictated by the capsular serotype *in vitro*. Th1 and Th17 immune responses were primed by DCs

previously exposed to K1 (W83) or K2 (HG184) serotypes (Vernal et al., 2014), which induce quantitatively stronger cytokine profiles (Vernal et al., 2009). A Th2 response was primed upon weak co-stimulation during antigen presenting and hence weak DC maturation by K3 (A7A1-28), K4 (ATCC41497) and K5 (HG1690) (Vernal et al., 2014). Interestingly, it has been suggested that the K^- strain (ATCC33277) (non-encapsulated) may prime a regulatory T cell (Treg) immune response characterized by IL-10 and TGF-β1 (Vernal et al., 2014).

A plethora of *P. gingivalis* virulence factors maintain its ability to colonize and survive in a host, with the pathogenicity predominantly aimed at suppressing the host's immune responses, including T cells (**table 1.3**).

Table 1.3. Virulence factors exerted by *P. gingivalis* that modulate T cell immunity.

Modulation of T cell immunity	***P. gingivalis* virulence**	**Reference**
Inhibition of IL-2 production	Arginine-specific gingipains	(Khalaf and Bengtsson, 2012)
Inhibition of T cell IFN-γ production	FimA	(Gaddis et al., 2013)
Activation of specific Th cell subset	Capsular serotype	(Vernal et al., 2014)
Cleavage of CD2 and CD4	Lysine and arginine-specific gingipains	(Yun et al., 2005)
Inhibition of Th1 and Th17 activation through TLR4 inhibition	C5 convertase-like enzyme	(Wang et al., 2010a)

1.3 T cells in PD

1.3.1 T cells

T cells are pivotal in the functioning of adaptive immunity. T cells are capable of direct killing of infected cells, and they have the ability to mediate the cellular microenviroment in which they reside (**table 1.4**). The importance of T cells is evident in X-linked SCID. Infants affected by this condition suffer from severe, persistent or recurrent infections and without reconstitution of the immune system, the infant will die, typically within the first year of life (Myers et al., 2002). Furthermore, deficiency of CD4+ T cells as a result of human immunodeficiency virus (HIV) leads to the devastating effects of acquired immunodeficiency syndrome (AIDS) that encompass opportunistic infections and cancer, ultimately resulting in death (Simon et al., 2006).

Table 1.4. Summary of T cell subsets - phenotypes and functions.

T cell subset	Cytotoxic T cell	Natural Treg	Naïve CD4+ T cell	Naïve CD8+ T cell	Th1 cell	Th2 cell	Th9 cell	Th17 cell	Th22 cell	Tfh cell	Central memory T cell	Effector memory T cell
Surface markers	CD3 CD8	CD3 CD4 CD25 CTLA4 GITR	CD3 CD4 CCR7 CD62L CD127	CD3 CD8 CCR7 $CD62L^{hi}$ CD127	CD3 CD4 IL-12R IFN-γR CXCR3	CD3 CD4 IL-4R IL-33R CCR4 IL-17RB	CD3 CD4	CD3 CD4 IL-23R CCR6 IL-1R	CD3 CD4 CCR10	CD3 CD4 CXCR5 SLAM OX40L CD40L ICOS IL-21R PD-1	CD3 CD4 or CD8 $CCR7^{hi}$ CD44 $CD62L^{hi}$ CD127 IL-15R	CD4 or CD8 $CCR7^{low}$ CD44 $CD62L^{low}$ CD127 IL-15R
Transcri-ption factors	EOMES T-bet BLIMP1	FOXP3 FOXO1 FOXO3 STAT5	THPOK	RUNX3	T-bet STAT4 STAT1	GATA3 STAT6 DEC2 MAF	PU.1	RORγt STAT3 RORα	AHR	Bcl-6 STAT3	Bcl-6 Bcl-6B MBD2 BMI1	BLIMP1
Effectors produced	IFN-γ Perforin Granzy-me	TGF-β IL-10 IL-35	-	-	IFN-γ IL-2 LT-α	IL-4 IL-5 IL-10 IL-13	IL-9 IL-10	IL-17A IL-17F IL-21 IL-22 CCL20	IL-22	IL-21	IL-2 CD40L	Inflamm-atory cytokines
Role	Direct and indirect killing of infected and transfor-med cells	Produced in thymus and mediates suppressi-on of immune response	Migrate through LNs scanning for cognate peptide present-ed within MHC-II	Migrate through LNs scanning for cognate peptide present-ed within MHC-I	Promote immunity to intra-cellular pathogen	Promote humoral responses and immunity to extra-cellular pathogen	Role in immunity to extra-cellular pathogen (mainly nemato-des)	Promote immunity to extra-cellular bacteria and funghi, mainly at mucosal sites	Linked with epiderm-al repair and found in inflamm-atory skin diseases	Promote germinal cell responses and provide help to B cells for class switching	Reside within second-ary lymphoid organs and mount recall responses to antigens	Found in periph-eral tissues and provide immed-iate defence upon antigen challenge

1.3.2 T cell development in the thymus

Lymphocyte progenitors leave the bone marrow and enter the thymus via the bloodstream, where the cells lose the potential to become B cells or natural killer (NK) cells and instead develop into T cells (**figure 1.5**). The complex architecture of the thymus and its array of specialized cell types are vital for the generation of antigen-specific T cells. Genetic defects in humans (e.g. DiGeorge syndrome), or thymectomy in neonatal mice that result in the lack of a thymus cause a marked reduction in T cell numbers both in circulation and in peripheral tissues resulting in immunodeficiency and premature death (Miller, 1961, Miller, 1962, Davies, 2013).

The committed T cell progenitors arrive in the thymus as double negative (DN) cells, thereby CD4 or CD8 molecules are absent. The progression of development of these DN cells is based on the expression of CD44 and CD25, whereby DN1 cells, which are CD44+ CD25-, sequentially develop to DN2 cells – CD44+ CD25+ – then DN3 cells – CD44- CD25+ – and finally DN4, which do not express either CD44 or CD25 (Godfrey et al., 1993).

The T cell receptor (TCR) is known to be composed of α and ß chains or γ and δ chains, and its presence is required for T cell development beyond DN3 (Malissen et al., 1995). The events that result in differentiation of DN cells to αß or γδ expressing T cells remain somewhat elusive, but strength of TCR signaling is thought to play a role (Hayes et al. 2005). Pre-TCRα is expressed by T cell precursors that develop into T cells expressing αß TCRs. This pre-TCRα pairs with a ß chain (von Boehmer and Fehling, 1997). Unlike the pre-TCRα chain that is the product of a non-rearranging locus, the ß chain is encoded by a locus that – through the expression of recombination-activating gene (RAG) 1 and RAG2 – undergoes somatic DNA arrangements. The ß chain is composed of *variable (V), diversity (D), joining (J)* and *constant (C)* regions (Abbey and O'Neill, 2007). The αß pre-TCR is associated with the CD3/ζ complex on the surface of the cell (van Oers et al., 1995) and providing the TCR has the capacity to successfully transmit signaling, the ß chain is selected for, allowing maturation of the T cell to continue. Precursor T cells in which the pre-TCR complex prevents important adaptor and enzyme expression, are

unable to actively signal and hence maturation is halted (Negishi et al., 1995, van Oers et al., 1996).

Following the selection of a ß chain, the T cell divides approximately six times and subsequently recombination of the genes at the TCRα locus occurs, producing the mature α chain of the TCR. The pre-TCRα is lost during this phase and so the T cell expresses small numbers of the αß TCR with the CD3/ζ complex on the cell surface (Hoffman et al., 1996, Dudley et al., 1994). The T cells at this stage begin to express CD8 and CD4 co-receptors, resulting in an abundance of CD8+ CD4+ (double positive (DP)) T cells expressing an αß TCR.

Selection of DP immature T cells expressing appropriate αß TCRs ensues by death by neglect, negative selection, positive selection and lineage-specific development (von Boehmer et al., 1989, Robey and Fowlkes, 1994). In the outer cortex of the thymus, DP cells interact with cortical epithelial cells that express high levels of MHC-I and MHC-II. The vast majority of DP cells exert weak, inadequate interactions between TCRs and MHC ligands expressing self-peptide, resulting in death by neglect, as the DP cell does not receive critical survival signals. Conversely, DP cells that bind to self-peptide presented within MHC too strongly receive signals that trigger rapid apoptosis – a process known as negative selection that typically occurs in the thymic medulla. Negative selection is a fundamental stage of T cell development as T cells with a high avidity for self-peptide (self-reactive) could elicit autoimmune pathology upon release from the thymus (Starr et al., 2003). Cells that bind self peptide with less avidity than those that are deleted can differentiate into Tregs (Maloy and Powrie, 2001). DP cells that engage with MHC-self-peptide with an appropriate intensity are positively selected for in the medulla. Positive selection occurs in fewer than 5% of DP cells, permitting survival of those with functional TCRs and supports downregulation of a co-receptor, giving rise to a population of single positive CD4+ or CD8+ T cell (Starr et al., 2003). T cells that recognize peptide presented within MHC-I or MHC-II become CD8+ or CD4+ lineage-specific T cells, respectively, and are permitted to exit the medulla for entry to peripheral lymphoid tissues.

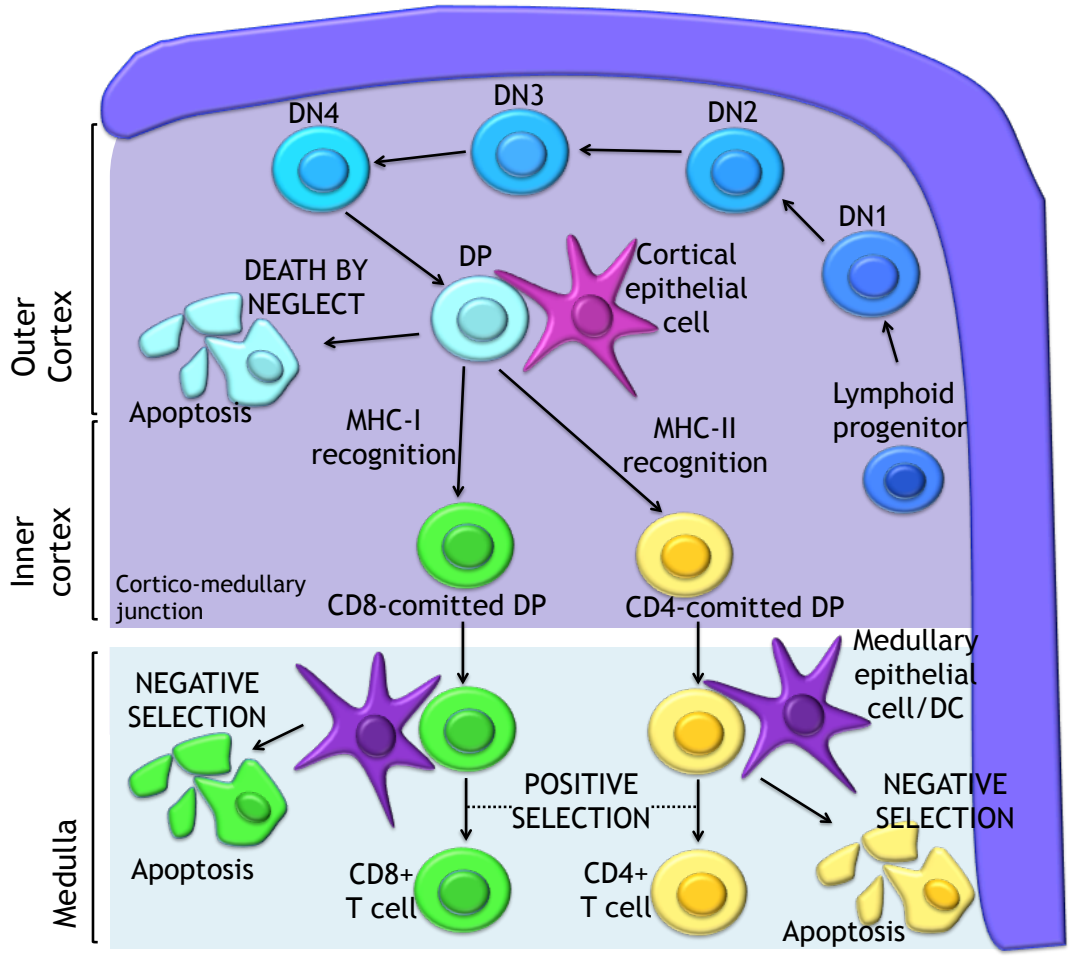

Figure 1.5. T cell development in the thymus.
Lymphocyte progenitors exit the bone marrow and enter the thymus via blood. The lymphocyte progenitors then become committed T cells. Initially, the committed T cells are absent of CD4 or CD8 surface expression and are known as double negative (DN) cells. DN cells undergo four stages, illustrated by the expression of CD44 and CD25: DN1 (CD44+ CD25-); DN2 (CD44+ CD25+); DN3 (CD44- CD25+); and DN4 (CD44- CD25-). Through differentiation of DN cells from DN2 to DN4, cells express a pre-TCR consisting of a non-rearranging pre-TCRα and a rearranging ß chain. Upon ß chain selection, the cells divide approximately six times and subsequently expression of pre-TCRα is replaced with a rearranged mature α chain. The cells expressing a mature αß TCR begin to express CD4 and CD8 and are, at this stage, known as double positive (DP) cells. DP cells engage with cortical epithelial cells through binding of their TCR to self-peptides presented within major histocompatibility complexes (MHC). DP cells that bind self-peptide-MHC with weak avidity undergo apoptosis through a lack of TCR-mediated survival signaling, a process known as death by neglect. DP cells that bind self-peptide-MHC too strongly also undergo apoptosis, however, this active negative selection results in rapid apoptosis. DP cells that bind self-peptide-MHC appropriately are positively selected and mature into single positive CD8 or CD4 T cells, depending on TCR recognition of MHC-I or MHC-II, respectively. Diagram adapted from (Germain, 2002).

1.3.3 Antigen presentation and T cells in PD

Dendritic cells (DCs) are antigen presenting cells (APCs) with the capacity to stimulate naïve T cell proliferation and activate a specific immune response, more potently than other APCs (Banchereau and Steinman, 1998, Banchereau et al., 2000). The maturation state and anatomical location in which the DCs reside dictate the morphology that the DC will assume. As the oral mucosa is composed of numerous microenvironments, oral DC phenotypes will differ depending on the site inhabited by the DC (**table 1.5**) (Hovav, 2014).

Whilst the oral cavity may be considered a site of tolerance induction (Novak et al., 2008), upon pathogen insult, DCs effectively prime a T cell response (Iwasaki and Medzhitov, 2015).

Table 1.5. DC subtypes that reside within the gingiva.

DC subtype	Cell surface markers	Location in gingiva
Langerhans cell	Langerin CD11c Ep-CAM MHC-II	Epithelium
Interstitial DC	CD11c CD11b MHC-II	Lamina propria
CD103+ Interstitial DC	CD11c CD11b CD103 MHC-II	Lamina propria
Macrophage-like DC	CD11b F4/80 MHC-II	Lamina propria

Adapted from (Wilensky et al. 2014).

DCs patrol the peripheral tissues in an immature state, characterized by optimal phagocytosis function. Pathogen associated molecular patterns (PAMPs) of invading pathogens are recognized through TLRs, stimulating phagocytosis and processing of the pathogen by DCs. The DC then matures and expresses chemokine receptor 7

(CCR7) on its surface, enabling migration to the draining lymph node (dLN). During migration, the DCs upregulate expression of MHC-II and co-stimulatory molecules to permit efficient activation of CD4+ T cells in dLNs (Wilensky et al., 2014) (**figure 1.6**). Clustering of mature DCs with CD4+ T cells has been observed in lamina propria of PD gingival tissues suggesting that in addition to activation of T cells within LNs, T cells might be primed at the local site of infection (Jotwani et al., 2001).

Langerhans cells (LCs) exist in low frequencies in health (Allam et al., 2008). An increase in abundance of gingival LCs followed accumulation of dental plaque and likewise, the numbers of LCs lessened with elimination of plaque (Dereka et al., 2004). In a model of gingivitis, numbers of LCs increased until day 14, following which the numbers decreased, reaching baseline frequencies at day 21 (Moughal et al., 1992). However, Gemmel et al (2002) reported no differences in LC number between health, gingivitis and PD (Gemmell et al., 2002) and further still, the majority of studies found a decrease in the presence of LC cells in PD (Crawford et al., 1989, Cury et al., 2008, Séguier et al., 2000, Stelin et al., 2009). The latter studies imply that LCs migrate out of gingival tissues as inflammation amplifies. Differences between the studies may be explained by varying sampling techniques and stages of disease. As a decrease in intraepithelial LC presence is observed in the aging population and the incidence of PD increases, Wilensky et al have speculated that the decrease in LCs in PD observed in some studies is likely a true reflection LC behaviour in disease (Wilensky et al., 2014).

Specific deletion of LCs was made possible through the use of langerin-DTR mice and was employed to evaluate LCs role in *P. gingivalis*-induced PD. A lack of LCs was concomitant with increased infiltration of T cells and B cells and exacerbated alveolar bone loss (Arizon et al., 2012). Furthermore, LCs were capable of stimulating Treg generation, which inhibited IFN-γ and subsequently resulted in a reduction in the expression of receptor activator of nuclear factor κB ligand (RANKL) on CD4+ T cells (Arizon et al., 2012). Furthermore, LCs are incapable of antigen presentation, which is instead primarily conducted – in the context of *P. gingivalis* antigens – by interstitial DCs (iDCs) to both CD4+ and CD8+ T cells, which

indicates that iDCs within the lamina propria can process and present oral pathogens causing activation of specific T cells. Rather, LCs inhibit the priming of specific T cells by iDCs (Arizon et al., 2012). DC subtypes within the oral cavity therefore play different roles in priming of T cells and regulating the inflammatory response characteristic of PD.

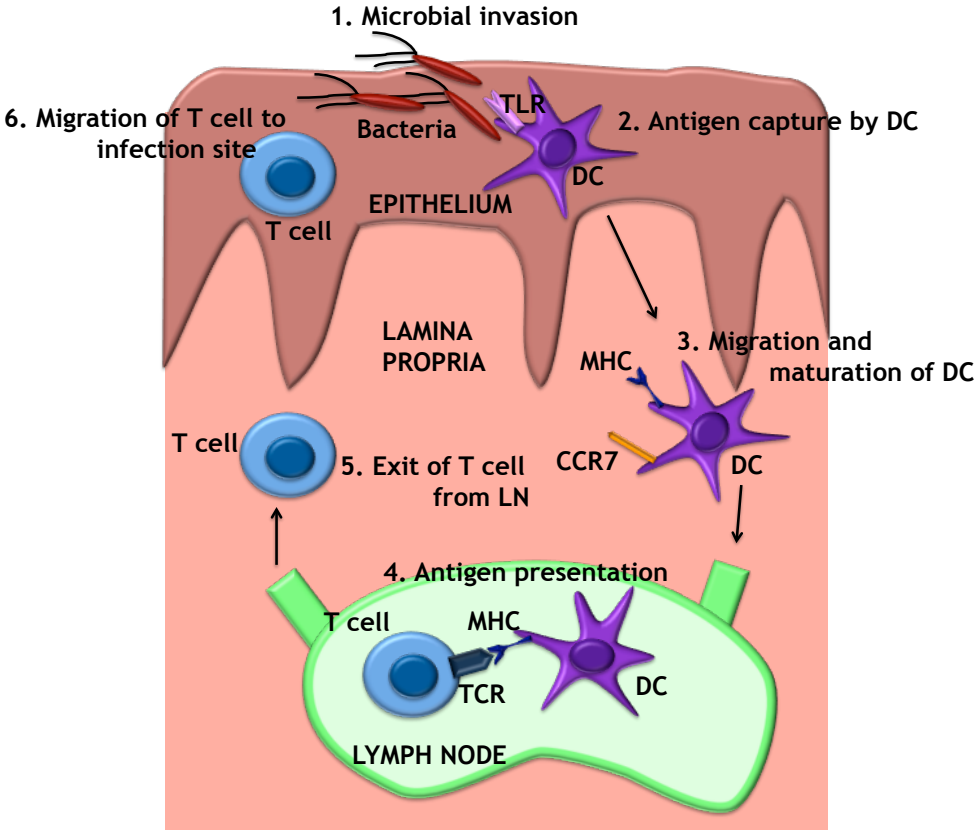

Figure 1.6. Priming of T cells by dendritic cells.
Dendritic cells (DC) patrol the peripheral tissues in an immature state. Pathogen associated molecular patterns of invading microbes are recognized through toll-like receptors (TLRs), stimulating phagocytosis and processing of the pathogen by DCs. The DC then matures and expresses chemokine receptor 7 (CCR7) on its surface, enabling migration to the draining lymph node (dLN). During migration, the DCs upregulate expression of MHC and co-stimulatory molecules to permit efficient activation of CD4+ T cells in lymph nodes (LN). Activated T cells exit the LN and migrate to the site of infection, where they exert effector functions and clear infection. Adapted from (Wilensky et al., 2014).

1.3.4 T cells in PD

1.3.4.1 Cytotoxic CD8+ T cells

Cytotoxic T cells are CD8+ cells that recognize altered self-antigen presented in MHC-I from infected host cells (Zinkernagel, 1997). Activation of naïve CD8+ T cells is dependent upon: 1) specific antigen stimulation through the TCR; 2) co-stimulation through binding of ligands to CD28, CD40 or ICOS; and 3) binding of cytokines (IFN-α and IL-12) to the receptor present on the cell surface (Curtsinger et al., 1999). Signals 1 and 2 alone will enable proliferation of the specific CD8+ T cells but only few will survive and these will become tolerant. Only in the presence of signal 3 will the activated T cells survive and develop effector function (Curtsinger et al., 2003). Clonal expansion of specific CD8+ T cells generates a vast pool of antigen-specific cytotoxic T cells that migrate to the site of infection. Pathogens are eliminated by host cell death through direct cell-cell contact or indirectly through the release of cytokines (Andersen et al., 2006). *P. gingivalis* is an interesting bacterium in that it invades and replicates within gingival epithelial cells (GECs) (Belton et al., 1999), suggesting a niche for CD8+ T cells in PD. Studies have implied that CD8+ T cell number (Cifcibasi et al., 2015b) and phenotype (Petit et al., 2001) differ in patients with established PD. However, there are few studies indicating the role of these cells in disease.

1.3.4.2 CD4+ T cells

Naïve CD4+ T cells, usually within secondary lymphoid organs, recognise their cognate antigen presented within MHC-II of an APC. Complete activation of specific naïve CD4+ T cells, like CD8+ T cells, is dependent on other signals. Binding of CD28, CD40 or ICOS to ligands present on APCs is necessary for the cell to receive co-stimulation signals. Whilst these two signals are sufficient for CD4+ T cell proliferation, IL-2 – as a third signal – doubles the proliferation rate of CD4+ T cells, hence three signals are necessary for optimal activation and proliferation (Curtsinger et al., 1999, Pape et al., 1997). The cytokine milieu in which antigen-specific naïve CD4+ T cells become activated dictates the genetic programming and subsequently differentiation into specific Th subsets (**figure 1.7**). Th subsets include Th1, Th2, Th17, Th9, Th22, Treg and T follicular helper cells (Tfh).

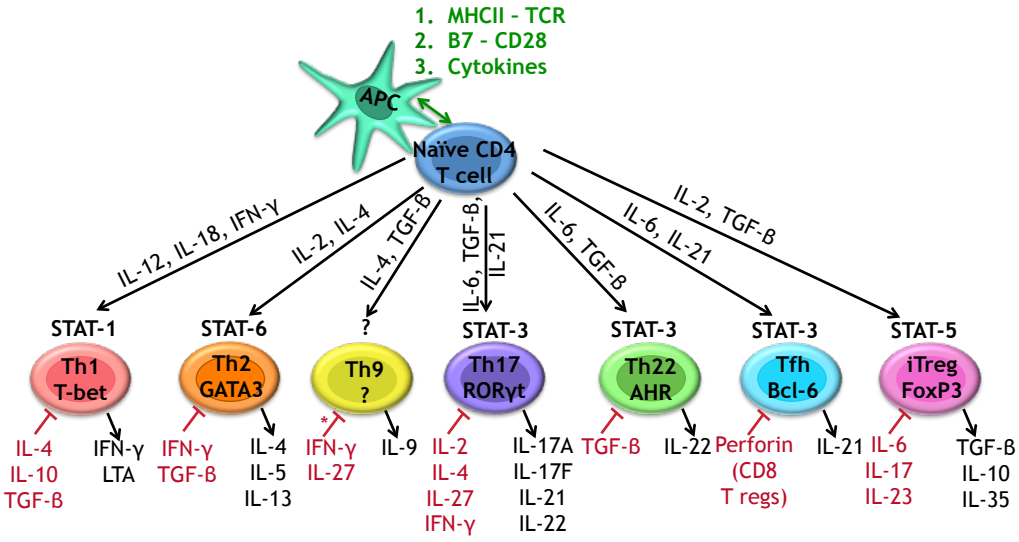

Figure 1.7. CD4+ T helper subsets.
Naïve CD4+ T cells become activated when presented with their cognate antigen non-covalently bound to MHC-II of an APC, with co-stimulation and appropriate cytokines. The cytokine milieu present (shown on the black arrows from naïve CD4+ T cells to specific subset) when naïve CD4+ T cells become activated dictate the Th subset into which the naïve cell will differentiate. Members of STAT family that are associated with specific subsets are shown above the cell and transcription factors are shown within the cell. The cytokines produced by each subtype are shown by the black arrows leaving the cells, and inhibitory cytokines are shown in red. *IFN-γ may not inhibit expansion of Th9 cells, but it inhibits the production of IL-9 by Th9 cells.

Deducing the CD4+ T cell contribution to PD has proven difficult. HIV-positive patients display reduced numbers of CD4+ T cells and are more commonly diagnosed with necrotizing periodontitis than their HIV-seronegative counterparts, which suggests a protective role of CD4+ T cells (Ryder et al., 2012). On the contrary, patients receiving immunosuppressive treatment, Cyclosporin A, often suffer gingival overgrowth but do not present with rapid progression of PD (Pejcic et al., 2014). This is despite a broad inhibition of T cells through blocking of calcineurin, which prevents nuclear factor of activated T cells (NFAT) activation (Ho et al., 1996). In a *P. gingivalis*-induced model of PD, C57BL/6J-*Tcra*$^{tm/Mom}$ mice deficient in T cells showed reduced alveolar bone loss compared to normal C57BL/6 mice (Baker et al., 2002). However, only depletion of CD4+ T cells, not CD8+ T cells

contributed to a reduction in alveolar bone loss (Baker et al., 1999a). A destructive role of CD4+ T cells in PD was thereby highlighted by the latter studies.

Furthermore, efforts to decipher specific CD4+ Th cell responses in PD have proven contradictory. Th1 responses promote immunity to intracellular pathogens, whilst Th2 responses are protective against extracellular pathogens. It was initially assumed that the potential of human PD to progress was linked to the ratio of Th1 to Th2 cells within gingival tissue. Th1 cytokines and chemokines were found more frequently in PD lesions than Th2 effectors, implying that Th1 cells posed a risk for development of PD (Seymour et al., 1993, Gamonal et al., 2001, Taubman and Kawai, 2001). Others demonstrated that unstimulated cells from patients with early-onset periodontitis (EOP, a form of aggressive periodontitis) (Manhart et al., 1994) or advanced PD (Lappin et al., 2001) produced predominantly Th2 cytokines. However, co-existence of Th1 and Th2 cells in PD was also suggested, as gingival CD4+ T cells from PD patients produced cytokines characteristic of both Th1 and Th2 (Takeichi et al., 2000, Berglundh et al., 2002).

Numerous studies have investigated the role of cytokines using animal models based on bacterial-induction of alveolar bone loss, using different members of the 'red complex'. In a *P. gingivalis*-induced model of PD, a lack of IFN-γ conferred protection against alveolar bone loss (Baker et al., 1999a), whilst infection of IFN-γ knockout (KO) mice with *A. actinomycetemcomitans* resulted in reduced bone loss but also increased acute phase immune reaction, dissemination of the bacterial infection and eventual death (Garlet et al., 2008). It can therefore be postulated that IFN-γ contributes to bone loss in PD, yet in some contexts also provides protection against periodontal bacterial infections. The contribution of Th2 cells to bone destruction has also been debated. Th2 cells specific for *A. actinomycetemcomitans* were transferred to athymic rats orally infected with *A. actinomycetemcomitans* and the rats subsequently displayed reduced bone destruction compared to their athymic counterparts that received no T cells. It was therefore suggested that Th2 cells ameliorated the clinical symptoms of PD (Eastcott et al., 1994). Opposing this finding, STAT-6 deficient mice infected with *T. forsythia* did not develop bone loss to the extent of WT mice. As STAT-6 plays a

role in Th2 polarisation through its involvement in downstream TLR2 signaling, this study implied that the TLR2-Th2 inflammatory response was a driver of alveolar bone loss (Myneni et al., 2011). Likewise, IL-33 – a Th2 cytokine - has recently been shown to exacerbate bone destruction following *P. gingivalis* infection (Malcolm et al., 2015a). Whilst there is a plethora of evidence indicating the presence of Th1 and Th2 cells and mediators in the oral mucosa in human and murine PD, no definite conclusion has been drawn regarding the role of these cells in PD.

With the emergence of Th17 cells, cytokines and chemokines emanating from the new Th subset were studied in PD, and IL-17A and IL-21 were identified in human periodontal lesions. The Th1/Th2 paradigm could not effectively describe the immune-mediated pathogenesis of PD (Gaffen and Hajishengallis, 2008). Th17 cells promote immunity to extracellular bacteria and fungi, particularly at mucosal sites; hence it seems plausible that they play a role in PD. Gingival tissue of PD patients have elevated gene expression of Th17 inducing cytokines (*il1β*, *il6* and *il21*) compared to control tissue (Cardoso et al., 2009, Dutzan et al., 2012a, Gaffen and Hajishengallis, 2008). Whilst lower levels of TGF-ß were found in disease (Dutzan et al., 2012a), it has been suggested that Th17 differentiation can occur in its absence (Ghoreschi et al., 2010). Further, IL-23p19-producing macrophages have been identified in severely inflamed PD lesion sites and have the potential to amplify the Th17 response through IL-23 secretion (Allam et al., 2011). IL-17, a cytokine indicative of an active Th17 response, has been identified at increased levels in PD patients compared to both gingivitis patients (Honda et al., 2008, Moutsopoulos et al., 2012) and healthy controls (Beklen et al., 2007, Cardoso et al., 2009, Allam et al., 2011, Adibrad et al., 2012, Awang et al., 2014), and T cells were shown to be the predominant source (Cardoso et al., 2009). The local cytokine milieu necessary for Th17 cell differentiation is likely promoted by the oral microbiota. Cell culture supernatants from human APCs stimulated by *P. gingivalis* induced a Th17 response – explained by the minimal release of IL-12p35, and the greater resistance of IL-1ß to proteolytic degradation by gingipains compared with IL-12 (Moutsopoulos et al., 2012). In addition to increased IL-17 in gingival crevicular fluid (GCF) from PD patients, IL-35 protein and *ebi3* and *il12a* mRNA (components of IL-35) were also

found to be elevated. As IL-35 is a suppressor of Th17, it may be found in PD to compensate for the increased numbers of Th17 cells (Mitani et al., 2015).

Whilst human studies found a clear association between Th17 cells and PD, the findings from mouse studies were ambiguous. Mice deficient in IL-17RA displayed increased alveolar bone loss when orally infected with *P. gingivalis*. In this model, IL-17-dependent neutrophil recruitment to the inflamed gingival tissue – imperative for defense against bacteria – was diminished, resulting in a total reduction of neutrophils to the site of infection and exacerbated bone loss (Yu et al., 2007). However, Del-1 deficient mice portrayed a role for IL-17 in the destruction of alveolar bone. Del-1 inhibits lymphocyte function-associated antigen (LFA)-dependent neutrophil adhesion but is itself blocked by IL-17. Conflicting the observations made by Yu et al (2007), increased production of IL-17 and recruitment of neutrophils was found to cause spontaneous PD in this study (Eskan et al., 2012). Although Th17 cells are present in experimental PD, unlike human studies, a role in protection or destruction cannot be appointed.

Perhaps, in part, explaining the conflicting evidence of Th cells identified in PD is Th cell plasticity. Th plasticity occurs when a differentiated Th cell expresses mediators associated with a different Th subtype. Whilst there is limited data supporting the occurrence of Th plasticity in PD, this phenomenon has been observed in other chronic inflammatory conditions. Th17 cells that display IL-12Rß2 have the capacity to co-express T-bet upon IL-12 stimulation, thereby enabling conversion to non-classical Th1 cells (Nistala et al., 2010). This has been observed in juvenile autoimmune arthritis, whereby the majority of Th17 cells in synovial fluid express both RORC2 and T-bet transcription factors (Nistala et al., 2010). In patients with fistulating Crohn's disease, Th1, Th7 and Th1/Th17 intermediate cells were found infiltrating the fistula in greater numbers than in peripheral blood and it was therefore postulated that Th1/Th17 intermediate cells were a feature of inflammatory sites (Maggi et al., 2013). Furthermore, by comparison to healthy controls, an increase in IL-17 producing 'Th2' cells was observed in patients with atopic asthma. These Th2/Th17 cells expressed classical Th2 cytokines together

with IL-17 and IL-22, and transcription factors of both Th2 and Th17 subsets (Wang et al., 2010b).

1.3.4.3 Memory T cells

Specific T cells undergo clonal proliferation upon recognition of their cognate antigen and migrate to the site of infection, where CD4+ T cell cytokine production amplifies the immune response to the pathogen, or CD8+ T cells mediate direct killing of infected-host cells. Most of the specific effector T cells die as the immune response comes to an end; however, a few of these will become memory cells (MacLeod et al., 2010). Memory cells present the host with the advantage of a fast and effective immune response in the event of re-infection. By comparison to naïve T cells, memory T cells can respond to lower doses of antigen and decreased levels of co-stimulation (London et al., 2000, Kaech et al., 2002). Memory T cells therefore respond to the pathogen at earlier stages of infection, before extensive damage has been caused. Unlike naïve CD8+ T cells, memory CD8+ T cells constitutively express cytotoxic mediators, including perforin and granzyme B, permitting an immediate response upon re-infection (Bachmann et al., 1999). As memory CD4+ T cells undergo fewer proliferation cycles than naïve cells, it has been suggested that the protective role of memory CD4+ T cells are exerted through cytokine production and their influence on other immune cells, rather than direct killing (MacLeod et al., 2008). Based on expression of CCR7 and CD62L - and hence their anatomical location - memory T cells can be divided into two subsets – central memory (TCM, CD44+ CD62L+ CCR7+) and effector memory (TEM, CD44+ $CD62L^{lo}$ $CCR7^{lo}$) T cells (Unsoeld and Pircher, 2005). This enables TCM cells to enter lymphatics from blood. Molecules on the surface of TEM cells enable their migration to the appropriate tissue type; for example, $\alpha_4\beta_7$ expression facilitates migration to the gut. More recently, a subset of memory T cells has been shown to reside within tissues – tissue-resident memory T cells (TRMs). TRMs are found within epithelial barrier tissues at the border between the host and the environment, with specificity to antigens previously encountered at that site. Thus, TRMs in the gut will have a specificity distinct from that of TRMs found within the lungs (Schlapbach et al., 2014). There is evolving knowledge that TRMs contribute to inflammatory

diseases (Park and Kupper, 2015). Psoriatic lesions can be cleared by appropriate treatments; however, upon disuse of the treatment the lesion will often return in the same position and to the same extent as prior to therapy. Analysis of resolved psoriatic skin lesions from patients identified T cells and cytokines that contribute to pathogenesis of the disease, suggesting that TRMs remain within lesion sites (Suárez-Fariñas et al., 2011). Furthermore, due to areas of disease being separated by areas of healthy mucosa within the gut in Crohn's disease, it has been postulated that TRMs mediate inflammation in this context (Kleinschek et al., 2009, Park and Kupper, 2015).

In human PD, CD4+ T cells were found to be the major source of increased IL-17 expression and upon further characterization of the cells, it was highlighted that TRMs (effector TRM: CD45RO+ CCR7- CD69+; central TRM: CD45RO+ CCR7+ CD69+) comprised the greatest proportion of CD4+ IL17+ cells (Dutzan et al., 2016). With regards to memory cells, early studies demonstrated that in both healthy and PD gingival samples, CD45RO+ memory cells predominate and few CD45RA+ naïve cells comprise the tissue. The memory cells were presumed to be specific for commensal bacteria present in oral plaque biofilms. Interestingly, it appeared that greater numbers of naïve cells were found in disease (Gemmell et al., 1992). Human studies have therefore illustrated that memory T cells are evident in gingival tissue irrespective of PD, yet the role of these cells in both health and disease remains an enigma. Memory T cell status of mice with experimental PD, however, remains completely unknown.

1.3.4.4 T cells and osteoimmunology

Binding of RANKL to RANK expressed on the surface of pre-osteoclasts induces differentiation to mature osteoclasts. RANKL-induced osteoclastogenesis is responsible for the alveolar bone destruction in PD and RANKL expression has been identified on T cells (Kawai et al., 2006, Vernal et al., 2006, Han et al., 2009). Therefore, it is plausible that T cells are directly involved in bone resorption of PD (Taubman and Kawai, 2001, Belibasakis and Bostanci, 2012).

1.3.4.5 Tregs in PD

Tregs function to suppress immune responses, which is important for many reasons. By generating and maintaining self-tolerance, Tregs prevent autoimmunity – a factor highlighted by immunodysregulation polyendocrinopathy enteropathy X-linked syndrome (IPEX). Owing to mutations in FOXP3, IPEX sufferers are deficient in Tregs and subsequently experience a range of autoimmune diseases, including type I diabetes and thyroiditis (Charbonnier et al., 2015). Arguably, most relevant to the study of the chronic inflammation associated with PD is that Tregs regulate the immune response mounted by Th cells (Oldenhove et al., 2003). As such, these cells have been the focus of many PD studies. Tregs have been identified in both gingivitis and PD patients, but an increase in both Tregs and their associated anti-inflammatory cytokines has been noted in PD (Nakajima et al., 2005, Cardoso et al., 2008b). Depletion of Tregs using anti-glucocorticoid-induced tumour necrosis factor receptor (GITR) in an *A. actinomycetemcomitans*-induced experimental PD model exacerbated alveolar bone loss, implying that Tregs regulate inflammation in the oral cavity in this environment (Garlet et al., 2010b). Nonetheless, the ability of Tregs to efficiently modulate inflammation has been under speculation. T cell proliferation can be inhibited by cell-cell contact through CTLA-4. However, whilst Tregs from active PD lesions showed increased expression of FOXP3, CTLA-4 expression was unchanged compared with gingival biopsies from stable lesions (Dutzan et al., 2009). This suggests that Tregs do not exhibit regulation through cell-cell contact but does not completely disregard these cells as mediators of inflammation in the context of PD. Despite the evidence that Tregs are present in periodontal tissues in PD, the role of Tregs in the initiation of disease is largely unknown.

1.3.4.6 Interaction between T cells and B cells in PD

B cells are constituents of adaptive immunity that respond to specific antigens. Unlike T cells that only recognize antigen presented within MHC by an APC, B cells can directly bind free antigen. Upon activation of B cells by specific antigen, the cells proliferate and differentiate to antibody-producing plasma cells or memory B cells (Warrington et al., 2011).

Within healthy gingival tissue, few leukocytes reside, with B cells and plasma cells comprising approximately 5% (Gemmell et al., 2002). However, the inflammatory infiltrate of PD lesions is comprised of around 70% B cells and plasma cells (Berglundh and Donati, 2005). As such, an increase in abundance of B cells and plasma cells has been linked with PD progression, severity and activity (Amunulla et al., 2008, Lappin et al., 1999, Thorbert-Mros et al., 2015). It is believed that B cells contribute to the pathogenesis of PD, possibly through their expression of RANKL (Kawai et al., 2006, Han et al., 2006).

IgG, IgA and IgM antibodies have been found within inflamed PD lesion sites – which is indicative of class-switching (Graswinckel et al., 2004, Okada et al., 1983, Ogawa et al., 1989). This evidence of B cell class switching and presence of plasma cells suggests a role for T cells. Upon specific-antigen recognition by T cells and B cells within the T cell zone and primary follicle, respectively, of a lymph node, the cells become activated and migrate to the interfollicular region. At this site, T cells and B cells interact, resulting in full activation of B cells and committed T cells differentiate into Tfh cells by upregulation of B cell lymphoma 6 (Bcl-6), CXC-chemokine receptor 5 (CXCR5), programmed cell death protein 1 (PD-1) and GL7. Tfh cells have the capacity to migrate into follicular region, where the activated B cells meet them (De Silva and Klein, 2015). Germinal centre (GC) B cells migrate through two distinct regions of the follicle: the light zone and dark zone. Within the light zone, GC B cells bind specific antigen and subsequently present antigen within MHC to Tfh cells. Tfh cells provide survival signals to the GC B cells, which then locate to dark zones to proliferate and undergo somatic hypermutation to generate B cell receptors with a range of affinities for specific antigens. Mutated GC B cells re-encounter Tfh cells in the light zone and only GC B cells with high affinities for antigen receive survival signals enabling further proliferation (Crotty, 2014). The differentiation of high affinity GC B cells into plasma cells has been shown to involve IL-21 signaling by Tfh cells that is induced by PD-1 signaling (Good-Jacobson et al., 2010, Hamel et al., 2010). Despite the role of Tfh cells in maturation of B cells and the accumulating evidence of B cells in PD pathogenesis, there is limited knowledge of the role of Tfh cells in PD.

On the other hand, B cells can also provide T cell help. B cells within severe PD lesions have been shown to express high levels of co-stimulatory molecules CD86 and CD83 (molecules found on mature DCs), which suggests that they play a role as APCs in PD, thereby activating T cells (Mahanonda et al., 2002).

Similar to T cell subsets, B cells can exert pro-inflammatory and anti-inflammatory functions. Regulatory B cells (Bregs) produce IL-10, IL-35 and TFG-β that subsequently inhibit differentiation of Th1, Th17 and cytotoxic T cells, and inhibit TNF-α and IL-12 production by monocytes and DCs respectively. Furthermore, Bregs are capable of stimulating Treg differentiation (Rosser and Mauri, 2015). In a mouse model of inflammatory bowel disease (IBD), activation of IL-10 producing Bregs through exogenous IL-33 and protected mice from inflammatory disease (Sattler et al., 2014). The value of Bregs in inflammatory disease was further highlighted in RA. RA patients displayed decreased frequencies of Bregs in peripheral blood than their healthy counterparts, and this negatively correlated with DAS28 scores (a measurement of disease activity) (Cui et al., 2015). In a collagen-induced arthritis model (experimental RA), adoptive transfer of IL-10 expressing B cells reduced both the incidence and severity of disease through inhibition of Th1 cell differentiation (Mauri et al., 2003). Likewise, there is evidence that Bregs can ameliorate inflammation in PD. Induction of local IL-10 producing Bregs in gingival tissues of mice through administration of low dose CD40L and cytidine-phosphate-guanosine oligodeoxynucleotide (CpG) reduced bone loss in a ligature model of PD. In the presence of increased IL-10 producing Bregs, alveolar bone loss was reduced with concomitant reductions in inflammatory cytokines and osteoclast numbers on the bone surface (Yu et al., 2016). Therefore, Bregs could serve as targets for novel therapeutics in PD.

1.4 Models of PD

1.4.1 Human *in vivo* models of PD

A human model of gingivitis was established by Löe et al (1965) to investigate the role of plaque in gingivitis induction. In this study, dental students ceased teeth brushing for 21 days, which illustrated that accumulation of plaque correlated with increased gingival inflammation and that removal of the plaque by restoration of

oral hygiene resulted in elimination of inflammation (Löe et al., 1965). This simple model was subsequently used as a platform for myriad investigations including those of inflammatory markers, induction and resolution transcriptome profiles of gingival lesions, differing inflammation in smokers versus non-smokers and the capacity of antimicrobials to lessen clinical parameters of gingival inflammation (Eberhard et al., 2013, Jönsson et al., 2011, Heasman et al., 1993, Dommisch et al., 2015, Offenbacher et al., 2009, Branco et al., 2015).

Experimental gingivitis has also been exploited to determine the composition of plaque in the transition from health to gingivitis by 454-pyrosequencing (Kistler et al., 2013). Further, the bacterial composition of plaque derived from smokers and non-smokers has been assessed using the experimental gingivitis model (Peruzzo et al., 2016). Such studies were conducted with the ultimate aim of identifying risk biomarkers for development of PD.

A limitation of experimental gingivitis is that it does not represent PD. The inflammation that occurs in the presence of the accumulating plaque is an acute response that does not cause destruction of local periodontal structures. However, PD is a chronic inflammatory condition that occurs over a period of months to years, rather than days to weeks, and causes irreversible damage to periodontal structures and bone.

Another means of researching the immune response and composition of the dental plaque biofilm in human disease is through extraction of gingival tissue lesions from patients with clinically diagnosed PD. Removal of inflamed tissue at periodontal surgery offers the potential for study of otherwise discarded tissue (**figure 1.8**). Whilst this provides a tool to understand the immune mechanisms in established PD, it does not enable the study of the immune response during the initiation and progression towards PD; in particular the dysregulated immune response that ultimately mediates bone destruction. Furthermore, it is difficult to precisely control, as patients will present at different stages of disease progression with varying severity of PD. Whilst the severity of disease can be accurately quantified clinically, there are no reliable clinical indicators of disease duration. Thus, studies

using experimental gingivitis and established PD in humans are complex, difficult to control, and confounded by patient heterogeneity.

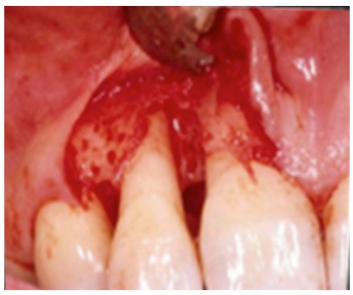

Figure 1.8. Surgical periodontal treatment.
Clinical photograph to show surgical periodontal treatment to permit better access for removal of inflamed tissue beneath the gingivae and to allow debridement of the root surfaces. Photograph also shows alveolar bone loss.

1.4.2 Animal *in vivo* models of PD

Animal models of PD offer numerous advantages over human studies including the potential to investigate mechanisms of evolving disease and disease intervention in controlled environments, by techniques not applicable to humans in the first instance because of ethical considerations. Due to the multifactorial nature and complexity of PD, *in vitro* models are insufficient in mirroring the immunopathogenesis of PD. *In vivo* models of PD encompass spontaneous and experimentally induced disease, in a number of different animals.

As there is a plethora of animal models of PD described in the literature, an appropriate model must be chosen based on both the scientific objectives and the specific experimental techniques i.e. consideration of feature of disease under investigation, experiment reproducibility, complexity, cost, ethical considerations an the time required for optimisation of the technique (Struillou et al., 2010).

Non-human primates are the most relevant animal models of PD due to their similarities in anatomy, immunology and microbiology to humans. Non-human primates are susceptible to naturally occurring PD and display comparable clinical symptoms to human disease. Disease can also be exacerbated through tying sutures round the teeth at gum level. Despite arguably baring the closest resemblance to

human PD of all the animal models, there are huge ethical implications, maintenance and appropriate housing are expensive, and non-human primates are susceptible to infectious diseases. For investigation of PD these animals are therefore rarely used (Oz and Puleo, 2011).

Dogs offer another platform for studying naturally occurring PD (Pavlica et al., 2004, Oliveira et al., 2016), and are susceptible to experimentally-induced disease by placement of sutures around teeth (Carcuac et al., 2013). Microbiologically, there is overlap between humans and dogs, with the subgingival plaques from dogs being composed of similar bacteria found in humans at the genus level, but not species level (Dahlén et al., 2012). Furthermore, as is evident in humans, severity of PD increases with age. However, not all breeds share equal disease susceptibility, likely due to differing genetics. The pattern of pathogenesis is dissimilar to that seen in humans; rather than affecting only the gingival tissue adjacent to the periodontal pocket, the entire width of the marginal gingiva is implicated in canine PD (Oz and Puleo, 2011). Moreover, maintenance of the dogs is costly and carries ethical considerations.

Rodents – mice and rats – are the most common animal type used for the investigation of PD *in vivo*. A particular benefit of rodents, and more so in mice, is the wide availability of experiment reagents for investigating the immune response, and the ability to generate genetically manipulated strains, which can assist the study of cause and effect relationships in disease settings. Rodents are relatively easy to handle, have high reproducibility rates and are fairly inexpensive and simple to maintain, offering further advantage. Disadvantages of rodents are that they tend to be naturally resistant to PD, and differ anatomically and microbiologically to humans. It has also been shown that female mice are more susceptible to alveolar bone loss than male mice, a contrast to that observed in humans (Duan et al., 2016). Even still, rodents are valuable tools for studying the complex pathogenesis of PD and a range of models are described in the literature.

The calvarial (scalp) model was first introduced in 1989 to investigate the role of cytokines in osteoclastogenesis (Boyce et al., 1989) and was subsequently adapted to determine the impact of oral pathogens on osteoclastogenesis. Specifically, this

model employed injections of *P. gingivalis* into the connective tissue overlying the skull to trigger inflammation and bone resorption (Graves et al., 2001). Whilst this model provides an insight into bacteria-induced immunity, it fails to assess the interactions between *P. gingivalis*, epithelial cells and mucosal tissue and ensuing downstream effects on osteoclastogenesis. Moreover, there is no evidence of the impact of *P. gingivalis* in the oral cavity in this model; the anatomical site affected in PD.

Originally developed to investigate synovial membrane function (Edwards et al., 1981), the air pouch model was adapted to study the host response to oral pathogens. Sterile air is injected subcutaneously into the dorsum of the mouse to create an air pouch, into which *P. gingivalis* is introduced. Infiltrating leukocytes and mediators are then determined by aspiration of the air pouch fluid, to assess the *P. gingivalis* induced inflammatory response (Pouliot et al., 2000). However, the chronic response to oral pathogens cannot be evaluated due to the short duration of the air pouch. This limitation was overcome through development of the chamber model. A coiled, stainless steel wire is inserted subcutaneously by surgical means into the dorsum of the mouse. To enable healing and epithelialisation, the mice are rested for 10 days, followed by injection of bacteria into the chamber (Genco et al., 1991). Both acute and chronic inflammatory responses can be determined through exudation of chamber fluid or the chamber can be removed for histological studies. As for the calvarial model, the chamber model does not provide a platform for studying the immune response to periodontal bacteria in the oral cavity; hence does not truly represent PD.

A successful model of PD in mice, initially described by Baker et al (1994), is achieved by orally introducing pathogenic, human PD-associated bacteria that are absent from murine microflora (Baker et al., 1994b). Prior to repeated oral inoculations, commensal microflora are depleted through administration of antibitoics to aid the colonisation of the foreign bacteria. Originally, and still currently, *P. gingivalis* is used to induce PD and its associated clinical symptoms; however, other 'red complex' bacteria including *A. actinomycetemcomitans* and *T. forsythia* can replace the role of *P. gingivalis* (Baker et al., 1994b, Garlet et al., 2008, Sharma et al., 2005). A major advantage of rodent models of PD is that the

immune response can be investigated at any stage pre or post infection, to understand the changes in immunity that occur along with the development of a dysbiotic biofilm and the mechanisms by which these causes alveolar bone resorption. However, caveats include the requirement of un-physiologically high numbers of bacteria and repeated inoculations to induce the clinical features of PD. Furthermore, the administered antibiotics are not specific for oral microbiota, hence gut microflora will also be affected, perhaps altering systemic immune responses.

An alternative method for investigating PD in rodents is the ligature model. Ligatures – typically cotton or silk – are placed around posterior teeth to promote the accumulation of bacteria and trigger an inflammatory response. The ligature may also be soaked with *P. gingivalis*. A benefit of using this model is that removal of the ligature enables assessment of resolving inflammation (Abe and Hajishengallis, 2013). Unlike the bacteria-induced PD model described above that typically takes four to six weeks to cause bone loss, the rodent ligature model requires only a matter of days for similar destruction to become evident (Bezerra et al., 2000, Li and Amar, 2007). A comparative study recently demonstrated that the ligature model is a more effective method than oral infections for investigating PD-associated inflammation at later stages of infection (45 and 60 days) (de Molon et al., 2016). Drawbacks of ligature-induced PD are that high technical skills are necessary to place the suture around teeth in such small animals, and this requires magnification with a surgical microscope. The ligature is prone to displacement; hence a larger number of animals are needed to appropriately power the experiments to compensate for this possibility.

No single animal model fully represents human PD, however, the models permit investigation of the inflammatory response to periodontal pathogens and the immune-mediated mechanisms of alveolar bone loss. Animal models therefore act as a bridge between hypotheses and human PD. Although each animal model of PD presents with advantages and disadvantages (**table 1.6**), mice have been described as the most convenient, adaptable and least expensive models (Graves et al., 2008) and subsequently have been the animal choice of all studies described in this thesis.

Table 1.6. Advantages and disadvantages of animal models of PD.

Animal	Advantages	Disadvantages	Models	References
Non-human primates	Comparable anatomy to humans Comparable oral microbiology to humans Naturally occurring PD	Expensive to house and maintain Ethical implications Susceptible to infectious diseases	Naturally-occurring PD Ligature	(Graves et al., 2008) (Oz and Puleo, 2011) (Struillou et al., 2010)
Dogs	Naturally occurring PD	Expensive to house and maintain Ethical implications Different pattern of PD pathogenesis	Naturally-occurring PD Ligature	
Rodents	Relatively inexpensive to maintain Easy handling Genetically modified strains available Rodent-specific reagents available High reproducibility rate of models	Different anatomy to humans Different oral microbiology to humans Resistant to PD	Air pouch Chamber Calvarial Oral infections Ligature	

1.5 Summary and Aims

In summary, PD is the most common chronic inflammatory disease in humans and is therefore a global health concern. A dysbiotic oral biofilm – found to be mediated in some instances by *P. gingivalis* – forms on the tooth surface altering host:biofilm interactions and ultimately results in a dysregulated immune response. The biofilm is necessary for PD to ensue but disease progression and destruction of periodontal structures are mediated by the immune response. Despite this, current PD treatment strategies remain focused on elimination of the dental plaque. With a greater understanding of the immunological basis of PD, novel and more efficient treatments can be designed.

The study of the inflammatory infiltrate of PD lesions in humans has suggested that T cells and their inflammatory effectors are predominant in disease. Furthermore, studies using CD4+ T cell KO mice imply a role for these cells in mediating alveolar bone destruction. The role of precise CD4+ T cell subsets in PD remains ambiguous, likely due to patients presenting with different severities and stages of disease and the use of different animal models.

It is hypothesized that CD4+ T cells in the oral cavity have a unique phenotype and that that will alter with functional consequence in response to oral *P. gingivalis*-infection and inflammation.

The overall aim of this thesis was to determine the phenotype and function of CD4+ T cells in a murine model of *P. gingivalis*-induced PD at early stages of disease.

The specific aims were:

1. To optimise a protocol for CD4+ T cell isolation from murine gingival tissue (**Chapter 3**).
2. To determine T cell subsets in the oral mucosa and whether these change with experimental PD, at different stages of disease progression (**Chapter 4**).
3. To identify a time-point at which the greatest difference between T cells in 'health' and PD could be observed in a murine model of PD (**Chapter 4**).

4. To determine the transcriptome of CD4+ T cells from the gingivae and dLNs of mice infected with *P. gingivalis* – at the time-point identified in aim 3 (**Chapter 5**).
5. To investigate systems to track the antigen specific CD4+ T cell response in the oral cavity, using an OVA-expressing transgenic strain of *P. gingivalis* (**Chapter 6**).

2 Materials and Methods

2.1 Materials

The materials and reagents used for the studies in this thesis are described in **table 2.1**.

Table 2.1. Suppliers of materials and reagents.

Material/Reagent	Supplier	Supplier location
Sterile de-ionised water from Milli-Q® Direct 8 Water Purification System	Merck Millipore	Hertfordshire, UK
Flow cytometry antibodies	eBioscience BD Biosciences Biolegend	Hatfield, UK Oxford, UK London, UK
Pipette tips	Starlab	Milton Keynes, UK
Minisart syringe filters	Sartorious Stedim Biotech	Göttingen, Germany
Needles	Henke Sass Wolf	Tuttlingen, Deutschland
Syringes	BD Biosciences	Oxford, UK
Cell strainers	eBioscience Greiner Bio-One	Hatfield, UK Gloucestershire, UK
Reaction tubes	Greiner Bio-One	Gloucestershire, UK
Western blot reagents and equipment	BIO-RAD*	California, USA
Multiplex Immunoassay reagents and equipment	BIO-RAD*	California, USA
Other plastic lab equipment	Sigma-Aldrich*	Dorset, UK
Chemicals	Sigma-Aldrich*	Dorset, UK
Culture media and supplements for mouse cells and microbiology	Thermo Fisher*	Paisley, UK

*Unless stated otherwise

2.2 *Porphyromonas gingivalis*

2.2.1 *P. gingivalis* W83 growth

Porphyromonas gingivalis W83 (ATCC BAA-308™, Middlesex, UK) originating from a human oral infection (isolated by Werner, H. in Germany in the 1950s (Loos et al., 1993) were maintained frozen in 10% glycerol at −80°C for long-term storage. Frozen bacteria were streaked onto Schaedler anaerobic agar supplemented with 10% heat-inactivated fetal calf serum (HI-FCS), 5% defibrinated horse blood (E&O laboratories, Bonnybridge, Scotland) and 1 µg/ml menadione, using sterile P200 pipette tips. The streaked agar plate was incubated in an anaerobic cabinet (Don Whitely, Yorkshire, UK) with 5% CO_2, 10% H_2 and 85% N_2 at 37°C for 72-96 hours. Two to three colonies were then inoculated into 35 ml of de-oxygenated Schaedler anaerobe broth supplemented with 1 µg/ml menadione and incubated anaerobically for a further 48 hours.

2.2.2 OVA-expressing *P. gingivalis* W83 (RgpbOVA-A) growth

P. gingivalis W83 was genetically modified to introduce OVA peptide (*ISQAVHAAHAEINEAGR*) into the RgpB gene LNE/SIA site (**table 2.2**) and the transgenic strain was resistant to tetracycline (kind gift of Jan Potempa, Jagiellonian University). The bacteria were maintained frozen in 10% glycerol at −80°C for long-term storage. Frozen bacteria were streaked onto Schaedler anaerobic agar supplemented with 10% HI-FCS, 5% defibrinated horse blood, 1 µg/ml menadione and 1 µg/ml tetracycline, using sterile P200 pipette tips. The streaked agar plate was incubated in an anaerobic cabinet with 5% CO_2, 10% H_2 and 85% N_2 at 37°C for 72-96 hours. Two to three colonies were then inoculated into 35 ml of de-oxygenated Schaedler anaerobe broth supplemented with 1 µg/ml menadione and 1 µg/ml tetracycline and incubated anaerobically for a further 48 hours.

Table 2.2. Amino acid sequence of RgpbOVA-A.

RgpbOVA-A amino acid sequence
MKKNFSRIVSIVAFSSLLGGMAFAQPAERGRNPQVRLLSAEQSMSKVQFRMDNLQFTGVQTSKGVA QVPTFTEGVNISEKGTPILPILSRSLAVSETRAMKVEVVSSKFIEKKDVLIAPSKGVISRAENPDQIPYV YGQSYNEDKFFPGEIATLSDPFILRDVRGQVVNFAPLQYNPVTKTLRIYTEIVVAVSETAEAGQNTIS LVKNSTFTGFEDIYKSVFMNYEATRYTPVEEKENGRMIVIVPKKYEEDIEDFVDWKNQRGLRTEVKV AEDIASPVTANAIQQFVKQEYEKEGNDLTYVLLVGHDKDIPAKITPGIKSDQVYGQIVGNDHYNEVF IGRFSCESKEDLKTQIDRTIHYERNITTEDKWLGQALCIASAEGGPSADNGESDIQHWNIIANLLTQY GYTKIIKCYDPGVTPKNIIDAFNGGISLANYTGHGSETAWGTSHFGTTHVKQLTNSNQLPFIFDVAC VNGDFLYNVPCFAEALMRAQKDGKPTGTVAIIASTINQSWASPMRGQDEMNEILCEKHPNNIKRTF GGVTMNGMFAMVEKYKKDGEKMLDTWTVFGDPSLLVRTLVPTKMQVTAPANISASAQTEEVACD YNGAIATLSDDGDMVGTAIVKDGKAIIKLNEISQAVHAAHAEINEAGRSIADETNLTLTVVGYNKVT VIKDVKVEGTSIADVANDKPYTVAVSGKTITVESPAAGLTIFDMNGRRVATAKNRMVFEAQNGVYA VRIATEGKTYTEKVIVK

OVA peptide is highlighted in yellow.

2.2.3 Preparation of *P. gingivalis* for final application

After the 48 hour incubation, the broths were centrifuged at 4000 x g for 20 minutes at room temperature. Most of the supernatant was discarded and the bacterial pellet was resuspended in the remaining broth, which was then transferred into 1.5 ml reaction tubes. The tubes were centrifuged at 14000 rpm (maximum speed) for 5 minutes and the supernatant was removed and discarded. The bacterial pellets were pooled and washed twice by resuspending in 1 ml phosphate buffered saline (PBS) per tube, centrifuging at 14000 rpm for 5 minutes and discarding the supernatant.

The bacteria were then prepared according to the final application:

(i) Oral Infections

After the addition of PBS for the second wash, around 20 µl was removed to determine the number of CFU of *P. gingivalis*. The bacteria were diluted 1/200 in PBS and the optical density (OD) measured at 600 nm using a GeneQuant spectrophotometer. Using a previously generated standard curve (kindly provided by Dr Emma Millhouse, University of Glasgow Dental School) the number of CFU could be determined and the bacteria were resuspended in 2% CMC in PBS to give a

final concentration of approximately 1 x 10^9 CFU per 75 µl (volume given to each mouse).

(ii) Assessment of anti-*P gingivalis* antibodies by ELISA

After the second wash with PBS, the supernatant was removed. The pellet was resuspended and 50 µl aliquots were transferred into 0.5 ml reaction tubes. The tubes were then sealed shut with parafilm M® (Bemis, Oshkosh, USA) and placed into a 50 ml centrifuge tube containing hot water. The centrifuge tube was then placed in a water bath at 60^{o}C for 30 minutes to heat-kill the bacteria. The aliquots were stored at -80^{o}C until required.

2.2.4 Recovery of live *P. gingivalis* after infection

In order to quantify the viability of the remaining *P. gingivalis* in the inoculum from the oral infections, the Miles and Misra method was used (Miles et al., 1938). The inoculum was serially diluted ten-fold to 10^{-10} with sterile PBS and 10 µl drop-plated in triplicate on blood agar. The agar plate was incubated in an anaerobic cabinet with 5% CO_2, 10% H_2 and 85% N_2 at 37°C for 48-72 hours (figure 2.1). The colonies were then counted and CFU/ml calculated: mean number of colonies in dilution x 100 x dilution factor. The average recovery was 3 x 10^8 CFU per 75 µl of bacterial inoculate.

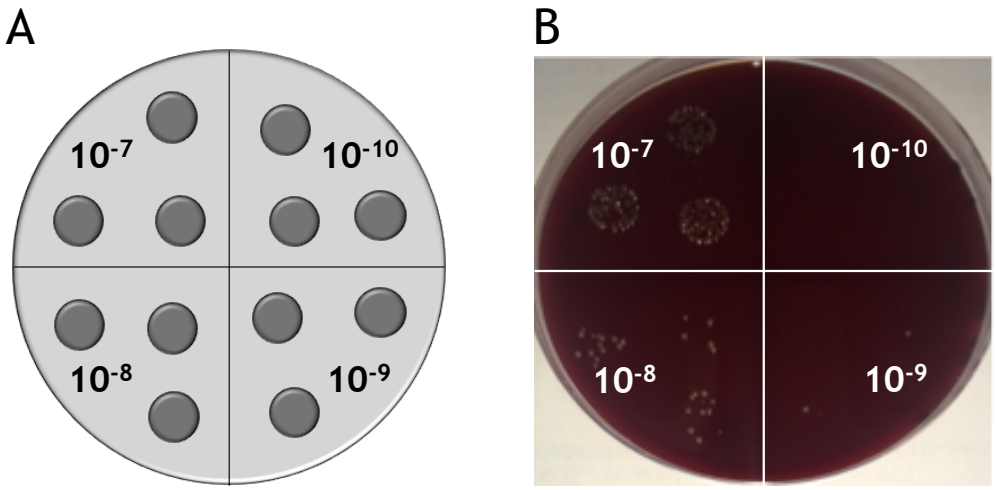

Figure 2.1. Quantification of viable *P. gingivalis* following oral infections.
Viable *P. gingivalis* were quantified following oral infections using the Miles and Misra method. The inoculum was serially diluted ten-fold to 10^{-10} with sterile PBS and 10 µl drop-plated in triplicate on blood agar. The agar plate was incubated in an anaerobic cabinet for 48-72 hours. (A) Representation of plating 10 µl of four lowest dilutions of *P. gingivalis*, represented as dark grey circles. (B) Growth of recovered, viable *P. gingivalis* on blood agar. Colonies were counted and CFU/ml calculated: mean number of colonies in dilution x 100 x dilution factor.

2.3 Mice

6-8 week female BALB/c mice were purchased from Harlan or Charles River Laboratories for all *in vivo* periodontal disease models and studies of gingival tissue. Ubiquitously expressing CRE mice (bred at the University of Glasgow Joint Research Facility) were also used for studies on gingival tissue (these mice were surplus to breeding colony requirements and phenotypically normal). A maximum of 10 mice were housed in standard cages and were maintained on a 12 hour light-dark cycle with *ad libitum* access to food and water. All mice were maintained and experiments carried out in accordance with local and UK home office regulations (Licences 60/4041 and 70/8166).

2.4 Murine models

2.4.1 Murine model of PD

Female BALB/c mice were pretreated with antibiotics (0.08% sulfamethoxazole and 0.016% trimethoprim) in drinking water for 10 days to deplete oral microflora and create a niche for *P. gingivalis* colonisation, followed by a 2-day antibiotic-free rest period. Mice were divided into separate cages and half were orally infected by gavage with 10^9 CFU *P. gingivalis* in 2% CMC, in a volume of 75 µl, administered using P200 pipette and tips (previously described by (Baker et al., 1994a). Sham-infected control groups were inoculated orally with an equal volume of 2% CMC only. Mice were infected 3 or 4 times within 7 days. One or two days before the 14 and 28 day post-infection end points, approximately 100 µl of blood was collected from each mouse by tail bleeding to determine the presence of anti-*P. gingivalis* IgG antibodies as an indication of infection status. At 7, 14 and 28 days post-infection, blood was collected by cardiac puncture under anesthetic, followed by euthanizing of the mice by dislocation of the neck. The timeline of the PD model is described in **figure 2.2**. Plaque was collected from the oral cavity of the mouse using eSwabs™ (Copan, USA) and these were placed in 1 ml liquid Amies transport medium. Gingivae, teeth, draining lymph nodes (cervical lymph nodes; dLN) and spleens were collected.

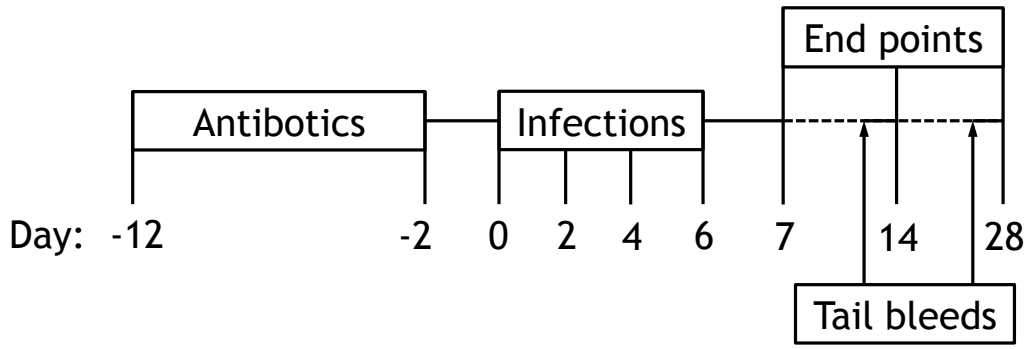

Figure 2.2. Timeline of murine experimental PD model.
BALB/c mice were treated with antibiotics for 10 days to deplete oral commensal bacteria. After a 2-day antibiotic-free rest period, mice were orally infected 3-4 times within one week with approximately 1 x 10^9 CFU of *P. gingivalis* W83 in CMC or sham-infected mice received CMC only. End points occurred 7, 14 and 28 days

post first infection, with tail bleeds being taken 1-2 days prior to end points to assess infection status of the mice.

2.4.2 Assessing OVA-specific T cell stimulation by RgpbOVA-A *in vivo*

Five DO11.10 4GET mice (with transgenic T cells specific for OVA) were sacrificed and their LNs and spleens were collected into a bijou containing 4 ml RPMI 1640 medium supplemented with 10% HI-FCS, 2 mM L-glutamine, 100 U/ml penicillin and 100 µg/ml streptomycin (complete media). A single cell suspension was obtained and counted, as described in **2.5.2**. To determine the percentage of viable, transgenic cells (CD4+ KJ1.26+) within the suspension, 5 x 10^5 cells were stained with viability dye, anti-CD4, anti-KJ1.26 and controls were stained with the isotype of anti-KJ1.26, rat IgG2a. The protocol described in **2.7.1** was followed and the cells were analysed using a MACSQuant® flow cytometer (Miltenyi Biotech) (**figure 2.3**). The total number of transgenic T cells in the sample was calculated using the total cells counts and proportion of CD4+ KJ1.26+ cells identified by flow cytometry. The cell were resuspended in a volume that gave 3 x 10^6 CD4+ KJ1.26+ in 100 µl of incomplete media (RPMI 1640 supplemented with 2 mM L-glutamine, 100 U/ml penicillin and 100 µg/ml streptomycin). Recipient BALB/c mice were placed into a heat box preheated to 37°C for 5 minutes. One hundred µl of cells were injected into the tail vein of each animal.

Twenty-four hours after the transfer of transgenic cells, each mouse was injected subcutaneously in the scruff with 100 µl Complete Freud's Adjuvant (CFA) only or CFA in combination with the following antigens: 1 x 10^8 CFU *P. gingivalis* W83; 1 x 10^8 CFU OVA-expressing *P. gingivalis*; or 1 x 10^8 CFU *P. gingivalis* W83 and 100 µg OVA protein (**table 2.3**). CFA was prepared by repeated aspiration until it formed an emulsion. Both strains of *P. gingivalis* were heat-killed for scruff and footpad injections as described in **2.3.3**.

Ten days after the scruff injections, mice received a second encounter with the antigen given previously with CFA. Fifty µl containing one or a combination of: 1 x 10^8 CFU *P. gingivalis* W83; 1 x 10^8 CFU OVA-expressing *P. gingivalis*; 100 µg OVA protein or PBS was injected into the footpad (**table 2.3**).

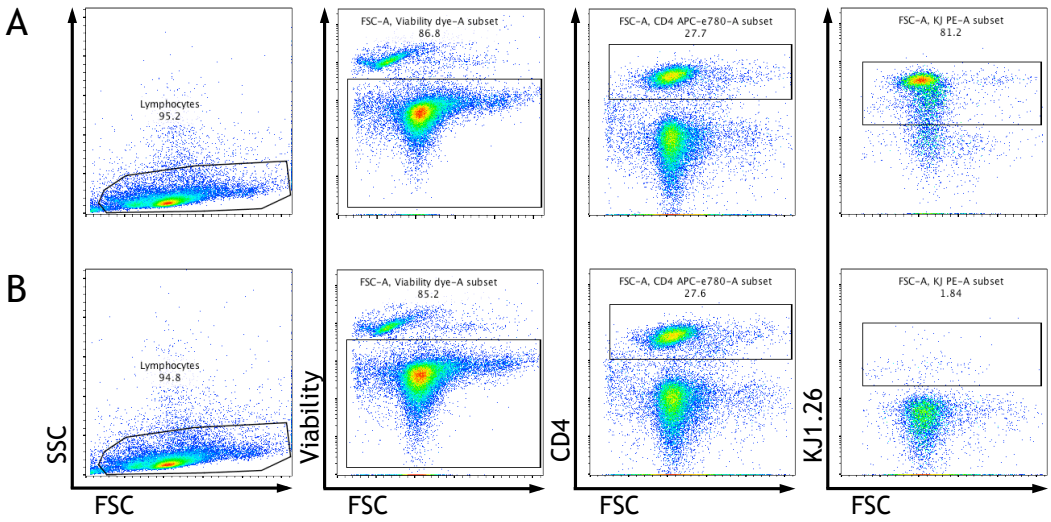

Figure 2.3. Example of flow cytometry plots used to identify CD4+ KJ1.26+ cells.
A single cell suspension of spleen and LNs was obtained and stained with viability dye, anti- CD4 and either (A) anti-KJ1.26 or (B) the isotype control, rat IgG2a. The samples were analysed by a MACSQuant® flow cytometer and FlowJo software. Lymphocytes were gated on based on their forward scatter (FSC) and side scatter (SSC). Viable lymphocytes were gated on based on the exclusion of viability dye. From this gate, CD4+ T cells could be gated on and subsequently the expression of CD4+ KJ1.26+ T cells could be identified.

Three days post-footpad injections, blood was collected by cardiac puncture under anesthetic, followed by euthanizing of the mice by dislocation of the neck. Popliteal LNs were collected into complete media. The timeline is described in **figure 2.4**.

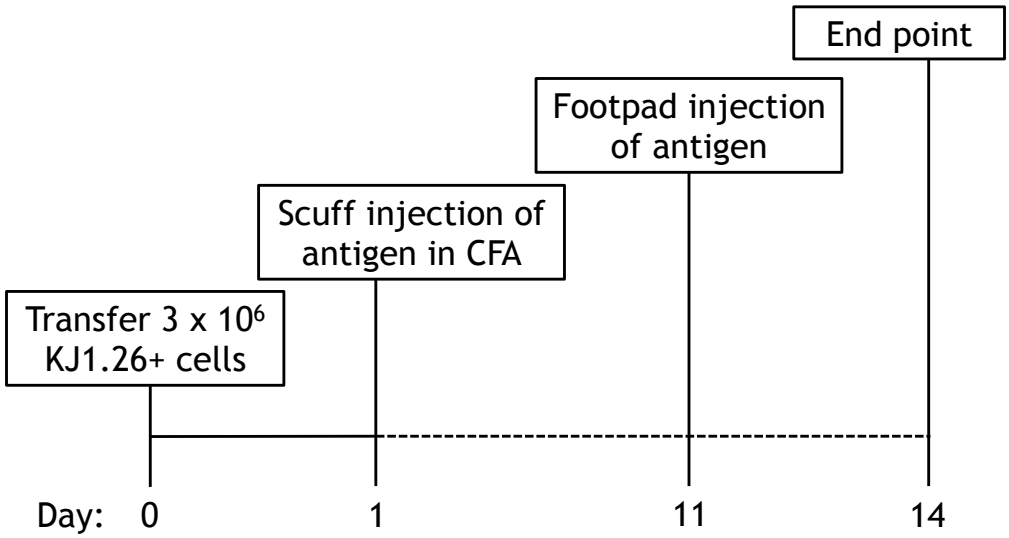

Figure 2.4. Timeline of *in vivo* testing of OVA-expressing *P. gingivalis*.
LN cells and splenocytes from DO11.10 mice were isolated and the percentage of KJ1.26+ CD4+ cells assessed by flow cytometry. Three million KJ.126+ CD4+ were transferred to recipient BALB/c mice by tail vein injection. Twenty-four hours post transgenic cell transfer, the mice were subcutaneously injected in the scruff with 100 µl Complete Freuds Adjuvant (CFA) or CFA in combination with 1 x 10^8 CFU *P. gingivalis* W83, 1 x 10^8 CFU OVA-expressing *P. gingivalis* or 1 x 10^8 CFU *P. gingivalis* W83 and 100 µg OVA protein. Ten days post scruff injection, the mice received a second encounter with the antigen previously given with CFA by footpad injections (50 µl). The mice that received CFA alone received 50 µl PBS footpad injection. Three days later, the mice were culled.

Table 2.3. Groups for assessing OVA-specific T cell stimulation by RgpbOVA-A *in vivo*.

Group (n=3)	Transfer DO11	Scruff injection	Footpad injections
1	✔	*P. gingivalis* W83 + CFA	*P. gingivalis* W83
2	✔	RgpbOVA-A + CFA	RgpbOVA-A
3	✔	*P. gingivalis* W83 + OVA protein + CFA	*P. gingivalis* W83 + OVA protein
4	✔	CFA only	PBS

2.5 Tissue harvest and cell isolation

2.5.1 Gingival tissue harvest

Whole palates were collected from euthanized mice by cutting both sides of the oral cavity, including cheeks and the ramus of the mandible with scissors. Soft and hard tissues were then cut 1 mm behind the third molars with a scalpel blade, followed by cutting the tissue that connects the maxilla to the cheek. The maxilla was then detached from the skull. The gingival and palatal tissues were then carefully removed from the maxilla using tweezers. For the majority of experiments, the entire palate was used but for trial experiments only gingival strips were taken (**figure 2.5**). The tissue was collected into PBS supplemented with 2% HI-FCS (PBS + 2% FCS).

2.5.2 Cell isolation

(i) Lymph nodes and spleen

LNs and spleens were collected into a 6-well plate containing complete media. LNs and spleens were then transferred to a 40 µm cell strainer and mashed using the plunger from a 2.5 ml syringe into complete media to generate a single cell suspension. LN cells were then counted. Splenocytes were washed using complete media and centrifuged at 400 x g for 5 minutes. Splenocytes were resuspended in 5 ml RBC lysis buffer (eBioscience) and incubated for 5 minutes at room temperature. Cells were washed (as described above) then resuspended in complete media for counting.

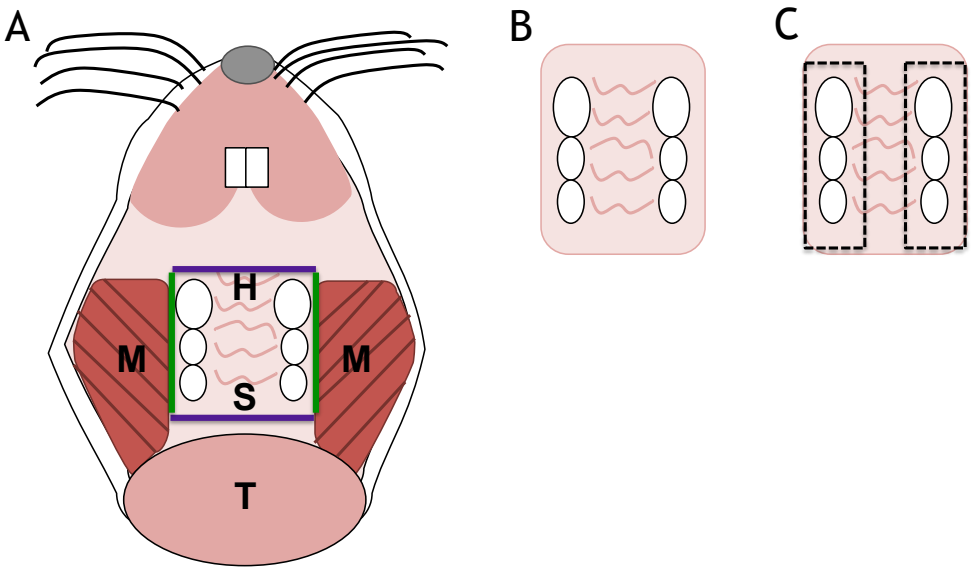

Figure 2.5. Dissection of murine palate and/or gingiva.
(A) The hard (H) and soft palates (S) were cut using a scalpel blade along the lines shown in purple. The gingival tissue was then cut away from the masseter muscle (M), shown in green, using scissors. The palate and teeth were removed from the mouse's head and the palate was carefully peeled away from the teeth. (B) The palatal tissue was used for the majority of experiments or (C) gingival strips were taken by cutting along the dashed lines as indicated. Abbreviations: M, masseter muscle; H, hard palate; S, soft palate; T, tongue.

(ii) Gingivae

Various methods of gingival digestion were performed to optimize a protocol:

MACS dissociation

The palate was collected as described in **2.5.1** and placed into a bijou containing 1 ml of cold PBS. Two hundred µl (500 µg) of dispase-high liberase (Roche, Indianapolis, USA), or collagenase D or no enzyme was added to the bijoux and the tissue was cut up into smaller fragments using scissors. The bijoux were then incubated at 37°C for 30-40 minutes with intermittent pipetting. The enzymatic reaction was inhibited through the addition of 3 ml complete media and the tissue suspension was transferred to a gentleMACS™ C tube (Miltenyi Biotech). A gentleMACS™ dissociator (Miltenyi Biotech) was used to homogenize the tissue further by running 2 cycles of one of the following programs: Protocol B; M_spleen; M_liver; or Program A. The cell suspension was strained over a 40 µm cell strainer

using the plunger from a 2.5 ml syringe and the cells were washed in complete media by centrifugation at 380 x g and 4°C for 5 minutes. The cells were resuspended in 5 ml complete media for counting.

Enzymatic and Mechanical Dissociation (Collagenase/DNAse based dissociation)

The palate was collected as described in **2.5.1** and digested with a modified protocol (Mizraji et al., 2013). Palatal tissue from a single mouse was minced using a no. 15 scalpel blade (Swann-Morton®, Sheffield, UK) in a 35 mm tissue culture dish containing 1 ml PBS + 2% FCS, 2mg/ml collagenase II (Lorne Laboratories, Berkshire, UK) and 1mg/ml DNase Type I. The minced gingival tissue and cells were transferred to a 15 ml centrifuge tube and the tissue culture dish was washed with 1 ml PBS + 2% FCS to collect remaining cells. The tubes were transferred to a shaking incubator (Innova™ 4400, New Brunswick™) for 30 minutes at 37°C and 200 rpm, with 0.5M EDTA added 10 minutes prior to the end of the incubation to stop the enzymatic reactions. The samples were removed from the incubator and topped up to 12ml with PBS + 2% FCS, then centrifuged at 400 x g for 8 minutes at 4°C. The supernatant was discarded and the pellet was resuspended in 2 ml of PBS + 2% FCS, then the cells were passed through a 70 µm strainer into a new 50 ml centrifuge tube to remove the remaining tissue. Strained cells were then centrifuged at 380 x g for 5 minutes and the supernatant was discarded. To allow for more accurate cell counting, the pellet was resuspended in 300 µl PBS + 2% FCS.

2.5.3 Cell counts

Ten µl of cells were mixed with 10 µl of 0.04% trypan blue and were counted using a haemocytometer (Naubeur improved, Marienfeld-Superior, Germany) and BH-2 light microscope (Olympus, UK). Dead cells were excluded by trypan blue staining of the cells (**figure 2.6**). The total cell count was calculated by: count x dilution factor x 10^4 x volume.

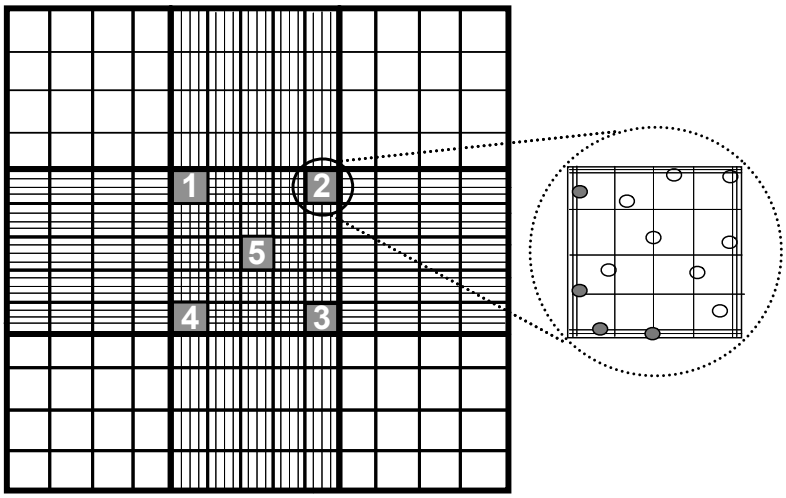

Figure 2.6. Cell counting using a haemocytometer.
Ten µl of cells mixed with an equal volume of trypan blue were pipetted onto a haemocytometer. The cells in all 25 boxes were counted for gingival tissue and LNs. For spleens only the 5 numbered boxes were counted. The zoomed in image of box 2 illustrates live (non-shaded) and dead cells (shaded) that have been stained with trypan blue and are therefore excluded from the cell count. Image generously donated by Ana Adrados-Planell.

2.6 T cell purification

2.6.1 Magnetic-activated cell sorting (MACS)

(i) Ficoll density gradient separation and positive selection with CD3ε Microbeads

A single cell suspension of dLNs and gingivae were prepared as described in **2.5** and were centrifuged at 400 x g for 5 minutes and the cell pellet was resuspended in 3 ml of room temperature PBS. The cells were then carefully layered over 3 ml of room temperature Histopaque® 1083 in a 15 ml centrifuge tube. The sample was centrifuged at 400 x g and room temperature for 30 minutes, with the brake off (**figure 2.7**). The mononuclear cell layer was carefully removed using a Pasteur pipette and transferred to a fresh 15 ml centrifuge tube. After 10 ml of incomplete media was added to the cells and the tube was inverted gently, several times, the tube was centrifuged at 250 x g for 10 minutes. The supernatant was removed and the pellet was resuspended in 0.5 ml of incomplete media, vortexed briefly and then an additional 4.5 ml of incomplete media was added, and mixed by inversion,

to wash away the remaining Histopaque®. The tube was centrifuged at 250 x g for 10 minutes and supernatant discarded. The wash step was repeated.

One hundred µl of MACS buffer (composed of PBS, 0.5% bovine serum albumin (BSA) and 2mM EDTA) was added to the cells, followed by the addition of 10 µl anti-mouse CD3ε-Biotin antibodies. This was incubated at 4°C for 10 minutes, followed by a wash with 1-2 ml of MACS buffer and centrifugation at 300 x g for 10 minutes. The supernatant was carefully pipetted off and the cell pellet was resuspended in 80 µl of MACS buffer, followed by 20 µl of Anti-Biotin MicroBeads. This was incubated at 4°C for 15 minutes then the cells were washed, as described above. An LD column (Miltenyi Biotech) was rinsed with 2 ml MACS buffer and placed in the magnetic field of a MACS™ separator (Miltenyi Biotech). The cells were resuspended in 500 µl MACS buffer and loaded onto the column. The unlabeled cells passed through, then the column was rinsed 3 times by adding 500 µl of MACS buffer. The column was removed from the magnetic separator and placed into a 15 ml centrifuge tube. One ml of MACS buffer was added to the column and the CD3+ T cells bound to the magnetic beads were immediately flushed out using the plunger supplied with the column. CD3+ T cells were then separated and ready for use in downstream applications.

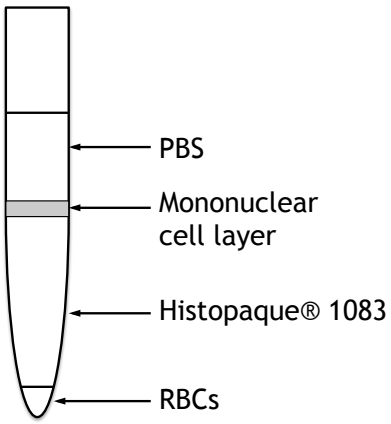

Figure 2.7. Cell layers following Histopaque® 1083 density gradient separation. To enable mononuclear cell separation, a single cell suspension of murine LN and gingival tissue was layered upon Histopaque® 1083. After centrifugation, distinct layers could be seen including PBS, mononuclear cells, Histopaque® 1083 and red blood cells (RBCs). The shaded mononuclear cell layer was aspirated for further analysis.

(ii) Dead Cell Removal and positive selection with CD90.2 MicroBeads

A single cell suspension of dLNs and gingivae were prepared as described in **2.5** and a maximum of 1 x 10^7 cells in complete media were centrifuged at 300 x g for 10 minutes. The supernatant was carefully and completely removed using a pipette and resuspended in 50 µl of MACS buffer. Five µl of Basic Microbeads (diluted 1 in 10 with MACS buffer) was added to the cells, mixed well and incubated at 4°C for 15 minutes. The Microbeads then bound to dead cells within the sample. The cells were washed with 1 ml of MACS buffer, followed by a centrifugation at 300 x g for 10 minutes. The supernatant was carefully removed with a pipette and the cells were resuspended in 500 µl of MACS buffer. An MS column (Miltenyi Biotech) was placed in the magnetic field of a MiniMACS™ separator (Miltenyi Biotech) and was prepared for separation by rinsing with 500 µl of MACS buffer. The cell suspension was added to the column, allowing unlabeled cells to pass through, and then the column was rinsed three times by adding 500 µl of MACS buffer. The unlabeled cells were collected.

The cells were washed, as above, at 300 x g for 10 minutes and the supernatant discarded. The pellet was resuspended in 90 µl of MACS buffer, followed by the addition of 10 µl CD90.2 MicroBeads (pan T cell marker). The cells were incubated at 4°C for 15 minutes then washed with 1-2 ml of MACS buffer. The pellet was resuspended in 500 µl of MACS buffer. An MS column was placed in the magnetic field of a MiniMACS™ separator and was prepared for separation by rinsing with 500 µl of MACS buffer. The cell suspension was added to the column, allowing unlabeled cells to pass through, and then the column was rinsed three times by adding 500 µl of MACS buffer. The column was then removed from the separator and placed into a 15 ml centrifuge tube. One ml of MACS buffer was added to the column and the CD90.2+ cells bound to the magnetic beads were immediately flushed out using the plunger supplied with the column. T cells were then separated and ready for use in downstream applications.

(iii) CD4 positive selection with MicroBeads

A single cell suspension of dLNs and gingivae were prepared as described in **2.5** and a maximum of 1 x 10^7 cells in complete media were centrifuged at 300 x g for 10 minutes. The supernatant was carefully and completely removed using a pipette and resuspended in 90 µl of MACS buffer. Ten µl of CD4 (L3T4) MicroBeads (Miltenyi Biotech) were added and mixed well, then incubated at 4^{o}C for 15 minutes. Anti-CD4 APC efluor 780 was added at a dilution of 1/400 to the sample and incubated at 4^{o}C for 5 minutes protected from light, as recommended by manufacturer's guide for flow cytometry analysis. Cells were washed with 1-2 ml of MACS buffer and centrifuged at 300 x g for 10 minutes. The supernatant was removed using a pipette and the pellet was resuspended in 500 µl of MACS buffer. An MS column was placed in the magnetic field of a MiniMACS™ separator and was prepared for separation by rinsing with 500 µl of MACS buffer. The cell suspension was added to the column, allowing unlabeled cells to pass through, and then the column was rinsed three times by adding 500 µl of MACS buffer. The column was then removed from the separator and placed into a 15 ml centrifuge tube. One ml of MACS buffer was added to the column and the CD4+ T cells bound to the magnetic beads were immediately flushed out using the plunger supplied with the column. CD4+ T cells were then separated and ready for use in downstream applications.

2.6.2 Fluorescence-activated cell sorting (FACS)

A single cell suspension of dLNs and gingivae were prepared and stained extracellularly for flow cytometry as described in **2.5** and **2.7.1**, respectively**.** The cells were stained with anti-CD45, anti-CD4, anti-CD8 antibodies and viability dye as described in **table 2.4**. The cells were passed through nitex prior to sorting using the BD FACSAria™ I or BD FACSAria™ III, depending on availability of the sorter. A 70 µm nozzle was used for sorting T cells and the set up was kindly conducted by Diane Vaughan (Flow Cytometry Facility Manager, University of Glasgow). Single, viable, CD45+ CD4+ and single, viable, CD45+ CD8+ T cells were sorted separately into 1.5 ml reaction tubes containing PBS or lysis buffer, depending on downstream analysis.

Table 2.4. Antibodies used for T cell sorting by FACS.

Antibody	Clone	Staining type	Final Dilution	Dilution Buffer	Supplier
CD45 FITC	30-F11	EC	1/200	FACS buffer	eBioscience
CD4 eFluor 780	RM4-5	EC	1/400	FACS buffer	eBioscience
CD8a PE	53-6.7	EC	1/200	FACS buffer	eBioscience
VD eFluor 450	-	EC	1/1000	PBS	eBioscience

Abbreviations: EC, extracellular; VD, viability dye.

2.7 Flow cytometry

2.7.1 Extracellular staining protocol

A single cell suspension of various tissue types was prepared as described in **2.5.** Cells were centrifuged at 400 x g for 5 minutes and resuspended in FcR blocking buffer (5% mouse serum in 2.4G2 hybridoma supernatant (containing monoclonal antibodies which block FcRs)) to give a concentration of approximately 1 x 10^6 cells/100 µl and this was incubated at 4^{o}C for 15 minutes. Extracellular antibodies were prepared in FACS buffer (composed of 0.01% NaN_3 and 2% HI-FCS in PBS) as shown in **table 2.5**, and 100 µl of the antibody preparation was incubated with 100 µl of cells in FcR blocking buffer for 20 minutes at 4^{o}C, protected from light. The cells were washed with 200 µl of PBS then centrifuged at 400 x g for 5 minutes at 4^{o}C. This step was repeated once more.

Viability dye was prepared as described in **table 2.5**. One hundred µl was added to 1 x 10^6 cells and incubated at 4^{o}C for 20 minutes, again protected from light. The cells were washed with 200 µl of PBS then centrifuged at 400 x g for 5 minutes at 4^{o}C. This step was repeated once more. Samples only having extracellular antibody staining were resuspended in 200 µl FACS buffer and passed through nitex nylon mesh prior to flow cytometry. Cells requiring intracellular staining were incubated with fix/perm buffer as described in **2.7.2**.

2.7.2 Intracellular staining

(i) Transcription factor staining

Intracellular staining for transcription factors was conducted using a Transcription Factor Buffer Set (BD Biosciences) following the manufacturer's guidelines. Briefly, cells were incubated with 100 µl of fix/perm at 4°C for 20 minutes in the dark. Cells were washed with 100 µl of perm/wash by centrifugation at 400 x g and 4°C for 5 minutes, the supernatant was discarded and the cells were washed again in 200 µl of perm/wash at the same centrifugation. The intracellular antibodies were prepared as described in **table 2.5** and 100 µl of the antibody preparation was added to 1 x 10^6 cells and incubated at 4°C for 50 minutes. The cells were washed with 100 µl of perm/wash by centrifugation at 400 x g and 4°C for 5 minutes, the supernatant was discarded and the cells were washed again in 200 µl of perm/wash at the same centrifugation. The cells were then resuspended in 200 µl of FACS buffer and passed through nitex nylon mesh prior to flow cytometry.

(ii) Cytokine staining

Intracellular staining for cytokines was conducted using a BD Cytofix/Cytoperm™ Plus Fixation and Permeabilisation kit (BD Biosciences) following the manufacturer's guidelines. Briefly, cells were incubated with 100 µl of BD Cytofix/Cytoperm™ at 4°C for 20 minutes in the dark. Cells were washed with 100 µl of BD Perm/Wash™ buffer by centrifugation at 400 x g and 4°C for 5 minutes, the supernatant was discarded and the cells were washed again in 200 µl of BD Perm/Wash™ buffer at the same centrifugation. The intracellular antibodies were prepared as described in **table 2.5**, and 100 µl of the antibody preparation was added to 1 x 10^6 cells and incubated at 4°C for 30 minutes. Cells were washed with 100 µl of BD Perm/Wash™ buffer by centrifugation at 400 x g and 4°C for 5 minutes, the supernatant was discarded and the cells were washed again in 200 µl of BD Perm/Wash™ buffer at the same centrifugation. The cells were then resuspended in 200 µl of FACS buffer and passed through nitex nylon mesh prior to flow cytometry.

2.7.3 Flow cytometry analysis

Cells were passed through nitex nylon mesh prior to flow cytometry using a MACSQuant® flow cytometer and were subsequently analysed using FlowJo® software (Tree Star Inc.).

Table 2.5. Antibodies used for flow cytometry staining.

Antibody	Clone	Staining type	Final Dilution	Dilution Buffer	Supplier
CD45 PerCP	30-F11	EC	1/200	FACS buffer	BD
CD4 eFluor 780	RM4-5	EC	1/400	FACS buffer	eBioscience
CD8a e450	53-6.7	EC	1/400	FACS buffer	eBioscience
CD8a PE-Cy7	53-6.7	EC	1/200	FACS buffer	eBioscience
CD44 APC	IM7	EC	1/400	FACS buffer	eBioscience
CD62L FITC	Mel-4	EC	1/200	FACS buffer	BD
CD69 PE	H1.2F3	EC	1/200	FACS buffer	BD
CD25 FITC	7D4	EC	1/200	FACS buffer	eBioscience
VD eFluor 450	N/A	EC	1/1000	PBS	eBioscience
VD eFluor 506	N/A	EC	1/1000	PBS	eBioscience
ICOS AF 88	C398.4A	EC	1/200	FACS buffer	BioLegend
PD-1 PE Cy7	J43	EC	1/400	FACS buffer	eBioscience
CXCR5 APC	2G8	EC	1/50	FACS buffer	BD
B220 eFluor 450	RA3-6B2	EC	1/400	FACS buffer	eBioscience
F4/80 eFluor 450	BM8	EC	1/400	FACS buffer	eBioscience
Ki67 PE-Cy7	SolA15	IC (1)	1/500	Perm/wash	eBioscience
Foxp3 APC	FJK-16s	IC (1)	1/200	Perm/wash	eBioscience
IFNγ PE-Cy7	B27	IC (2)	1/200	Perm/Wash	BioLegend
IL-4 biotin	BVD6-24G2	IC (2)	1/200	Perm/Wash	BD
IL-17A PE	TC11-18H10	IC (2)	1/200	Perm/Wash	BD
SA PerCP	N/A	IC (2)	1/200	Perm/Wash	BD
Bcl6 PE	K112-91	IC (2)	1/50	Perm/wash	BD

(1) – Transcription factor staining; (2) – cytokine staining
Abbreviations: AF, alexa fluor; EC, extracellular; IC, intracellular; N/A, not applicable; SA, streptavidin; TF, transcription factor; VD, viability dye.

2.8 Immunohistochemistry

2.8.1 Whole-mount staining for fluorescent microscopy

Palates were collected as described in **2.5.1** and fixed using 1% paraformaldehyde (PFA) in PBS overnight at 4°C. The tissue was then washed 3 times using whole-mount buffer (1% BSA, 0.3% Triton™ X-100, 0.2% NaN_3). For each wash, tissue was incubated at 4°C for 1 hour then the buffer was removed. The tissue was transferred to a 48-well plate and incubated overnight at 4°C with 300 µl of appropriate combinations of fluorescently labeled antibodies in whole-mount buffer (**table 2.6**). The tissues were then transferred to bijoux and washed by adding 4 ml cold PBS followed by an incubation at 4°C for 30 minutes. PBS was discarded and the wash step repeated another 2 times (3 washes total). The tissue was further washed by adding 4 ml whole-mount buffer to the bijoux and incubating at 4°C for one hour. Whole-mount buffer was discarded and the wash step repeated twice more (3 washes total). The samples were transferred into PBS for mounting. The tissue was blotted dry then placed onto a Superfrost™ Plus Microscope Slide (Thermo Fisher) with the inside of the palate facing up. ProLong® Gold Antifade Mountant (Thermo Fisher) was added to the tissue and a coverslip was placed on top carefully to avoid creating air bubbles. The coverslip was sealed using clear nail varnish. The samples were then incubated at room temperature for 24 hours to allow ProLong® Gold to cure. With thanks to Owain Millington at University of Strathclyde, the palates were imaged by confocal microscopy and analysed using Volocity™ software (Improvision, Perkin Elmer).

Table 2.6. Antibodies used for whole-mount staining and confocal microscopy.

Antibody	Clone	Final Dilution	Dilution Buffer	Supplier
CD4 AF 647	RM4-5	1/100	Whole-mount buffer	BD
B220 PE	RA3-6B2	1/100	Whole-mount buffer	eBioscience

Abbreviations: AF, alexa-fluor.

2.8.2 Haematoxylin and eosin staining

Palates were collected as described in **2.5.1** and were kindly processed by Jim Reilly and Shauna Kerr (Histology department, III, University of Glasgow). Palates were fixed in 10% formalin then embedded in paraffin. A Leica-LM microtome (Leica Microsystems, Germany) was used to cut 5 µm sections and these were placed onto Superfrost™ Ultra Plus Microscope Slides (Gerhard Menzel, Germany). Sections containing gingival tissue were heated at 60^{o}C for 35 minutes to soften the wax. In order to remove the paraffin and rehydrate the sections, the sections were immersed in xylene for 3 minutes. This step was repeated, as were all subsequent steps until water washing. The sections were immersed in 100% ethanol, then 90% ethanol and finally 70% ethanol, each for 3 minutes. The sections were immersed in running water for 3 minutes.

The sections were then stained by immersion in Harris haematoxylin for 2 minutes followed by washing in running water for 3 minutes. To reduce the background staining, the sections were dipped twice into 1% HCl in 70% ethanol, rinsed in running water then immersed in Scotts tap water substitute for 30 seconds. The sections were again rinsed in running water before counter staining with 1% eosin in tap water for 2 minutes. The excess stain was washed off by running water. The sections were dehydrated in 70% ethanol for 30 seconds, followed by 1 minute in 90% ethanol. The sections were then immersed in 100% ethanol for 3 minutes, transferred to fresh 100% ethanol for another 3 minutes before being immersed in xylene in for 3 minutes, followed by a final immersion in fresh xylene for another 3 minutes. The sections were mounted with DPX.

2.9 Measurement of bone loss

The maxilla was separated from the skull and gingiva removed as described in **2.5.1**. The remaining tissue on the maxilla was removed by enzymatic digestion with 100 U/ml DNase I, 4 mg/ml collagenase IV and 2 mg/ml hyaluronidase (from bovine testes) in PBS. Five hundred µl of the enzyme digestion mix was added to the maxillae of one mouse in a well of a 24-well plate. Plates were transferred to a

shaking incubator for 30 minutes at 37°C and 100 rpm. The enzymatic reaction was stopped by adding complete media and the teeth were washed using tap water after this step and all subsequent steps. The teeth were incubated at 4°C overnight with 3% H_2O_2, fixed with 4% PFA at 4°C overnight, then were stained with 0.5% methylene blue in dH_2O for 30 minutes at room temperature. The teeth were given a final wash with tap water and were left to air-dry. Images were captured using an Olympus SZX7 stereo zoom microscope fitted with SC100 digital colour camera. Measurements of the distance between the cemento-enamel junction and the alveolar bone crest were made using cellSens software (Olympus) to assess alveolar bone loss. Both the left and right maxillae were measured by taking 12 measurements from the 3 molars on the palatal side of the bone, resulting in a total of 24 measurements per mouse (**figure 2.8**). The mean of the 24 measurements was the final alveolar bone level for the mouse. All measurements were conducted with the examiner blinded to the experimental group of each maxilla.

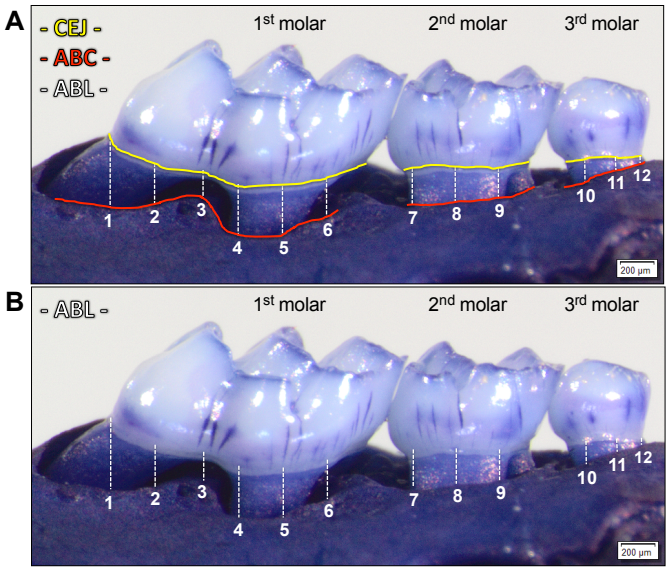

Figure 2.8. Measurement of alveolar bone loss in mice.
Maxillae from mice were excised, defleshed and stained for imaging. Images of the maxillae were captured using Olympus SZX7 stereo zoom microscope fitted with SC100 digital colour camera. (A) The assessment of alveolar bone loss was determined by applying 12 vertical measurements (white dashed lines) between the cemento-enamel junction (CEJ) (yellow line) and the alveolar bone crest (ABC) (red line) on the palatal side of the maxillae, using the cellSens software (Olympus). (B) The vertical measurements represent the alveolar bone loss.

2.10 Detection of antibodies by ELISA

2.10.1 Processing of murine blood

Murine blood was collected by tail bleeds (approximately 100 µl) prior to experiment end-points or at end-points by cardiac puncture (approximately 700 µl) under terminal anesthesia. Blood was transferred into 1.5 ml reaction tubes and allowed to clot by incubating at room temperature for a minimum of 2 hours. The reaction tubes were centrifuged at 12000 rpm in an Eppendorf™ microcentrifuge for 12 minutes and the supernatants (serum) transferred to fresh reaction tubes. Serum samples were then aliquoted and stored at -20 °C.

2.10.2 Anti-*P. gingivalis* ELISA

P. gingivalis W83 was grown as described in **2.2.1**. Aliquots of frozen heat-killed *P. gingivalis* were thawed at room temperature then resuspended at an OD of 0.02 at 600 nm (4 x 10^7 CFU/ml) in 0.5 M carbonate-bicarbonate buffer. Immulon 1B ELISA plates (Fisher Scientific) were coated with 100 µl/well *P. gingivalis* in carbonate-bicarbonate buffer and incubated overnight at 4°C. The plates were washed with 0.05% Tween-20 in PBS (PBS-T) 3 times after this step and all subsequent steps until the addition of TMB stop solution. The plates were blocked with 200 µl/well blocking buffer (10% HI-FCS in PBS) at 37°C for 1 hour. Serial dilutions of serum ranging from 1/50 to 1/400 were made using dilution buffer (0.2% HI-FCS in PBS-T) and 50 µl of each diluted sample was added to duplicate wells. Previously tested positive and negative serum samples were included in each plate, as well as a no-sample blank control. The plates were incubated for 2 hours at 37°C or overnight at 4°C. Fifty µl/well of the detection goat anti-mouse antibody conjugated to horseradish peroxidase (HRP) (**table 2.7**) was then added and incubated for 1 hour at 37°C before the reaction was visualized by the addition of 100 µl/well of TMB stop solution. The reaction was stopped using 50 µl/well of 10% HCl and the plate was read by a microplate absorbance reader at 450 nm with a reference wavelength of 630 nm.

2.10.3 Anti-OVA ELISA

One hundred µl of 20 µg/ml OVA protein in 0.5 M Carbonate-Bicarbonate buffer was added to a 96 well plate and incubated overnight at 4°C. The plates were washed with PBS-T 3 times after this step and all subsequent steps until the addition of TMB stop solution. The plates were blocked with 200 µl/well blocking buffer at 37°C for 1 hour. Serial dilutions of serum ranging from 1/100 to 1/6400 were made using dilution buffer and 50 µl of each diluted sample was added to duplicate wells. Previously tested positive and negative serum samples were included in each plate, as well as a no-sample blank control. The plates were incubated for 2 hours at 37°C or overnight at 4°C. Fifty µl/well of the detection goat anti-mouse (**table 2.7**) antibody was then added and incubated for 1 hour at 37°C before the reaction was visualized by the addition of 100 µl/well of TMB stop solution. The reaction was stopped using 50 µl/well of 10% HCl and the plate was read by a microplate absorbance reader at 450 nm with a reference wavelength of 630 nm.

Table 2.7. Detection antibodies used in anti-*P. gingivalis* and anti-OVA ELISAs.

Detection antibody	Dilution	Supplier
Anti-mouse IgG (HRP)	1/10000	Southern Biotech
Anti-mouse IgG1 (HRP)	1/10000	Southern Biotech
Anti-mouse IgG2a (HRP)	1/10000	Southern Biotech

Antibody concentrations were previously optimized by Ana Adrados Plannell.

2.10.4 Calculation of ELISA units (EU)

A mean blank-corrected value was obtained for each dilution of each serum sample by subtracting the mean OD of blank wells from the mean sample ODs. The y-intercept of the slope of the blank-corrected ODs from all serial dilutions was determined and this value was multiplied by 1000 to give ELISA units (EU), as previously described (Gmür et al., 1986).

2.11 Quantification of cytokines by ELISA and multiplex assay

2.11.1 Anti-IFN-γ ELISA

The concentration of IFN-γ from cell culture supernatants (described in **2.14.1**) was measured using IFN-γ ELISA Ready-SET-Go! Kit (eBioscience) following the manufacturer's guide. One hundred µl of diluted capture antibody in 1X Coating buffer was added to each well of a 96-well plate and incubated overnight at 4^{o}C. The plates were washed with PBS-T 3 times after this step and all subsequent steps until the addition of Avidin-HRP. The plates were blocked with 200 µl/well 1X ELISA diluent and incubated for 1 hour at room temperature. Standards were serially diluted two-fold and ranged from 15 pg/ml to 2000 pg/ml. Samples were diluted 1/2 with 1X ELISA diluent. One hundred µl/well of standards and samples were added and incubated for 2 hours at room temperature. Detection antibody was diluted in 1X ELISA diluent and incubated for 1 hour at room temperature. One hundred µl/well avidin-HRP was diluted in ELISA diluent and incubated for 30 minutes at room temperature. The plates were washed at least 5 times, followed by visualization by the addition of 100 µl/well TMB stop solution (KPL, Maryland, USA). The reaction was stopped using 50 µl/well of 10% HCl and the plate was read by a microplate absorbance reader (Sunrise™, Tecan) at 450 nm with a reference wavelength of 570 nm.

A mean blank-corrected value was obtained for each standard and sample by subtracting the mean OD of blank wells from the standard or sample ODs. The blank-corrected OD of each serially diluted standard was used to generate a standard curve, from which concentrations of IFN-γ in each cell culture supernatant were calculated.

2.11.2 Bio-Plex® Multiplex Immunoassay

The Bio-Plex® Multiplex Immunoassay was used to identify IL-6, IL-10, IL-13, IL-17A and IFN-γ from cell culture supernatants (described in **2.14.1**) and the protocol from the manufacturer's guide was followed. Standards provided in the kit were prepared by reconstitution with 500 µl of complete media. Standards were then

vortexed and incubated on ice for 30 minutes, and then serially diluted four-fold to have 8 standards containing known concentrations of the cytokines, the ranges of which are described in **table 2.8**. Cell culture supernatants were centrifuged at 1000 x g for 15 minutes at 4^{o}C to remove cellular debris. The beads for each cytokine in this assay are distinctly coloured by use of different ratios of two fluorescent dyes (red and infrared). The beads are then conjugated to anti-cytokine antibodies. The cytokine beads diluted to a 1X concentration in assay buffer were vortexed and 50 µl added to each well of the flat-bottom 96-well plate provided. The plate was then washed twice with 100 µl Bio-Plex® wash buffer using the Bio-Plex handheld magnetic washer, as were all subsequent wash steps. Fifty µl of vortexed diluted standards, blanks (complete media) and neat samples were transferred to wells of the 96-well plate. The plate was covered with sealing tape and aluminum foil to protect from light and was incubated on a shaker at 850 +/- 50 rpm for 30 minutes at room temperature. The plate was then washed 3 times with 100 µl wash buffer and 25 µl of 1X biotinylated detection antibodies added to each well. The plate was sealed and incubated on a shaker at 850 +/- 50 rpm overnight at 4 ^{o}C. After 3 washes with 100 µl wash buffer, 50 µl of 1X streptavidin-PE was added to each well and the plate sealed and incubated on a shaker at 850 +/- 50 rpm for 10 minutes at room temperature. The plate was then washed 3 times with 100 µl wash buffer and beads resuspended in 125 µl assay buffer. Prior to plate reading, the plate was shaken at 850 +/- 50 rpm for 30 seconds. The plate was read on a BIO-RAD Bio-Plex 100 at a low RP1 (PMT) setting. A mean blank-corrected value was obtained for each standard and sample by subtracting the mean fluorescence of blank wells from the standard and sample fluorescences. The blank-corrected fluorescence of each serially diluted standard was used to generate a standard curve for each cytokine, from which concentrations of cytokines in each cell culture supernatant were calculated.

Table 2.8. The concentration range of multiplex cytokine standards.

Cytokine	Highest standard concentration (pg/ml)	Lowest standard concentration (pg/ml)
IL-6	20,832	1.27
IL-10	19,679	1.20
IL-13	19,968	1.22
IL-17A	44,706	2.73
IFN-γ	13,205	0.81

2.12 Molecular Biology

2.12.1 RNA extraction

(i) Qiagen RNeasy® Micro kit

RNA extraction was performed using the Qiagen RNeasy® Micro kit (Qiagen, The Netherlands) following the manufacturer's guidelines. In brief, cells in a 1.5 ml reaction tube were centrifuged at 3000 x g for 5 minutes and the supernatant was discarded. To lyse the cells, the pellet was loosened and resuspended in 350 µl Buffer RLT. The sample and buffer were mixed by vortexing and the cells were homogenized by passing lysate 10 times through a 20-gauge needle attached to a 1 ml plastic syringe. Three hundred and fifty µl of 70% ethanol was added to the lysate and was mixed by pipetting. The sample was transferred to an RNeasy MinElute spin column placed in a 2 ml collection tube and was centrifuged at 8000 x g for 15 seconds. The flow-through was discarded and 350 µl Buffer RW1 was added to the spin column, and then it was centrifuged at 8000 x g for 15 seconds. To remove genomic DNA (gDNA), 80 µl of DNase I incubation mix (70 µl Buffer RDD and 10 µl DNase I stock solution) was added directly to the column membrane and was incubated at room temperature for 15 minutes. Three hundred and fifty µl of Buffer RW1 was added to the column and it was centrifuged at 8000 x g for 15 seconds and the collection tube and flow through were discarded. Five hundred µl Buffer RPE was added to the column, then placed in a new 2 ml collection tube, and was centrifuged at 8000 x g for 15 seconds. The flow through was discarded and 500 µl of 80% ethanol was added to the column. The column was centrifuged at 8000 x g for 2 minutes to wash the membrane then the collection tube and flow through were discarded. The column was placed onto a new 2 ml collection tube and with the lid opened to dry the column membrane it was centrifuged at full speed for 5 minutes. The collection tube and flow through were discarded and the column was placed on a new 1.5 ml collection tube. Fourteen µl of RNase-free water was added to the column membrane and the column was centrifuged at full speed for 1 minute to elute the RNA. RNA samples were stored at -80^{o}C until required.

(ii) RNAqueous-Micro® total RNA Isolation kit

RNA extraction was performed using RNAqueous-Micro® total RNA Isolation kit (Thermo Fisher) following the manufacturer's guidelines. In brief, cells in a 1.5 ml PCR tube were centrifuged at 3000 x g for 5 minutes and the supernatant was discarded. One hundred µl of Lysis Solution was added to the cells and vortexed vigorously. Fifty µl of 100% ethanol was added to the sample, followed by a brief vortex. The lysate/ethanol mixture was loaded onto a Micro Filter Cartridge Assembly and centrifuged at full speed for 10 seconds to allow the RNA to bind to the filter. One hundred and eighty µl of Wash Solution 1 was added to the Micro Filter Cartridge Assembly then centrifuged at 16000 x g for 10 seconds. One hundred and eighty µl of Wash Solution 2/3 was added to the Micro Filter Cartridge Assembly then centrifuged at 16000 x g for 10 seconds. This step was repeated and the flow-through was discarded. To dry the filter, the filter cartridge was centrifuged at full speed for 1 minute and the filter cartridge was placed in a new 1.5 ml collection tube. Five µl of prehreated (75^{o}C) Elution Solution was added directly to the membrane of the filter cartridge and incubated at room temperature for 1 minute. The filter cartridge was centrifuged at full speed for 30 seconds to elute the RNA. A second 5 µl of Elution Solution was added to the membrane and all subsequent steps were repeated. To remove gDNA, 1 µl of 10X DNase I Buffer and 1 µl of DNase I was added to the sample and mixed, then incubated at 37^{o}C for 20 minutes. Two µl of DNase Inactivation Reagent was added to the sample and was incubated at room temperature for 2 minutes, vortexing once during the incubation. The tube was centrifuged at full speed for 1.5 minutes to pellet the DNase Inactivation Reagent and the supernatant (containing RNA) was transferred to a fresh RNase free 0.5 ml PCR tube. RNA samples were stored at -80^{o}C until required.

(iii) Arcturus® PicoPure™ RNA Isolation kit

RNA extraction was performed following the manufacturer's guidelines. In brief, for trial experiments, cells in a 1.5 ml PCR tube were pelleted by centrifugation at 3000 x g for 5 minutes and the supernatant was discarded. The cell pellet was resuspended in 100 µl of Extraction Buffer and mixed by pipetting. For T cell sorting

for RNA-sequencing, cells were sorted into 1.5 ml PCR tubes containing 100 µl of Extraction Buffer. The cell/Extraction Buffer mix was incubated at 42^{o}C for 30 minutes followed by a centrifugation at 3000 x g for 2 minutes. The supernatant containing the RNA was transferred to a fresh 1.5 ml PCR and an equal volume of 70% ethanol was added and was mixed by pipetting. The cell extract/ethanol mixture was added to a column pre-conditioned with Conditioning Buffer. RNA was bound to the column by centrifugation at 100 x g for 2 minutes, followed by a centrifugation at 16000 x g for 30 seconds to remove the flow through. One hundred µl Wash Buffer 1 was added to the column and was centrifuged at 8000 x g for 1 minute. Genomic DNA was then removed from the column by mixing 5 µl of DNase I Stock Solution (Qiagen) to 35 µl Buffer RDD (Qiagen) (not supplied with RNA extraction kit) and adding the total 40 µl directly to the purification column. The DNase mix was incubated on the column at room temperature for 15 minutes. Forty µl of Wash Buffer 1 was added to the column containing the DNase mix and the column was centrifuged at 8000 x g for 15 seconds. One hundred µl of Wash Buffer 2 was added to column and centrifuged at 8000 x g for 1 minute. This step was repeated with the centrifugation being increased to 16000 x g for 2 minutes. The column was transferred to a new 0.5 ml PCR tube and 11 µl of Elution Buffer was pipetted directly onto the membrane of the column. The column was incubated for 1 minute at room temperature then centrifuged at 1000 x g for 1 minute to ensure the Elution Buffer was distributed across the membrane, followed by a centrifugation at 16000 x g for 1 minute to elute the RNA. RNA samples were stored at -80^{o}C until required.

(iv) Cells-to-CT™ kit

For RNA-sequencing verification experiments, CD4+ T cells were.sorted from cell isolates of 5 pooled gingivae or dLNs. Owing to the low numbers of CD4+ T cells sorted from gingivae (approximately 1 x 10^4), the Cells-to-C_T™ Kit (Thermo Fisher) was used and protocol from the manufacturer's guide followed. Cells-to-C_T™ enables reverse transcription of lysates from 10 to 1 x 10^5 cells, without the typical initial RNA purification step that can result in loss of RNA from small samples. Sorted cells were transferred to a 96-well plate and resuspended in 50 µl of cold PBS, then washed by centrifugation at 400 x g for 3 minutes. DNase I was diluted in

Lysis Solution at 1/100 to remove gDNA. Fifty µl of Lysis Solution was added to each sample and mixed by pipetting up and down 5 times. After the lysis reaction was incubated for 5 minutes, 5 µl Stop Solution was added and mixed by pipetting 5 times, followed by a 2 minute incubation. Ten 10 µl of lysate was added to 40 µl of master mix containing 25 µl 2X RT Buffer, 2.5 µl 20X RT Enzyme Mix and 12.5 µl of nuclease-free water in a 0.2 ml PCR tube on ice. The PCR tubes were briefly centrifuged to ensure that all contents were collected at the bottom, and then were loaded into an Applied Biosystems Veriti thermal cycler (Thermo Fisher) and the program described in **table 2.9** was run. The quantitative RT-PCR was conducted as described in **2.11.4**.

Table 2.9. Thermal cycling program for reverse transcription using Cells-to-C_T™ kit.

Stage	No. of cycles	Temperature (°C)	Time (minutes:seconds)
1	1	37	60:00
2	1	95	05:00
3	1	4	Infinity

2.12.2 Assessment of RNA quality and concentration

(i) Nanodrop

The concentration and quality of isolated RNA was evaluated by measuring the absorbance of 1.5 µl sample at 230 nm, 260 nm, 280 nm and 340 nm with a Nanodrop1000 spectrophotometer (Thermo Fisher). The absorbance at 230 corresponds with organic compounds including phenol and also peptide bonds in proteins. The absorbance at 260 nm corresponds with the peak absorption of nucleic acid, and at 280 nm with proteins and phenol. The absorbance at 340 nm establishes a baseline close to zero for the spectrum normalization. The Beer-Lambert Law was used to determine the concentration of RNA in each sample: RNA concentration (ng/µl) = (Abs_{260} – Abs_{340}) x 40.

The ratio of absorbance at 260/280 indicates the purity of the RNA sample, with a desirable ratio being approximately 2.0. As a second measure of purity, the ratio of absorbance at 260/230 should range between approximately 2.0 and 2.2.

(ii) Bioanalyzer

As a more sensitive means of RNA concentration and quality determination, the Agilent RNA 6000 Pico Kit was used along with the Agilent 2100 Bioanalyzer instrument (Agilent, Cheshire, UK). The detection range of RNA concentrations was between 200 and 5000 pg/µl. Each RNA chip contained an interconnected set of microchannels that were used for separation of nucleic acid fragments based on size during electrophoresis. The protocol as described in manufacturer's guide was followed. First, the chip priming station was set up by replacing the old syringe with the new one provided in the kit and the base plate was adjusted to position C. The ladder was briefly centrifuged and transferred to a PCR tube, and then heat denatured for 2 minutes at 70^{o}C on a heat block and immediately cooled on ice. After the addition of 90 µl RNase-free water, the prepared ladders were aliquoted and stored at -70^{o}C. All reagents were equilibrated to room temperature before subsequent steps were conducted. Five hundred and fifty µl of RNA gel matrix was transferred to a spin column and centrifuged at 1500 x g for 10 minutes at room temperature, and then 65 µl aliquots stored in 0.2 ml PCR tubes at 4^{o}C for a maximum of 4 weeks. The gel-dye mix was then prepared by vortexing the RNA dye concentrate for 10 seconds and briefly centrifuging to bring all contents to the bottom of the tube. To a 65 µl aliquot of gel, 1 µl of dye was added, gel-dye mix was then vortexed and centrifuged at 13000 x g for 10 minutes at room temperature. The prepared gel-dye mix was used within 1 day. To prepare the RNA chip for assessment by the Bioanalyzer, 9 µl of gel-dye mix was loaded into the appropriate marked well of the chip positioned in the chip priming station. The plunger of the syringe was adjusted to 1 ml position and the chip priming station was closed. The plunger was pressed down until held by the clip and after 30 seconds the clip was released. After 5 seconds, the plunger was pulled back up to the 1 ml position. The chip priming station was then opened and 9 µl of gel-dye mix added to remaining marked wells. Nine µl and 5 µl of RNA conditioning solution and RNA marker, respectively, were added to appropriate wells. One µl of heat-

denatured ladder was added to the appropriate well, followed by the addition of 1 µl of each sample (maximum 11 per chip) to appropriate sample wells of the chip. Samples were previously heat denatured at 70°C on a heat block for 2 minutes and cooled on ice. The chip was then vortexed at 2400 rpm for 1 minute on the IKA vortexer and immediately run on the bioanalyzer. Thanks go to Dr Donna Nile (Beatson Institute, Glasgow) for providing advice and access to equipment.

2.12.3 Reverse Transcription

Reverse transcription of RNA to cDNA was carried out using the Applied Biosystems High Capacity cDNA Reverse Transcription Kit (Thermo Fisher). Into 0.2 ml PCR tubes, 5 µl of RNA template was added (as the amount of extracted RNA from different RNA extraction kits was being compared), along with 5 µl of nuclease-free H_2O and 10 µl of master mix from the reverse transcription kit. This master mix contained manufacturer optimised concentrations of $MgCl_2$, along with deoxynucleotide triphosphates (dNTPs), random primers and MultiScribe™ reverse transcriptase enzyme (RT). A negative RT control was also included, whereby RT was excluded and instead replaced with an equal volume of nuclease-free H_2O to determine the presence of contaminating gDNA. The PCR tubes were briefly centrifuged to ensure that all contents were collected at the bottom then were loaded into a thermal cycler and the program described in table **2.10** was run.

Table 2.10. Thermal cycling program for reverse transcription using High Capacity cDNA Reverse Transcription Kit.

Stage	No. of Cycles	Temperature (°C)	Time (minutes:seconds)
1	1	25	10:00
2	1	37	120:00
3	1	85	05:00
4	1	4	Infinity

2.12.4 Quantitative RT-PCR

Quantitative RT-PCR (qRT-PCR) was carried out using Taqman® reagents (Thermo Fisher) and reactions were prepared in MicroAmp® 96-well reaction plates (Thermo Fisher). Each reaction consisted of between 1-100 ng of cDNA in a volume of 0.5-9 µl, 1 µl Taqman® Primer Probe Assay Mix, 10 µl Taqman® Fast Universal PCR Master Mix and a volume of nuclease-free H_2O to make the reaction volume 20 µl. The 96-well plate was then sealed shut and briefly centrifuged to bring all components to the bottom of the wells. The plate was placed in an Applied Biosystems 7500 Fast Real-Time PCR System (Thermo Fisher), and a thermal cycling program was conducted as described in **table 2.11**. The threshold cycle (C_T) for each well was calculated using the Real-Time PCR System software and expression relative to housekeeping gene calculated in excel.

Table 2.11. Thermal cycling program for qRT-PCR amplification of cDNA using 7500 Fast Real-Time PCR system.

Stage	No. of Cycles	Temperature (^oC)	Time (minutes:seconds)
1	1	95	0:20
2	40	95	0:03
		60	0:30

2.12.5 RT^2 Profiler PCR Array

Cells were isolated from single gingiva and dLNs of a single mouse as described in **2.5.2.** RNA was extracted using the Arcturus® PicoPure™ RNA Isolation kit. A cytokine and chemokine RT^2 profiler PCR Array (Qiagen) was used to assess RNA isolated from gingivae and dLNs of mice sham and *P. gingivalis*-infected. The protocol was followed as described in the manufacturer's guide. Each sample was diluted to 400 ng of RNA in 8 µl using RNase-free H_2O (recommended by manufacturer), to which 2 µl of Buffer GE was added for gDNA elimination. The RNA-gDNA elimination mixture was mixed gently by pipetting up and down, then centrifuged briefly. The RNA-gDNA elimination mixture was incubated at 42^{o}C for 5

minutes, then immediately placed on ice for at least 1 minute. The reverse-transcription mix was prepared as described in **table 2.12** and 10 µl added to 10 µl RNA-gDNA elimination mixture. The mixture was then mixed gently by pipetting and incubated at 42^{o}C for 15 minutes. To stop the reaction, mixtures were immediately incubated at 95^{o}C for 5 minutes. Ninety-one µl of RNase-free H_2O was added to each sample and mixed. The PCR component mix was prepared as described in **table 2.13** for each sample. Ten µl of PCR component mix was added into the appropriate wells of the 384 well array plate that already contained forward and reverse primers of the genes of interest. The plate was sealed with an optical adhesive film and centrifuged at 1000 x g for 1 minute at room temperature to bring contents to the bottom of the plate and remove bubbles. The plate was placed in an Applied Biosystems 7900HT Fast Real-Time PCR System (Thermo Fisher), and a thermal cycling program was conducted as described in **table 2.14**. The C_T for each well was calculated using the Real-Time PCR System software and expression relative to housekeeping gene calculated in excel.

Table 2.12. Reverse-transcription mix per reaction.

Reverse-transcription component	Volume (µl)	Total Volume (µl)
5X Buffer BC3	4	10
Control P2	1	
RE3 Reverse transcriptase mix	2	
RNase-free H_2O	3	

Table 2.13. PCR component mix for each sample (for use in 384 well plate - 4 x 96 well format).

PCR component	Volume (µl)	Total Volume (µl)
2X RT^2 SYBR Green Mastermix	650	1300
cDNA synthesis reaction	102	
RNase free H_2O	548	

Table 2.14. Thermal cycling program for qRT-PCR amplification of cDNA using 7900HT Fast Real-Time PCR system.

Stage	No. of Cycles	Temperature (°C)	Time (minutes:seconds)
1	1	95	10:00
2	40	95	00:15
		60	01:00

2.12.6 Pre-amplification of RNA

Clonetech SMART-Seq® v4 Ultra® Low Input RNA kit for sequencing (Takara Bio, Saint-Germain-en-Laye, France) was used to pre-amplify the RNA isolated from CD4+ T cells for RNA-sequencing. The amplification was performed following the manufacturer's guidelines. The components of all buffers required for pre-amplification are described in **table 2.15.** In brief, 1–9.5 µl RNA (**table 2.16**) was added to a 0.5 ml RNase free PCR tube. The volume was then increased to 9.5 µl with the addition of nuclease-free H_2O and 1 µl of 10X Reaction Buffer was added. Whilst the samples were on ice, 2 µl of 3' SMART-Seq CDS Primer II A (12 µM) was added. The samples were incubated for 3 minutes in a thermal cycler at 72°C, followed by an incubation on ice for 2 minutes. The thermal cycler was pre-heated to 42°C and 7.5 µl master mix was added to the samples. The samples and master mix were mixed by gentle pipetting then were briefly centrifuged to ensure the contents were collected at the bottom of the PCR tubes. The samples were placed in a thermal cycler and the program described in **table 2.17** was run for first strand cDNA synthesis. For cDNA amplification by long distance PCR, 30 µl of PCR mastermix was added to 20 µl of first-strand cDNA product and mixed well. Again the samples were centrifuged to ensure the contents were collected at the bottom of the PCR tubes. The samples were placed in a thermal cycler and the program described in **table 2.18** was run. The samples were shipped on dry ice to Source BioScience for all downstream steps of the SMART-Seq® v4 Ultra® Low Input RNA kit: purification of amplified cDNA using the Agencourt AMPure XP kit; validation using the Agilent 2100 BioAnalyzer and Illumina library preparation using Nextera DNA library preparation kits.

Table 2.15. Components of buffers required for pre-amplification.

Buffer	Components	Volume (µl)	Total volume (µl)*
10X Reaction Buffer	10X lysis buffer	19	20
	RNase Inhibitor	1	
First Strand cDNA Synthesis Master Mix	5X Ultra Low First-Strand Buffer	4	5.5
	SMART-Seq v4 Oligonucleotide (48 µM)	1	
	RNase Inhibitor (40 U/µl)	0.5	
PCR Master Mix	2X SeqAmp PCR Buffer	25	30
	PCR Primer II A (12 µM)	1	
	SeqAmp DNA Polymerase	1	
	Nuclease-Free H_2O	3	

*Volume per reaction.

Table 2.16. Concentration of RNA used for pre-amplification.

Experimental Repeat	Sample	RNA for pre-amplification (ng)	Volume of RNA (µl)*	Volume of H_2O
1	CMC LN	10	5	4.5
	PG LN	10	5	4.5
	CMC G	10	6.9	2.6
	PG G	5.814	9.5	0
2	CMC LN	10	5	4.5
	PG LN	10	5	4.5
	CMC G	7.825	9.5	0
	PG G	10	9.5	0
3	CMC LN	10	5	4.5
	PG LN	10	5	4.5
	CMC G	8.313	9.5	0
	PG G	6.873	9.5	0

*RNA from LN samples were previously diluted in H_2O.
Abbreviations: CMC, carboxymethylcellulose; PG, *P. gingivalis*-infected; LN, lymph node; G, gingivae.

Table 2.17. Thermal cycling program for first strand cDNA synthesis.

Stage	No. of Cycles	Temperature (°C)	Time (minutes:seconds)
1	1	42	90:00
2	1	70	10:00
3	1	4	Infinity

Table 2.18. Thermal cycling program for cDNA amplification.

Stage	No. of Cycles	Temperature (°C)	Time (minutes:seconds)
1	1	95	1:00
2	10	98	0:10
		65	0:30
		68	3:00
3	1	72	10:00
4	1	4	Infinity

2.12.7 RNA-sequencing

RNA-sequencing workflow is shown in **figure 2.9**. RNA-sequencing was conducted by Source BioScience on the Illumina NextSeq 500 v2 platform using one High-Output flow cell (12 indexes per flow cell) at 75bp paired-end. RNA-sequencing analysis was conducted by a bioinformatician at Source BioScience and included five steps: adaptor and quality trimming of data using Skewer (version 0.1.12); spliced mapping of trimmed reads based on a Mus Musculus reference genome (UCSC (mm10)) using HISAT (version 0.1.6); gene-wise read counting based on reference genome using DESeq2; calculation of differential gene expression between groups using DESeq2; and gene-set enrichment analysis using fold changes obtained from sample comparisons in previous step.

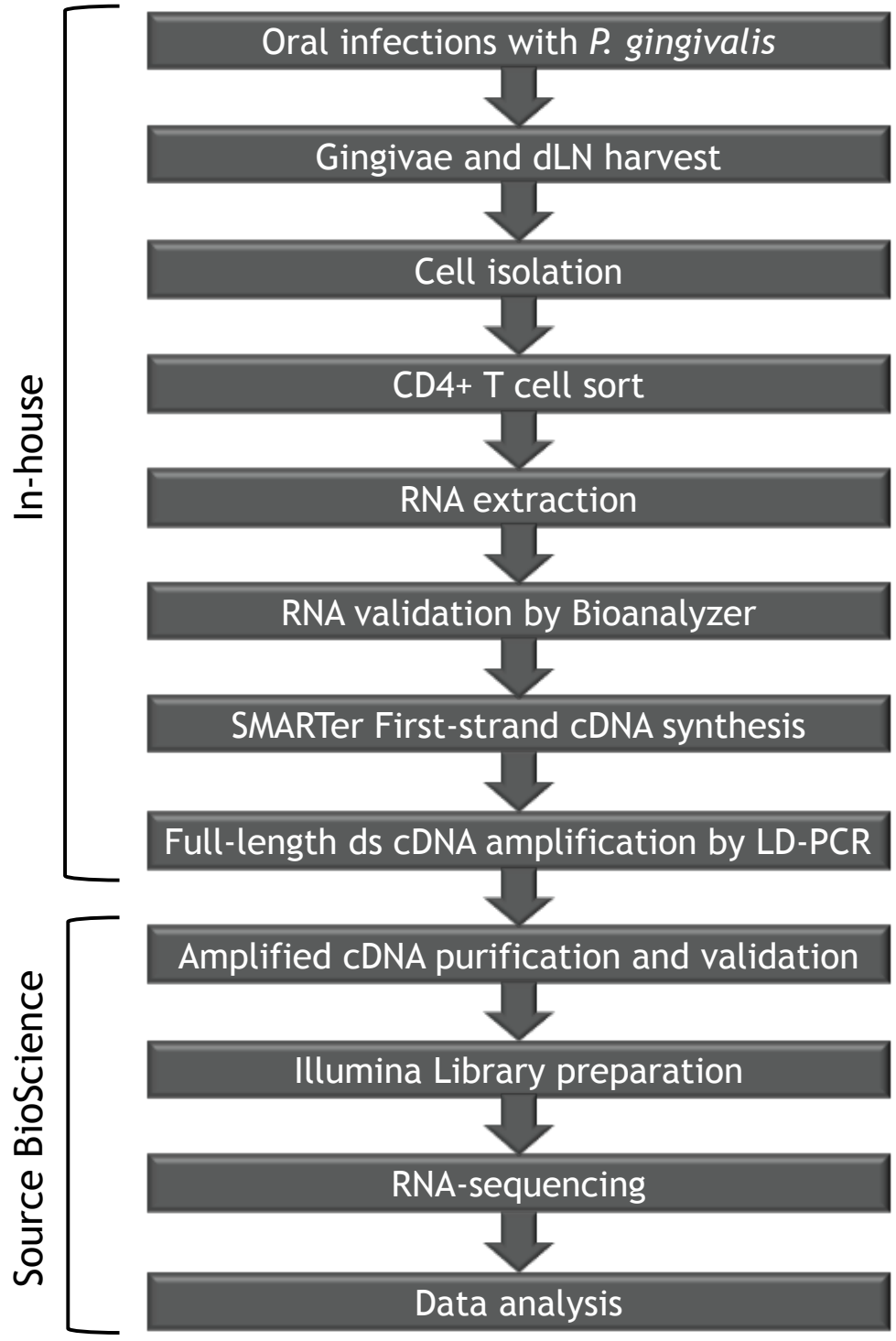

Figure 2.9. Work flow of RNA-sequencing.
The steps required for RNA-sequencing, from oral infections of mice to end point data analysis. The location in which each step was conducted is described on the left. Abbreviations: dLN, draining lymph node; ds, double-stranded; LD PCR, long distance polymerase chain reaction; *P. gingivalis*, *Porphyromonas gingivalis*.

2.12.8 Bacterial DNA extraction from oral swabs and PCR

Oral swabs were taken from mice at the end point of the murine models of PD, as described in **2.4.1**. The swabs were placed into the container with 1 ml of liquid amies transport medium and vortexed to ensure the release of bacteria from the swab. The transport medium and any bacteria were then transferred to 1.5 ml PCR tubes and stored long term at -80^{o}C. Bacterial DNA was isolated using the MasterPure™ Gram Positive DNA Purification Kit (Epicentre, Wisconsin, USA), following the manufacturer's guidelines with a few modifications. In brief, the bacteria were pelleted by centrifugation at full speed for 10 minutes in a microfuge and the supernatant was discarded. One hundred and fifty µl of TE buffer was added and the bacterial pellet was resuspended by vortexing. One µl of Ready-Lyse Lysosyme was added, followed by an incubation at 37^{o}C for 2 hours. One µl of Proteinase K (50 µg/µl) was mixed with 150 µl of Gram positive Lysis Solution and added to the sample, and this was incubated at 70^{o}C for 15 minutes, vortexing the sample every 5 minutes. After cooling the samples to 37^{o}C, they were placed on ice for 5 minutes. One hundred and seventy five µl of MPC Protein Precipitation Reagent was added to the sample and was mixed vigorously for 10 seconds. The samples were centrifuged at full speed for 10 minutes at 4^{o}C and the supernatants were transferred to fresh 1.5 ml PCR tubes, avoiding pick up of pelleted debris. One µl of RNase A (5 µg/µl) was added to the samples and incubated at 37^{o}C for 30 minutes. Next, 500 µl of isopropanol was added and this was mixed with the sample by inverting approximately 40 times. The DNA was pelleted by centrifugation at full speed for 10 minutes and the supernatant was discarded, followed by rinsing of the pellet with 200 µl of 70% ethanol. DNA from each sample was resuspended in 35 µl TE buffer.

One µl of extracted DNA was added to a PCR mixture composed of 10 µl SYBR® Select Master Mix (Thermo Fisher), 7 µl nuclease-free H_2O, 1 µl forward primers and 1 µl reverse primers (giving a final concentration of 10 µM) (**table 2.19**). The primers were supplied by Integrated DNA technologies (Leuven, Belgium). The reaction mixture was prepared in a MicroAmp® 96-well plate, sealed shut and briefly centrifuged to bring all components to the bottom of the wells. The plate

was placed in an Applied Biosystems 7500 Fast Real-Time PCR System, and a thermal cycling program was conducted as described in **table 2.20**.

Table 2.19. DNA primers used for identification of bacteria found in the oral cavity of *P. gingivalis*-infected mice.

Primer	Sequence (5'-3')	Reference
P. gingivalis rpoB	Forward: GGA AGA GAA GAC CGT AGC ACA AGG A Reverse: GAG TAG GCG AAA CGT CCA TCA GGT C	(Park et al., 2011)
Universal 16S	Forward: ACT CCT ACG GGA GGC AGC AGT Reverse: TAT TAC CGC GGC TGC TGG C	(Matsuda et al., 2011)

Abbreviations: *rpoB*, RNA polymerase ß-subunit gene.

Table 2.20. Thermal cycling program for PCR amplification of DNA from bacteria found in the oral cavity of *P. gingivalis*-infected mice.

Step	No. of cycles	Temperature (^{o}C)	Time (minutes:seconds)
1	1	50	2:00
2	1	95	2:00
3	40	95	0:15
		60	1:00

2.13 Assessment of RgpbOVA-A OVA expression by western blot

2.13.1 Isolation of bacterial protein

P. gingivalis W83 and OVA-expressing *P. gingivalis* were cultured as described in **2.2**, for 24 hours. In 1.5 ml reaction tubes, 1.5 ml of the cultures were centrifuged at full speed for 10 minutes. The supernatant was discarded and the pellets from 2 reaction tubes were pooled (i.e. a pellet from 3 ml of culture) then frozen at -80^{o}C overnight, or until required. Upon thawing, the bacterial pellets were resuspended in 250 µl bacterial lysis buffer (composed of 50 mM Tris, 10% glycerol, 0.1% Triton

X-100, 100 µl/ml lysozyme, 1 miniTab protease inhibitor, 3 units DNase and 2 mM $MgCl_2$ in dH_2O) and were then incubated at 15 minutes on a heat-block at 30°C. After transferring the samples to ice for another 15 minute incubation, the samples were sonicated 3 times, each for 20 seconds with a 10 second rest using a Soniprep 150 (MSE, London, UK). The samples were centrifuged at full speed and 4°C for 20 minutes and the supernatants were collected and transferred to fresh 1.5 ml reaction tubes.

To ensure that the same amount of protein was used for western blotting, a Bradford Assay was conducted to determine the concentration of protein in the lysed bacterial samples, relative to a control. Protein Assay Dye Reagent Concentrate was diluted 1/5 with dH_2O and was filtered using a sterile filter. Five dilutions of BSA were made in dH_2O, to give a standard curve ranging from 0.5 mg/ml to 0.05 mg/ml. Ten µl of standards and samples were added to separate wells of a 96 well plate in triplicate, followed by the addition of 200 µl of diluted dye reagent. The samples and dye were mixed by repeated aspiration and dispersion using a pipette and the plate was incubated at room temperature for at least 5 minutes, but no longer than 1 hour. The plate was read by a microplate absorbance reader at 595 nm. The OD of each serially diluted standard was used to generate a standard curve for BSA, from which concentrations of bacterial protein in each cell culture supernatant were calculated. The mean concentration from 'blank' wells (which were not incubated with protein samples but otherwise treated the same as the other wells) was subtracted from the concentration of all other wells to give the final concentration.

2.13.2 Western blot

Samples were diluted in dH_2O to give a final concentration of 20 µg in 32 µl and positive control samples OVA peptide (0.5 µg and 0.1 µg) or OVA protein (10 µg, 5 µg and 1 µg) were diluted in dH_2O to give a final volume of 32 µl. Eight µl of 5X sodium dodecyl sulfate (SDS) loading buffer was added to each sample to give a total loading volume of 40 µl. SDS loading buffer was composed of 5% ß-mercaptoethanol, 0.02% bromophenol blue, 30% glycerol, 10% SDS and 250mM Tris-

Cl (pH 6.8). Two 18% Ready Gel® Tris-HCl gels were placed into the modules of a Mini-PROTEAN® electrophoresis Tetra system and 1X TGS buffer was added to the cell up to the fill line of the tank. The samples and 10 µl of neat Precision Plus Protein Dual Xtra Standards were loaded into the wells of the gel and electrophoresis was conducted by setting the voltage to 120V for around 1 hour (or until the bands of the standards had separated appropriately).

The proteins from the gel were then transferred to nitrocellulose membranes using the Mini Trans-Blot® Electrophoretic Transfer Cell following the manufacturer's instructions. In brief, the gel sandwich was prepared by placing the cassette grey side down, then one fibre pad pre-wetted in 1X TG buffer was placed on. Pre-wetted filter paper was then placed on top, following the addition of the gel and another piece of pre-wetted filter paper. To ensure the removal of bubbles, a 50 ml centrifuge tube was carefully rolled over the sandwich and the other fibre pad was placed on top of the filter and the cassette was closed. The cassette was placed in the module and together with a frozen blue cooling unit, was placed in the tank of the Tetra system. The voltage was set to 100 V and was run for 1 hour.

The nitrocellulose membrane was blocked in 5% milk in PBS-T for 1 hour then blocking buffer was removed and the primary antibody added and incubated at 4^{o}C on a shaker overnight. The membrane was washed with PBS-T on a shaker at room temperature for 10 minutes. Fresh PBS-T was added and the process was repeated 3 times. The secondary antibody was added and incubated on a shaker at room temperature for 1 hour. Antibodies used in western blots are described in **table 2.21** and were diluted in PBS-T. The membrane was washed with PBS-T as previously described. The membrane was placed onto cling film and bands of the ladder marked with a chemiluminescent pen. Equal parts of WesternBright™ Sirius™ luminol/enhancer solution (Advansta, California, USA) and WesternBright™ peroxide chemiluminescent detection reagent (Advansta) were mixed and poured over the membrane and the reaction was developed for 2 minutes. The membrane was placed in a development machine (LI-COR®, Cambridge, UK) to visualize the western blot images.

Table 2.21. Antibodies used for western blots.

Primary antibody	Dilution	Secondary antibody	Dilution	Supplier
Anti-GroEL	1/1000	Goat anti-rabbit IgG (HRP)	1/50000	Both - Abcam (Cambridge, UK)
Anti-OVA 323-339	1/1000	Goat anti-rabbit IgG (HRP)	1/50000	Primary – Innovagen (Lund, Sweden) Secondary – Abcam (Cambridge, UK)

2.14 *In vitro* cell culture assays

2.14.1 Restimulation of splenocytes with *P. gingivalis*

A single cell suspension of splenocytes was obtained as described in **2.5.2** and 2 x 10^5 cells in 200 µl of complete media were added into each well of a round bottom 96-well plate. *P. gingivalis* W83 was cultured and heat-killed as described in **2.2.3** and 50 CFU/cell were added to the wells. The cells were stimulated separately with 0.5 µg/ml anti-CD28 antibody in wells pre-coated overnight at 4°C with 1 µg/ml anti-CD3 antibody in PBS as a positive control or complete media only as a negative control. After 72 hours of incubation at 37°C with 5% CO_2, the plate was centrifuged at 400 x g for 3 minutes and the supernatants transferred to a fresh 96-well plate. The cells were stained with anti-CD45, anti-CD4, anti-CD8, anti-Ki67 and viability dye to assess the proliferation of T cells by flow cytometry (described in **2.7**).

2.14.2 Stimulation of OVA-specific T cells with RgpbOVA-A

A single cell suspension of splenocytes and cervical LN cells from DO11.10 4GET mice were obtained as described in **2.5.2**. As a source of APCs, 2 x 10^5 splenocytes in 100 µl complete media were added to the wells of a round bottom 96-well plate and incubated at 37°C with 5% CO_2 for 2 hours. The non-adherent cells in the supernatant were removed, leaving the adherent, APCs in the wells. One hundred µl OVA protein (1 mg/ml), 1 x 10^7 CFU *P. gingivalis* W83, 1 x 10^7 CFU *P. gingivalis* W83

with OVA protein (1 mg/ml), 1 x 10^7 CFU RgpbOVA-A, anti-CD3 antibody or media were added to the wells and incubated with APCs at 37°C with 5% CO_2 for 20 minutes. *P. gingivalis* W83 and RgpbOVA-A used in this assay were cultured and heat-killed as described in **2.2.3**. To the wells, 2 x 10^5 LN cells in 100 µl complete media were added and the plate was incubated at 37°C with 5% CO_2 for 72 hours. After the incubation, the plate was centrifuged at 400 x g for 3 minutes and supernatants were discarded. The cells were stained with anti-CD4, anti-KJ1.26, anti-CD69, anti-Ki67 antibodies and viability dye to assess the activation state and proliferation of the transgenic T cells by flow cytometry (described in **2.7**).

2.14.3 Stimulation of gingival and LN cells for assessment of cytokine production by flow cytometry

A single cell suspension of gingival tissue and LNs were obtained from sham and *P. gingivalis*-infected mice as described in **2.5.2**. To a round bottom 96 well plate, 5 x 10^5 cells were added in 200 µl complete media, followed by the addition of 2 µl of a stimulation mix or BD GolgiStop™ alone. The mix was composed of 10 ng/ml PMA, 500 ng/ml ionomycin and BD GolgiStop™ (4 µl in every 6 ml of complete media (BD Biosciences)). BD GolgiStop™ was added to inhibit protein transport, causing an intracellular accumulation of cytokines. The 96 well plate was incubated at 37°C with 5% CO_2 for 4 hours. After the incubation, the plate was centrifuged at 400 x g for 3 minutes and the supernatant was discarded. The cells were stained with viability dye, anti-CD45, anti-CD4, anti-CD8, anti-IFNγ, anti-IL-17A and anti-IL-4 antibodies and were analysed by flow cytometry (described in **2.7**).

2.15 Statistics

All statistical analysis was performed using GraphPad Prism® software version 6 (GraphPad Software, California, USA). For RNA-sequencing and qRT-PCR, where gene expression was shown as fold change or relative expression, data were log transformed to conduct statistical analysis. All other statistical analysis was conducted on raw data. To test if the means of two samples differed when the data was normally distributed, two-tailed unpaired T tests were employed. To test if the

means of two samples differed when the data was non-normally distributed, Mann-Whitney tests were employed. To test if the means of two samples from a larger data set differed, multiple unpaired T tests followed by Holm-Sidak multiple comparison correction was employed. To compare the means of samples from the same mouse, two-tailed paired T tests were employed. To test if the means of more than two samples differed, a one-way ANOVA was employed. Differential gene expression from RNA-sequencing was determined using Wald-test (P value) followed by Benjamini-Hochberg correction (adjusted P value, Padj). A P value < 0.05 was considered significant for T tests, Mann-Whitney tests and one-way ANOVA. A Padj value < 0.1 was considered significant for Wald-test and Benjamini-Hochberg correction.

3 Optimizing a protocol for digesting gingival tissue

3.1 Introduction

The immune response can localize to tissue specific sites, and the response is influenced by the architecture and milieu of cells and their products present within that given site. The phenotype and function of immune cells residing within specific anatomical locations will, therefore, be unique (Kroemer et al., 1993). The hallmark of PD is alveolar bone destruction. Gingival tissue is located in close proximity to alveolar bone, therefore is a propitious site to study the immune response that mediates bone remodeling in inflammation. Whilst the murine model offers an advantage to deciphering the immunological basis of PD over human studies (discussed in **chapter 1.4**), the small size of the mouse's gingiva complicates isolation of the residing cells.

To isolate cells of murine LNs, the LNs are removed and mashed over a cell strainer. Gingival tissue is extremely tough by comparison, as it is composed of a dense network of predominantly collagen fibres (Laurell et al., 1987). Gingivae are thereby resistant to processing by manual techniques appropriate for LNs. Enzymatic digestions are commonly used for isolating cells from gut tissue (Goodyear et al., 2014) and typically utilize collagenase and dispase I, combined with DNase and EDTA to enhance tissue disruption and reduce clumping of cells. However, the integrity of the cell surface may be impeded, affecting expression of surface markers and function (Ford et al., 1996). Despite this caveat, cells cannot be reliably obtained from certain tissue types using mechanical disruption alone (Autengruber et al., 2012).

Investigating the cellular composition of gingivae is fundamental to understanding the immune response in PD; therefore the aims of this chapter were to:

- Optimize a method for gingival tissue digestion.
- Optimize a T cell purification method for downstream analysis of this specific cell type.

3.2 Results

This project sought to determine the role of CD4+ T cells in PD, including investigating CD4+ T cells at the local site of infection. As such, initial experiments focused on optimizing a protocol for efficiently obtaining a viable, single cell suspension of cells isolated from the gingivae of mice. The original gingival digestion protocol (method A) had been used for previous studies, but only highlighted the need for an improved protocol as cell numbers greatly varied between experiments and cell viability was poor. With the aim of achieving improved reproducibility and viability, six protocols were constructed, as described in **table 3.1**, using a combination of enzymes with four tissue disruption methods. These protocols were based on studies previously carried out within the group (Malcolm et al., 2015b), protocols that were previously published (Mizraji et al., 2013, Goodyear et al., 2014), and others were discussed with MACS manufacturer.

Table 3.1. Methods of gingival digestion.

Method	Enzymatic digestion	Tissue Disruption
A	Liberase DH	GentleMACS™ dissociator Program A
B	No enzyme	GentleMACS™ dissociator Program M_liver
C	Collagenase D	GentleMACS™ dissociator Program M_liver
D	Collagenase D	GentleMACS™ dissociator Program M_spleen
E	Collagenase D	GentleMACS™ dissociator Program A
F	Collagenase II + DNase I	Manual disruption with scalpel blade

Abbreviations: DH, dispase high.

Gingival tissue was excised from four (methods A-E) or five (method F) female BALB/c mice and cells isolated according to one of the six protocols. The cells were then stained with anti-CD4, anti-CD8 and viability dye for flow cytometry analysis. The plots in **figure 3.1** clearly illustrate that methods B-E failed to achieve a suspension of predominantly viable cells and instead depict small, poorly defined populations of viable CD4+ and CD8+ T cells. Whilst both methods A and F generate largely viable cell populations, method F yielded a greater population of CD4+ and an identifiable CD8+ population. This, however, is not simply a reflection of using an additional mouse in the group of pooled gingivae. **Figure 3.2** and **table 3.2** both demonstrate cell numbers per individual mouse and show that numbers of lymphocytes, viable lymphocytes, viable CD4+ and viable CD8+ cells are all greatest when using method F. Method F was therefore deemed the preferred protocol for cell isolations from gingival tissue.

In some experiments, gingival strips were obtained (**figure 2.5C**). However, very few cells were isolated from gingival strips, compared with gingival and palatal tissue described above. On average, 76 viable CD4+ T cells and 8 viable CD8+ T cells were obtained per gingival strip (data not shown). Pooling the gingival strips from five mice would still give T cell numbers insufficient for analysis. As the main aim was to investigate oral mucosal T cells, and therefore encompass the oral mucosal tissue, and given the very low cell numbers obtained from gingival strips, in subsequent experiments, gingival tissue investigations in this thesis included palatal tissue.

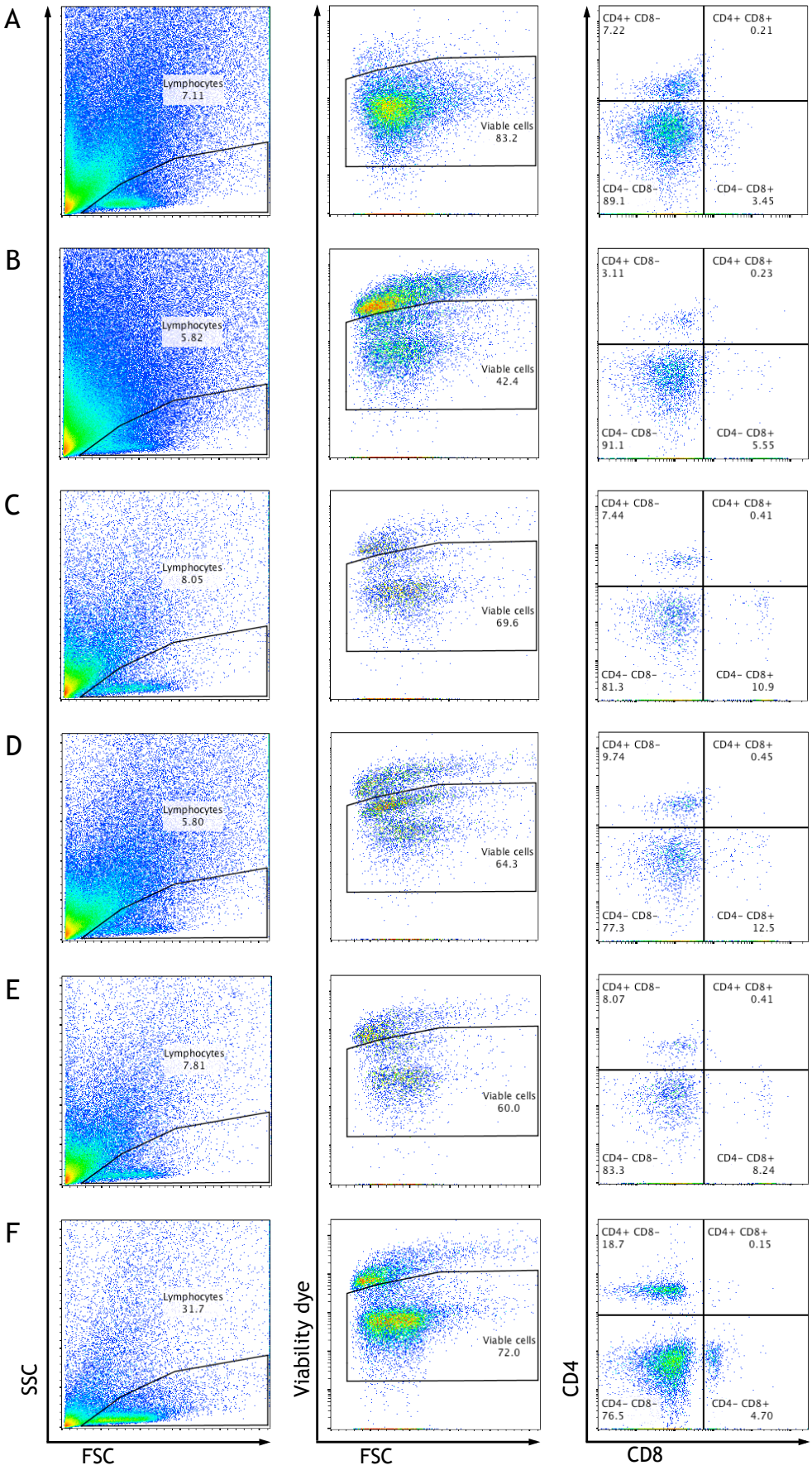
A
Lymphocytes
7.11
Viable cells
83.2
CD4+ CD8-
7.22
CD4+ CD8+
0.21
CD4- CD8-
89.1
CD4- CD8+
3.45
B
Lymphocytes
5.82
Viable cells
42.4
CD4+ CD8-
3.11
CD4+ CD8+
0.23
CD4- CD8-
91.1
CD4- CD8+
5.55
C
Lymphocytes
8.05
Viable cells
69.6
CD4+ CD8-
7.44
CD4+ CD8+
0.41
CD4- CD8-
81.3
CD4- CD8+
10.9
D
Lymphocytes
5.80
Viable cells
64.3
CD4+ CD8-
9.74
CD4+ CD8+
0.45
CD4- CD8-
77.3
CD4- CD8+
12.5
E
Lymphocytes
7.81
Viable cells
60.0
CD4+ CD8-
8.07
CD4+ CD8+
0.41
CD4- CD8-
83.3
CD4- CD8+
8.24
F
Lymphocytes
31.7
Viable cells
72.0
CD4+ CD8-
18.7
CD4+ CD8+
0.15
CD4- CD8-
76.5
CD4- CD8+
4.70
SSC
FSC
Viability dye
FSC
CD4
CD8

Figure 3.1. Flow cytometry of cells obtained following different gingival digest protocols.
Single cell suspensions were obtained from gingival tissue of BALB/c mice by combinations of different enzymatic digestion followed by different tissue disruption methods, as summarized in **table 3.1**. The resulting cell suspensions from each protocol were stained with cell viability dye, anti-CD4 and anti-CD8 antibodies then analysed by flow cytometry. (A) Liberase DH with gentleMACS™ dissociator Program B; (B) No enzyme with Program M_liver; (C) Collagenase D with Program M_liver; (D) Collagenase D with Program M_spleen; (E) Collagenase D with Program A; (F) Collagenase II and DNase I with manual disruption with scalpel blade.

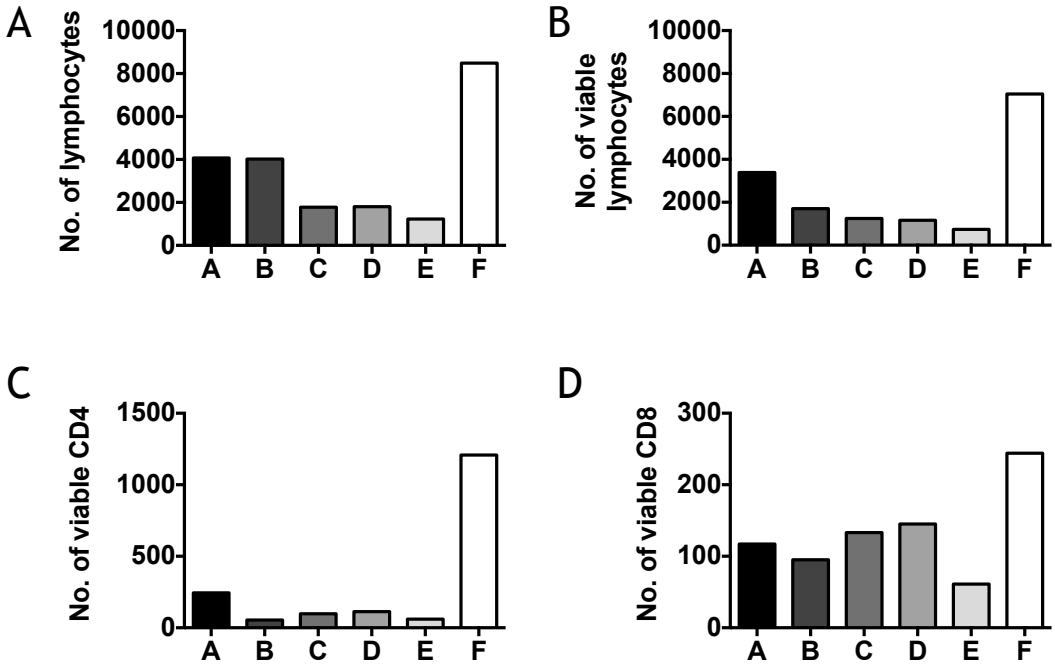

Figure 3.2. Numbers of cells obtained following different gingival digest protocols, per mouse.
Single cell suspensions were obtained from gingival tissue of BALB/c mice by combinations of different enzymatic digestion followed by different tissue disruption methods, as summarized in **table 3.1**. The resulting cell suspension from each protocol was stained with cell viability dye and anti-CD4 and anti-CD8 antibodies then analysed by flow cytometry. Cells were pooled from 4 or 5 mice for processing and analysis but normalized numbers per mouse are plotted. (A) Liberase DH with gentleMACS™ dissociator program Program B; (B) No enzyme with programs Program M_liver; (C) Collagenase D with Program M_liver; (D) Collagenase D with Program M_spleen; (E) Collagenase D with Program A; (F) Collagenase II and DNase I with manual disruption with scalpel blade. Each bar represents the cell numbers per mouse. (A) Number of lymphocytes; (B) Number of live lymphocytes; (C) Number of live CD4 cells; (D) Number of live CD8 cells.

Table 3.2. Proportions and total number of CD4 and CD8 T cells obtained following different gingival digest protocols.

Method	Lymphocytes	Viable Lymphocytes		Viable CD4		Viable CD8	
	No.	No.	%	No.	%	No.	%
A	4067	3384	83.2	244	7.2	117	3.5
B	4024	1706	42.4	53	3.1	95	5.6
C	1782	1243	69.8	98	7.9	133	10.7
D	1805	1160	64.3	113	9.7	145	12.5
E	1230	738	60.0	60	8.1	61	8.3
F	8486	7049	83.1	1208	17.1	244	3.5

A, Liberase DH with Program B; B, No enzyme with Program M_liver; C, Collagenase D with Program M_liver; D, Collagenase D with Program M_spleen; E, Collagenase D with Program A; F, Collagenase II and DNase I with manual disruption. No. = cell number per mouse; % is of total number of lymphocytes.

As enzymatic digestion can affect the extracellular expression of some markers, the next experiment assessed whether the use of collagenase II and DNase I affected the expression of the memory marker CD62L that is particularly prone to cleavage from the cell surface. To address this, cells were isolated from inguinal LNs by mechanical tissue disruption (no enzymes) or by method F enzymatic digestion, and were stained with viability dye, anti-CD45, anti-CD4, anti-CD62L and anti-CD44 for analysis by flow cytometry. The expression of CD62L by memory CD4+ T cells (CD45+ CD4+ CD62L+/- and CD44+/-) was evaluated (**figure 3.3**) and highlighted that the entire cell populations had slightly altered forward/side scatter following isolation by enzymatic digestion. Applying identical gates to cells from both disruption types suggested that expression of CD62L differed when cells were isolated in the presence of enzymes (CD62L+ cell numbers: mean 17147 +/- 108.5 no enzymes vs. mean 15984 +/- 59 enzymes, $P < 0.05$) (**table 3.3**). However, when the gating strategy was slightly modified, to better fit the cell populations from enzymatically-digested tissues, the expression of CD62L was similar to that of cells isolated by non-enzymatic disruption (CD62L+ cell numbers: mean 17147 +/- 108.5 no enzymes vs. mean 17431 +/- 575 enzymes, NS). Therefore, the use of DNase I and collagenase II did not appear to affect antibody binding to these lymphocyte

cell surface molecules, which were used for phenotyping cells in subsequent experiments.

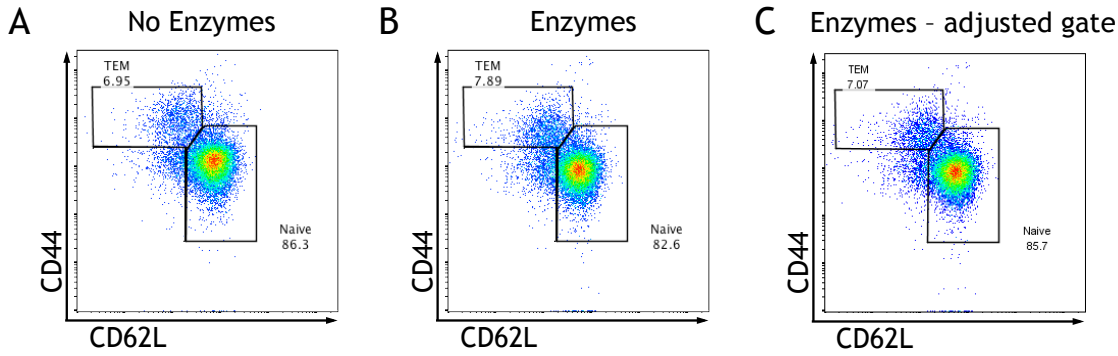

Figure 3.3. Effect of enzymatic digest on cleavage of CD62L from cell surface. Single cell suspensions were obtained from inguinal LNs by (A) mechanical tissue disruption (no enzymes) or (B and C) enzymatic digestion (Method F). The resulting cell suspensions were stained with cell viability dye, anti-CD45, anti-CD4, anti-CD44 and anti-CD62L for analysis of memory CD4+ T cells by flow cytometry. (A and B) Cell gates were applied based on mechanical tissue disruption. (C) Gate in B was moved to better fit the populations' slightly altered FSC/SSC. Populations of naïve and effector memory T cells (TEM) are highlighted by black gates.

Table 3.3. Effect of enzymatic digest on cell surface CD62L expression.

Cell isolation type*	Mouse No.	No. of CD62L+ cells (same cell gate)	No. of CD62L- cells (same cell gate)	Ratio of CD62L+ To CD62L-	No. of CD62L+ cells (gate adjusted)	No. of CD62L- cells (gate adjusted)	Ratio of CD62L+ To CD62L-
No enzymes	1	17255	1984	8.7	-	-	-
No enzymes	2	17038	2034	8.4	-	-	-
Enzymes	1	15925	2876	5.5	16586	1950	8.5
Enzymes	2	16043	4506	3.6	18006	2546	7.1

*No enzymes, non-enzymatic mechanical tissue disruption; Enzymes, enzymatic digestion (Method F).

To analyse T cells in PD by RNA-sequencing, the T cells would have to be purified from the total gingival tissue cell population. Therefore, the next experiments were conducted in order to optimize T cell purification. Two methods were trialed; using either magnetic-labeled antibody cell selection or flow cytometry based sorting (fluorescence-activated cell sorting, FACS).

To improve the efficiency of binding of magnetic-labeled antibody beads to cells and therefore of cells to the column, the T cell population within the gingival cell suspension was enriched by eliminating other populations; either by using ficoll gradient separation, or by using MACS® Basic MicroBeads to remove dead cells. The T cells were purified from the enriched fraction using positive selection with either anti-CD3ε magnetic-labeled antibody beads, or anti CD90.2-labeled beads; the latter are reported to cause no T cell stimulation. In all cases, the purity was assessed by flow cytometry (**table 3.4**). These methods of T cell purification had limited success. Using ficoll and anti-CD3ε-labeled beads (**figure 3.4**), the purified population was comprised of around 22% viable CD3+ cells and 21% of viable CD3- cells. Using Basic Microbeads and CD90.2-labeled beads resulted in poor viability, with only 8% of cells being viable and positive for CD3 and CD4 (**figure 3.5)**.

Table 3.4. Antibody panel used to assess purity of separated T cells.

Protocol	Antibody Panel
Ficoll + anti-CD3ε beads	Viability dye, anti-CD3, anti-CD4
Basic Microbeads + anti-CD90.2 beads	Viability dye, anti-CD3, anti-CD4
Basic Microbeads + anti-CD4 beads	Viability dye, anti-CD45, anti-CD4
FACS	Viability dye, anti-CD45, anti-CD4

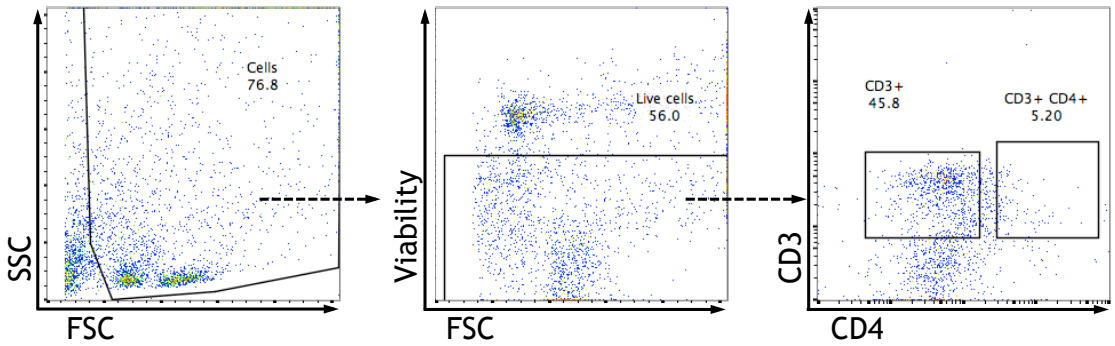

Figure 3.4. T cell purification using ficoll and magnetic-labeled antibody beads. Single cell suspensions were obtained from gingival tissue of BALB/c mice, by liberase DH enzymatic digestion followed by Program B gentleMACS™ dissociation. Mononuclear cells were separated by Histopaque® 1083 density gradient separation then T cells purified using MACS® CD3ε MicroBeads. Cells were stained with cell viability dye, anti-CD3 and anti-CD4 antibodies then were analysed by flow cytometry. The dashed arrows indicate gating strategy.

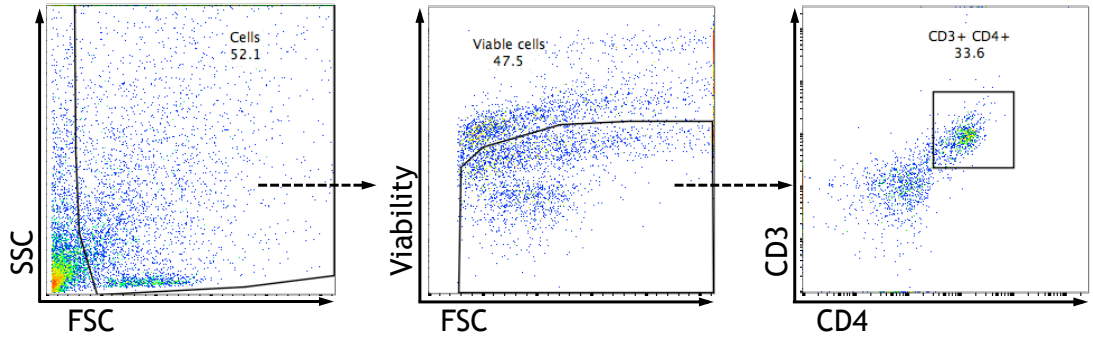

Figure 3.5. T cell purification using magnetic-labeled antibody beads. Single cell suspensions were obtained from gingival tissue of BALB/c mice, by liberase DH enzymatic digestion followed by Program B gentleMACS™ dissociation. Dead cells were removed using MACS® Basic MicroBeads then T cells were purified by MACS® CD90.2 MicroBeads. Cells were stained with cell viability dye, anti-CD3 and anti-CD4 antibodies then were analysed by flow cytometry. The dashed arrows indicate gating strategy.

In addition to the poor viability and purity, there was potential for anti-CD3ε beads to activate T cells and interfere with downstream analysis, and anti-CD90.2 could purify innate lymphoid cells (ILCs) (Hams et al., 2014). Therefore, the next experiments purified the CD4+ T cell population using anti-CD4-labeled beads in combination with Basic Microbeads. In these experiments, anti-CD45 was used for

flow cytometry to help identify CD4+ T cells and confirm purity as CD45 allows discrimination of leukocytes from non-hematopoietic cells. This was necessary since CD3 was removed from the panel to avoid stimulating the cells (**table 3.4**). The cells purified using anti-CD4 beads were stained with viability dye, anti-CD45 and anti-CD4 antibodies (**figure 3.6B)**. Flow cytometry indicated that of the total population purified, only 11.1% were viable cells but 93.9% of the viable cells were CD4+.

Using the antibodies in **table 3.4**, viable CD45+ CD4+ T cells were sorted by FACS (**figure 3.6A)**, which yielded 100% pure, viable CD4+ T cells. Thus, the cells obtained by FACS were of greater viability and purity. Moreover, using magnetic-labeled antibody beads requires the purified populations to be assessed for purity. By comparison, the total FACS sorted CD4+ T cell population can be used for downstream analysis (**table 3.5**). FACS sorting was therefore the preferred method for obtaining viable, CD4+ T cells for RNA-sequencing.

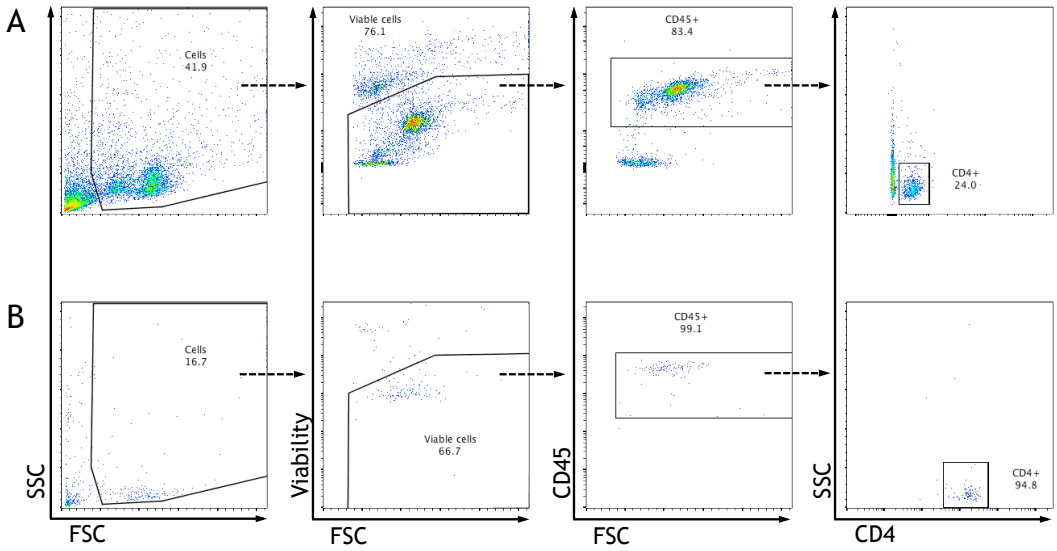

Figure 3.6. CD4+ T cell purification using fluorescence-activated cell sorting and magnetic-labeled antibody beads.
Single cell suspensions were obtained from gingival tissue of BALB/c mice, by collagenase II and DNase I enzymatic digestion followed by manual disruption with a scalpel blade (**table 3.1**, protocol F). (A) The unsorted cell suspension was stained with cell viability dye, anti-CD45 and anti-CD4 antibodies. (B) The cell suspension was CD4 purified using MACS® Basic MicroBeads followed by CD4 MicroBeads. The purified cells were stained for flow cytometry (as in A) to assess purity. The dashed arrows indicate gating strategy.

Table 3.5. Purity of T cells following different separation methods.

Purification method	No. of cells post purification	Can all purified cells be used for downstream analysis?	Percentage of pure, viable T cells	Estimation of T cell no. for downstream analysis***
Histopaque® 1083 and MACS® CD3 MicroBeads*	2.0×10^4	No; purity must be assessed	21.9	3.3×10^3
MACS® Basic MicroBeads and CD90.2 MicroBeads**	1.1×10^5	No; purity must be assessed	8.3	6.8×10^3
MACS® Basic MicroBeads and CD4 MicroBeads	1.4×10^4	No; purity must be assessed	10.5	7.9×10^2
Flow-cytometry based CD4 cell sorting	1.2×10^4	Yes	100.0	1.2×10^4

*CD3 beads may activate T cells thus interfering with downstream analysis
** CD90.2 beads may not be specific for T cells; could purify ILCs
***Estimation based on percentage of pure T cells and ¼ of purified sample being assessed by flow cytometry.

3.3 Discussion

As the overall aim of this thesis was to determine the role of CD4+ T cells in PD, it was crucial to explore the immune response in the gingiva. Specific anatomical locations are home to distinct immune cells. For example, there is discrete distribution of Ig class by plasma cells in the gut compared to LNs and bone marrow (Crabbe et al., 1965). Likewise, the oral mucosa is populated by different immune components (Horav 2014). It was therefore imperative to define a protocol that enabled isolation of viable and functionally active cells from the gingiva.

Due to the tough nature of gingival tissue, manual dissociation in the absence of enzymes failed to disrupt the tissue enough to allow the release of cells – in contrast to LNs and spleens which are readily disrupted by manual dissociation. These data indicate that specific enzymes in combination with tissue disruption methods were crucial variables in optimizing gingival T cell isolation. Rather unexpectedly, enzymes proved non-essential when using GentleMACS™ dissociation to obtain viable lymphocytes, however, a lack of enzymes resulted in the poorest retrieval of CD4+ T cells. It was demonstrated that using a combination of DNase I and collagenase II effectively isolated viable CD4+ and CD8+ T cells. This was similar to previous studies that substantiated a combination of liberase, DNase and collagenase was optimal for the isolation of cells from the small intestine from various strains of mice (Goodyear et al., 2014). The mouse lung is another tough tissue type to digest, and likewise has been dissociated with DNase, however GentleMACS™ was necessary to aid in the isolation of cells (Jungblut et al., 2009). Ideally, every combination of enzyme and mechanical disruption would have been assessed. However, this would have used an unacceptable number of animals. Despite this, protocol F that required manual dissociation with a scalpel blade proved to produce viable lymphocytes, and in particular T cells, in a reproducible manner.

A concern when using enzymatic digests is alteration of true cell phenotype through cleavage of cell-surface markers (Autengruber et al., 2012). Although not always possible, the isolation of tissue resident cells can be achieved without the use of

enzymes. One such technique is the 3D explant method in which tissue samples are placed over a titanium matrix and cultured in media (Henderson et al., 2014). In this model, cells migrate out of the sample into media leaving behind the tissue structure. Whilst this system avoids the use of enzymes, a disadvantage is the bias of obtaining only cells with migratory capacity. Moreover, the relatively small number of CD4+ T cells available in the gingival tissue would potentially limit the usefulness of this passive migration method. Optimized method F illustrated that enzymes were crucial for optimal isolation of CD4+ T cells from gingival tissue; however, it was demonstrated that these enzymes did not affect the expression of memory marker CD62L, which is prone to enzymatic cleavage. Therefore, it seemed unlikely that the phenotype of gingival cells would be affected by either collagenase II or DNase I in the context of tissue digest.

The combination protocol F enabled the phenotype and potential function of T cells from the oral mucosa to be determined using flow cytometry. However, to evaluate CD4+ T cells in an unbiased manner, further aims of this project were to conduct transcriptomic studies. For this technique, T cells must be purified from the total gingival cell isolate. Magnetic-labeled antibody beads have allowed successful separation of a plethora of cells including DCs (Arora and Porcelli, 2016), neutrophils (Hasenberg et al., 2011), mast cells (Jamur et al., 2001) and B cells (Cato et al., 2011). Purification of the total T cell population using anti-CD3 magnetic-labeled antibody beads was not an appropriate method as there was potential for the T cells to become activated – the reason for the use of CD90.2 beads. Whilst CD90.2 beads do not activate T cells, a caveat is the potential isolation of ILCs. Moreover, the particular focus of these studies was to address the contribution of CD4+ T cells in PD, hence anti-CD4 magnetic-labeled antibody beads and FACS sorting of CD4+ T cells were compared. Despite the high purity rate of cells separated by beads, only a small percentage of the total population were viable cells and further, a fraction of the CD4+ T cells were required for cell type confirmation by flow cytometry. By contrast, cell sorting by FACS allowed simultaneous cell purification and analysis of the purified population. The FACS sorted CD4+ T cells could have been re-assessed by flow cytometry to determine the absolute specificity of the sorter and viability of the cells post-sort; however, it

was optimal to keep numbers as high as possible for downstream analysis. Whilst the target population described could be identified through the use of only three antibodies (viability dye, anti-CD45 and anti-CD4), FACS offers numerous advantages over other conventional sorting methods. For example, cells can be sorted based on expression of numerous proteins, internal protein expression and density of expression (Basu et al., 2010). A caveat of FACS is the expense of the sorter and the slow rate at which target populations are purified. A fairly recently developed method for cell sorting that surpasses the limitations of FACS is buoyancy-activated cell sorting (BACS). This technique employs antibody-conjugated microbubbles that bind targeted cells, which then float to the surface of the liquid based sample and are harvested. BACS is inexpensive and the absence of magnetic beads means that magnetic-induced damage to cells will not occur. Instead, the stress and tension of the rising of the cell to the surface is incapable of impacting cell integrity (Liou et al., 2015). As with MACS, a proportion of the BACS-sorted cells would have to be assessed for purity, therefore the number of cells for downstream analysis would be limiting. Another novel method of sorting for downstream analysis is PCR-activated cell sorting (PACS), which exploits multiplexed TaqMan assays to evaluate individual cells in microfluidic droplets for transcripts, non-coding RNAs or genomic DNA then appropriate cells are sorted (Pellegrino et al., 2016). Similar to FACS, a pre-selection of known phenotype is required for sorting, as is it a high throughput and highly specific sorting technique. Therefore, PACS would not have provided any benefits over the chosen method of FACS for the sorting of CD4+ T cells. Rather, the transcriptome may not truly reflect the protein expression of a cell (Vogel and Marcotte, 2012).

In conclusion, gingival tissue is composed of a dense network of collagen fibres making it resistant to digestion methods appropriate for LNs and spleens. However, a method for obtaining viable lymphocytes from the oral mucosa has been optimized with the use of an enzymatic digest combined with mechanical disruption. For downstream analysis of CD4+ T cells specifically, FACS sorting was found to purify the greatest yield with the greatest purity. This will enable efficient analysis of CD4+ T cells by transcriptomic methods.

Key findings from chapter 3:

- A combination of DNase I and collagenase II with manual dissociation enables efficient isolation of gingival cells.
- The enzymatic digestion does not affect cell surface expression of CD62L.
- FACS sorting enables efficient purification of CD4+ T cells from total gingival cell isolate.

4 Phenotype of CD4+ T cells in PD

4.1 Introduction

Characterization of immune cells in a disease setting aids understanding of the immunological basis of the disease and the development of potential new treatments. For example, evidence that aberrant T cells play a predominant role in the activation of the inflammatory cells infiltrating the synovial membrane of RA led to development of treatments targeting T cells (Cope, 2008). Abatacept is a blockade of co-stimulation and modulates the interaction of CD80/CD86 with CD28 to inhibit T cell activation and consequently reduces inflammation (Westhovens and Verschueren, 2010). Evidence of T cell responses in PD has been reported in human and murine studies. Unquestionably, these studies have illustrated that T cells are present in PD, yet their function remains disputed.

Flow cytometry is a powerful method for single-cell analysis of components of the immune system. Various parameters of single cells can be evaluated, which facilitates the characterization of individual cells from small or large samples of tissue. To determine the immune response associated with PD in human studies, IHC, ELISA and PCR were most commonly employed (Gamonal et al., 2001, Lappin et al., 2001, Berglundh et al., 2002, Takeichi et al., 2000, Cardoso et al., 2009, Dutzan et al., 2012b, Honda et al., 2008, Beklen et al., 2007, Adibrad et al., 2012). Flow cytometry was used in a small number of studies investigating T cell subsets. More commonly, cell lines were stimulated with periodontal pathogens and then assessed by flow cytometry (Moutsopoulos et al., 2012).

The immune response associated with PD in murine models has been studied by flow cytometry. The majority of these studies have evaluated responses in spleen and draining lymph nodes, and only a very few have evaluated the cells infiltrating the gingival tissues. Inflammation at the local infection site was investigated at multiple time points – 14 days or more post infection - in an *A. actinomycetemcomitans*-induced PD mouse model (Garlet et al., 2010a).

Developments in flow cytometers and fluorochromes allow a greater number of markers of phenotype and function to be measured in a single experiment. A disadvantage, however, is that cells must be crudely disrupted from their location within tissue, preventing analysis of cell-cell interactions and expression characteristics. For example, it is known that antigens of varying shapes and sizes are presented by APCs to T cells. However, the use of multi-photon imaging confirmed that contact duration between DCs and T cells was increased in presentation of large antigens, whilst velocity was reduced (Benson et al., 2015). Thereby, the imaging of cells in their natural anatomical location can provide further insights into the behaviour and function of cells in a disease milieu. Light and fluorescent microscopy have identified subsets of T cells in gingival biopsies of PD patients, but there is a lack of similar investigations in mouse models of the disease.

In this chapter, detailed analysis of T cell phenotype at both the local and draining site of infection in a *P. gingivalis*-induced PD model will be investigated. In an attempt to understand the changes in the immune response that ultimately result in alveolar bone loss – rather than immunology of established disease - the specific T cell phenotypes will be investigated at 7, 14 and 28 days post infection using flow cytometry and IHC.

The aims of this chapter were to:

- Phenotype CD4+ and CD8+ T cells at early stages of experimental PD by flow cytometry.
- Determine the systemic immune response at early stages of experimental PD by flow cytometry, and *ex vivo* cell culture.
- Determine the localization of T cells in the oral mucosa at early stages of experimental PD.

4.2 Results

To investigate whether signs of PD could be established in mice at 28 days post infection, alveolar bone loss was assessed in mice orally infected with CMC (sham) or *P. gingivalis* (**figure 4.1**). There was a trend towards increased bone loss in *P. gingivalis*-infected mice (mean 0.345 +/- 0.0023 mm sham vs. 0.366 +/- 0.0110 mm *P. gingivalis*, NS). Serum anti-*P. gingivalis* IgG titres were measured and highlighted that whilst there was a significant increase in infected mice (56.70 +/- 17.27 EU sham vs. 351.3 +/- 96.45 EU *P. gingivalis*, $P < 0.05$), two animals from this group displayed antibody titres mimicking that of sham-infected mice. As a result of this finding, bone loss in each mouse was viewed in relation to antibody titre, demonstrating that the absence of antibody associated with absence of bone loss (**figure 4.1E**). The infected two mice with low antibody titres were excluded from the data set and alveolar bone loss reanalyzed. *P. gingivalis*-infected mice then showed significantly greater bone loss than their infected counterparts (mean 0.345 +/- 0.0023 sham vs. 0.382 +/- 0.0078 *P. gingivalis*, $P < 0.05$), indicating that *P. gingivalis* infection induced PD at 28 days post infection; however, only in the presence of specific bacterial IgG antibodies.

In the above experiments, serum antibodies were assessed after mice were sacrificed. For analysis of gingival cells, gingival tissue from 5 mice were pooled, therefore, cells from mice not displaying PD could potentially skew the investigation of T cells in the disease model. Data from **figure 4.1** suggests that serum anti-*P. gingivalis* IgG titres reflect alveolar bone loss and hence establishment of PD. For this reason, mice from all subsequent PD models were tail bled prior to the cull day to examine serum antibodies and only those mice with antibodies greater at least one standard deviation greater than the average of the control were sacrificed. This would increase the likelihood of phenotyping cells from mice only with PD.

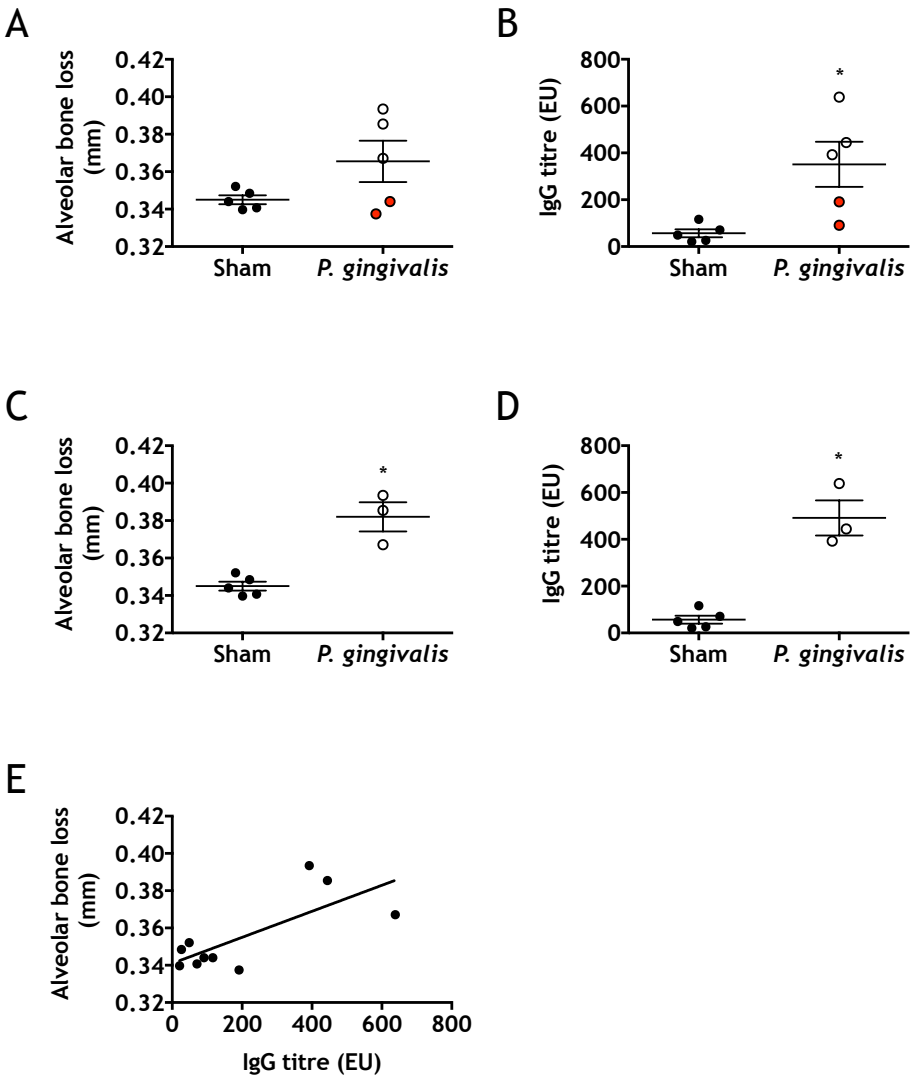

Figure 4.1. Alveolar bone loss and anti-*P. gingivalis* IgG titres at 28 days post *P. gingivalis* infection.

Mice were orally infected with *P. gingivalis* or were sham-infected (sham) with carrier vehicle, CMC, only. At 28 days post infection, alveolar bone loss and anti-*P. gingivalis* IgG titres were measured. (A) Alveolar bone loss data are shown as mean per mouse (symbols) with mean +/- SEM for each group (lines), n = 5 mice/group. Red symbols indicate two infected mice with low bone loss that were removed in reanalysis. (B) Anti-*P. gingivalis* IgG titres in serum were measured by ELISA. Data are ELISA Units (EU) shown as individual mice (symbols) with mean +/- SEM for each group (lines), n = 5 mice/group. Red symbols indicate two infected mice with low IgG titres that were removed in reanalysis. (C) Alveolar bone loss is represented as described for A with the exception that two mice with low anti-*P. gingivalis* IgG titres are excluded from the graph. (D) Anti-*P. gingivalis* IgG titres are represented as described in B with the exception that two mice with low anti-*P. gingivalis* IgG titres are excluded from the graph. (E) Alveolar bone loss in relation to *P. gingivalis* IgG antibody titre. Antibody titre and bone loss from each of the ten sham or *P. gingivalis*-infected mice with line of best fit (R^2 = 0.56). Statistical significance was determined by Mann-Whitney test, as indicated on the graph (*P < 0.05).

To gauge a clearer understanding of the contribution of the immune response to the initiation, progression and ultimately establishment of PD, sham or *P. gingivalis*-infected mice were culled prior at 7, 14 and 28 days post infection. Initially, IgG isotypes were investigated to determine whether Th1 or Th2 responses predominated in this model (**figure 4.2**). Greater serum anti-*P. gingivalis* IgG titres were apparent in the majority of infected mice at 14 and 28 days post infection compared to sham-infected mice (Day 7: mean 46.54 +/- 11.75 sham vs. mean 249.77 +/- 155.82 *P. gingivalis*, NS. Day 14: mean 22.62 +/- 7.89 sham vs. mean 786.25 +/- 189.60 *P. gingivalis*, $P < 0.0001$. Day 28: mean 97.51 +/- 24.63 sham vs. mean 675.54 +/- 174.39 *P. gingivalis*, $P < 0.001$). No significant differences in serum IgG1 between control and infected mice at any of the time-points investigated were observed. IgG2a was significantly increased in *P. gingivalis*-infection at 14 days post infection (mean 1.27 +/- 1.27 sham vs. mean 91.44 +/- 43.46 *P. gingivalis*, $P < 0.05$). Thus an association of Ig2a isotype with PD was noted; therefore, serum IgG titres to *P. gingivalis* suggested the presence of a Th1 response.

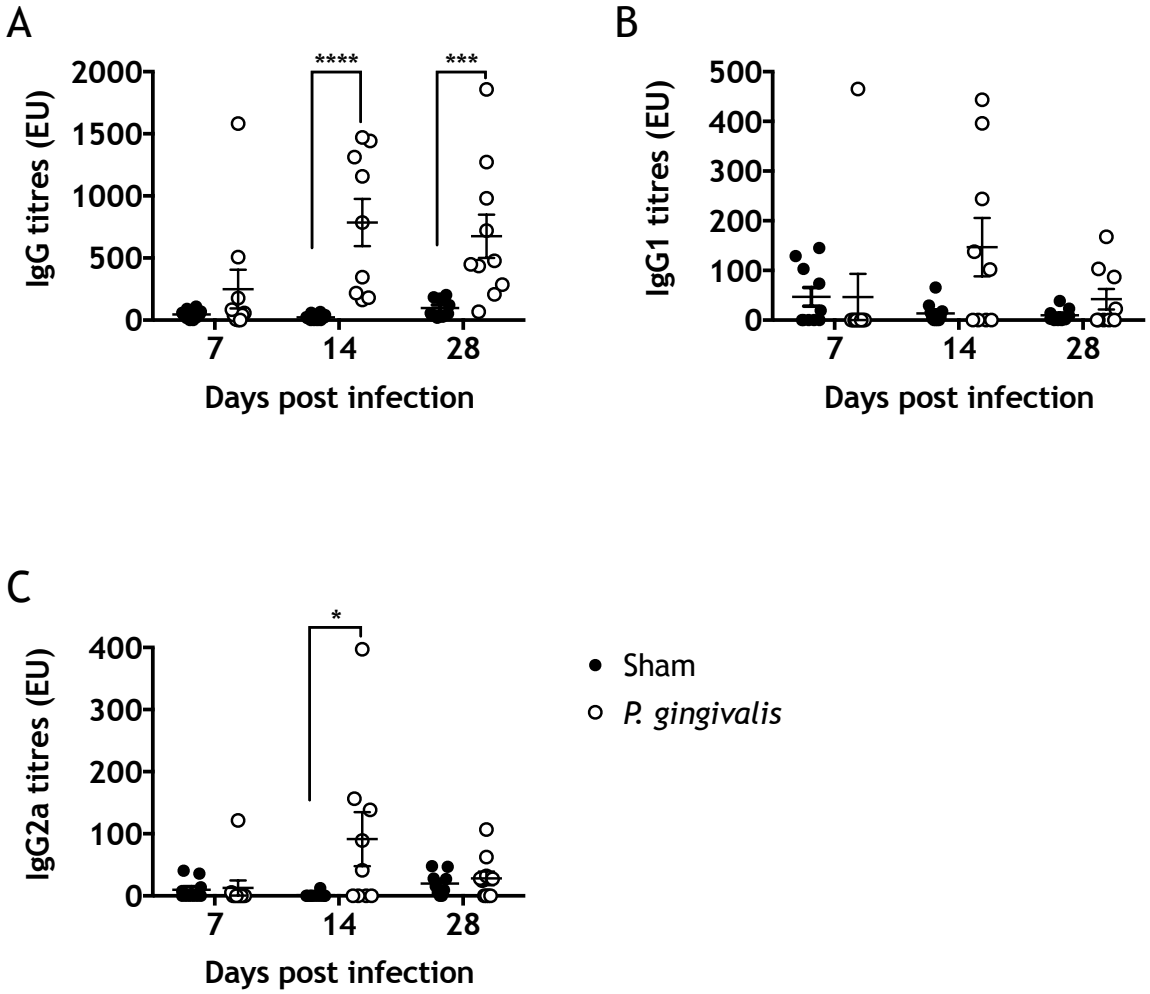

Figure 4.2. Anti-*P. gingivalis* antibody titres at 7, 14 and 28 days post *P. gingivalis* infection.
Mice were orally infected with *P. gingivalis* or were sham-infected (sham) with carrier vehicle, CMC, only. Anti-*P. gingivalis* (A) IgG, (B) IgG1 and (C) IgG2a titres in serum were measured by ELISA at 7, 14 and 28 days post infection. Data are ELISA Units (EU) shown as individual mice (symbols) with mean +/- SEM for each group (lines). Data are combined from 2 independent experiments, n = 5 mice/group at each time-point. Statistical significance was determined by Mann-Whitney tests comparing sham and *P. gingivalis*-infection at each time point (*P < 0.05, **P < 0.01, ***P < 0.001 and ****P < 0.0001).

Alveolar bone loss was determined at 7, 14 and 28 days post infection (**figure 4.3**). In these experiments, there was no evidence of significant alveolar bone loss at any time point, despite high *P. gingivalis*-specific IgG titres in serum at both 14 and 28 days. Compared with bone levels at 7 days, naturally occurring bone loss could be seen at 14 and 28 days post sham-infection (**figure 4.3D**).

With the exception of the initial model described in **figure 4.1**, alveolar bone loss did not occur in any PD model, hence it was necessary to ascertain successful colonization of *P. gingivalis*. The oral cavity of each mouse was swabbed and the presence of *P. gingivalis gpoB* was determined by qRT-PCR. Irrespective of stage of infection (mid-infections, 7, 14 or 28 days post infection), *P. gingivalis gpoB* was undetectable by this method (data not shown), preventing the confirmation of oral colonization. The *P. gingivalis* primers were able to detect DNA from cultured *P. gingivalis*, the positive control sample. Universal 16S primers were able to detect the presence of bacteria on the swabs. As only small numbers of *P. gingivalis* are required to modulate oral commensal bacteria and elicit the immune response associated with PD, the mass of the bacteria present may have been below the lower detection limit of 1000 *P. gingivalis* per mouse - rather than being completely absent (Dr Jessica Oliver-Bell, Ph.D. thesis). Previous studies have found *P. gingivalis* to comprise less than 0.01% of the total bacterial cell counts from oral swabs, the difference of which being 4 – 5 $\log_{10}$ units (Hajishengallis et al., 2011a).

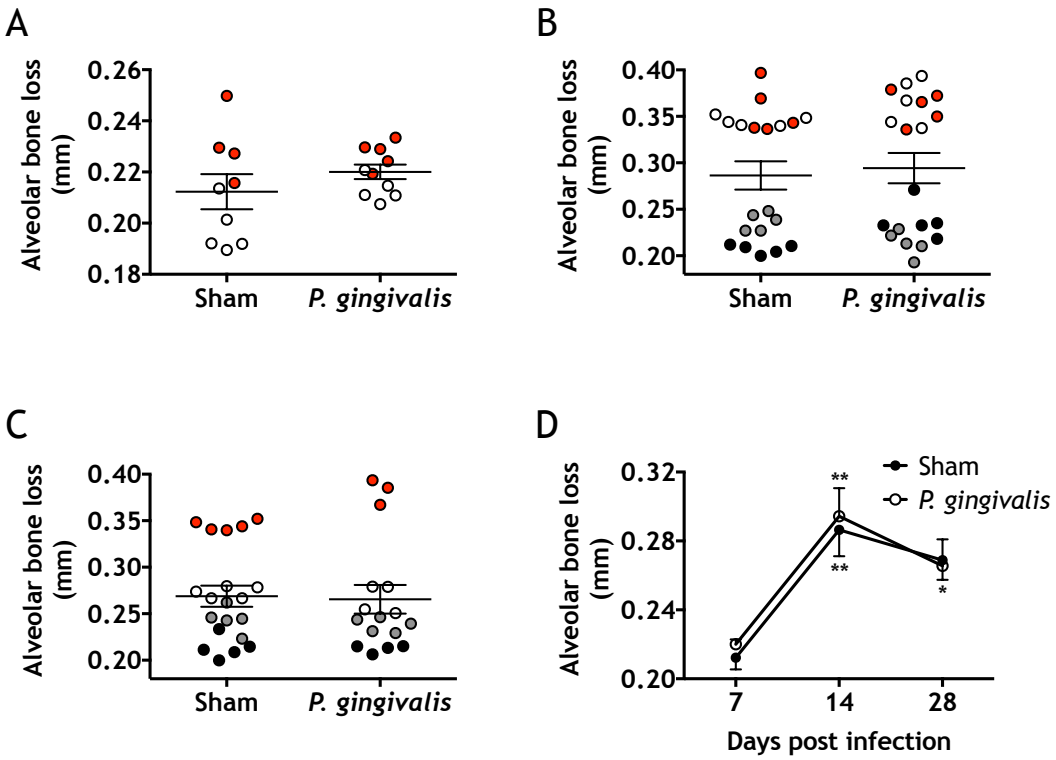

Figure 4.3. Alveolar bone loss at 7, 14 and 28 days post *P. gingivalis* infection. Mice were orally infected with *P. gingivalis* or were sham-infected (sham) with carrier vehicle, CMC, only. At (A) 7, (B) 14 and (C) 28 days post infection alveolar bone loss was measured. Data are shown as mean per mouse (symbols) with mean +/- SEM for each group (lines), from 2 independent experiments at 7 days post infection and 4 independent experiments at 14 and 28 days post infection, n = 3 - 5 mice/group. (D) Mean alveolar bone loss over time. Data are shown as mean per group (symbols) +/- SEM (lines) at 7, 14 and 28 days post infection. (A–C) Statistical insignificance was determined by unpaired T test. (D) Statistical significance was determined by Tukey's comparison 2way ANOVA comparing mean bone loss at each time-point (sham vs. sham and *P. gingivalis* vs. *P. gingivalis*) (*P < 0.05, **P < 0.01).

As antigen from the oral cavity is thought to drain to superficial cervical LNs (Yamazaki et al., Walk et al., 2015, Mkonyi et al., 2012), four of these LNs were excised from the mice. Antigen presentation in LNs can initiate an adaptive immune response, signified by T and B cell proliferation; therefore cell counts were performed on single cell suspensions of the dLNs, as well as the gingivae (**figure 4.4**). At 7 days post infection, a greater number of cells were present in the dLNs from *P. gingivalis*-infected mice compared to the sham-infected controls (mean 9.696×10^6 +/- 9.035×10^5 sham vs. mean 1.651×10^7 +/- 2.823×10^6 *P. gingivalis*, P < 0.05). The cell counts at later time-points did not differ. Gingival cell counts appeared similar irrespective of infection status, at all time-points. This was also

true for the proportions of CD4+ and CD8+ T cells of the total viable cell suspension in both gingivae and dLNs, as defined by flow cytometry analysis. The gating strategy to identify CD4+ and CD8+ T cells has been illustrated in the first five plots of **figure 4.5**.

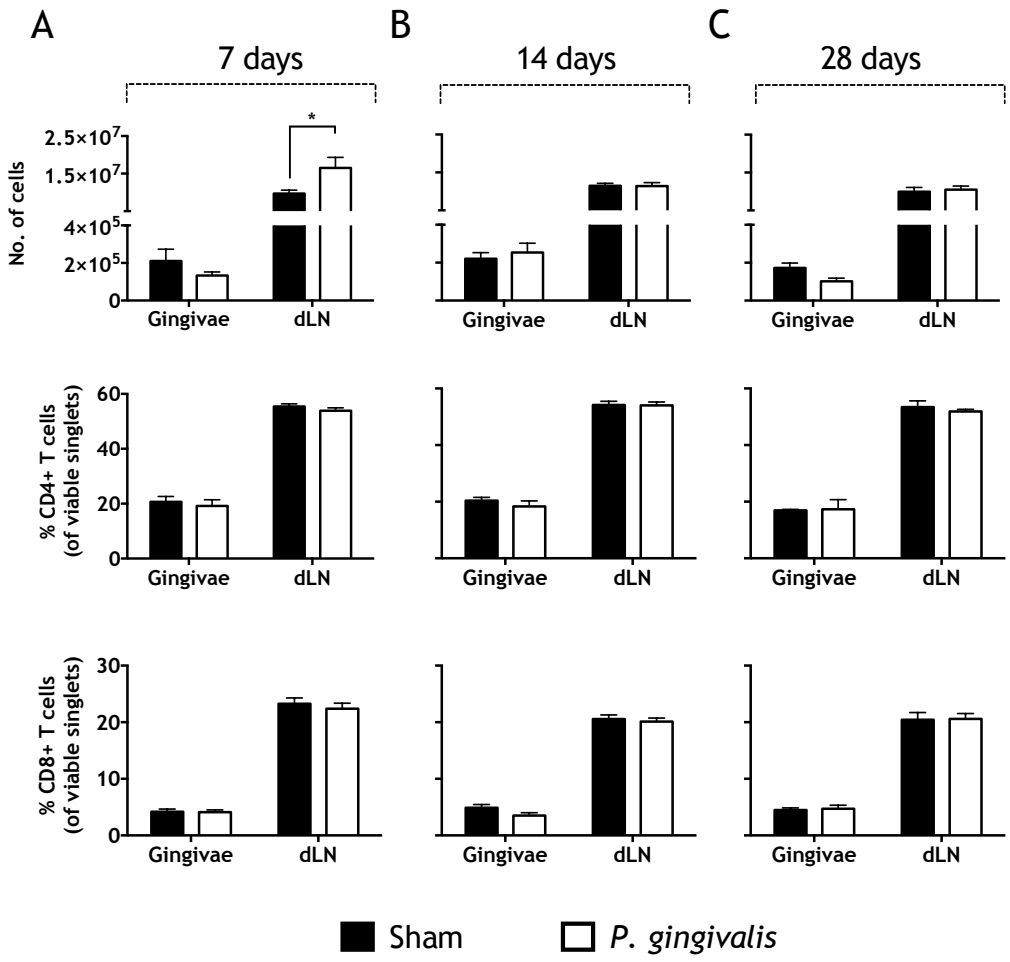

Figure 4.4. Counts of cells and percentages of T cells isolated from gingivae and draining lymph nodes at 7, 14 and 28 days post *P. gingivalis* infection.
Mice were orally infected with *P. gingivalis* or were sham-infected (sham) with carrier vehicle, CMC, only. At 7, 14 and 28 days post infection cells were isolated from gingivae and draining lymph nodes. (A) Number of cells isolated from indicated tissues at each time-point, counted using a haemocytometer. Percentages of (B) CD4+ and (C) CD8+ T cells from their parent single, viable cell populations at each time-point, analysed by flow cytometry. For total cell counts, single gingivae and draining lymph nodes were counted. For CD4+ and CD8+ T cell analysis, cells from 5 gingivae of each group were pooled, as were draining lymph node cells. Data are shown as mean + SEM. Data are combined from 5 independent experiments at 7 days post infection and 4 independent experiments at 14 and 28 days post infection, n = 5 mice/group at each time-point. Statistical significance was determined by unpaired T test for each tissue at each time-point (*P < 0.05).

Whilst the percentage of T cells infiltrating the gingivae and dLNs did not change in infection, other T cell characteristics were investigated to definitively conclude whether *P.* gingivalis-infection influenced changes in T cells. As the *P. gingivalis*-induced PD model is a chronic infection, memory T cells were analysed by flow cytometry (**figure 4.5**). Memory cells were identified based on their lymph node homing receptors and ligands, CCR7 and CD62L. Attempts were made to identify CCR7 by flow cytometry. However, positive staining could not be achieved on gingival cells (data not shown). This was likely due to the enzymatic digest that potentially cleaved some markers from the cell's surface. The majority of CD4+ T cells were naïve (CD44- CD62L+) at each time-point in both the gingivae and dLNs, with a small percentage of CD4+ T cells being TEM (CD44+ CD62L-) and even less being TCM cells (CD44+ CD62L+) (**figure 4.6A, C**). The proportions of memory cells were similar irrespective of infection. At each time-point, regardless of infection, there was a predominance of naïve CD8+ T cells in both gingivae and dLNs, with no significant changes in percentage of this cell type between control and infected mice (**figure 4.6B, D**). Similar to CD4+ memory T cells, only a small percentage of the total CD8+ T cell population were TEM and TCM cells. However, these cells were found in a lower abundance than those of the CD4+ T cell population. Again, there were no significant changes in the disease state.

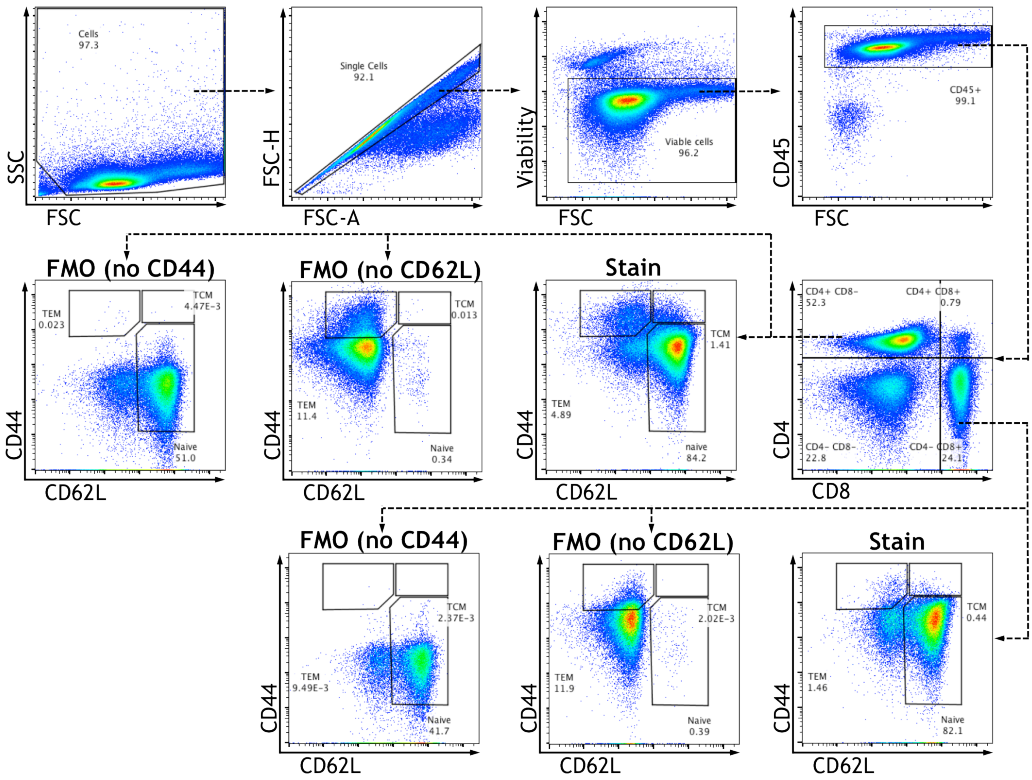

Figure 4.5. Example of gating strategy used to identify memory T cells by flow cytometry.
Mice were orally infected with *P. gingivalis* or were sham-infected (sham) with carrier vehicle, CMC, only. At 7, 14 and 28 days post infection cells were isolated from gingivae and draining lymph nodes and memory T cells analysed by flow cytometry. Dead cells and debris were excluded, based on forward scatter (FSC) and side scatter (SSC), followed by doublet discrimination. Viable, CD45+ cells were then gated upon to assess CD4+ and CD8+ T cells. Memory cells were identified using CD44 and CD62L in both CD4+ and CD8+ T cell populations, as indicated in the stained samples. Naïve cells were identified as CD44- CD62L+, T effector memory (TEM) as CD44+ CD62L- and T central memory cells (TCM) as CD44+ CD62L+. The fluorescence minus one (FMO) control samples were stained with all of the markers in the gating strategy, excluding CD44 or CD62L, as indicated in the figure. The example plot is from sham-infected LN cells at 7 days post infection.

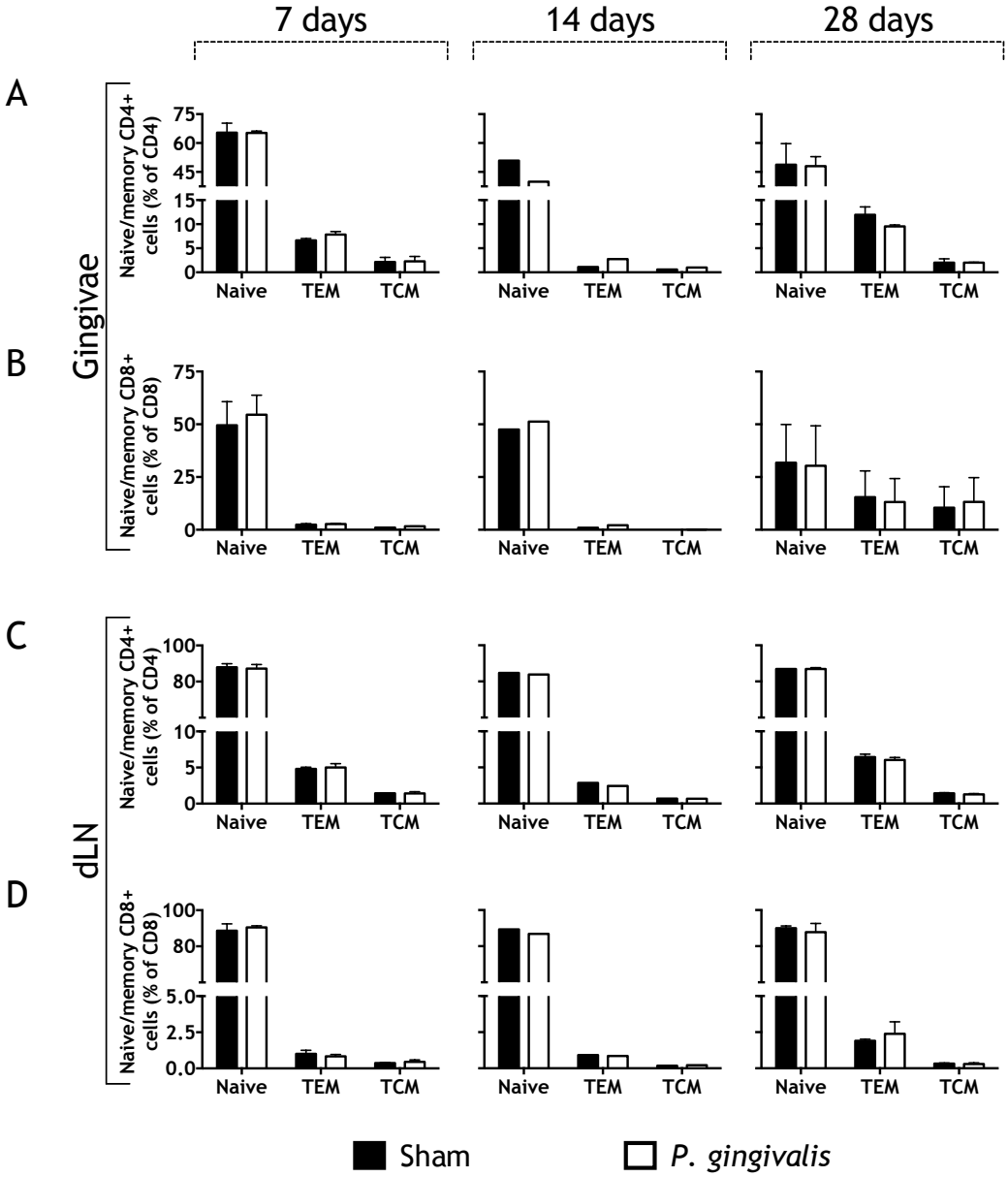

Figure 4.6. Memory T cells from gingivae and draining lymph nodes at 7,14 and 28 days post *P. gingivalis* infection.

Mice were orally infected with *P. gingivalis* or were sham-infected (sham) with carrier vehicle, CMC, only. At 7, 14 and 28 days post infection cells were isolated from gingivae and draining lymph nodes and memory T cells analysed by flow cytometry. Naïve cells were identified as CD44- CD62L+, T effector memory (TEM) as CD44+ CD62L- and T central memory cells (TCM) as CD44+ CD62L+. Percentage of CD4+ (A and C) and CD8+ (B and D) memory T cells of the total CD4+ or CD8+ T cell population at each time-point in (A and B) gingivae and (C and D) draining lymph nodes (dLN). Cells from 5 gingivae of each group were pooled, as were lymph node cells. Data are shown as mean + SEM and are from 1 experiment at 14 days and combined from 2 independent experiments at 7 and 28 days, n = 5 mice/group at each time-point. Statistical insignificance was determined by unpaired T tests.

The hallmark of PD is alveolar bone destruction that occurs from, arguably, reduced regulation of the immune response. As the role of Tregs is to maintain an appropriate immune response, the number and proportion of these cells within the gingivae and dLN were investigated by flow cytometry (**figure 4.7**). However, no differences were found in Treg numbers or percentages of the total CD4+ population in infection compared with controls at 7 and 14 days post infection, in either gingivae or dLNs (**figure 4.8**). Whilst not significant, there was a trend towards a decrease in Tregs within the gingivae in *P. gingivalis*-infection at 28 days post infection, both in percentage (mean 8.82 +/- 1.68 sham vs. mean 7.11 +/- 1.47 *P. gingivalis*, NS) and number (mean 1191.5 +/- 141.5 sham vs. mean 642 +/- 189.0 *P. gingivalis*, NS). This was comparable to dLNs in infection, whereby a decrease in Tregs could be seen – again in both percentage (mean 12.6 +/- 1.0 sham vs. mean 12.1 +/- 0.4 *P. gingivalis*, NS) and number (mean 1.56 x 10^4 +/- 695 sham vs. mean 1.30 x 10^4 +/- 498 *P. gingivalis*, NS) – but this did not reach statistical significance.

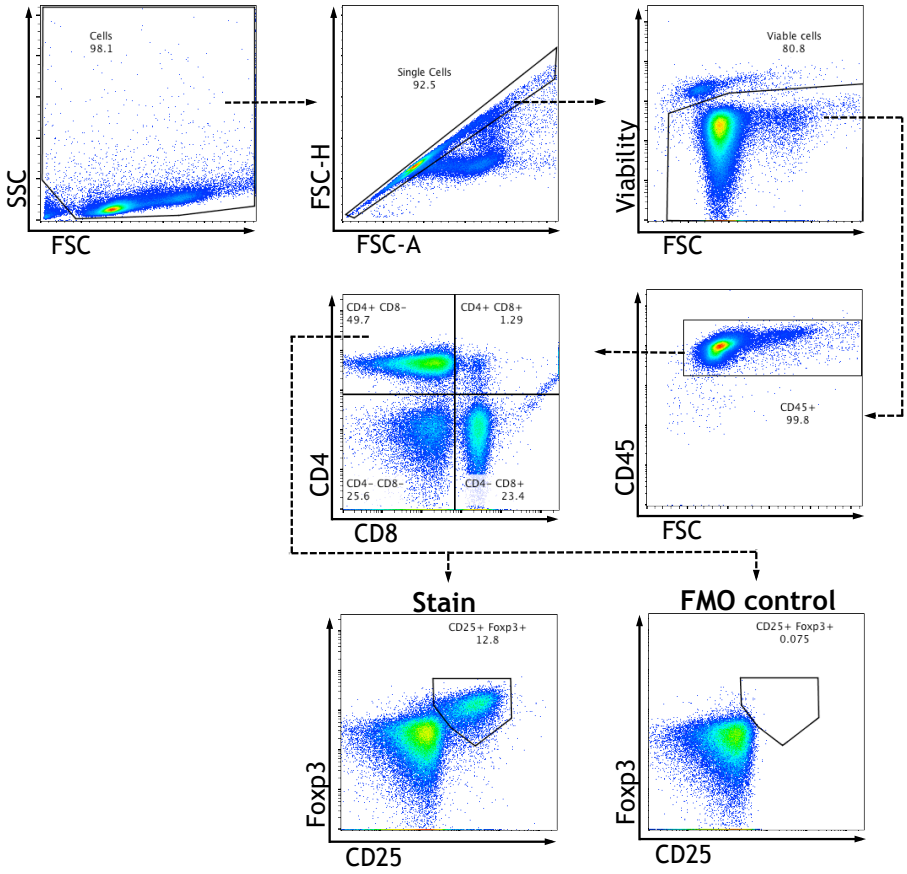

Figure 4.7. Example of gating strategy used to identify regulatory T cells by flow cytometry.

Mice were orally infected with *P. gingivalis* or were sham-infected (sham) with carrier vehicle, CMC, only. At 7, 14 and 28 days post infection cells were isolated from gingivae and draining lymph nodes and regulatory T cells (Tregs) analysed by flow cytometry. Dead cells and debris were excluded, based on forward scatter (FSC) and side scatter (SSC), followed by doublet discrimination. Viable, CD45+ cells were then gated upon to assess CD4+ and CD8+ T cells. Tregs can be identified in the CD4+ T cell population based on expression of both CD25 and Foxp3. The fluorescence minus one (FMO) control sample was stained with all of the markers in the gating strategy, excluding Foxp3 and CD25. The example plot is from sham-infected LN cells at 7 days post infection.

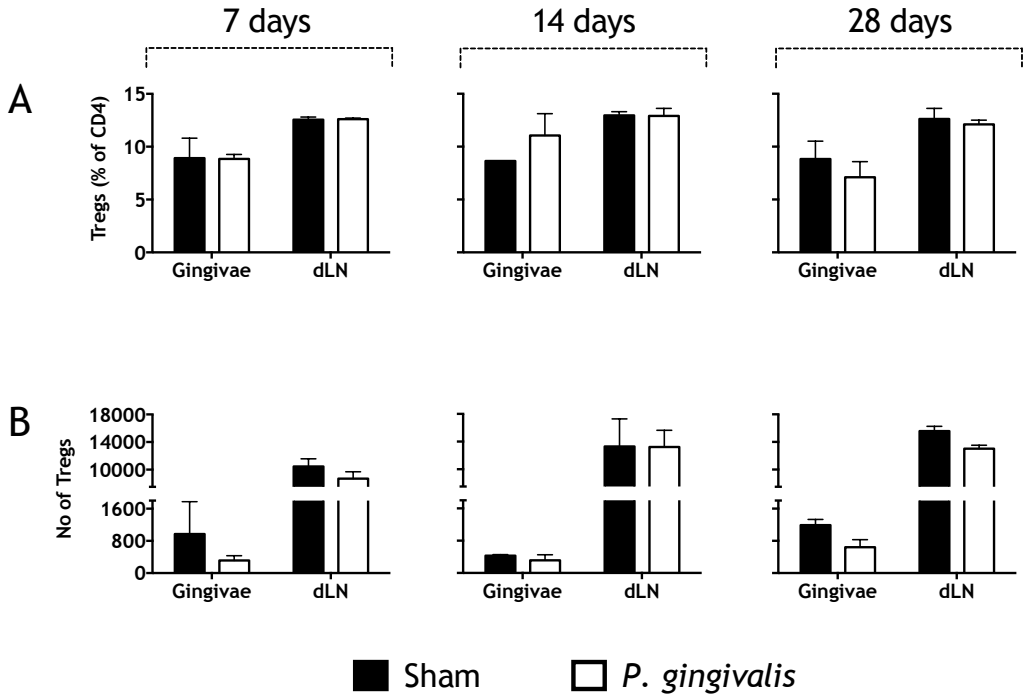

Figure 4.8. Regulatory T cells from gingivae and draining lymph nodes at 7, 14 and 28 days post *P. gingivalis* infection.
Mice were orally infected with *P. gingivalis* or were sham-infected (sham) with carrier vehicle, CMC, only. At 7, 14 and 28 days post infection cells were isolated from gingivae and draining lymph nodes and regulatory T cells (Tregs) analysed by flow cytometry. Tregs were identified as CD4+ CD25+ FOXP3+ cells. (A) Percentage of Tregs of the total CD4+ T cell population in indicated tissues at each time-point. (B) Number of Tregs in indicated tissues at each time-point. Cells from 5 gingivae of each group were pooled, as were lymph node cells. Data are shown as mean + SEM and are combined from 2 independent experiments, n = 5 mice/group. Statistical insignificance was determined by unpaired T tests.

As mice produced anti-*P. gingivalis* IgG antibodies systemically, it could be concluded that B cells were playing a role in the infection. B cells require help from Tfh cells to differentiate into antibody producing plasma cells. Therefore, the proportion of Tfh cells in the dLN following infection was analysed by flow cytometry (**figure 4.9**). Bcl-6 is a transcription factor required for the development of Tfh cells and with the upregulation of CXCR5, Tfh cells can migrate to germinal centres within LNs to provide B cell help (Baumjohann and Ansel, 2013). Tfh cells have also been shown to produce high levels of both ICOS and PD-1 (Crotty, 2011, Haynes et al., 2007). As such, these markers were used to identify Tfh cells. At 14 days post *P. gingivalis* infection, the percentage of CD4+ T cells that expressed Bcl-

6 was significantly increased by comparison to cells from control dLNs (mean 0.127 +/- 0.012 sham vs. mean 0.336 +/- 0.019 *P. gingivalis*, P < 0.0001). This was also true of the numbers of CD4+ Bcl6+ cells (mean 171.4 +/- 10.95 sham vs. mean 459.8 +/- 35.48 *P. gingivalis*, P < 0.0001) (**figure 4.10**). The population of CD4+ Bcl6+ cells was too small to accurately quantify the proportions of cells expressing ICOS and PD-1. Nonetheless, there were a greater proportion of CD4+ cells with expression of both ICOS and PD-1 (mean 0.456 +/- 0.046 sham vs. mean 1.862 +/- 0.188 *P. gingivalis*, P < 0.0001). The increase in CD4+ ICOS+ PD-1+ cell numbers in infection was also statistically significant (mean 637.2 +/- 100.9 sham vs. mean 3465 +/- 712.7 *P. gingivalis*, P < 0.01). No cells were stained with anti-CXCR5 antibody. Limitations of time and resource prevented further investigation and optimization of this staining. Without this marker, the presence of Tfh cells cannot be definitively concluded, however, with the presence of Bcl-6, ICOS and PD-1, it is likely that the dLNs of mice infected with *P. gingivalis* did contain Tfh cells.

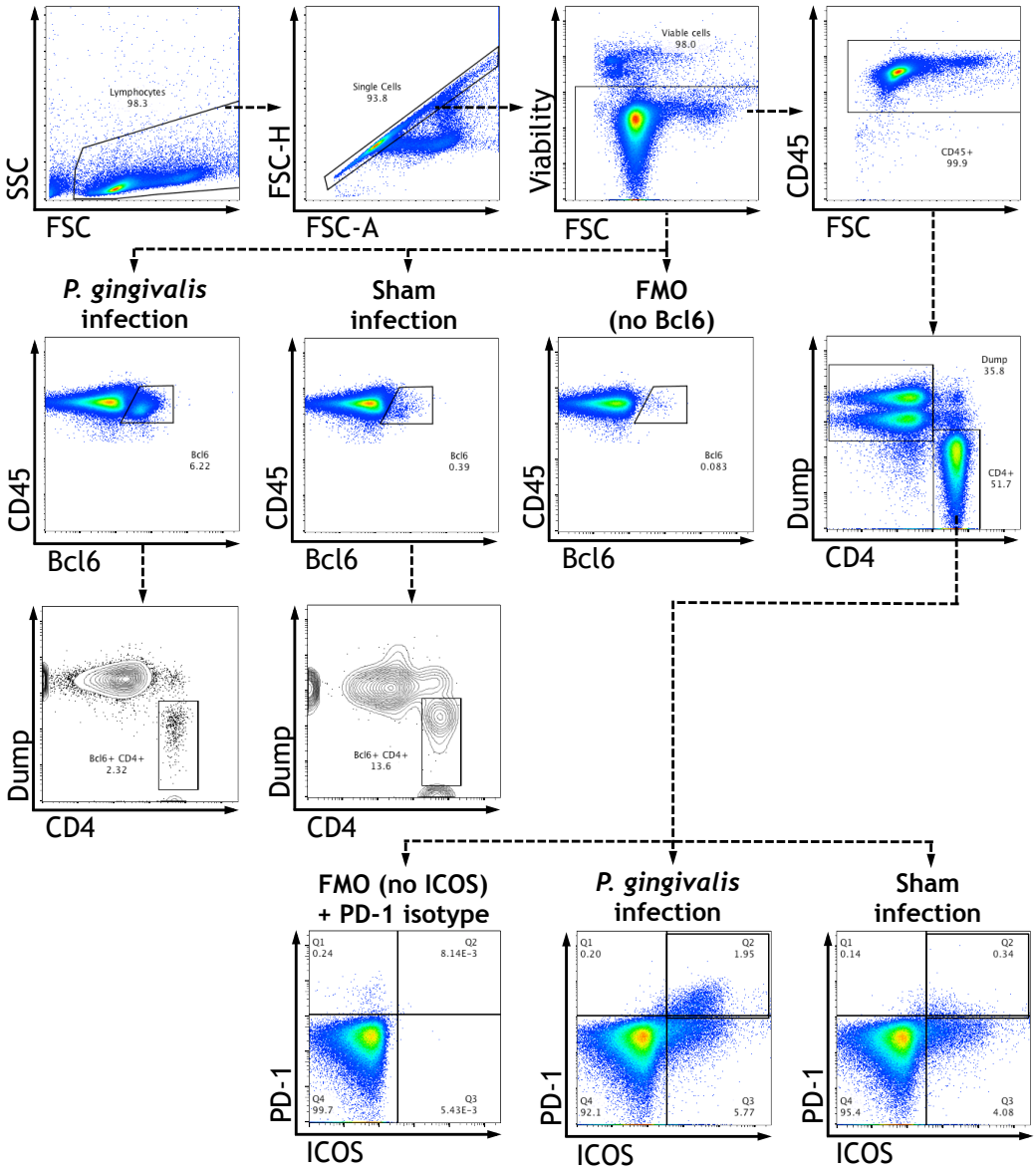

Figure 4.9. Example of gating strategy to identify T follicular helper cells by flow cytometry.
Mice were orally infected with *P. gingivalis* or were sham-infected (sham) with carrier vehicle, CMC, only. At 14 days post infection cells were isolated from draining lymph nodes and T follicular helper cells analysed by flow cytometry. Dead cells and debris were excluded, based on forward scatter (FSC) and side scatter (SSC), followed by doublet discrimination. Viable, CD45+ Bcl6+ cells were then gated to assess CD4+ T cells with T follicular helper cell transcription factor expression. A dump gate included CD8, B220 and F4/80 to ensure no inclusion of the cells commonly known to express T follicular helper markers. The fluorescence minus one (FMO) control samples were stained with all of the markers in the gating strategy, excluding Bcl6 or ICOS along with a PD-1 isotype control antibody, as indicated in the figure. The example plots are from sham and *P. gingivalis*-infected LN cells.

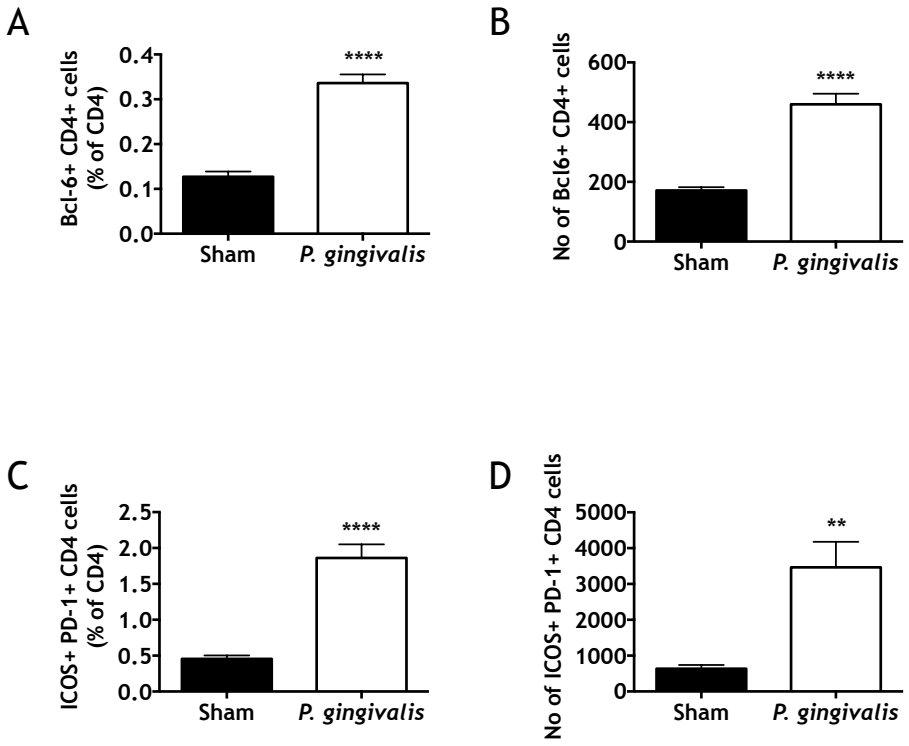

Figure 4.10. T follicular helper cells in draining lymph nodes at 14 days post *P. gingivalis* infection.
Mice were orally infected with *P. gingivalis* or were sham-infected (sham) with carrier vehicle, CMC, only. At 14 days post infection cells were isolated from draining lymph nodes and T follicular helper cells analysed by flow cytometry. (A) Percentage of Bcl6+ CD4+ T cells of the total CD4+ T cell population. (B) Number of Bcl6+ CD4+ T cells. (C) Percentage of ICOS+ PD-1+ CD4+ T cells of the total CD4 population. (D) Number of ICOS+ PD-1+ CD4+ T cells. Data are shown as mean + SEM from 1 experiment, n = 5 mice/group, LN from each mouse analysed individually. Statistical significance was determined by unpaired T tests, as indicated on the graph (**P < 0.01, ***P < 0.001 and ****P < 0.0001).

Serum IgG antibodies suggested that mice infected with *P. gingivalis* generated a systemic response reflecting that of Th1 immunity. To determine the Th response locally, cytokines indicative of Th subsets were analysed. Mice were orally infected with sham or *P. gingivalis* and at 7, 14 and 28 days post infection cells from gingivae and dLNs were isolated. The percentage and number of cytokine producing cells were assessed by intracellular cytokine staining and flow cytometry (**figure 4.11**). At 7 days post infection, there were no differences in cytokine production, although the experiment was conducted only once (**figure 4.12**). As no obvious

trends between control and infection could be seen, repetition of the experiment and use of additional mice could not be justified. At 14 days post infection, although no changes in IL-4 and IL-17A production by the infected group were found, there was a trend towards an increased percentage of IFN-γ producing cells of the CD4+ population in dLNs (mean 0.664 +/- 0.119 sham vs. 0.968 +/- 0.243 *P. gingivalis*, NS). A similar pattern of cytokine expression could be observed at 28 days post infection, whereby IFN-γ production was increased in *P. gingivalis* infection in dLNs, particularly when comparing control and infection by fold change of media control (mean 7.569 +/- 1.985 sham vs. 28.394 +/- 6.843 *P. gingivalis*, NS). As observed at previous time points, at day 28 there were no differences in IL-4 and IL-17A.

The cytokine production by T cells in the gingivae did not resemble the seemingly increased Th1 response from dLNs, but instead highlighted no differences between control and infected mice at any of the time-points (**figure 4.13**).

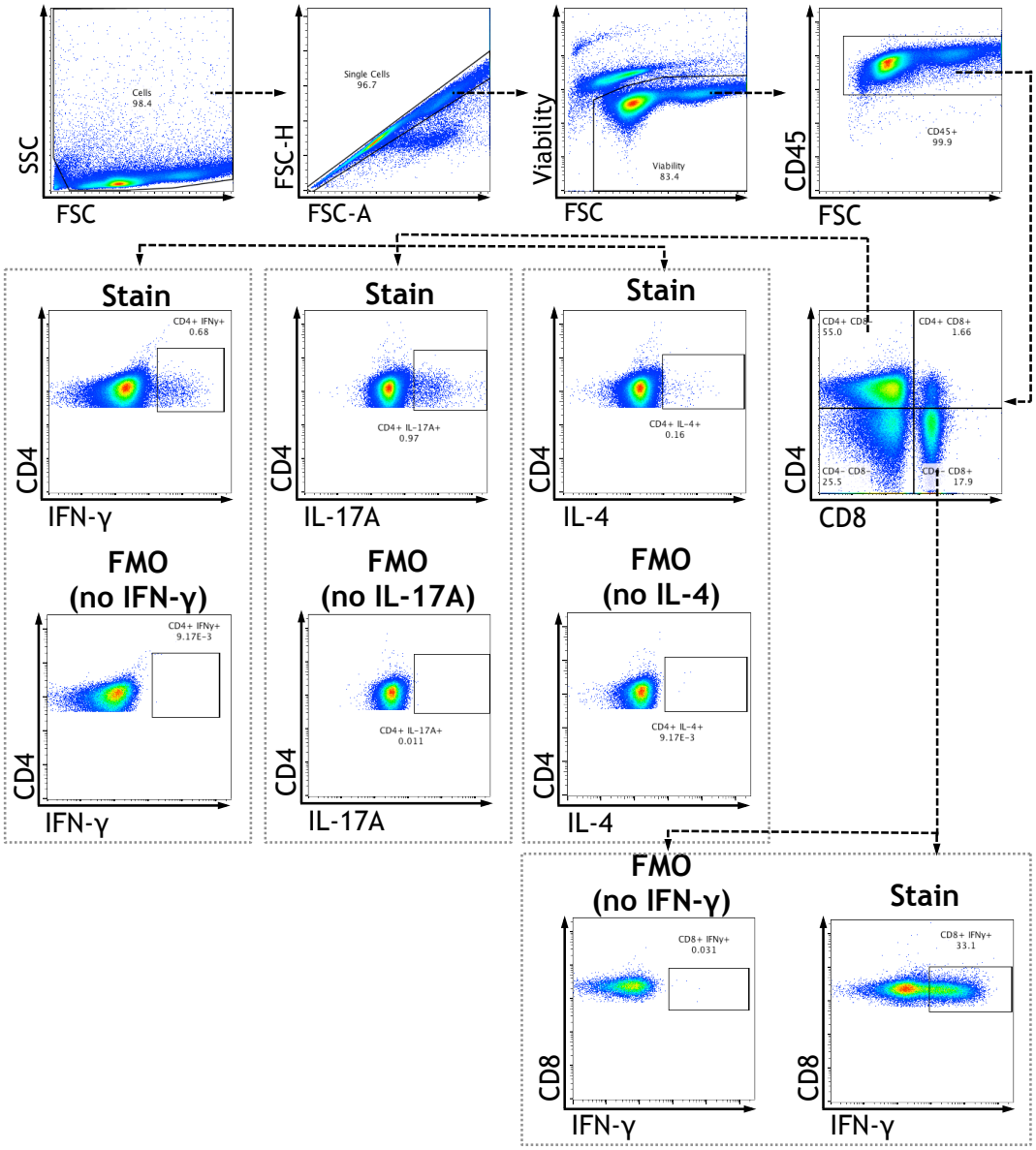

Figure 4.11. Example of gating strategy used to identify cytokine producing T cells.

Mice were orally infected with *P. gingivalis* or were sham-infected (sham) with carrier vehicle, CMC, only. At 7, 14 and 28 days post infection cells were isolated from draining lymph nodes. The isolated cells were stimulated with PMA/ionomycin or controls received only media and also incubated with BD GolgiStop™ for 4 hours then analysed by flow cytometry. Dead cells and debris were excluded, based on forward scatter (FSC) and side scatter (SSC), followed by doublet discrimination. Viable, CD45+ cells were then gated to identify CD4+ and CD8+ T cells. Cytokine producing CD4+ and CD8+ T cells were then identified. The fluorescence minus one (FMO) control samples were stained with all of the markers in the gating strategy, excluding IFN-γ, IL-17A or IL-4, as indicated in the figure. The example plots are from sham-infected lymph node cells stimulated with PMA/ionomycin from a 7 days post infection model.

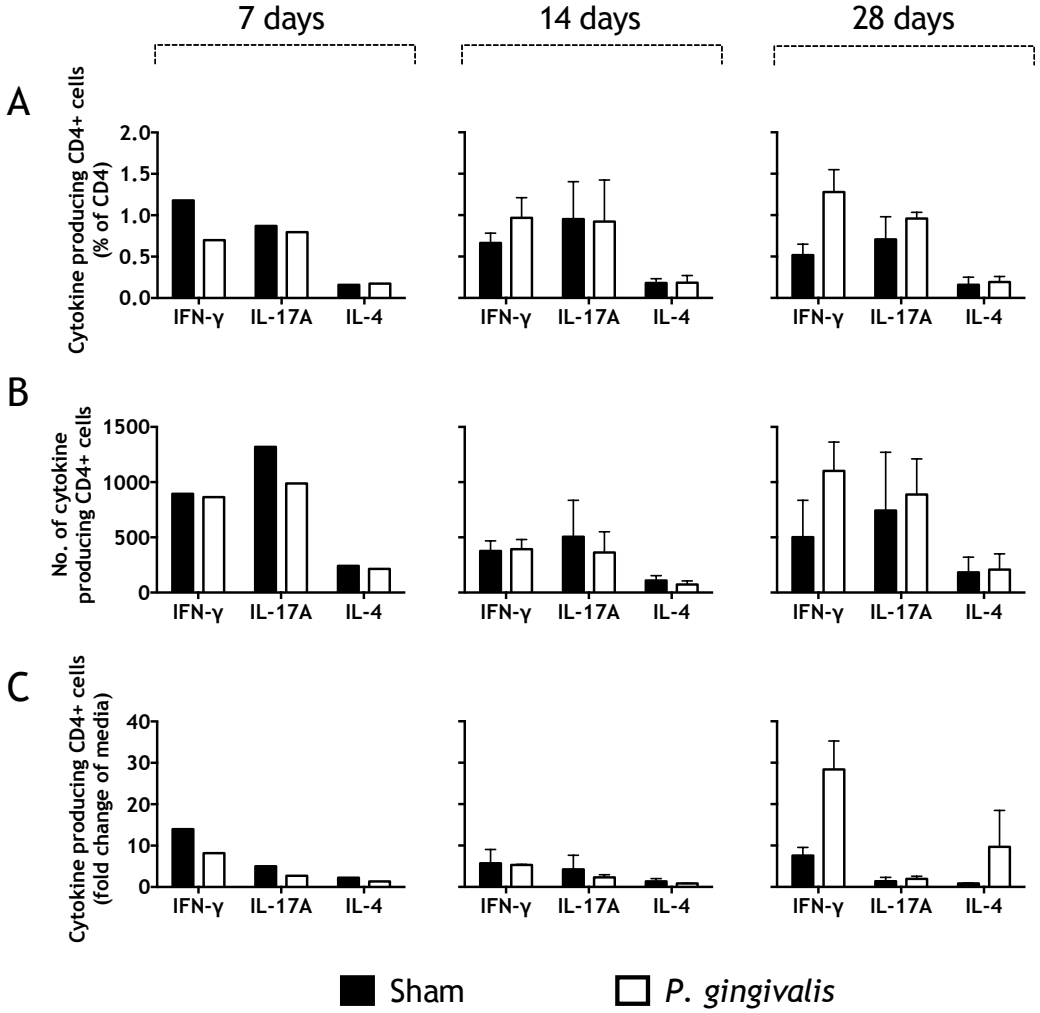

Figure 4.12. T helper cell cytokine production in draining lymph nodes at 7, 14 and 28 days post *P. gingivalis* infection.

Mice were orally infected with *P. gingivalis* or were sham-infected (sham) with carrier vehicle, CMC, only. At 7, 14 and 28 days post infection cells were isolated from draining lymph nodes. The isolated cells were stimulated with PMA/ionomycin or controls received only media and all were incubated with BD GolgiStop™ for 4 hours then analysed by flow cytometry. (A) Percentage of PMA/ionomycin-stimulated CD4+ T cells producing indicated cytokines of the total CD4+ T cell population, at each time-point. (B) Number of PMA/ionomycin-stimulated CD4+ T cells producing indicated cytokines at each time-point. (C) Fold change of number of stimulated cytokine-producing CD4+ T cells compared to number of cytokine-producing CD4+ T cells from media controls. Cells from 5 lymph nodes were pooled from each group. Data are shown as mean + SEM from 1 experiment at 7 days and combined from 2 independent experiments at 14 and 28 days, n = 5 mice/group at each time-point. Statistical insignificance was determined by unpaired T test.

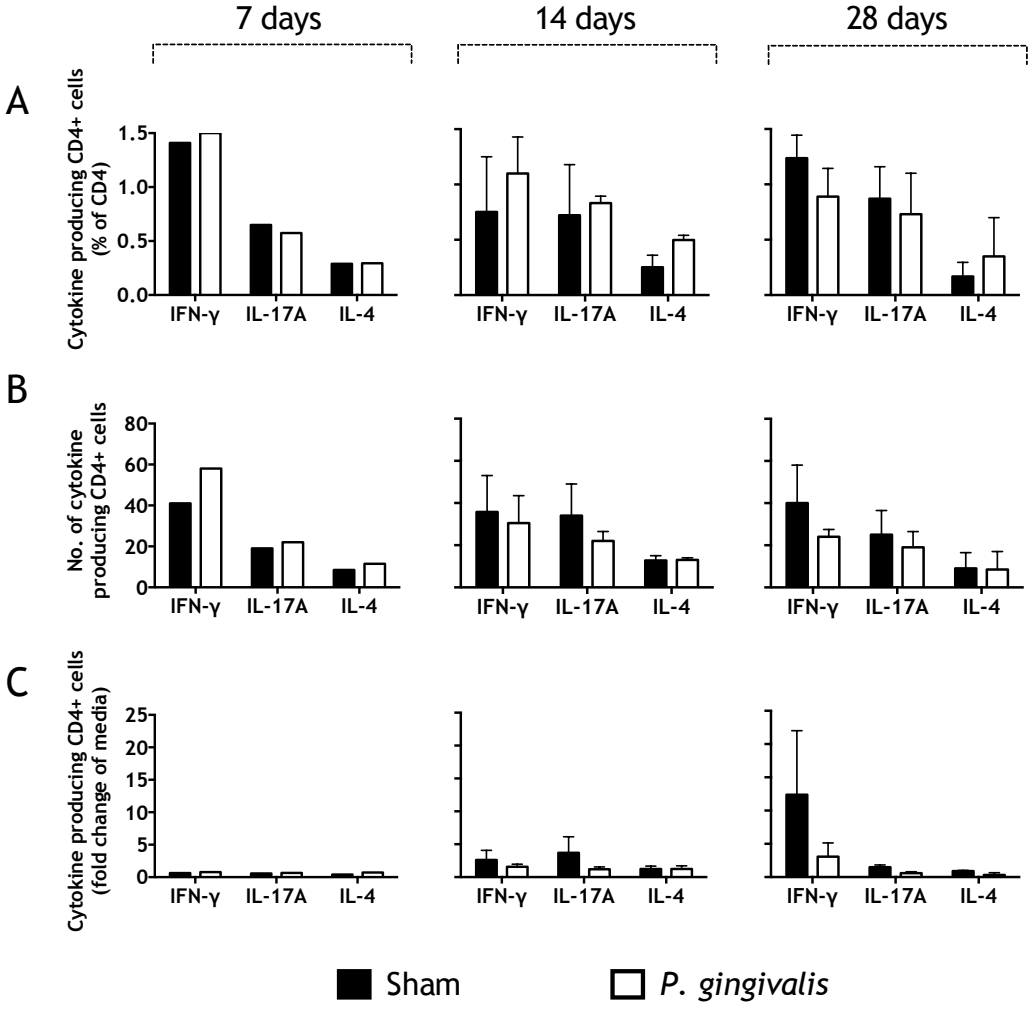

Figure 4.13. T helper cell cytokine production in gingivae at 7, 14 and 28 days post *P. gingivalis* infection.

Mice were orally infected with *P. gingivalis* or were sham-infected (sham) with carrier vehicle, CMC, only. At 7, 14 and 28 days post infection cells were isolated from gingivae. The isolated cells were stimulated with PMA/ionomycin or controls received only media. Cells were incubated with BD GolgiStop™ for 4 hours then analysed by flow cytometry. (A) Percentage of PMA/ionomycin-stimulated CD4+ T cells producing indicated cytokines of the total CD4+ T cell population, at each time-point. (B) Number of PMA/ionomycin-stimulated CD4+ T cells producing indicated cytokines at each time-point. (C) Fold change of number of stimulated cytokine-producing CD4+ T cells compared to number of cytokine-producing CD4+ T cells from media controls. Cells from 5 gingivae were pooled from each group. Data are shown as mean + SEM from 1 experiment at 7 days and combined from 2 independent experiments at 14 and 28 days, n = 5 mice/group at each time point. Statistical insignificance was determined by multiple unpaired T tests.

As *P. gingivalis* has the ability to infect cells intracellularly, CD8+ T cell IFN-γ production was next assessed by flow cytometry. Infected and sham control animals showed similar proportions of IFN-γ producing CD8+ T cells at 7 or 28 days post infection in the gingivae. At 14 days, the percentage of CD8+ T cells producing IFN-γ was greater in the gingivae of *P. gingivalis* infected mice (mean 9.32 +/- 0.96 sham vs. mean 20.85 +/- 1.70 *P. gingivalis*, $P < 0.05$) (**figure 4.14**). At both 7 and 14 days post infection, there were no effects of *P. gingivalis*-infection on the percentage or number of IFN-γ-producing CD8+ T cells from dLNs. At 28 days post infection, there was an increase in IFN-γ production by CD8+ T cells, although this did not reach statistical significance (mean 222.26 +/- 189.35 sham vs. 892.40 +/- 767.21 *P. gingivalis*, NS). The variation between experiments was high; thereby the increase in IFN-γ by CD8+ T cells at this time-point was not significant. However, consistent in both experiments was that cytokine production is approximately 4 times (3.804 from experiment 1 and 4.032 from experiment 2) greater in dLNs of mice infected with *P. gingivalis* than sham-infected control, using data from fold change of media control.

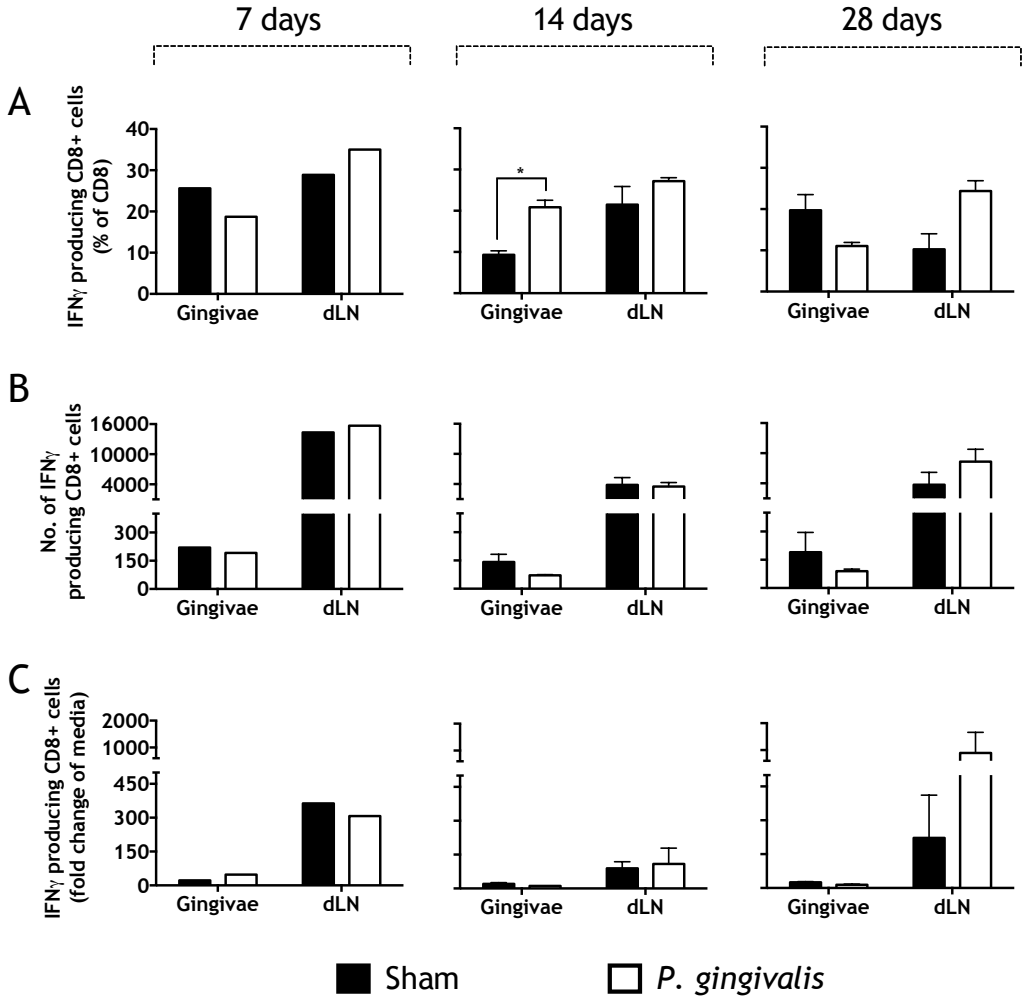

Figure 4.14. IFN-γ producing CD8+ T cells in gingivae and draining lymph nodes at 7, 14 and 28 days post *P. gingivalis* infection.
Mice were orally infected with *P. gingivalis* or were sham-infected (sham) with carrier vehicle, CMC, only. At 7, 14 and 28 days post infection cells were isolated from gingivae and draining lymph nodes. The isolated cells were stimulated with PMA/ionomycin or controls received only media and were incubated with BD GolgiStop™ for 4 hours then analysed by flow cytometry. (A) Percentage of PMA/ionomycin-stimulated CD8+ T cells producing IFN-γ of the total CD8+ T cell population, at each time-point. (B) Number of PMA/ionomycin-stimulated CD8+ T cells producing IFN-γ at each time-point. (C) Fold change of number of stimulated IFN-γ-producing CD8+ T cells compared to number of IFN-γ-producing CD8+ T cells from media controls. Cells from 5 gingivae were pooled from each group, as were lymph node cells. Data are shown as mean + SEM from 1 experiment at 7 days and combined from 2 independent experiments at 14 and 28 days, n = 5 mice/group. Statistical significance was determined by unpaired T tests, as indicated on the graph (*$P < 0.05$).

To assess the systemic response in the PD model, splenocytes from sham and *P. gingivalis*-infected mice were restimulated with *P. gingivalis*, incubated for 72 hours and the proliferation (anti-Ki67) state of CD4+ and CD8+ T cells was determined by flow cytometry. The results indicated that *P. gingivalis* induced a similar extent of splenocyte proliferation from sham and *P. gingivalis*-infected mice. The proliferation stimulated by *P. gingivalis* was lower than that induced by anti-CD3 and anti-CD28 (data not shown). The supernatants from the assays were collected and the level of IFN-γ measured by ELISA. IFN-γ was selected due to indications from flow cytometry experiments that there were trends towards increased production of this cytokine by CD4+ and CD8+ T cells at 28 days post infection. The ELISA demonstrated that IFN-γ was increased by splenocytes from *P. gingivalis*-infected mice upon restimulation with *P.* gingivalis at 28 days post infection (mean 1132.10 +/- 193.53 pg/ml sham vs. mean 2028.90 +/- 315.67 pg/ml *P. gingivalis*, $P < 0.05$) (**figure 4.15**).

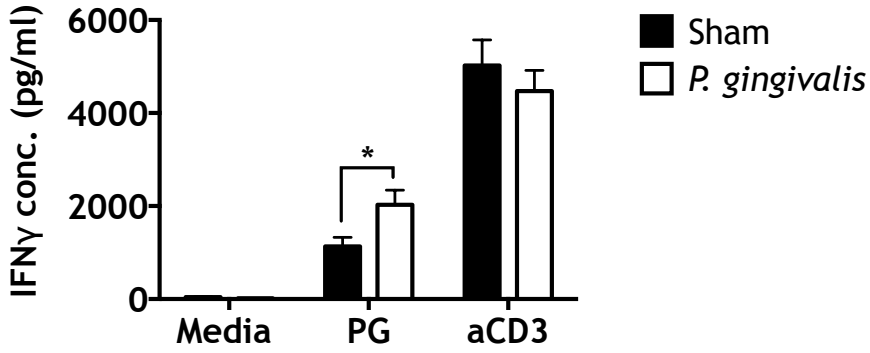

Figure 4.15. IFN-γ production by splenocytes incubated with *P. gingivalis*.
Mice were orally infected with *P. gingivalis* or were sham-infected (sham) with carrier vehicle, CMC, only. At 28 days post infection, cells were isolated from spleens and stimulated with heat-killed *P. gingivalis* (PG), media (negative control) and anti-CD3 and anti-CD28 (aCD3) (positive control) for 72 hours. The supernatants were analysed for IFN-γ by ELISA. Data are shown as mean + SEM from 1 experiment, n = 5 mice/group. Statistical significance was determined by unpaired T tests, as indicated on the graph (*$P < 0.05$).

The concentrations of IL-6, IL-10, IL-13, IL-17A and IFN-γ in supernatants were then determined by multiplex to further evaluate systemic Th responses (**figure 4.16**). The production of all cytokines investigated was upregulated somewhat – although not significantly – by splenocytes from *P. gingivalis*-infected mice at 7, 14 and 28 days post infection. At 14 days post infection, there was a significant increase in IFN-γ, IL-13 and IL-10 production by splenocytes from *P. gingivalis* infected mice (IFN-γ: mean 500.59 +/- 180.63 pg/ml sham vs. 2627.48 +/- 589.944 pg/ml *P. gingivalis*, $P < 0.05$. IL-13: mean 1410.98 +/- 540.13 pg/ml sham vs. mean 4555.44 +/- 942.35 pg/ml *P. gingivalis*, $P < 0.05$. IL-10: mean 83.83 +/- 22.53 pg/ml sham vs. mean 339.50 +/- 88.26 pg/ml *P. gingivalis*, $P < 0.05$). At 28 days post infection, IL-6 was significantly increased from splenocytes of *P. gingivalis*-infected mice (mean 169.36 +/- 15.76 pg/ml sham vs. mean 296.95 +/- 41.00 pg/ml *P. gingivalis*, $P < 0.05$). As a number of cytokines were elevated by re-stimulation of splenocytes from *P. gingivalis*-infected mice, there was a suggestion of a systemic inflammatory response. There was no obvious cytokine profile of a particular Th response in *P. gingivalis* infection from splenocytes.

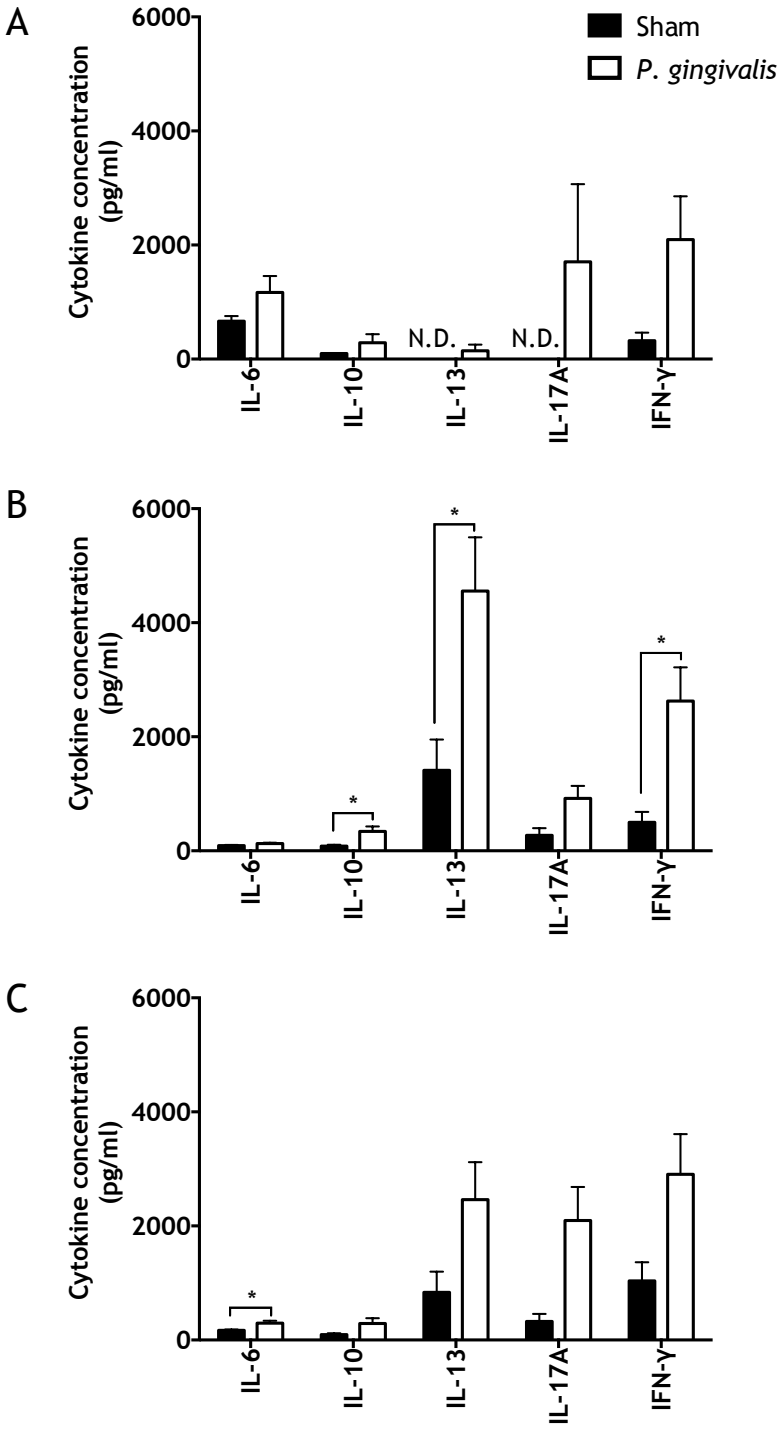

Figure 4.16. Cytokine production by *P. gingivalis* stimulated splenocytes
Mice were orally infected with *P. gingivalis* or were sham-infected (sham) with carrier vehicle, CMC, only. At 7, 14 and 28 days post infection, cells were isolated from spleens and stimulated with heat-killed *P. gingivalis* for 72 hours. The supernatant was analyzed for cytokines using multiplex technology. Concentrations of IL-6, IL-10, IL-13, IL-17A and IFN-γ at (A) 7 days, (B) 14 days and (C) 28 days post infection. Data are shown as mean + SEM from 1 experiment at 7 days post infection, and combined from 3 and 4 independent experiments at 14 and 28 days post infection, respectively, n = 5 mice/group. Statistical significance was determined by multiple T tests and Holm-Sidak multiple comparison correction, as indicated on the graph (*P < 0.05).

Thus far, phenotyping of T cells has involved the disruption of cells from their anatomical position within tissue. For this reason, the next experiments looked to address the location and distribution of T cells within tissue. Initially, gingival tissue was fixed and embedded in paraffin wax, then sectioned. H&E staining of the sections (**figure 4.17**) revealed that an even section could not be obtained, the 'ruffled' architecture of the palatal ruggae caused large gaps in the section and that the tissue was prone to tearing. As a result, gingivae were stained 'wholemount' with fluorescent antibodies to CD4 and B220 and were imaged using a confocal microscope (**figure 4.18**).

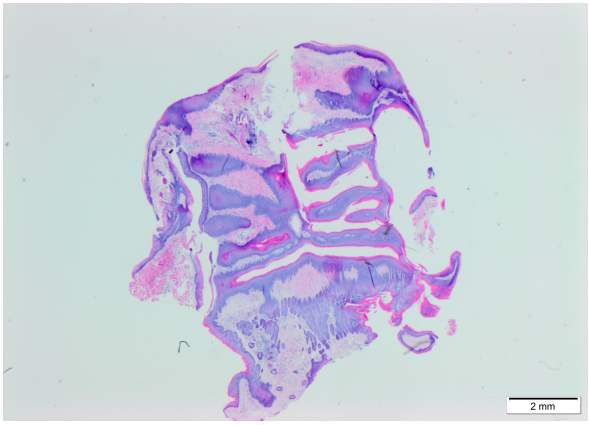

Figure 4.17. H&E staining of sectioned gingiva.
Gingiva was extracted from the mouth of a mouse, formalin fixed and paraffin embedded. Five µm sections were cut using a microtome and stained by H&E. Olympus SZX7 stereo zoom microscope fitted with SC100 digital color camera was used to capture the image. Scale bar represents 2 mm.

The images in **figure 4.20A** enabled visualization of CD4+ T cells and B220+ B cells within lymphoid aggregates, in which CD4+ T cells clustered around a clearly defined B cell population. Very few CD4+ T cells or B cells were visible out with these aggregates. The single stain controls illustrated that the staining of the cells was not simply the result of autofluorescence (**figure 4.20B-C**). To determine the orientation of the lymphoid structures a suture was placed in the bottom right hand side of the palate. With the suture in place, the location of these aggregates was found to be within the hard palate, at the uppermost region closest to the central incisors.

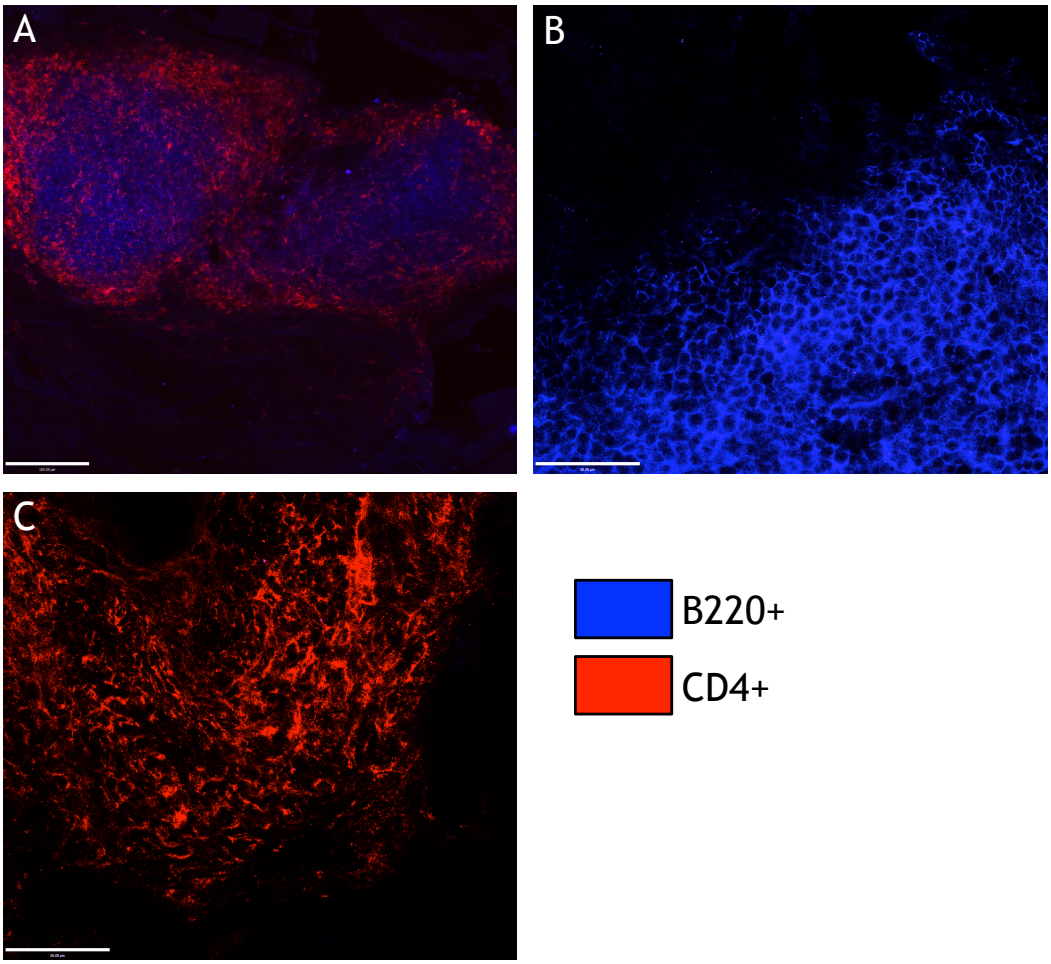

Figure 4.18. Fluorescent microscopy of intact gingiva.
Gingivae were extracted from the mouths of mice and paraformaldehyde fixed. Samples were stained with fluorescent anti-B220 (blue) and anti-CD4 (red) antibodies then visualized using a confocal microscope. (A) Gingiva stained with anti-B220 and anti-CD4. Scale bar represents 150 µm (B) Gingiva single stain control stained with anti-B220 only. Scale bar represents 50 µm (C) Gingiva single stain control stained with anti-CD4. Scale bar represents 50 µm.

Next, mice were sham- or *P. gingivalis*-infected and the lymphoid aggregates within the oral mucosa were imaged at various stages post infection to assess whether *P. gingivalis* influenced a notable change in these structures. At 14, 35 and 49 days post infection, irrespective of infection status, clearly defined populations of CD4+ T cells and B cells were seen (**figure 4.19**). As implied by the memory T cell data by which the gingivae was predominated by naïve T cells (**figure 4.6A**), lymphoid aggregates were present in this tissue irrespective of *P. gingivalis*-infection. Although the majority of CD4+ T cells resided around a clustering of B cells in both

control and infected mice, a number of CD4+ T cells migrated into the B cell area. These data suggest that CD4+ T cells may be providing B cell help in both oral infection states.

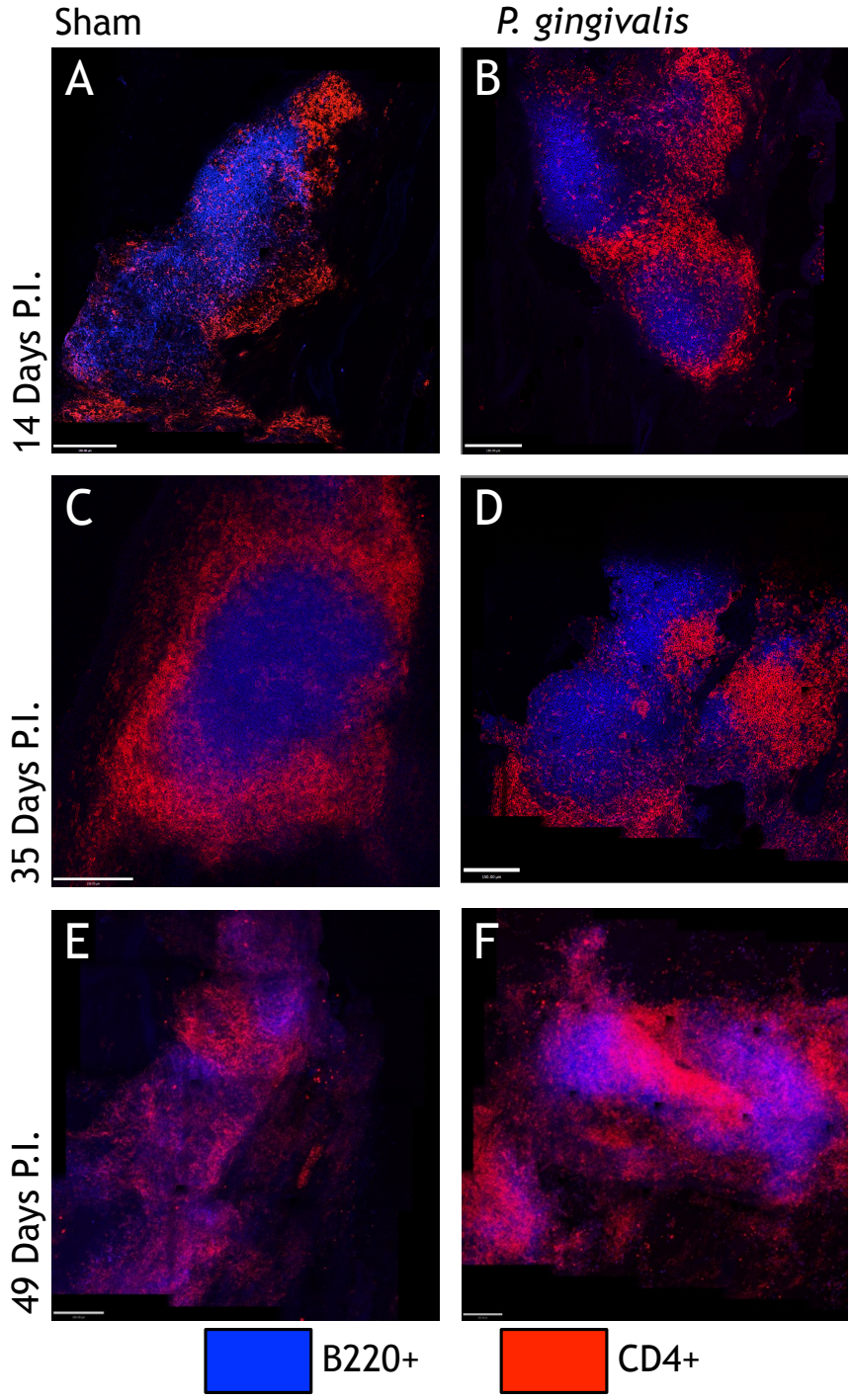

Figure 4.19. Fluorescent microscopy of intact gingivae at 14, 35 and 49 days post *P. gingivalis* infection.
Mice were orally infected with *P. gingivalis* (B, D, F) or were sham-infected (sham) with carrier vehicle, CMC (A, C, E), only. At 14 (A and B), 35 (C and D) and 49 (E and F) days post infection gingivae were extracted from the mouths of mice and paraformaldehyde fixed. Samples were stained wholemount with fluorescent anti-B220 (blue) and anti-CD4 (red) antibodies then visualized using a confocal microscope. (A-D) Scale bar represents 150 µm. (E-F) Scale bar represents 100 µm. Representative of n = 3.

To investigate the expression of a broader range of cytokines and chemokines than could be practically achieved by intracellular staining and flow cytometry, gene expression was next assessed by qRT-PCR using a Qiagen cytokine and chemokine array. As the greatest trends in CD4+ T cell cytokine production and numbers of Tregs were noted at 28 days post infection, along with an interest in the stage at which alveolar bone loss develops, this time point was investigated. Mice were sham or *P.* gingivalis-infected as previous PD models. Groups contained three mice. For the array, the entire gingival cell isolate from a single mouse was sufficient for analysis, hence three mice per group enabled generation of three independent data points. Cells from three sham-infected and three *P. gingivalis*-infected mice expressed each of the housekeeping genes in the array. Likewise, positive PCR controls and reverse transcription controls were positive for each sample. There was indication of gDNA contamination in both the gingivae and dLN samples from one of the three experiments. This experimental replicate was therefore excluded from further analysis. Of the 5 housekeeping genes in the assay, *Actb* expression (actin ß) was the most conserved amongst the samples, hence was chosen to determine relative expression of test genes.

From the 84 test genes in the array, 21 genes were differentially expressed between the groups compared (control vs infection and gingivae vs. dLN) and are shown in **figure 4.20**. Six genes were significantly differentially expressed in gingivae from sham compared to *P. gingivalis*-infected mice (**figure 4.20A**). Il-1α is released from stressed or dead cells and acts as an alarmin. The expression of *ila* was – not surprisingly – increased in *P. gingivalis* infection (mean 7.38×10^{-3} +/- 8.79×10^{-4} sham vs. mean 1.55×10^{-2} +/- 1.67×10^{-3} *P. gingivalis*, $P < 0.05$). IL-7 is important for lymphocyte development in the bone marrow and thymus. It also interacts with TCRs on mature CD4+ and CD8+ cells to promote survival (Kondrack et al., 2003, Kaech et al., 2003). Expression of *Il7* gene was reduced in *P. gingivalis*-infection (mean 1.85×10^{-3} +/- 7.00×10^{-5} sham vs. mean 6.78×10^{-4} +/- 5.96×10^{-5} *P. gingivalis*, $P < 0.01$). Cardiotrophin-1 is involved in the protection of cardiac myocytes from injury due to ischemia or reperfusion, and also prevents apoptosis. *Ctf1* expression was upregulated in *P. gingivalis* infection (mean 1.00×10^{-3} +/- 5×10^{-5} sham vs. mean 3.00×10^{-3} +/- 4×10^{-4} *P. gingivalis*, $P < 0.05$). The product of

Gpi1 expression is glucose phosphate isomerase 1. Glucose phosphate isomerase 1 exerts a range of effects, including an involvement in the interconversion of glucose-6-phosphate to fructose-6-phosphate. Perhaps most interesting with regard to the PD model, glucose phosphate isomerase 1 stimulates immunoglobulin secretion (https://www.ncbi.nlm.nih.gov/gene – accessed on 04/04/17). Glucose phosphate isomerase 1 was increased in *P. gingivalis* infection (mean 6.20×10^{-2} +/- 5.21×10^{-3} sham vs. mean 1.31×10^{-1} +/- 5.00×10^{-4} *P. gingivalis*, $P < 0.05$), possibly reflecting the increase in anti-*P. gingivalis* IgG. *Bmp4* expression was also upregulated in gingivae of *P. gingivalis*-infected mice (mean 3.00×10^{-3} +/- 5.00×10^{-5} sham vs. mean 4.00×10^{-3} +/- 4.00×10^{-4} *P. gingivalis*, $P < 0.05$). Embryos of the bone morphogenetic protein (BMP) 4 KO mice develop bilateral cleft lip; therefore BMP4 has been described as a regulator of lip fusion during midfacial morphogenesis. The final gene differentially expressed (down-regulated) in the gingivae of *P. gingivalis*-infected mice was *Tnfsf13b*. TNF (ligand) superfamily member 13B (otherwise known as B-cell activating factor) plays a role in proliferation and differentiation of B cells (Mackay and Browning, 2002).

Within the dLNs, only *Bmp7* expression was down-regulated upon *P. gingivalis* infection (mean 2.00×10^{-4} +/- 4.28×10^{-6} sham vs. mean 1.00×10^{-4} +/- 1.08×10^{-6} *P. gingivalis*, $P < 0.01$) (**figure 4.20B**). BMP7 plays a role in eye, brain, palate and ear development (Wyatt et al., 2010). The greatest variation in gene expression was noted between gingivae and dLN (**figure 4.20C-D)**. Genes differentially expressed between the two different tissues and their functions are described in **table 4.1** and **table 4.2**.

As the RT^2 profiler was employed as an exploratory platform to identify chemokine and cytokine genes that were differentially expressed in the PD model, the statistical analysis was devoid of post hoc corrections for multiple T tests. A caveat of this approach was that false positives could be incorporated into the analysis. However, the application of post hoc correction may have included false negatives. Therefore, it was concluded that as an exploratory experiment to pinpoint potential gene candidates it was more beneficial to eliminate false negative statistical tests.

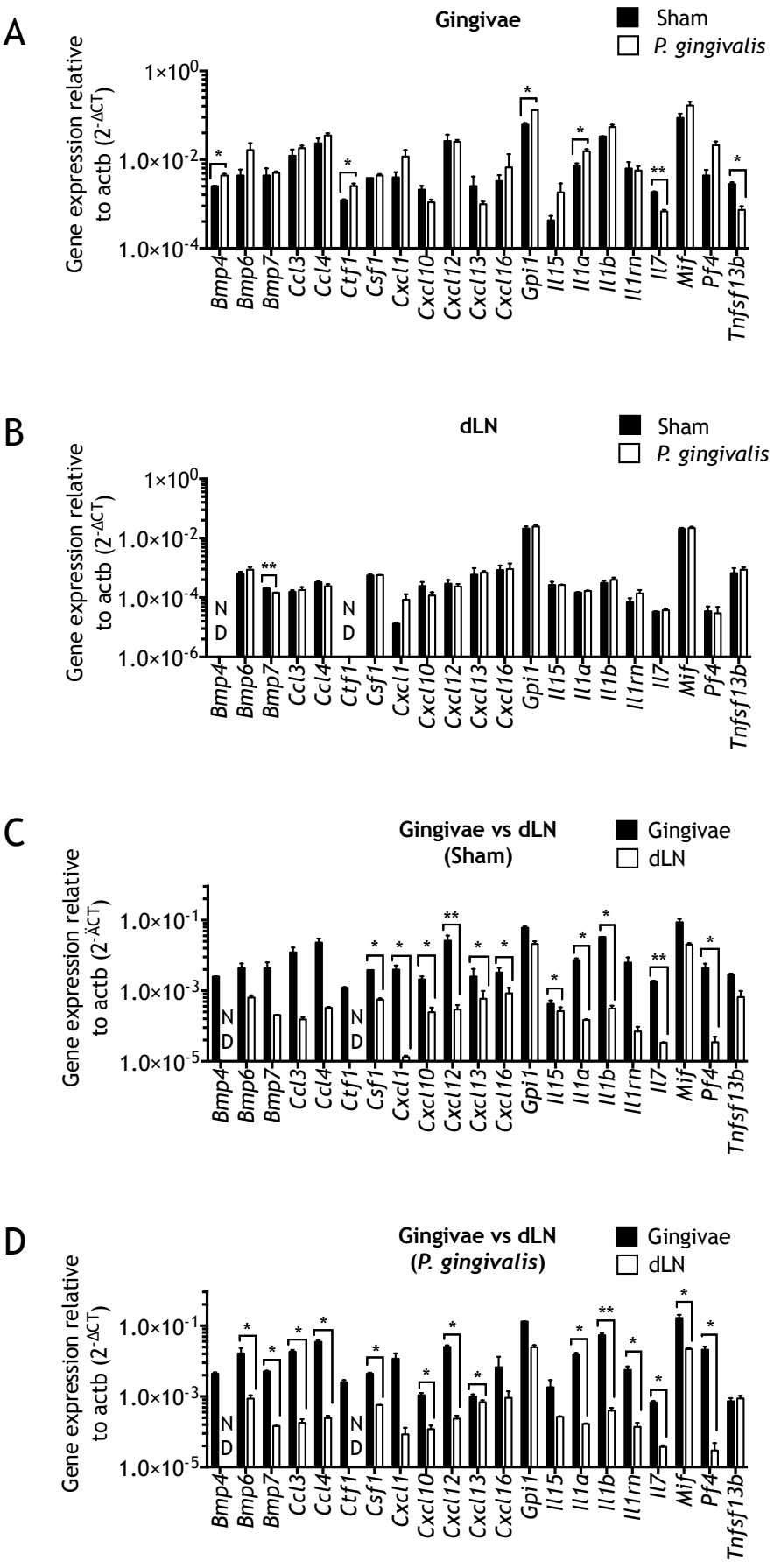
A
Gingivae
Sham
P. gingivalis
Gene expression relative to actb (2-ΔCT)
1×100
1.0×10-2
1.0×10-4
Bmp4
Bmp6
Bmp7
Ccl3
Ccl4
Ctf1
Csf1
Cxcl1
Cxcl10
Cxcl12
Cxcl13
Cxcl16
Gpi1
Il15
Il1a
Il1b
Il1rn
Il7
Mif
Pf4
Tnfsf13b
B
dLN
Sham
P. gingivalis
Gene expression relative to actb (2-ΔCT)
1×100
1.0×10-2
1.0×10-4
1.0×10-6
ND
C
Gingivae vs dLN
(Sham)
Gingivae
dLN
Gene expression relative to actb (2-ΔCT)
1.0×10-1
1.0×10-3
1.0×10-5
D
Gingivae vs dLN
(P. gingivalis)
Gingivae
dLN
Gene expression relative to actb (2-ΔCT)
1.0×10-1
1.0×10-3
1.0×10-5

Figure 4.20. Differential gene expression within gingivae and draining lymph nodes from sham and *P. gingivalis*-infected mice.
Mice were orally infected with *P. gingivalis* or were sham-infected with carrier vehicle, CMC, only. At 28 days post infection, cells were isolated from gingivae and dLN. RNA was extracted, reverse-transcribed to cDNA and the expression of cytokine and chemokine genes determined by qRT-PCR using Qiagen RT^2 profiler PCR array. Graphs show gene expression relative to *Actb* and the 21 genes that were differentially expressed between groups are presented. (A) Gingival gene expression, comparing sham and *P. gingivalis*-infection. (B) dLN gene expression, comparing sham and *P. gingivalis*-infection. (C) Gene expression from sham-infected mice, comparing gingivae and dLN. (D) Gene expression from *P. gingivalis*-infected mice, comparing gingivae and dLN. Data are shown as mean + SEM combined from one independent experiment, n = 2 mice/group. Statistical analysis was conducted on log transformed data (raw data shown on graph). (A and B) Statistical significance was determined using multiple unpaired T tests. (C and D) Statistical significance was determined using paired T tests as gingivae and dLN were harvested from the same mouse. Statistical significance is indicated on the graph (*P < 0.05 and **P < 0.01). ND, not detected.

Table 4.1. Expression of cytokine and chemokine genes in gingivae and draining lymph nodes of sham and *P. gingivalis*-infected mice.

	***P. gingivalis* vs Sham**		**dLN vs gingivae**	
Gene	**Gingivae**	**dLN**	**Sham**	***P. gingivalis***
Bmp4	↑*	N/A	N/A	N/A
Bmp6	NS	NS	NS	↓*
Bmp7	NS	↓**	NS	↓*
Ccl3	NS	NS	NS	↓*
Ccl4	NS	NS	NS	↓*
Ctf1	↑*	N/A	N/A	N/A
Csf1	NS	NS	↓*	↓*
Cxcl1	NS	NS	↓*	NS
Cxcl10	NS	NS	↓*	↓*
Cxcl12	NS	NS	↓**	↓*
Cxcl13	NS	NS	↓*	↓*
Cxcl16	NS	NS	↓*	NS
Gpi1	↑*	NS	NS	NS
Il15	NS	NS	↓*	NS
Il1a	↑*	NS	↓*	↓*
Il1b	NS	NS	↓*	↓**
Il1rn	NS	NS	NS	↓*
Il7	↓**	NS	↓**	↓*
Mif	NS	NS	NS	↓*
Pf4	NS	NS	↓*	↓*
Tnfsf13b	↓*	NS	NS	NS

Statistical significance is represented as *P < 0.05 and **P <0.01(determined by unpaired T tests for *P. gingivalis* vs. sham and paired T tests for gingivae vs. dLN). Abbreviations: dLN, draining (cervical) lymph nodes; N/A, not applicable (due to no detection of gene expression in at least one sample); NS, not significant; ↑, upregulated; ↓, downregulated.

Table 4.2. Functions of cytokine and chemokine genes expressed in gingivae and draining lymph nodes of sham and *P. gingivalis*-infected mice.

Gene	Gene product	Function
Bmp4	BMP 4	Regulator of limb and lip development (Wang et al., 2014)
Bmp6	BMP 6	Regulator of hepcidin expression and iron metabolism (Andriopoulos et al., 2009)
Bmp7	BMP 7	Role in eye, brain, palate and ear development (Wyatt et al., 2010)
Ccl3	CCL3	CD8+ T cell and B cell chemoattractant (O'Grady et al., 1999)
Ccl4	CCL4	Naïve CD4+ T cell chemoattractant (O'Grady et al., 1999)
Ctf1	Cardiotrophin-1	Protects cardiac myocytes from ischemic and reperfusion injury (Bristow and Long, 2002)
Csf1	CSF-1	Differentiation of haematopoietic cells to macrophages (Rettenmier et al., 1988)
Cxcl1	CXCL1	Neutrophil chemoattractant (Moser et al., 1990)
Cxcl10	CXCl10	Monocyte, T cell and NK cell chemoattractant (Liu et al., 2011, Carlsen et al., 2002)
Cxcl12	CXCL12	Role in monocyte extravasation and recruitment (Sánchez-Martín et al., 2011)
Cxcl13	CXCL13	B cell chemoattractant and plays role in development of lymphoid structure organization (Carlsen et al., 2002)
Cxcl16	CXCL16	Chemoattractant for activated CD8+ T cells and NKT cells expressing CXCR6 (Tohyama et al., 2007)
Gpi1	GPI-1	Functions as glycolytic enzyme, promotes skeletal motor neurons and sensory neurons and stimulates Ig secretion (NCBI Gene)
Il15	IL-15	Plays a role in NK cell development and proliferation of T cells and NK cells (Di Sabatino et al., 2011)
Il1a	IL-1α	Acts as an alarmin and is pro-inflammatory (Di Paolo and Shayakhmetov, 2016)

Il1b	IL-1ß	Pro-inflammatory (Di Paolo and Shayakhmetov, 2016)
Il1rn	IL-1R antagonist	Inhibitor of pro-inflammatory IL1- α and IL-1ß (Perrier et al., 2006)
Il7	IL-7	Role in T cell and B cell development (Kittipatarin and Khaled, 2007)
Mif	MIF	Role in activation and proliferation of T cells and regulates lymphocyte trafficking (Calandra and Roger, 2003)
Pf4	PF4	Role in wound repair and inflammation (Lord et al., 2017)
Tnfsf13b	TNF (ligand) superfamily, member 13B	Role in proliferation and differentiation of B cells (Mackay and Browning, 2002)

(https://www.ncbi.nlm.nih.gov/gene?cmd=Retrieve&dopt=Graphics&list_uids=14751 - accessed on 04/04/17). Abbreviations: BMP, bone morphogenetic protein; CCL, chemokine (C-C motif) ligand; CXCL, chemokine (C-X-C motif) ligand; CSF, Colony stimulating factor; GPI, glucose phosphate isomerase; IL, interleukin; MIF, macrophage migration inhibitory factor; PF, platelet factor; TNF, tumour necrosis factor.

Principle component analysis was conducted on the samples analyzed by RT^2 profiler, which highlighted that gingival gene expression clustered irrespective of infection and clustered separately from dLN. dLN gene expression also clustered irrespective of infection (**figure 4.21**)

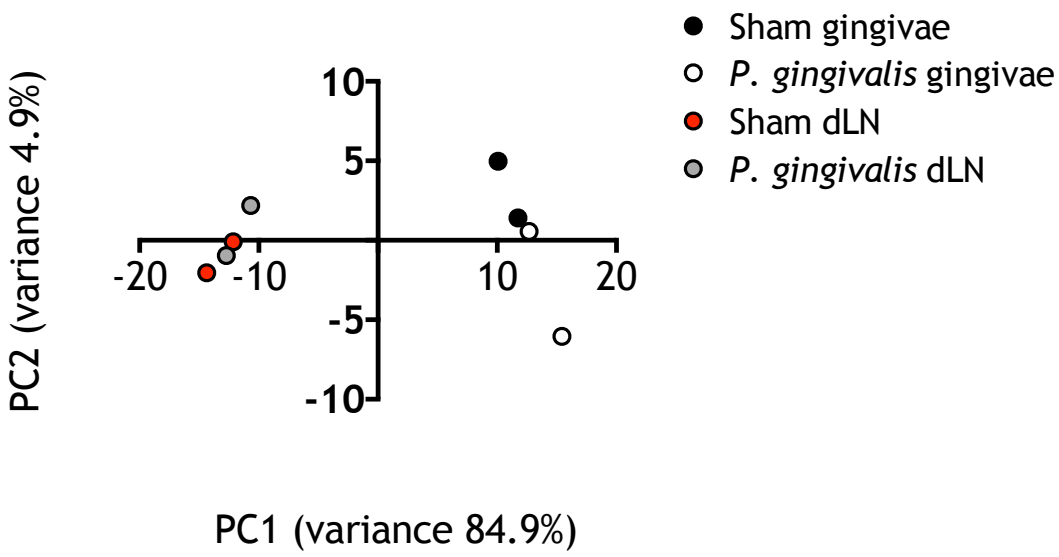

Figure 4.21. Principle component analysis (PCA) plot of gene expression from gingivae and draining lymph nodes of sham and *P. gingivalis*-infected mice.
Mice were orally infected with *P. gingivalis* or were sham-infected with carrier vehicle, CMC, only. At 28 days post infection, cells were isolated from gingivae and dLN. RNA was extracted, reverse-transcribed to cDNA and the expression of cytokine and chemokine genes determined by qRT-PCR using Qiagen RT^2 profiler PCR array. Gene expression relative to *Actb* was calculated ($2^{-\Delta CT}$) and log transformed. The log transformed data was input into PAST software to generate the PCA plot.

A number of genes associated with T cell development, activation and migration were differentially expressed in gingivae compared to dLNs, which suggested that chemokines and cytokines play a role in the movement and homing of T cells to the oral mucosa. However, the chemokine and cytokine gene expression from this experiment do not solely regulate T cells, therefore their presence may have influenced changes in other cell types. The use of the array highlighted that gene expression differs in cells from gingivae of sham vs. *P. gingivalis*-infected mice. However, gene expression was determined from a mixed cell population from each tissue, and there were no immediately obvious signatures of any particular cell type; therefore gene expression attributed to CD4+ T cells remained elusive.

4.3 Discussion

These data document for the first time the chemokine signature of gingival tissue relative to draining lymph node. To the best of the author's knowledge, this is also the first description of Tfh cells in the oral cavity, despite previous evidence of an increased presence of B cells and antibodies in PD. Furthermore, a novel protocol for visualizing cells within the intact murine oral mucosa has been established and has illustrated that CD4+ T cells and B cells form aggregates in this tissue irrespective of infection.

Initial studies proved that alveolar bone loss occurred only in the presence of anti-*P. gingivalis* serum titres at 28 days post infection, similar to previous findings at 42 days post infection (Oliver-Bell et al., 2015). However, the elevated antibody titres of latter experiments were not reflected by significant alveolar bone loss. A potential explanation is that the detection method used was not reliable. A highly accurate and reproducible methodology used to assess rodent alveolar bone loss is micro-computed tomography (micro-CT). Using micro-CT, mandibles and maxillae are imaged at the micron level enabling precise analysis of bone architecture (Park et al., 2007). Therefore, this technique has frequently been employed for identification of bone resorption in experimental PD (Zhang et al., 2014, Kim et al., 2015, Huang et al., 2016, Xu et al., 2014). What the studies described in this chapter have perhaps highlighted is the requirement for an efficient method for identification of bone loss in mice infected with PD prior to culling, particularly for analysis of the local immune response in which the gingivae of 5 mice were pooled. IVIS Luminex XR has been utilized for several years to assess hind limb bone density following spinal cord injury (McManus and Grill, 2011), a method that enables longitudinal measurements in a living mouse. A similar technique could be valuable for bone loss measurements in experimental PD; however, to date there is no literature describing bone density assessment in the oral cavity, likely due to the size and anatomy of the murine mouth. A limitation in the studies described in this chapter was the lack of alveolar bone loss, preventing the validation of experimental PD in mice. Whilst previous studies described the presence of bone destruction as early as 26 days post infection (Baker et al., 1999b), the majority of

murine models of PD are examined at least 42 days post infection (Yu et al., 2007, Baker et al., 1999a, Malcolm et al., 2015b, Oliver-Bell et al., 2015, Malcolm et al., 2016, Myneni et al., 2011), so perhaps at the early stages of *P. gingivalis*-infection bone loss had not yet occurred. It is also noteworthy that oral commensal bacteria have a significant impact upon the induction of bone loss, so much so that co-caging of GF mice with SPF mice enables complete transmission of commensals to GF and promotes alveolar bone loss (Hajishengallis et al., 2011c). The commensal bacteria present within the oral cavity of BALB/c mice have been shown to differ when purchased from different suppliers, a phenomenon that persists for at least one week after recaging in-house (Rodrigue and Lavoie, 1996). It is important to note that initial studies in this chapter were conducted from BALB/c mice that originated from Harlan, whilst latter studies were conducted on mice supplied by Charles River and all mice began antibiotic treatment within one day of arrival. Altogether, these studies suggested that the oral commensal bacteria present within the oral cavity of each mouse greatly influenced the ability of *P. gingivalis* to induce bone destruction. Whilst mice in our studies were pre-treated with antibiotics, oral microflora was not completely depleted and therefore may have influenced the colonization of *P. gingivalis* and development of alveolar bone loss. The identification of *P. gingivalis*-specific antibodies did suggest a successful infection, but the technologies readily available were unable to confirm oral colonization. Other investigators have determined *P. gingivalis* colonization by harvesting and lysing palatal and gingival tissues to remove gDNA then bacterial numbers quantified by qRT-PCR (McIntosh and Hajishengallis, 2012). As an aim of this chapter was to address the immune response at the local site of infection, this method could not be employed. However, to enhance detection of *P. gingivalis* obtained by oral swabs, more sensitive primers – such as *P. gingivalis ISPg1* gene primers – could be used (McIntosh and Hajishengallis, 2012).

A major caveat with regard to the study of the local site of infection is the small size of the murine gingivae. Despite optimization of cell isolation, the entire palate and gingivae were excised from each mouse as too few cells were obtained from the narrow strips of gingival tissue only (data not shown). It is likely that the inflammation associated with PD would be located proximal to

alveolar bone – in gingival tissue – and consequently the immune components at the infection site are potentially being diluted out. Interpretation of gingival cells only is plausible but would require an increase in the number of mice used per group. Further, the disease can be localised to specific sites in humans (Armitage, 2004), and tissue around these teeth are often studied as a means of investigating the immune response in PD. Given the small size of the oral cavity of the mouse, it is impossible to assign disease sites by clinical techniques used for human examination that are readily available, therefore any immune responses specific to *P. gingivalis* infection could be masked by collection of the whole gingival tissues. For this reason, gingival tissue data should be interpreted with a degree of caution.

In early studies of PD in mice, Baker demonstrated that whilst the differences were not as profound as in B cell ablated mice, the depletion of CD4+ T cells contributed to a reduction in alveolar bone loss (Baker et al., 1999a). Yet, the differences in percentages of CD4+ and CD8+ T cells in sham vs. infected mice were non-existent irrespective of infection stage. Likewise, *P. gingivalis*-infection had no impact on the balance of memory and naïve T cells in both local and draining sites of infection. Human gingival tissue was found to harbour memory T cells regardless of disease (Gemmell et al., 1992). However, the current paradigm of TEM and TCM is under scrutiny following the identification of TRM cells. In RA, another immune-mediated bone destructive disease, TRMs constitute a large proportion of both CD4+ and CD8+ T cells in synovium, which are though to contribute to chronic inflammation at sites of disease (Henderson et al., 2014). As the transcriptional status of TRMs is distinct to that of TEMs or TCMs (Mackay et al., 2013), it would be interesting to assess the presence and function of TRMs at early stages of *P. gingivalis*-infection, particularly as the role of memory T cells in PD remains elusive.

At 28 days post infection there was a trend towards a decrease in both the number and percentage of Tregs in gingival tissue in PD, however as mentioned previously there are limitations with the platforms employed. As pooling of five gingivae may dilute out the immune response, it could be speculated that the tendency towards fewer Tregs in infection would be significant at the true sites of disease. A similar trend was noted in dLNs. Treg data from other studies have in fact shown the

opposite. Both an increase in Treg numbers and cytokines have been observed in lesion sites from PD patients (Nakajima et al., 2005, Cardoso et al., 2008a), however, as mentioned previously, these patients had chronic PD, in which clinical parameters of disease were established. In an *A. actinomycetemcomitans* model of mouse PD, depletion of Tregs exacerbated alveolar bone loss, which suggested that the presence of Tregs was preventing further progression of disease (Garlet et al., 2010a). Like in a murine model of LMCV clone 13 infection, in which the expansion of splenic Tregs dipped in very early stages, followed by a sharp increase in numbers (Punkosdy et al., 2011), perhaps the decrease in Tregs at 28 days post *P. gingivalis*-infection would have preceded a proliferation of Tregs that mimics human chronic PD. To test this hypothesis, the duration of the murine model of PD could be extended to determine the composition of Tregs in a more chronic phase of infection.

As previously discussed, anti-*P. gingivalis* antibodies were an important factor in defining successful infection in the PD model, yet they also signified a role for Tfh cells. Thus far, there is no literature discussing either the role or presence of this cell type in PD. Whilst the flow cytometry data of dLN cells was not entirely conclusive as to the presence of Tfh cells due to a lack of CXCR5 expression, the upregulated expression of Bcl-6, ICOS and PD-1 on CD4+ T cells was suggestive of Tfh cells. For the first time, it has been implied that *P. gingivalis* infection induces Tfh cell expansion within cervical LNs, likely providing GC B cell help to support the generation of high-affinity antibodies. However, despite the presence of *P. gingivalis*-specific antibodies in experimental PD, they do not protect mice from disease-associated bone loss (Baker et al., 1999b).

Since the discovery of Th cells, attempts have been made to assign Th subsets to the protection or progression of disease. Initial studies evaluated the role of Th1 and Th2 cells in PD (Seymour et al., 1993, Eastcott et al., 1994, Manhart et al., 1994, Baker et al., 1999a, Gamonal et al., 2001, Lappin et al., 2001, Berglundh et al., 2002). As the existence of other Th subsets was revealed, the nature of the T cell-mediated immune response in PD grew more complex. In more recent studies, a correlation between Th17 cells and their cytokines have been associated with the

pathogenesis of human PD (Cardoso et al., 2009, Dutzan et al., 2012b, Allam et al., 2011, Honda et al., 2008, Moutsopoulos et al., 2012, Beklen et al., 2007, Adibrad et al., 2012, Awang et al., 2014). From the two repeats of the experiment, an association of gingival Th cell subtype with disease progression could not be commented upon. Nonetheless, our flow cytometry results assessing Th cells in dLNs of *P. gingivalis*-infected mice showed clearer trends of cytokine production but did not corroborate the link between Th17 and disease. The mice were used as a platform to explore the early immune response that ultimately causes disease, yet as discussed previously, Th17 responses were noted in patients with established PD. Furthermore, a definitive role of Th17 cells has not been concluded in other mouse models of PD (Yu et al., 2007, Eskan et al., 2012).

Whilst a pattern of CD4+ T cell cytokine production in gingivae was not notable in our studies, CD8+ T cells elevated IFN-γ production in gingival tissue at 14 days post infection. Furthermore, although not significant, at 28 days post-infection an increase in IFN-γ production by CD4+ T cells was observed (implying a Th1 response) in dLNs. Similarly, CD8+ T cells produced insignificantly increased concentrations of IFN-γ in dLNs from *P. gingivalis*-infected mice. The lack of significance was likely due to repetition of the experiment only twice, therefore a further repeat would be necessary to argue the definite presence of Th1 cells and IFN-γ production at early stages of PD. In addition to cytokine production, a Th cell can be identified based on the expression of transcription factors. The presence of Th1 and Th2 cells in human PD gingival tissue biopsies were evaluated by transcription factors T-bet and GATA-3, respectively, through qRT-PCR (Rajesh et al., 2015). Transcription factors could have been assessed in our studies by qRT-PCR or intracellular flow cytometry staining (similar to identification of Foxp3 expression by Tregs).

Systemically, IFN-γ was upregulated in spleen supernatants in *P. gingivalis*-infection at 14 and 28 days post infection by luminex and ELISA, respectively. Together with suggested CD4+ and CD8+ T cell IFN-γ production in both gingivae and dLNs, it is implicated that *P. gingivalis* may induce local and systemic Th1 responses. In support of these findings, Baker *et al*. (1999) demonstrated that genetic deletion of IFN-γ ameliorated alveolar bone loss in mice infected with *P. gingivalis* (Baker et

al., 1999a). This was perhaps a little surprising considering that in other studies IFN-γ directly inhibited osteoclastogenesis (Fox and Chambers, 2000). However, the stimulation of T cells by IFN-γ induced secretion of osteoclastogenic cytokines RANKL and TNF-α, outweighing its inhibitory effects on osteoclasts, and thereby promoted bone loss (Gao et al., 2007).

Although flow cytometry is unequalled as a technology for single-cell analysis, a limitation is its dependence on fluorochromes. The use of greater numbers of fluorescently labeled antibodies can increase autofluorescence and spectral overlap, hence impeding efficiency. Furthermore, a maximum of eight fluorochromes could be analysed by the MACSQuant used in these studies, thereby cells were either split into different panels or were harvested from mice of repeated experiments to assess different T cell types. Due to the limited number of cells isolated from the gingivae, experiments were typically repeated, resulting in increased consumption of time and resources. Mass spectrometry, otherwise known as CyTOF (Cytometry by Time-Of-Flight), is an emerging technology that permits phenotyping of cells through detection of 40 markers from small sample sizes (starting from as few as 10,000 cells). In CyTOF, fluorochromes are replaced with rare heavy metal ion-labeled antibodies that prevent autofluorescence and there is very little overlap between channels. CyTOF works in a similar manner to mass spectrometry in that cells are accelerated through an electrical field and the time taken by ions to reach the detector is measured – lighter ions will reach the detector more quickly than heavier ions (Yao et al., 2014). CyTOF could have enhanced the flow cytometry analysis described in this chapter; however acquisition is slower and reagents are more expensive.

A different approach to identifying a role for T cells in PD was microscopy. This enabled the visualization of cells in their anatomical position within intact tissue – as the cells would have been in the murine mouth. Whilst obtaining sections of gingival tissue was unsuccessful in this model, sections of human gingival tissue are commonly assessed to determine specific cells and cytokines within disease (Gamonal et al., 2001, Lappin et al., 2001, Berglundh et al., 2002, Cardoso et al., 2009, Dutzan et al., 2016). Human tissue is larger and can be easily placed in the

correct position for embedding, and sections with recognizable architecture cut. The small and thin tissue obtained from mice was difficult to position appropriately for embedding and consequently the sections cut by the microtome were uneven and caused the tissue to tear. Conversely, staining the tissue wholemount enabled clear imaging of cells within the hard palate. Due to the position of the lymphoid aggregates at the front of the hard palate, it was likely that these cells comprised the nasal-associated lymphoid tissue (NALT) (Wu et al., 1997). As the NALT was in close proximity to the gingival tissue, it seemed plausible that this immunological tissue played a role in the induction of the immune response in PD. This has not been widely described in the literature, however, it has been found that nasal immunization of BALB/c mice with a fusion protein composed of the 25kDa antigenic region of *P. gingivalis* haemagglutinin A and the maltose binding protein of *Escherichia coli* (25k-hagA-MBP) conferred protection against *P. gingivalis*-induced alveolar bone loss. Bone loss was prevented from one week to one-year post-immunisation (Du et al., 2011), suggesting a role for NALT in oral immunity.

It was therefore hypothesized that a greater number of CD4+ T cells would migrate into B cell regions in NALT to provide B cell help upon bacterial insult in the oral cavity. However, there appeared to be no obvious differences in the structure and B cell and CD4+ T cell composition of the aggregates. Upon intranasal immunization with flagellin-modified circumsporozite protein, typical organization of the T cells and B cells is very apparently lost and lymphocyte arrangement is notably different by eye (Nacer et al., 2014). It therefore seems unlikely that *P. gingivalis* infection caused any differences in NALT lymphocyte structure. Computational analysis of the precise numbers of CD4+ T cells within B cell regions may have proven otherwise. There were various issues regarding this technique. Ideally, numbers of CD4+ T cells would have been counted using Volocity software but T cells resided close to each other, preventing discrimination of individual cell borders. A more appropriate measurement was the area of red (CD4+ T cells) within areas of blue (B cells); however, a major caveat of wholemount staining was that the depth of tissue at which images were taken was difficult to control. Furthermore, the location of T cells and B cells within the NALT of rats has been shown to differ (Kuper et al., 1990), which is a possibility within the mouse. Therefore, it would not be possible

to differentiate between true differences in migratory CD4+ T cells between infection states and whether the images had been captured at different sites within the gingivae. Nevertheless, these data suggest that CD4+ T cells provided B cell help under both steady state and infection conditions. Microbiota that reside within the oral cavity induce an immune response despite usually being harmless to the host. It is thought that the induction of innate (e.g. mucins) and adaptive immunity (e.g. secretory IgA) maintains homeostasis between commensal bacteria and the host (Marcotte and Lavoie, 1998), which potentially explains the reason for which T cells appear to communicate with B cells in the palate of control mice. The use of germ-free (GF) mice has illustrated that commensal flora contribute to the structure and function of paranasal sinuses, including NALT. NALT was evident in GF mice, but was a smaller size compared to that of SPF mice (Jain et al., 2016).

As flow cytometry had revealed an upregulation of IFN-γ by CD8+ T cells in the gingivae of mice, it would have been interesting to visualize the production of the cytokine within the oral mucosa by confocal microscopy. For this experiment, mice could be orally infected with sham or *P. gingivalis* and sacrificed at different days post infection. As positive controls, mice could be given OVA emulsified in CFA in the scruff as this has been reported to stimulate IFN-γ production (Ke et al., 1995). The intact palatal tissue from *P. gingivalis*-infected mice and dLNs from OVA-CFA mice could be stained wholemount with anti-IFN-γ, anti-CD4 and anti-CD8 antibodies, as previously described and visualized by fluorescent confocal microscopy.

Whilst the data generated from this study have revealed a subtle role of T cells in PD, perhaps repeating the experiments would have identified statistically significant differences in the cells in infection. It is also important to note that the entire T cell population was analyzed in this chapter; therefore the function of the *P. gingivalis*-specific T cells in experimental PD remains unknown. The antigen-specific T cells would likely be involved in at least the early stages of infection after their activation and expansion. The antigen-specific T cells at the infection site would then orchestrate the ensuing immune response. Thus, assessing *P.*

gingivalis-specific cells could provide a different insight into CD4+ T cell response in experimental PD (**Chapter 6**).

In conclusion, oral *P. gingivalis*-infection in BALB/c mice induced a slight increase in IFN-γ production by CD8+ T cells from gingivae, CD4+ and CD8+ T cells from dLNs and systemically by splenocytes. Therefore, it seemed likely that infection by these 'red complex' bacteria induced some Th1 differentiation, however, the contribution of Th1 skewed immunity towards development of PD cannot be commented upon due to the lack of alveolar bone loss in these animal models. Furthermore, NALT has been imaged in the context of PD for the first time. This technique highlighted that CD4+ T cells within the lymphoid structure migrate to B cell areas, seemingly to provide B cell help, irrespective of oral *P. gingivalis* infection.

Key findings from chapter 4:

- There was a trend towards a decrease in number and percentage of Tregs in gingivae and dLNs at 28 days post *P. gingivalis*-infection.
- The identification of CD4+ T cells expressing Bcl-6, ICOS and PD-1 suggested that oral *P. gingivalis* infection induced Tfh cell expansion in dLNs.
- There was a trend towards an increase in IFN-γ production by CD4+ and CD8+ T cells in dLNs and a significant increase in gingival CD8+ T cell IFN-γ production from infected mice, along with a systemic elevation of IFN-γ in response to *P. gingivalis* stimulation.
- CD4+ T cells predominantly clustered around B cells in NALT, with some CD4+ T cells migrating to B cell regions – irrespective of infection.

5 Transcriptome of CD4+ T cells in PD

5.1 Introduction

The murine model of PD described in **chapter 4** illustrated subtle changes in T cell phenotypes upon oral infection with *P. gingivalis*. A caveat of this approach was the biased manner in which T cell phenotypes were assessed, possibly masking changes in T cells in PD. Global detection of genes, transcripts, proteins and metabolites through 'omics' technologies is conducted in an untargeted manner and eliminates the bias of assessing only preselected targets.

'Omics' have the potential to define physiological processes and disease pathologies through simultaneous quantification of numerous molecules. Genomics is the study of the entire genome – total DNA – of a cell or organism. Whilst this technique can identify disease-associated sequence polymorphisms, it does not reveal functionality of DNA. Active gene expression and regulation is evaluated through RNA transcripts by transcriptomics. This enables recognition of cell-specific or disease-specific gene expression, but may not be a true representation of down-stream protein translation (Wang et al., 2009). Proteomics assesses the proteome of a cell, to determine protein pathways and functions in a given environment. However, limitations include poor sensitivity of low abundance proteins and analysis of protein complexes (Chandramouli and Qian, 2009). Metabolomics can be defined as the assessment of the metabolic profile of a cell. It is considered the truest reflection of the cell phenotype, as metabolites – final product of gene expression and environmental stimulus – can be amplified in response to small changes in transcriptomics and proteomics. However, unlike the other 'omics' technologies in which a single instrument is capable of conducting analysis, metabolomics requires a variety of instrumentation (Wishart, 2016).

Although disease characteristics cannot be fully explored by transcriptomics in an equal manner to metabolomics, small sample quantities can be readily evaluated by transcriptomics. The cell's transcriptome can be analysed by qRT-PCR, microarrays and RNA-sequencing. As mentioned above, bias-driven experimentation is not

optimal, eliminating qRT-PCR and microarray assays. RNA-sequencing, however, enables universal quantification of a cell's transcripts.

Human PD has been assessed at the transcriptome level, with a particular focus on peripheral blood monocytes (Liu et al., 2016) or the total cell composition of the gingivae (Davanian et al., 2012, Lundmark et al., 2015) using RNA-sequencing. Further, this technique has been used to characterise the microbial dysbiosis that associates with disease (Szafrański et al., 2015).

Whilst RNA-seq has provided a greater insight into gene expression and regulation in human PD in some studies, there is a complete lack of equivalent analysis in the mouse model, and minimal analysis of discrete cell populations. For this reason, the transcriptomes CD4+ T cells in the oral mucosa and dLNs were analysed by RNA-sequencing to better define the disease phenotype of PD.

The aims of this chapter were to:

- Optimize an RNA extraction method.
- Determine a PD gingival CD4+ T cell transcriptome profile.
- Determine a PD dLN CD4+ T cell transcriptome profile.

5.2 Results

The aim of this chapter was to assess the transcriptome of CD4+ T cells from the local and draining sites of *P. gingivalis*-infection. Limited cell numbers could be obtained from the gingivae, of which even fewer were CD4+ T cells (1.2×10^4 cells from five mice; **chapter 3**). Therefore, initial experiments were conducted to determine the optimal method for RNA extraction from low cell numbers. Three RNA extraction kits were selected based on the manufacturer specification for use with small cell numbers; Qiagen RNeasy® Micro Kit (≤ 5×10^5 cells), Ambion™ RNAqueous® - Micro Total RNA Isolation Kit (≤ 5×10^5 cells) and Arcturus® PicoPure® RNA Isolation Kit (< 10 cells, maximum cell number not specified). Cells from cervical LNs not required in other experiments were isolated and resuspended at 10^6, 5×10^5, 5×10^4, 5×10^3 and 5×10^2 cells for RNA extraction using the RNeasy® Micro Kit. For the other kits, cervical LN cells were resuspended at 10^6, 10^5, 10^4, 10^3 and 10^2 cells. The concentration of RNA was assessed by spectrophotemtry, using a nanodrop (**table 5.1**). Only small amounts of RNA were obtained from the RNeasy® Micro Kit, regardless of cell number, and RNA concentration did not increase in a linear manner with increasing cell number. Both RNAqueous® and PicoPure® kits extracted concentrations of RNA that better reflected the cell count; however, the concentrations remained relatively low. The ratio of absorbance at 260/280 indicates the purity of the RNA sample, with a desirable ratio being approximately 2.0. With a few exceptions, the majority of the samples fell below or above the acceptable range. A low 260/280 ratio may be indicative of contamination with phenol or a reagent used in the extraction method, or may result from concentrations of RNA lower than 10 ng/µl. As a second measure of purity, the ratio of absorbance at 260/230 should range between approximately 2.0 and 2.2. All samples failed to reach purity, substantially, by this ratio, ranging between 0.02 and 0.88, which can often signify phenol or guanidine contamination.

Table 5.1. Assessment of RNA by nanodrop.

RNA extraction kit	Cell number	Concentration (ng/µl)*	Ratio of absorbance at 260/280	Ratio of absorbance at 260/230
Qiagen RNeasy® Micro Kit	10^6	10.3	1.83	0.20
	5×10^5	11.4	1.33	0.20
	5×10^4	3.0	1.77	0.06
	5×10^3	7.4	1.44	0.64
	5×10^2	11.5	1.86	0.77
Ambion™ RNAqueous®-Micro Total RNA Isolation Kit**	10^6	62.3	1.83	0.77
	10^5	12.7	1.91	0.26
	10^4	2.1	1.83	0.1
	10^3	1.4	1.3	0.05
	10^2	1.4	2.25	0.02
Arcturus® PicoPure® RNA Isolation Kit**	10^6	74.1	1.99	0.88
	10^5	13.0	1.53	0.23
	10^4	4.8	1.32	0.13
	10^3	4.8	1.55	0.16
	10^2	7.4	1.37	0.28

* RNA was eluted into the same volume of buffer hence concentration of RNA from each extraction method can be compared.
**Representative of 2 independent experiments.

To further investigate the quality and quantity of these small amounts of RNA, a bioanalyser pico chip was used to ensure maximum sensitivity. A bioanalyser is a capillary electrophoresis machine that analyses DNA, RNA and protein. Whilst a nanodrop assesses concentration and the presence of contamination in a sample, it will not determine the presence of contaminating DNA and whether the RNA samples are intact or fragmented. The RNA integrity number (RIN) generated by the bioanalyser is far more comprehensive and gives details of sample integrity based on electropherograms. The number of CD4+ T cells to be sorted from gingival tissue by flow cytometry was expected to be within the range of 5×10^5 and 10^3, due to the results of trial sorts (**chapter 3**) and so in the interests of conserving resources, RNA from 10^6 and 10^2 cells were not analysed by this method. The electropherograms generated using the bioanalyzer (**figure 5.1**) show marker peaks (control to indicate a successful run) and where applicable 18S and 28S ribosomal peaks. Small peaks at 18S and 28S were found only from RNA extracted from 5×10^5 cells using the RNeasy® kits. There were 18S and 28S peaks from RNA extracted from 1×10^5 cells RNA using the RNAqueous extraction kit. There was no detectable

RNA obtained following extraction of RNA from cell numbers below 1 x 10^5 from both the RNeasy® kit and the RNAqueous kit. Due to a labeling error using Picopure® kit, the only sample known was that from 10^3 cells. The other samples were estimated based on their ribosomal peaks. However, it can clearly be concluded that this kit could isolate quantifiable RNA from even 10^3 cells, with 18S and 28S peaks having far greater height than the RNA from corresponding cell counts using the other kits.

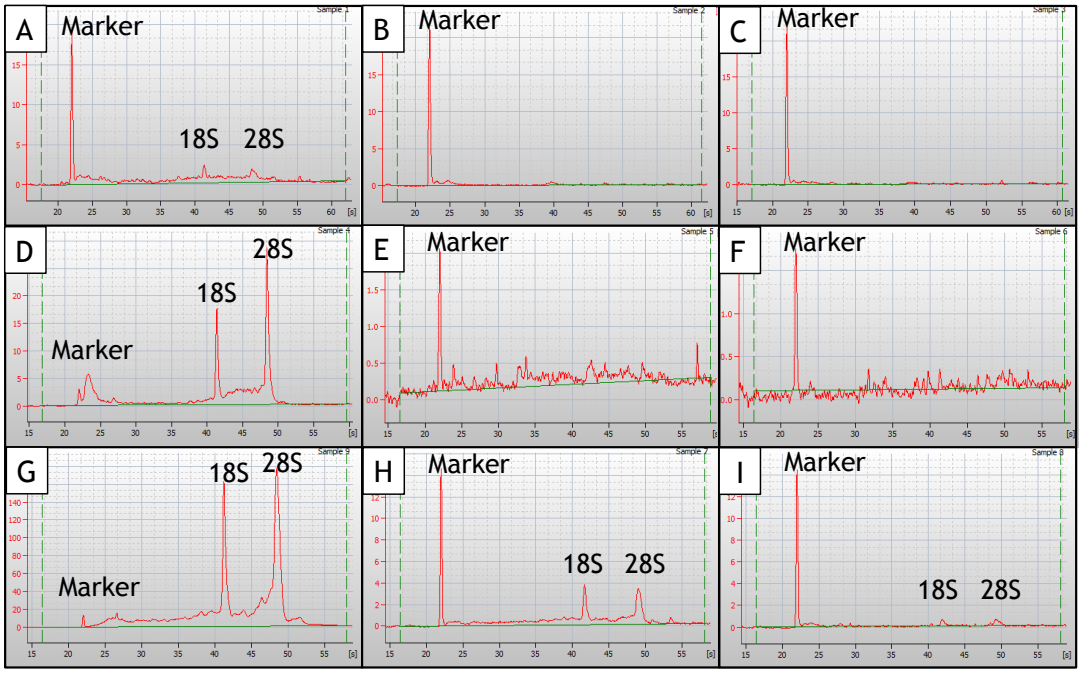

Figure 5.1. Assessment of RNA extracted using three different kits.
RNA was extracted from mouse lymphocytes and the quality of the RNA extraction by each kit was assessed using a Bioanalyzer. (A-C) Electropherograms of RNA extracted using the Qiagen RNeasy® from (A) 5 x 10^5, (B) 5 x 10^4 and (C) 5 x 10^3 cells. (D-F) RNA extracted by Ambion™ RNAqueous®-Micro Total RNA Isolation Kit from (D) 10^5, (E) 10^4 and (F) 10^3 cells. (G-I) Electropherogram of RNA extracted by Arcturus® PicoPure® RNA Isolation Kit* from (G) 10^5, (H) 10^4 and (I) 10^3 cells. 'Marker' is a positive control indicative of a successful run and is shown on the electropherograms along with ribosomal 18S and 28S in A, D, G-I.
*10^3 cells is the only sample that is known due to a labeling error, 10^4 and 10^5 have been estimated based on their peaks.

The bioanalyzer also determined RIN – a measurement of quality whereby a range of between 8 and 10 is usually accepted for NGS – as well as RNA concentration (**table 5.2**). The RIN from each of the RNA samples isolated by RNeasy® kit was lower than required for RNA-sequencing. A high RIN of 8.5 was assigned to RNA obtained from 10^5 cells by RNAqueous® kit, but the quality of the samples of lower cell counts was so poor that RINs could not be determined. As suggested by the electropherograms, the RNA from Picopure® kit was generally of greater quality, with 10^3 cells having a RIN of 4.8, 10^4 having a RIN of 7.6 and 10^5 with a RIN of 7.8. Although not optimal, RNA from 10^5 and 10^4 cells were of borderline quality and 10^3 quite low, however, the lower cell count samples were of greater quality from Picopure® kit than the others.

Table 5.2. Assessment of RNA extraction kits by Bioanalyzer.

RNA extraction kit	Cell number	RIN	Concentration (pg/µl)
Qiagen RNeasy® Micro Kit	5 x 10^5	5	105.0
	5 x 10^4	1	22.1
	5 x 10^3	1	21.8
Ambion™ RNAqueous®-Micro Total RNA Isolation Kit	10^5	8.5	298.0
	10^4	N/A	19.3
	10^3	N/A	6.1
Arcturus® PicoPure® RNA Isolation Kit	10^5 *	7.8	2820.5
	10^4 *	7.6	86.3
	10^3	4.8	13.0

* Due to a labeling error, 10^3 cells is the only sample that is known, 10^4 and 10^5 have been estimated based on their peaks on the electropherograms (**figure 5.1**).

The results from bioanalyzer analysis seemed more informative than those of the nanodrop and so RNA samples were reverse-transcribed to cDNA and qRT-PCR conducted to determine whether 18S expression could be identified with such low quantities of starting RNA. **Figure 5.2** shows that 18S expression was found in all samples from each kit and indicated that the greater the starting cell count, the

lower the CT value. The change in CT value best represented the changes in starting cell numbers using cDNA from RNA from the Picopure® kit.

Whilst expression of the 18S housekeeping gene could be identified in all samples, the bioanalyzer results indicated that Picopure® kit extracted the best quality of RNA from lower cell counts. This kit was then trialed for extraction of RNA from CD4+ T cells sorted from the gingivae and dLNs of five mice. Analysis of RNA by the bioanalyzer highlighted that high quality RNA could be extracted from gingival and dLN CD4+ T cells (RIN of 9 and 9.4, respectively) (**table 5.3**), hence was selected for use for the RNA-sequencing experiment. The concentrations of RNA from gingival cells were low, suggesting that greater numbers of mice may be required.

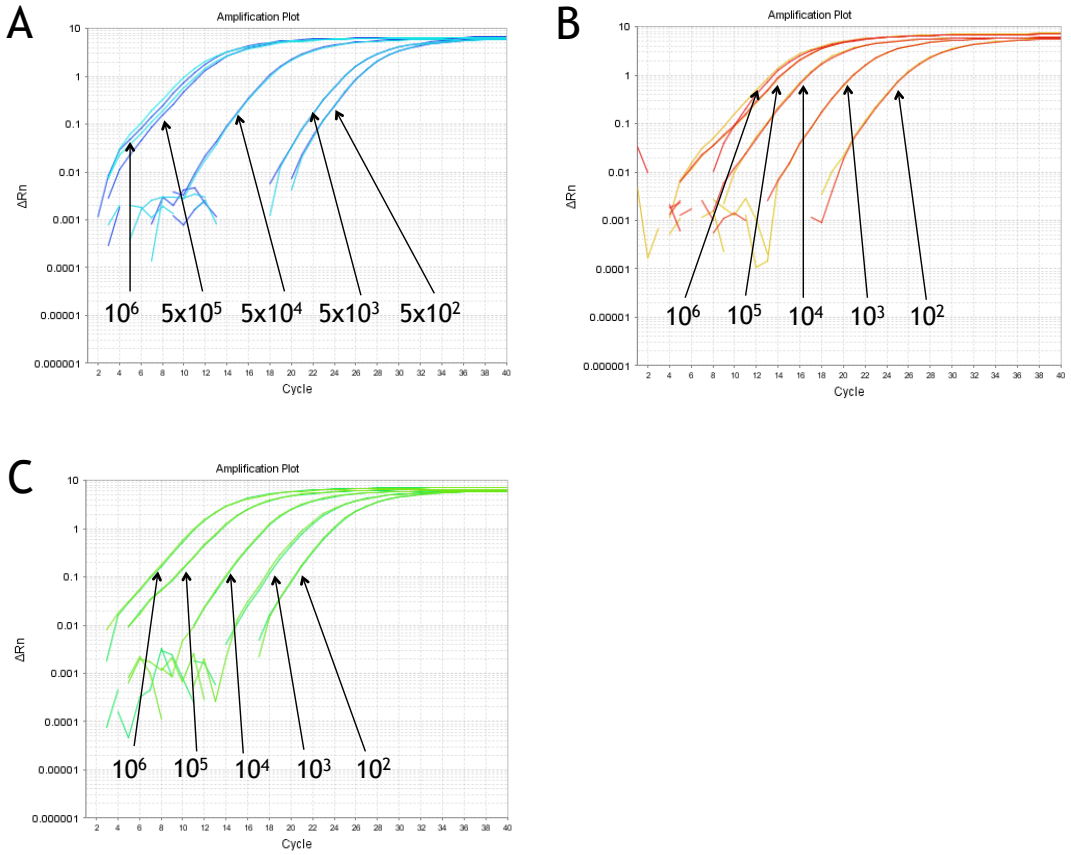

Figure 5.2. Amplification plots of PCR for 18S of cDNA generated from RNA extracted using different RNA extraction kits.
RNA was extracted from cervical lymph node cells using (A) Qiagen RNeasy® Micro Kit, (B) Ambion™ RNAqueous®-Micro Total RNA Isolation Kit or (C) Arcturus® Picopure® RNA Isolation Kit. RNA was extracted from the cell numbers indicated on the plots and reverse transcribed to cDNA and expression of 18S determined by qRT-PCR.

Table 5.3. Concentrations of RNA extracted using Picopure® kit following FACS sort of gingival and draining lymph node CD4+ T cells.

Tissue	No. of mice	Cell no. pre-sort	CD4+ T cell no. post-sort	Total RNA (ng)	RIN
Gingivae	5	$7.0 \times 10^{5*}$	7.4×10^{3}	3	9
dLN	5	$1.5 \times 10^{6**}$	3.7×10^{5}	170	9.4

*Cells from 5 gingivae were pooled and all cells were used for sort.
**Cells from 5 dLNs were pooled (approximately 5×10^{7} cells) but only 1.5×10^{6} were used for sort.

The initial analysis of gene expression in whole gingivae or dLN was carried out using a selection of genes and cell surface molecules speculated to contribute to PD progression. The data presented in **chapter 4** suggest subtle alterations in T cell phenotype in *P. gingivalis*-infection, and that perhaps the changes were not fully exposed with the methodology used. Subsequently, the transcriptome of CD4+ T cells from experimental PD models were analyzed by NGS. Due to the cost of the RNA-sequencing experiment, it was not feasible to assess CD4+ T cells at all time-points. The data from **chapter 4** implied that IFN-γ production by both CD4+ and CD8+ T cells within the dLNs of infected mice increased at 28 days post infection, along with a trend towards a decrease in Tregs. Furthermore, it was of interest to determine T cell responses occurring at the time of alveolar bone loss development. Therefore, RNA-sequencing of gingival and dLN CD4+ T cells was conducted at 28 days post infection.

As discussed in **chapter 4**, serum anti-*P. gingivalis* IgG titres reflected alveolar bone loss in initial studies. Although in some models serum antibody was observed with minimal bone loss, previous models and some replicates of these studies demonstrated that an absence of serum antibody was likely to represent failed infection and absence of bone loss. Therefore, antibody titres were assessed using serum obtained by tail bleed, prior to cull. RNA-sequencing experiments excluded mice that did not produce IgG to *P. gingivalis*. Groups of 20 mice were used for each experiment, with 10 orally infected with CMC/sham and 10 mice infected with *P. gingivalis*. The rationale behind the increased group size was that around 7000 CD4+ T cells could be sorted from the gingivae pooled from 5 mice, from which

around 3 ng of RNA could be extracted (**table 5.3**). The recommended minimum concentration of cDNA required was 10 ng at a concentration of 1 ng/µl. Of mice infected with *P. gingivalis*, a maximum of 20% of the infected animals had very low or undetectable IgG titres. As an appropriate control, the same numbers of sham-infected mice were also excluded. Therefore, an experiment with 10 mice per group would allow the exclusion of *P. gingivalis*-antibody negative mice, whilst increasing the number of CD4+ T cells to be sorted.

The serum antibody titres of the mice used for RNA-sequencing experiments are described in **figure 5.3.** The infected mice had significantly greater serum antibody titers than their sham-infected counterparts (mean 148.7 +/- 30.3 EU sham vs. mean 1569.0 +/- 101.6 EU *P. gingivalis*, $P < 0.0001$). Despite this, the mice developed alveolar bone loss mirroring that of the sham-infected mice (mean 0.229 +/- 0.005 mm sham vs. mean 0.231 +/- 0.006 mm *P. gingivalis*, NS). To investigate whether the duration of the infection was insufficient to cause bone destruction, five supplementary mice were orally infected with the same cultures of *P. gingivalis,* concurrently with a group of animals from which cells were used for RNA-sequencing and similarly, five extra mice were sham-infected. The mice infected for 49 days displayed increased anti-*P. gingivalis* IgG titres (mean 157.8 +/- 39.36 EU sham vs. mean 1675.0 +/- 47.27 EU *P. gingivalis*, $P < 0.0001$) (**figure 5.3C**). Further more, alveolar bone loss was apparent in four of the five mice at 49 days post infection compared to control mice (mean 0.270 +/- 0.004 mm sham vs. mean 0.290 +/- 0.007 mm *P. gingivalis*, $P < 0.05$) (**figure 5.3D**). The data therefore suggested that in this system, at 28 days post-infection, the local and potentially systemic changes that lead to development of PD were occurring and the RNA-sequencing data would pinpoint the correlating changes in CD4+ T cell gene expression – perhaps corroborating the suggested association of CD4+ T cell IFN-γ production and PD (**chapter 4**).

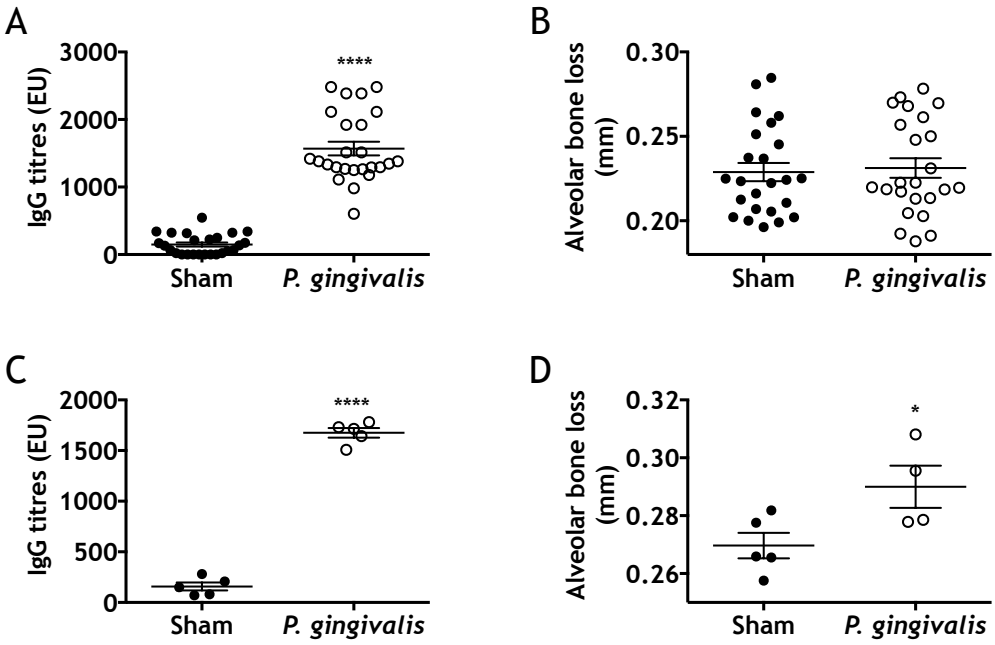

Figure 5.3. Anti-*P. gingivalis* IgG titres and alveolar bone loss at 28 and 49 days post *P. gingivalis* infection.
Mice were orally infected with *P. gingivalis* or were sham-infected (sham) with carrier vehicle, CMC, only. (A and B) 28 days post infection; (C and D) 49 days post infection. (A and C) Anti-*P. gingivalis* IgG titres in serum were measured by ELISA. Data are ELISA Units (EU) shown as individual mice (symbols) with mean +/- SEM for each group (lines). (B and D) Alveolar bone loss. Data are shown as mean per mouse (symbols) with mean +/- SEM for each group (lines). (A and B) Data are combined from 3 independent experiments, n = 4-5 mice/group. (C and D) Data are combined from 1 experiment, n = 4-5 mice/group. Statistical significance was determined by unpaired T test, as indicated on the graph (*P < 0.05, ****P < 0.0001).

A total of three independent experiments were set up for RNA-sequencing, each consisting of sham infected mice (n = 10) and *P. gingivalis*-infected mice (n = 10). In the tables below, the independent experiments are designated '3', '4', and '5' as experiments '1' and '2' were unusable due to RNA degradation. Cells from gingivae of each group were pooled and sorted by flow cytometry. Two to three million cells from a pooled population of dLN cells were similarly sorted. Surplus lymphocytes were used for compensation controls. Details of the mice, CD4+ T cells sorted and RNA extracted are described in **table 5.4**. From the gingivae, the number of CD4+ T cells sorted ranged from 1.2 x 10^4 to 3.5 x 10^4 and the extracted RNA samples had RINs of at least 8.6. From the dLNs, between 3.0 x 10^5 and 1 x 10^6 CD4+ T cells were sorted, giving extracted RNA with RINs of at least 9.0 (sham dLN from batch 3 was

not analysed by the bioanalyzer due to an error in the loading of the chip). All samples were of sufficient quality for RNA-sequencing. However, with low starting concentrations of RNA, the sequencing platform used from Source BioScience advised a pre-amplification step.

Table 5.4. RNA of CD4+ T cells sorted from gingivae and draining lymph nodes of sham and *P. gingivalis*-infected mice.

Sample		No. of mice	CD4+ T cell count post sort	RIN	Conc. of RNA (ng/µl)	Total RNA (ng)
Name	Repeat*					
Sham gingivae	3	8	3.2×10^4	9.3	1.46	14.6
P. gingivalis gingivae	3	8	3.5×10^4	9.4	0.58	5.8
Sham dLN**	3	8	1.0×10^6	-	-	-
P. gingivalis dLN	3	8	1.0×10^6	9.4	47.8	478
Sham gingivae	4	8	1.9×10^4	8.8	0.78	7.8
P. gingivalis gingivae	4	8	2.3×10^4	8.6	1.01	10.1
Sham dLN	4	8	5.0×10^5	9.0	72.4	724
P. gingivalis dLN	4	8	4.9×10^5	9.4	33.1	331
Sham gingivae	5	9	2.2×10^4	9.2	0.83	8.3
P. gingivalis gingivae	5	9	1.2×10^4	9.1	0.69	6.9
Sham dLN	5	9	3.0×10^5	10	20.5	205
P. gingivalis dLN	5	9	3.7×10^5	9.6	29.2	292

*RNA-sequencing was performed on 3 independent experiments. Experiment repeats were assigned numbers 3, 4 or 5. Experiments 1 and 2 were not used due to RNA degradation.
**No Bioanalyzer readout for Sham dLN due to error loading sample into chip
Abbreviations: No., number; RIN, RNA integrity number; conc., concentration; dLN, draining (cervical) lymph node.

The SMART-Seq® v4 Ultra® Low Input RNA Kit was used to generate full-length cDNA from low concentrations of RNA (10 pg – 10 ng). SMART (Switching Mechanism at 5' End of RNA Template) technology generates full length cDNAs by exploiting the switching activity of reverse transcriptases. Defined PCR adapters are added to both ends of first strand cDNA. These adaptors are meant to ensure that final cDNA libraries contain the 5' end of mRNA and this should help accurate representation of the initial mRNA transcripts. A maximum of 10 ng could be used for first-strand cDNA was synthesis, therefore RNA from dLNs were diluted but the whole sample of gingivae RNA was used. cDNA was amplified by 'long distance PCR'; a technique that enables amplification of DNA lengths (>30 kb) that conventional PCR methods are unable to amplify. Amplified cDNA was then sent to Source BioScience for purification and validation using Agilent's 2100 Bioanalyzer and high sensitivity DNA kit. All samples passed quality control testing and concentrations of each sample ranged between 0.41 and 2.64 ng/µl. The samples were diluted to 1 ng total cDNA for preparation of Nextera XT libraries and all libraries were validated using the Bioanalyzer. NGS was then conducted using the NextSeq 500 platform. This platform is advantageous in that it provides highly accurate results in rapid turnaround times (48 hours). Differential gene expression and gene set enrichment analysis were conducted by Source BioScience using DESeq2.

The heatmap in **figure 5.4** depicts the expression of the 50 most highly expressed genes. The clustering analysis shows 2 primary branches, one of which groups gingival samples and the other groups the dLNs. Thirty-nine of the 50 genes appear to be expressed fairly similarly by the all samples irrespective of tissue origin and infection status. However, the remaining genes are differentially expressed between gingivae and dLNs – particularly *Ppp1r15a*, *Vps37b*, *Tnfaip3*, *Junb*, *Hspa5*, *Ier2* and *Pnrc1*. The expression of these genes does not differ in infection compared to control. There is some variation in expression between different experimental replicates, which is especially evident in expression of *Gm26917*, *Ppp1r15*a, *Tnfaip3*, *Junb* by dLN replicates. Along with the clustering analysis, these data suggest that *P. gingivalis* infection does not cause great changes in gene expression of CD4+ T cells.

These findings are consolidated by the MA-plot (**figure 5.5A**), which is a visual representation of genomic data with log ratio plotted against mean expression for a set of genes. In this plot comparing gene expression from CD4+ T cells of sham and *P. gingivalis*-infected gingivae, it was clearly demonstrated that only 3 genes are upregulated in disease at 28 days post infection. The difference between control and *P. gingivalis*-infection in dLNs is even smaller; with the down-regulation of a single gene being the only difference in CD4+ T cell gene expression corresponding with infection (**figure 5.5B**). As the data from the heatmap implied, the majority of differential gene expression occurs between gingivae and dLN (**figure 5.5C-F**).

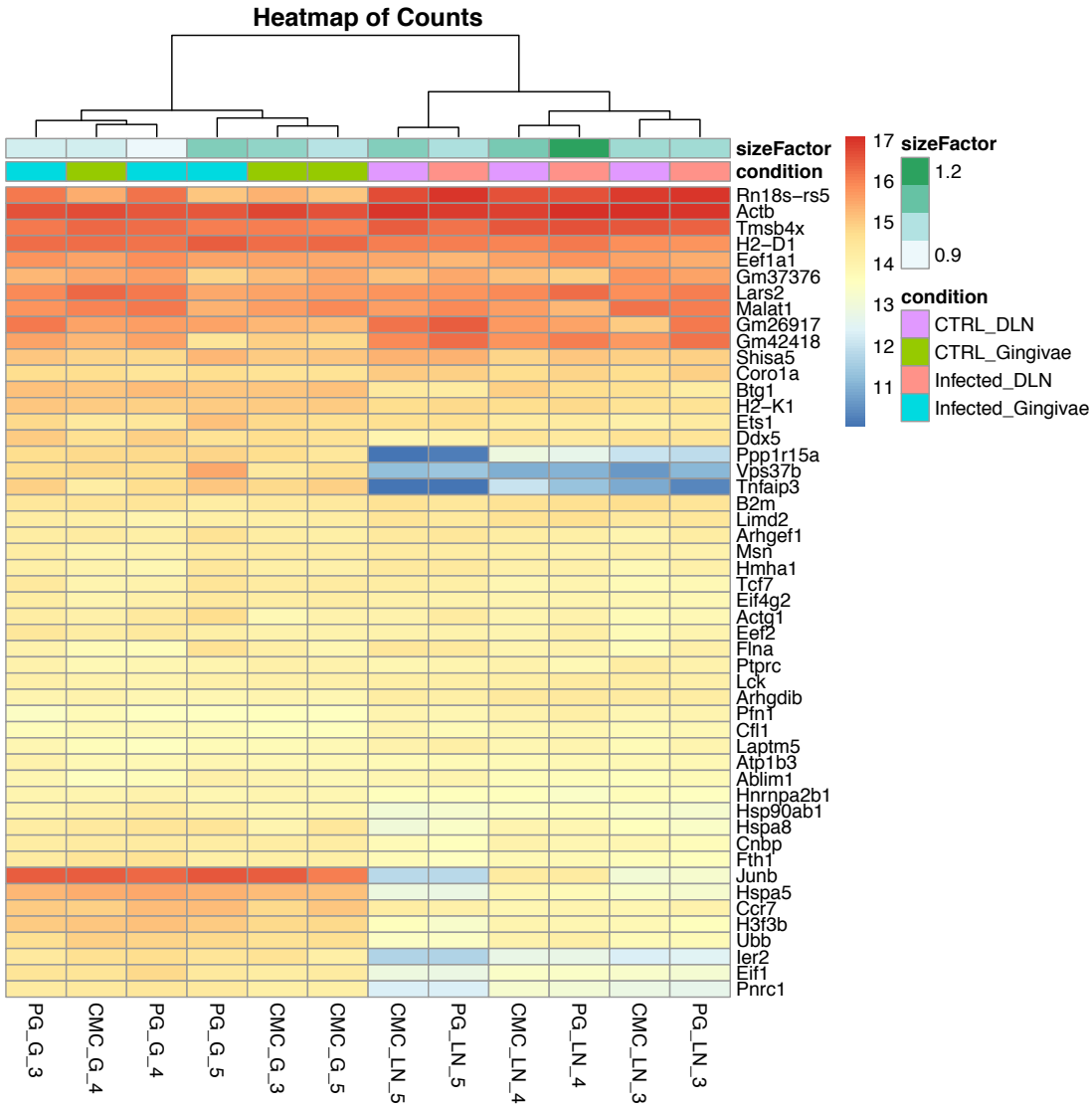

Figure 5.4. Heatmap of the 50 most highly expressed genes in CD4+ T cells isolated from the gingivae and draining lymph nodes of sham and *P. gingivalis*-infected mice.

Mice were orally infected with *P. gingivalis* or were sham-infected with carrier vehicle, CMC, only. At 28 days post infection, cells were isolated from gingivae and draining lymph nodes and CD4+ T cells were sorted. RNA was extracted, pre-amplified, then reverse transcribed for next-generation sequencing using NextSeq platform. DESeq2 was used to determine differential gene expression and generate heatmaps. The data were transformed by variance stabilizing transformation prior to clustering. The length and grouping of the branches correspond to similarity of the samples. The branching and height of the tree reflects the distance. Size factor indicates how much sequencing differs between samples; 0.9 indicates a sample in which 90% of the mean total reads mapped are different. PG - *P. gingivalis* infection, CMC - sham infection, G - gingivae, LN - draining lymph node and the following number represents the independent experiment batch number.

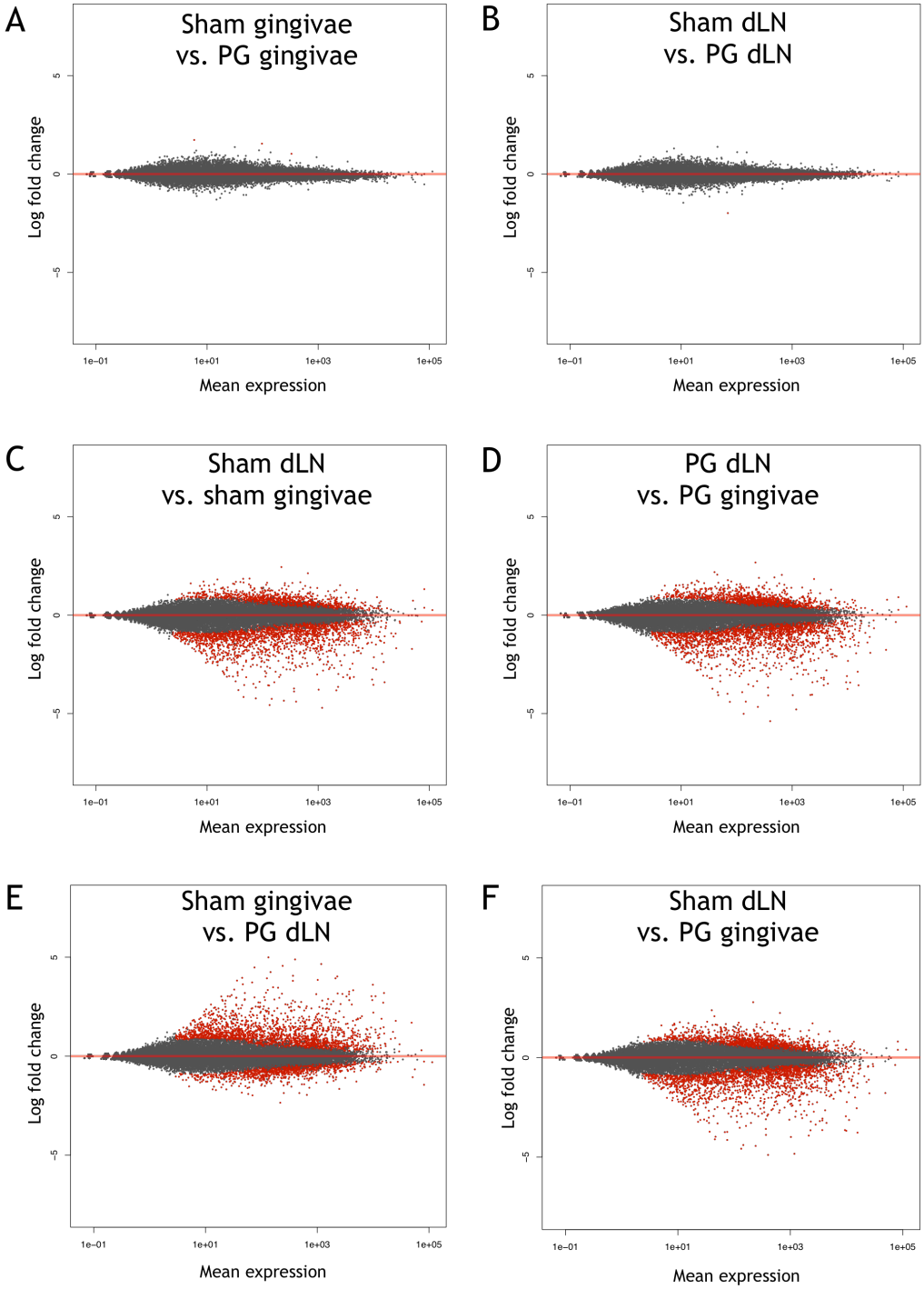

Figure 5.5. MA-plots of gene expression from CD4+ T cells isolated from sham versus *P. gingivalis*-infected gingivae and draining lymph nodes.
Samples were prepared as in **figure 5.4.** DESeq2 was used to determine differential gene expression and generate MA-plots. MA-plots showing log2 fold change of gene expression against their mean expression comparing CD4+ T cell expression from (A) gingivae of sham and *P. gingivalis*-infected mice, (B) draining lymph nodes of sham and *P. gingivalis*-infected mice, (C) sham-infected draining lymph nodes and sham-infected gingivae, (D) *P. gingivalis*-infected draining lymph nodes and *P. gingivalis*-infected gingivae, (E) sham-infected gingivae and *P. gingivalis*-infected draining lymph nodes and (F) sham-infected draining lymph node and *P. gingivalis*-infected gingivae.

As the MA-plot and heatmap suggested, the clustering of samples occurred between gingivae irrespective of infection and dLNs irrespective of infection, and this is similarly represented in the PCA plot (**figure 5.6**). A similar pattern of clustering of gene expression from total cell isolate of gingivae and dLNs was noted using the RT^2 profiler in **chapter 4** (**figure 4.16**).

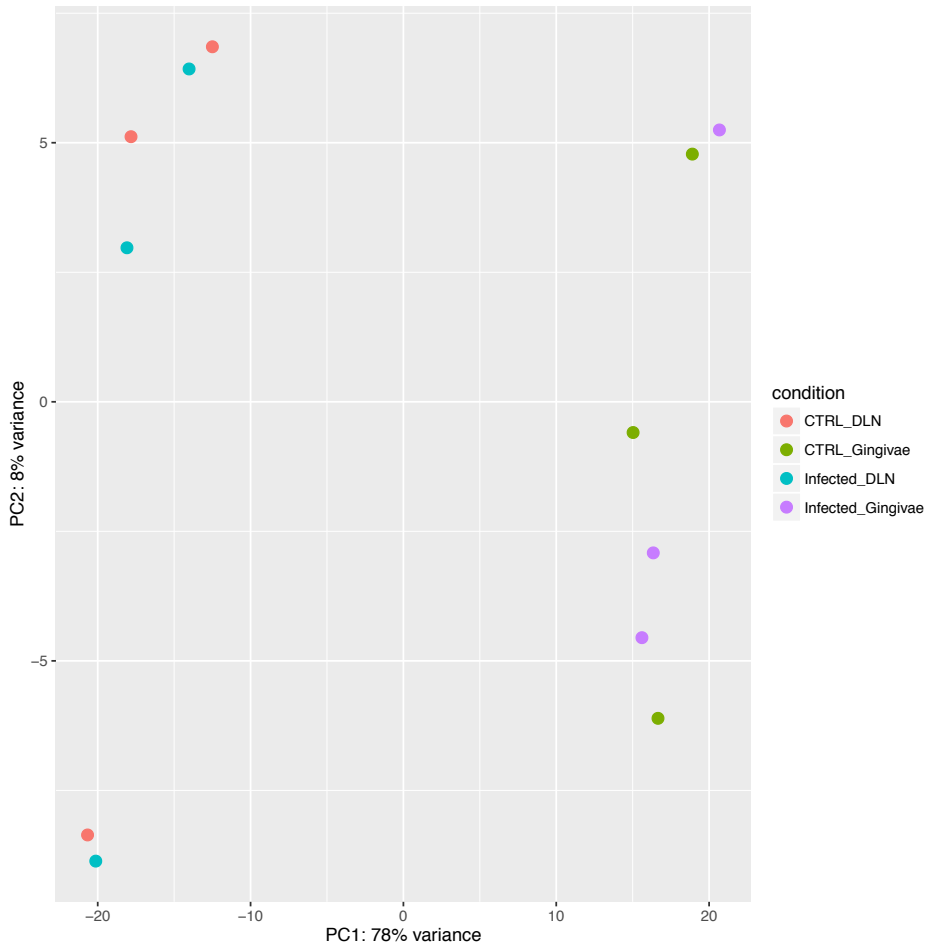

Figure 5.6. Principle component analysis (PCA) of CD4+ T cells from sham and *P. gingivalis*-infected mice.
Samples were prepared as in **figure 5.4.** DESeq2 was used generate PCA plot.

The three genes statistically significantly upregulated by CD4+ T cells from gingivae of infected mice were *Btg3*, *Gm20634* and *Gm20633* (**figure 5.7A**). The functions of each of these genes are described in **table 5.5**. In the dLNs in *P. gingivalis* infection, CD4+ T cells were found to down-regulate the expression of *Gm5451* compared with its expression in sham-infection (**figure 5.7B**). The details of *Gm5451* are described in **table 5.5**.

The four genes described above were significantly differentially expressed in infection when analysed to obtain a Padj value – a corrected P value that eliminates random events falsely appearing as significant in high throughput experimentation. P values are generally insufficient for identifying statistical significance in such high throughput experiments. However, given the surprisingly small number of differentially expressed genes identified, to further interrogate the data, the genes with the lowest P values (but a Padj value of > 0.1) are shown in **figure 5.7C-D**. Using this method, within the gingivae, two genes were found to be upregulated - *Hmgb1-ps1* and *Bc147527* – and three genes were found to be down-regulated – *Prdm2, Gm13169* and *Tcf20*. *Gm14173* and *Gm10231* were upregulated by CD4+ T cells in dLNs of *P. gingivalis*-infected mice, whilst there was a down-regulation of *Trav6-d6*.

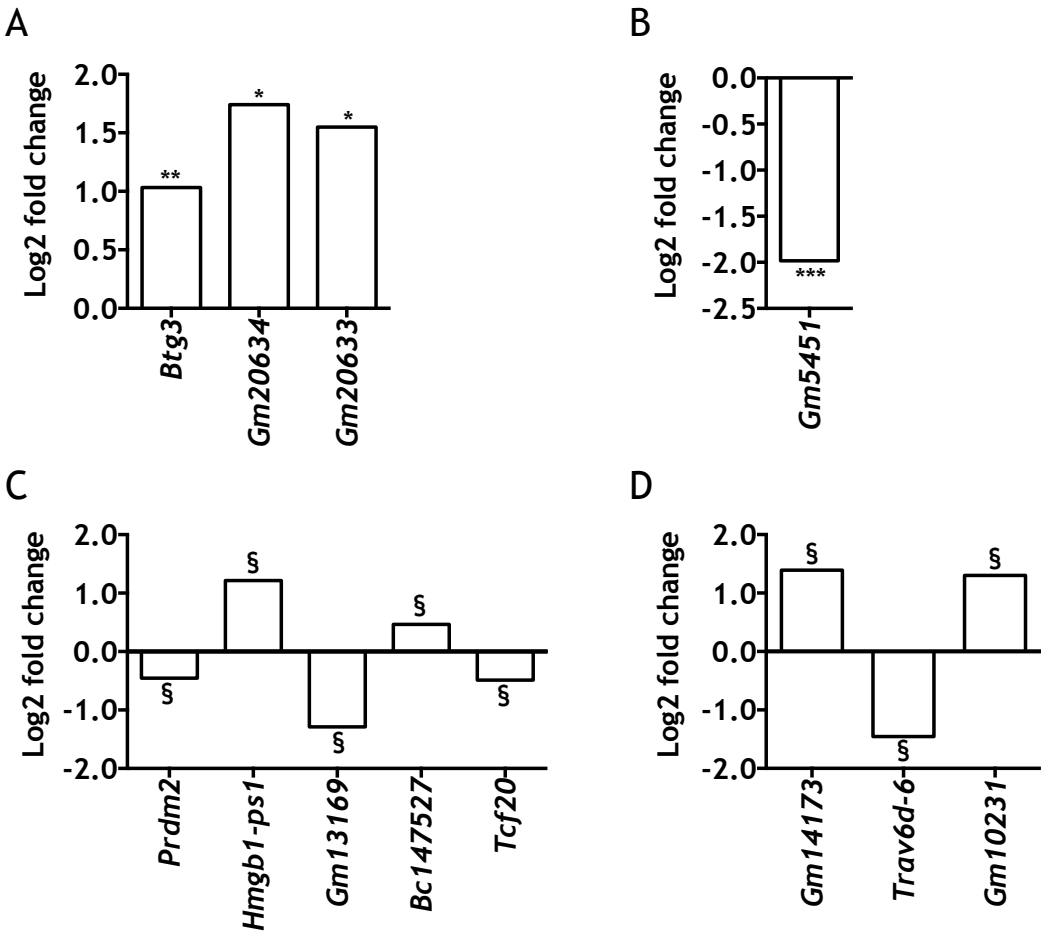

Figure 5.7. Differential CD4+ T cell gene expression in gingivae and draining lymph nodes from sham and *P. gingivalis*-infected mice.
Samples were prepared as in **figure 5.4.** DESeq2 was used to determine differential gene expression. (A) Genes significantly differentially expressed in the gingivae of *P. gingivalis*-infected mice, determined by Padj value. (B) Single gene significantly differentially expressed in the draining lymph nodes of *P. gingivalis*-infected mice, determined by Padj value. (C) Genes differentially expressed in gingivae of *P. gingivalis*-infected mice, determined by P value. (D) Genes differentially expressed in draining lymph nodes of *P. gingivalis*-infected mice, determined by P value. Data shown are mean log2 fold change of *P. gingivalis*-infection compared to sham-infection, from 3 independent experiments, n=1/group. Statistical significance was determined using Wald-test (P value) followed by Benjamini-Hochberg correction (adjusted P value, Padj) (*Padj < 0.1, **Padj < 0.05, ***Padj < 0.01 and §P < 0.001).

Table 5.5. Details of genes with differential expression in *P. gingivalis* infection.

Gene symbol	Gene name	Chromosome location	Function	Reference
Btg3	B cell translocation gene 3	16	Anti-proliferation	(Du et al., 2015)
Gm20634	Predicted gene 20634	3	Unclassified non-coding gene	Mouse Genome Informatics
Gm20633	Predicted gene 20633	3	Anti-sense lncRNA gene	Mouse Genome Informatics
Gm5451	Predicted gene 5451	13	Pseudogene	Mouse Genome Informatics
Prdm2	PR domain containing 2, with ZNF finger	4	Protein coding gene	Mouse Genome Informatics
Hmgb1-ps1	High mobility group box 1, pseudogene 1	11	Pseudogene	Mouse Genome Informatics
Gm13169	Predicted gene 13169	4	Pseudogene	Mouse Genome Informatics
Bc147527	cDNA sequence Bc147527	13	Protein coding gene	Mouse Genome Informatics
Tcf20	Transcription factor 20	15	Protein coding gene	Mouse Genome Informatics
Gm14173	Predicted gene 14173	2	Pseudogene	Mouse Genome Informatics
Trav6d-6	T cell receptor alpha variable 6D-6	14	Gene that rearranges at the DNA level and encodes variable region of TCRs	Ensembl
Gm10231	Predicted gene 10231	17	Pseudogene	Mouse Genome Informatics

http://www.informatics.jax.org/marker/MGI:5313081 (accessed on 03/02/17)
http://www.informatics.jax.org/marker/MGI:5313080 (accessed on 03/02/17)
http://www.informatics.jax.org/marker/MGI:3643790 (accessed on 03/02/17)
http://www.informatics.jax.org/marker/MGI:107628 (accessed on 03/02/17)
http://www.informatics.jax.org/marker/MGI:3768536 (accessed on 03/02/17)
http://www.informatics.jax.org/marker/MGI:3651793 (accessed on 03/02/17)
http://www.informatics.jax.org/marker/MGI:4840510 (accessed on 03/02/17)
http://www.informatics.jax.org/marker/MGI:108399 (accessed on 03/02/17)
http://www.informatics.jax.org/marker/MGI:3650930 (accessed on 03/02/17)
http://www.ensembl.org/Mus_musculus/Gene/Summary?g=ENSMUSG00000094176;r=14:52821922-52822359;t=ENSMUST00000197754 (accessed on 03/02/17)
http://www.informatics.jax.org/marker/MGI:3704468 (accessed on 03/02/17)

Since analysis of dLN T helper cytokine production by flow cytometry (**chapter 4**) suggested that *P. gingivalis*-infection induced IFN-γ but not IL-17A or IL-4 production, the expression of these genes, as found by RNA-sequencing, was assessed (**figure 5.10**). Similar to the findings by flow cytometry of gingivae, there were no differences in the expression of *Ifnγ, Il17A* or *Il4* by CD4+ T cells from sham or *P. gingivalis*-infected mice. Likewise, the results of cytokine production in dLNs by flow cytometry were mirrored in the RNA-sequencing experiment, whereby *Ifnγ* expression was increased in *P. gingivalis*-infection. This finding was not significant by corrected P value, Padj, but had a P value < 0.05.

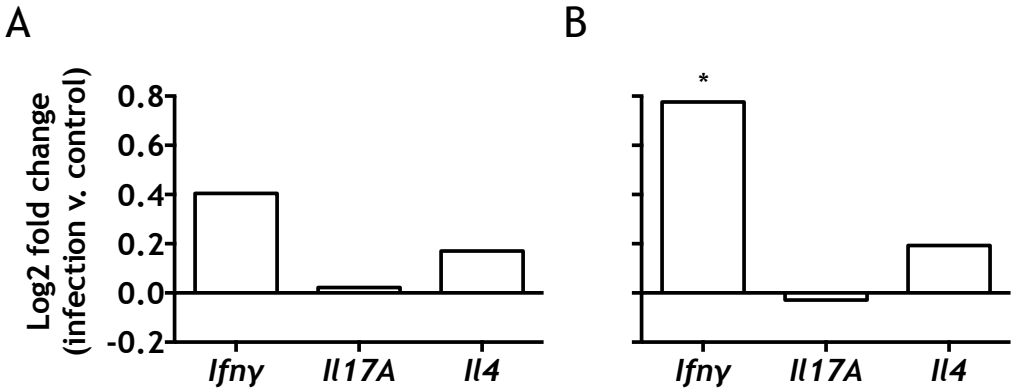

Figure 5.8. Differential gene expression of CD4+ T helper cytokines in gingivae and draining lymph nodes from sham and *P. gingivalis*-infected mice.
Samples were prepared as in **figure 5.4**. DESeq2 was used to determine differential gene expression. Log2 fold change of *Ifnγ*, *Il17a* and *Il4* gene expression in (A) gingivae and (B) draining lymph nodes. Data is shown as mean log2 fold change of *P. gingivalis*-infection compared to sham-infection, from 3 independent experiments, n=1/group. Statistical insignificance was determined using Wald-test (P value) followed by Benjamini-Hochberg correction (adjusted P value, Padj). * represents P < 0.05 as indicated on the graph.

As a trend towards a decrease in the proportion of Tregs in *P. gingivalis*-infection was also observed by flow cytometry at 28 days post infection, Treg markers were evaluated from the RNA-sequencing data-set. There was, however, no difference in expression of *Cd25*, *Foxp3*, *Il10*, *Ctla4*, *TgfB1* or *TgfB2* between CD4+ T cells from control and infected mice, in both gingivae and dLNs (**figure 5.9**). To further compare the flow cytometry data to that of RNA-sequencing, Tfh gene expression

was assessed. However, no differential expression of *Bcl6*, *Cxcr5*, *Icos*, *Pd1* or *Il21* was found in CD4+ T cells from dLNs of sham or *P. gingivalis*-infected mice (data not shown).

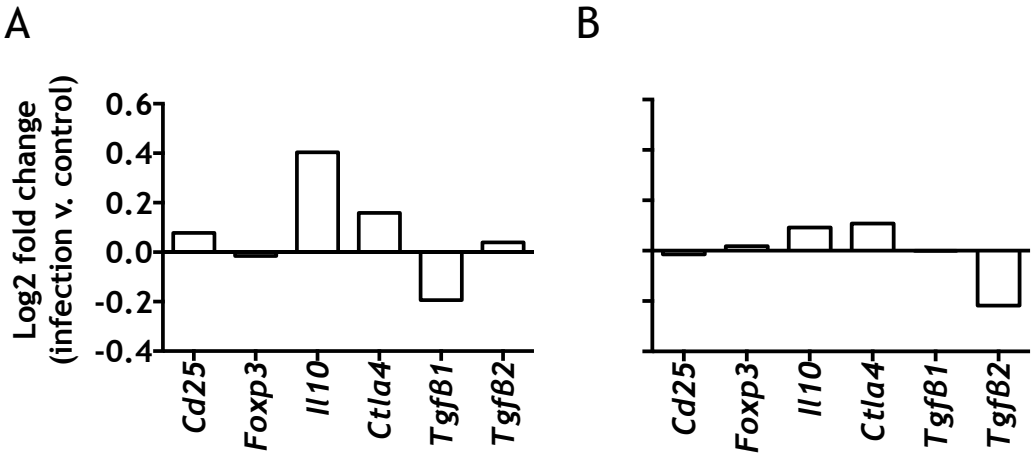

Figure 5.9. Differential gene expression of regulatory T cell associated genes in gingivae and draining lymph nodes from sham and *P. gingivalis*-infected mice. Samples were prepared as in **figure 5.4.** DESeq2 was used to determine differential gene expression. Log2 fold change of *Cd25*, *Foxp3*, *Il10*, *Ctla4*, *Tgfb1* and *Tgfb2* gene expression in (A) gingivae and (B) draining lymph nodes. Data is shown as mean log2 fold change of *P. gingivalis*-infection compared to sham-infection, from 3 independent experiments, n=1/group. Statistical insignificance was determined using Wald-test (P value) followed by Benjamini-Hochberg correction (adjusted P value, Padj).

As shown by the MA-plots, the greatest differences were of gene expression of CD4+ T cells from different sites. Specifically, 4277 genes were expressed differently between gingivae and dLNs from sham-infected mice. Between gingivae and dLNs from *P. gingivalis*-infected mice, 4576 genes were differentially expressed. Of the top 20 differentially expressed genes upregulated in sham gingivae compared to sham dLNs and of the top 20 differentially expressed genes upregulated in infected gingivae compared to infected dLN, 15 genes were commonly upregulated within the gingivae, irrespective of infection status (**table 5.6**). Of the top 20 differentially expressed genes down-regulated in sham gingivae compared to sham dLNs and of the top 20 differentially expressed genes down-regulated in infected gingivae compared to infected dLN, 9 genes were commonly down-regulated (**table 5.6**). These genes may give an indication as to why particular CD4+ T cells reside

within the gingivae. *Maff* was the gene with the greatest decrease in expression by CD4+ T cells from dLNs. This gene encodes a transcription factor that is thought to play a role in blood coagulation and skeletal muscle development amongst others (http://www.uniprot.org/uniprot/O54791- accessed 03/02/17). Of the genes increased in the dLNs compared to the gingivae, *Clec2d* had the highest fold change. Clec2d encodes C-type lectin domain family 2, member d (https://www.ncbi.nlm.nih.gov/gene/93694 - accessed 03/02/17), which is a negative regulator of osteoclast differentiation and plays a role in protection against NK cell mediated cytotoxicity. As the gingivae is proximal to alveolar bone and teeth, it is not surprising that a gene involved in negatively regulating osteoclast differentiation is found downregulated in the gingival CD4+ T cells. Thus implying that these CD4+ T cells are more likely to promote osteoclast differentiation. Interestingly, *Cx3cl1* expression was increased in gingival CD4+ T cells compared to dLN CD4+ T cells. CX3CL1 has been shown to promote immune cell migration, particularly T cells, B cells, NK cells and monocytes (Ferretti et al., 2014). CX3CL1 is typically expressed by neurons, gut, vascular and airway epithelium but not usually T cells (Johnson and Jackson, 2013). Perhaps some of the CD4+ T cells isolated from gingivae were intraepithelial lymphocytes and shared the immune trafficking behaviour that epithelial cells can exert.

Of the genes statistically significantly expressed differently by CD4+ T cells of gingivae and dLN, a number of these genes were previously identified through the RT^2 profiler (**table 4.1**) This included a down-regulation of *Cxcl10* by cells of dLN compared to gingivae in both sham and *P. gingivalis* infection, a down-regulation of *Cxcl16* in dLN compared to gingivae in sham-infection and a decrease in *Ccl4* expression in dLN compared to gingivae in *P. gingivalis*-infection.

Table 5.6. Genes differentially expressed in CD4+ T cells from gingivae compared to draining lymph nodes.

Transcript	Log2 fold change (dLN v. gingivae)*		Padj value	
	Sham	*P. gingivalis*	Sham	*P. gingivalis*
Maff	-4.39	-5.38	5.57×10^{-70}	3.64×10^{-97}
Fosl2	-4.70	-4.79	5.25×10^{-92}	1.07×10^{-96}
Vegfa	-4.34	-4.65	1.86×10^{-59}	3.67×10^{-66}
Chad	-4.22	-4.40	1.51×10^{-35}	2.18×10^{-37}
Rnd1	-4.25	-4.39	1.62×10^{-53}	1.26×10^{-57}
Cdkn1a	-3.88	-4.07	2.24×10^{-25}	5.67×10^{-28}
4930438A08Rik	-3.55	-4.06	1.67×10^{-21}	2.28×10^{-28}
Errfi1	-3.78	-4.06	6.89×10^{-67}	2.33×10^{-77}
Crem	-3.81	-4.05	3.22×10^{-75}	4.98×10^{-85}
Tgif1	-3.64	-4.04	1.49×10^{-64}	6.66×10^{-79}
Ccno	-3.49	-3.99	1.78×10^{-28}	4.41×10^{-36}
Dusp8	-4.15	-3.91	4.60×10^{-32}	2.68×10^{-29}
Nr4a1	-3.54	-3.75	6.86×10^{-27}	2.68×10^{-30}
Cx3cl1	-3.80	-3.73	1.66×10^{-24}	1.14×10^{-23}
Pmaip1	-3.72	-3.68	1.40×10^{-74}	3.79×10^{-72}
Clec2d	2.45	2.69	7.41×10^{-23}	1.13×10^{-26}
RP24-417N13.5	1.69	2.19	1.18×10^{-05}	1.01×10^{-08}
2010008C14Rik	1.85	2.06	2.90×10^{-08}	7.07×10^{-10}
Ifit1	2.13	2.06	6.53×10^{-17}	8.50×10^{-16}
Gm12250	1.68	1.92	1.90×10^{-12}	2.22×10^{-16}
Lpar5	1.63	1.90	1.19×10^{-08}	1.03×10^{-11}
Al467606	1.52	1.84	1.65×10^{-25}	2.40×10^{-37}
Ifit1bl1	1.64	1.66	2.61×10^{-10}	1.40×10^{-10}
Gm37766	1.81	1.63	4.39×10^{-05}	2.69×10^{-04}

*Gene expression comparisons are shown as an up/downregulation in the draining lymph node compared to the gingivae in either sham-infection vs. sham-infection or *P. gingivalis*-infection v. *P. gingivalis* infection.
Abbreviations: dLN, draining (cervical) lymph nodes

Gene set enrichment analysis was conducted to determine whether defined sets of genes (i.e. genes that are together involved in a pathway) were significantly different in CD4+ T cells from gingivae or dLNs. The computational gene set enrichment analysis highlighted pathways that were differentially regulated, and those with a false discovery rate (FDR) < 1 were defined as being statistically significant. Twenty-two pathways were down-regulated in CD4+ T cells from the dLN compared to gingivae from sham-infected mice. The five pathways with the lowest FDR were cytokine-cytokine receptor interaction, osteoclast differentiation, MAPK signaling, TNF signaling and apoptosis pathways. As aforementioned the

gingiva is within close location of bone, therefore it is not unexpected that osteoclast differentiation pathways were upregulated in CD4+ T cells of gingival tissue. Of the pathways upregulated in CD4+ T cells from dLN compared to gingivae from sham-infected mice, three were statistically significant. The pathways included ribosome, oxidative phosphorylation and proteasome pathways. Comparing CD4+ T cell pathways from gingivae and dLN of *P. gingivalis*-infected mice, 16 pathways were downregulated in the dLN. The five pathways with the lowest FDR were the same as those from sham-infected mice. Of the pathways upregulated in CD4+ T cells from dLNs of *P. gingivalis*-infected mice compared to that of sham-infected mice, only two pathways were statistically significant; ribosome and oxidative phosphorylation pathways. Therefore, the changes in pathway gene expression in gingivae and dLN occur irrespective of *P. gingivalis* infection.

To verify the RNA-sequencing results by qRT-PCR, another two PD models were set up as previously described, with the exception that five mice per group were used. Each of the infected mice displayed serum anti-*P. gingivalis* IgG but once more did not exhibit alveolar bone loss (data not shown) at 28 days post infection. Curiously, the only RNA-sequencing-flagged gene of known function that was upregulated by CD4+ T cells in *P. gingivalis* infection in the gingivae was Btg3. This begged the question of whether B cells were sorted along with CD4+ T cells. CD4+ T cells were sorted based on positive selection for expression of CD45 and CD4. However, studies have shown that Epstein-Barr virus-immortilised B cells (Hoennscheidt et al., 2009) and Hodgkin's lymphoma B cells (Tzankov et al., 2005), can too express CD4. To address whether B cells contaminated the sorted CD4+ T cell population, an extra antibody was added to the sorting antibody panel to identify B cells – B220. In sham-infected mice, CD4+ B cells (CD45+ CD4+ B220+) were sorted from both gingivae and dLN at a ratio of approximately 1 B cell:1000 CD4+ T cells (CD45+ CD4+ B220-). In *P. gingivalis*-infection, the ratio was a little tighter, with on average 1 B cell:588 CD4+ T cells (**table 5.7**). In both groups the number of interfering B cells was small and therefore unlikely to contribute to the RNA-sequencing results. To confirm this, RNA from sorted CD4+ T cells and CD4+ B cells was extracted, reverse-transcribed to cDNA and 18S expression was analysed by qRT-PCR. Expression of 18S could be found in CD4+ T cells but not of the CD4+ B cells from any of the samples

(data not shown). It can be concluded that CD4+ B cells are very unlikely to have contributed to the results of the RNA-sequencing experiment.

Table 5.7. Interference of B220+ cells in the CD4+ cell gate.

Sample	No. of sorted CD4+ B220- T cells	No. of sorted CD4+ B220+ cells	Ratio CD4+ B220- T cells:CD4+ B220+ cells	Expression of target genes by CD4+ B220+ cells?
Sham gingivae	9931	10	993:1	No
P. gingivalis gingivae	10144	15	676:1	No
Sham dLN	100244	106	946:1	No
P. gingivalis dLN	100229	200	500:1	No

To determine whether the differential gene expression of CD4+ T cells in *P. gingivalis*-infection - identified by RNA-sequencing – was reproducible, qRT-PCR was conducted. Of the 4 genes with significantly different expression in CD4+ T cells from gingivae or dLNs from *P. gingivalis*-infected mice, only the primers for Btg3 were readily available and optimized in the available time. As the changes in expression of Prdm2, Bc147527 and Tcf20 were of borderline significance, their expression was also evaluated by qRT-PCR. The qRT-PCR suggested that increased expression of *Btg3* was observed in CD4+ T cells from only gingivae of infected mice (mean relative expression 6×10^{-5} +/- 4×10^{-6} sham vs mean relative expression 1×10^{-4} +/- 1×10^{-5} *P. gingivalis*, $P < 0.05$) (**figure 5.10**). However, using 18S primers that are known to amplify both cDNA and gDNA, contamination was detected in these samples. The Btg3 primers also amplify both cDNA and gDNA therefore changes in expression of *Btg3* could not be definitely defined.

Expression of *Prdm2* could not be detected in CD4+ T cells from sham gingivae but could be detected in infected gingival CD4 T cells. The expression of *Bc147527* was not detected in CD4+ T cells from gingivae of either control or infected animals.

CD4+ T cells from the gingivae of infected mice appeared to express Tcf20 more than cells of control mice. However, expression of this gene was only detected in sham-infected gingivae from one experiment so the data were not significantly different. The findings of qRT-PCR do not entirely reflect the pattern of expression determined by RNA-sequencing. However, the expression of *Btg3*, *Prdm2*, *Bc147527* and *Tcf20* by CD4+ T cells of dLNs was not found to be different in either infection state – both by RNA-sequencing and qRT-PCR.

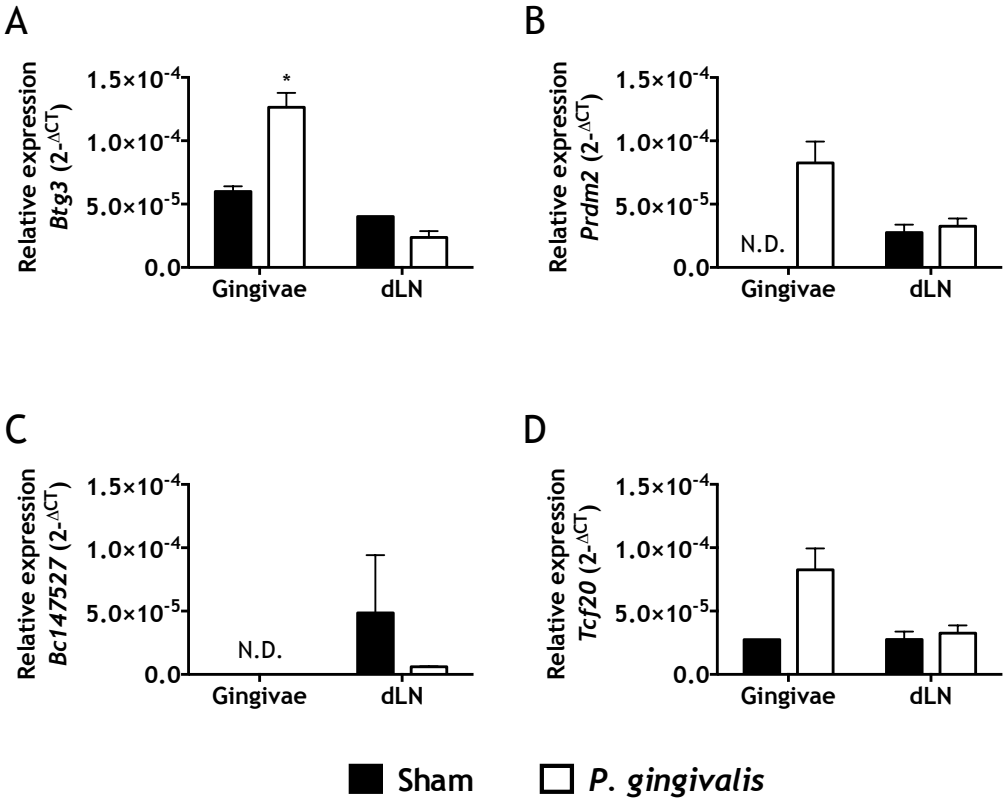

Figure 5.10. Verification of up- and down-regulation of genes in the gingivae from *P. gingivalis*-infected mice by quantitative real-time PCR.
Mice were orally infected with *P. gingivalis* or were sham-infected with carrier vehicle, CMC, only. At 28 days post infection, cells were isolated from gingivae and draining lymph nodes and CD4+ T cells were sorted. RNA was extracted and reverse transcribed to cDNA to determine expression of (A) *Btg3,* (B) *Prdm2,* (C) *Bc147527* and (D) *Tcf20* relative to 18S by quantitative PCR. Not determined (N.D.) represents no expression of the appropriate gene. Data are shown as mean + SEM, combined from 2 independent experiments, n = 5/group from which cells were pooled. Statistical analysis was conducted on log transformed data (raw data shown on graph). Statistical significance was determined by unpaired T tests, as indicated on the graphs (*P < 0.05).

5.3 Discussion

The data presented in **chapter 4** demonstrated that subtle changes in T cell phenotype occurred in response to oral *P. gingivalis* infection at 28 days post infection. These studies were based on analysis of a small selection of cell surface markers and cell products that were thought to contribute to PD. Therefore, alterations in T cell phenotype may not have been completely exposed. RNA-sequencing was therefore employed as a platform to fully explore the phenotype and function of CD4+ T cells at the transcriptome level, in a non-biased manner. However, commensurate with the data in chapter 4, very few differences in gene expression were found between sham and *P. gingivalis* infection in CD4+ T cells.

For these studies, RNA-sequencing was selected over microarray technology as the former permits identification of novel transcripts, gene fusions and insertions and deletions, as opposed to the requirement of transcript-specific probes. The Next-seq platform was used to conduct RNA-sequencing as it is highly accurate and data can be generated in 48 hours. As the amount of RNA in gingival samples was limiting, perhaps a better sequencing platform would be Helicos due to simple sample preparation. A true and direct reflection of gene expression is likely achieved using the Helicos system, as reverse transcription, PCR amplification and cDNA are not required. Whilst Helicos may be advantageous for low RNA concentrations, a major limitation with this platform is the high rate of error (~5%), predominantly insertions and deletions, making matching of sequencing reads to a reference genome difficult. Illumina (NextSeq, HiSeq and MiSeq) and SOLiD sequencing platforms, however, have low error rates (<1%) (Chu and Corey, 2012). SOLiD sequencing takes 6-7 days to generate high quality data, of which there is less output than illumina platforms. Of the illumina platforms, HiSeq generates higher quality data than that generated by MiSeq or NextSeq but has longer turnaround times (11-14 days) (Gupta and Gupta, 2014). Furthermore, large-scale projects are better suited to NextSeq or HiSeq, and despite long turnaround times, HiSeq is more cost efficient (Glenn, 2011). The Hi-Seq platform may have provided better quality data, and may have highlighted other differences in CD4+ T gene expression in PD, however, the faster turnaround time, accurate data generation

and cost efficiency of the NextSeq platform was advantageous for the study described in this chapter.

Of the total transcriptome analyzed by RNA-sequencing, only three genes were significantly differentially expressed by CD4+ T cells in gingivae from *P. gingivalis*-infected mice. These genes did not encode proteins that were analysed in **chapter 4**, confirming that the bias-driven manner in which previous experiments were executed may mask the PD phenotype of CD4+ T cells. The number of genes up or down-regulated upon *P. gingivalis* infection was surprisingly low, considering that an initial human PD RNA-sequencing study of gingival tissue determined that 453 genes were differentially expressed in disease (Davanian et al., 2012). However, it is important to note that the complete cell composition of gingival tissue was analyzed in the human study, rather than a single cell population. Nonetheless, of the known genes found to be significantly (*Btg3*) or close to being significantly (*Prdm2*, *Hmgb1-ps1*, *Bc147527*, *Tcf20*) differentially expressed in murine gingivae by CD4+ T cells, none were differentially expressed in human PD RNA-sequencing studies (Davanian et al., 2012, Lundmark et al., 2015, Kim et al., 2016). This does not completely refute our findings, as the difference in gene expression of other cell types in health versus disease may have been greater, therefore the difference in *Btg3* expression may have been evident but not significant. Furthermore, Davanian *et al*. claimed that the gene expression patterns of PD gingival tissue were distinct from those of healthy gingival tissue, yet the healthy and diseased gingival sites of three of their ten participants clustered together. This was potentially explained by underlying subclinical disease, but like our study it also highlights that a PD phenotype may be difficult to define. Similarly, distinct gene expression profiles could not be assigned to chronic and aggressive PD (Papapanou et al., 2004). The gene expression findings in numerous PD studies starkly contrast identification of specific gene expression patterns in other diseases; for example, a gene expression signature can distinguish between metastatic and localized breast cancer. This has been of huge beneficiary as it enables patient survival predictions and patient-tailored treatment (van 't Veer et al., 2002).

Moreover, numerous studies investigated the transcriptome present in PD, both by RNA-sequencing and microarrays; however, no similar expression pattern was found in any of these studies. Particularly, differential gene expression by the same research group but in separate studies described 453 PD-associated genes (Davanian et al., 2012) and 1268 PD-associated genes (Lundmark et al., 2015), respectively. Whilst the latter study employed substantially more patients, the gene with the greatest differential expression – Muc4 – wasn't included in the 50 most differentially expressed genes in their earlier study. The only upregulated gene found to be in both data sets (as presented in the paper) was MMP7. Furthermore, others found 12,744 probe sets to be expressed differently in PD by human genome array, yet Muc4 did not reach the 50 most up-regulated genes (Demmer et al., 2008). Additionally, four genes with greatest difference in expression in PD were shared between Lundmark's and Kim's RNA-sequencing studies, once again highlighting very little overlap (Lundmark et al., 2015, Kim et al., 2016). Therefore, a defined transcriptome of PD has not been described. Perhaps discrimination of ethnicity, sex, age and environment would allow identification of a PD transcriptome for groups of similar patients. Likewise, IL-1 (Papapanou et al., 2001, Archana et al., 2012) and Fcγ (Wolf et al., 2006) polymorphisms can indicate the severity of PD in only some ethnic or racial populations. What has been defined by transcriptome analysis however, is that there is an upregulation of inflammatory mediators and cytokines in PD. Gene expression of such markers were not found to be differentially expressed in our murine RNA-sequencing data from CD4+ T cells, implying that inflammation at the local site of infection is not mediated by T cells – at least in the mouse model.

Th subsets can be delineated by RNA-sequencing. Although not significant, the transcriptome identified in this chapter revealed that IFN-γ was upregulated by CD4+ T cells in disease – as was found by flow cytometry. However, RNA-sequencing in humans found no correlation between IFN-γ and PD, rather Th17 cytokine genes were upregulated significantly (Kim et al., 2016). There was no difference in Tfh cell genes in CD4+ T cells from dLNs of *P. gingivalis* infected mice. RNA-sequencing was conducted at 28 days post infection, whilst flow cytometry of Tfh cells was conducted at 14 days post infection, highlighting that an extensive time course of

gene expression studies would be required to identify the kinetics of the T cell response.

There have been no other RNA-sequencing studies conducted in mouse cervical LNs in experimental PD, therefore no comparison can be made between dLN data from this RNA-seq experiment and others. The only gene found to be significantly differentially expressed by CD4+ T cells from the dLNs in *P. gingivalis*-infection was *Gm5451*. As this is a predicted mouse gene, there have been no studies investigating its role in any disease. To explore it's function, and the function of predicted genes found to be differentially expressed by gingival CD4+ T cells, the genes could be silenced. RNA interference (RNAi) can silence genes by inhibiting transcription or most commonly by acting post-transcriptionally by sequence-specific RNA degradation. For research purposes, long double-stranded (ds) RNAs can be delivered to a cell. The dsRNA is then cleaved by dicer, resulting in small interfering RNAs (siRNAs) that bind to target mRNA. The mRNA that is bound by siRNA is cleaved and cleaved mRNAs are degraded, therefore preventing protein synthesis (Agrawal et al., 2003).

The use of qRT-PCR to determine the expression of *Btg3*, *Prdm2*, *Bc147527* and *Tcf20* by CD4+ T cells isolated from the gingivae of sham and *P. gingivalis*-infected mice only partially supported the RNA-sequencing data. With regard to the latter three genes, expression was not detected in at least one replicate gingival CD4+ T cell sample replicate. Therefore, repitition of the experiment with increased cell numbers – hence increased mice per group – would enable extraction of greater quantities of RNA and likely better quality of cDNA that would provide a true representation of expression. Whilst the expression of *Btg3* did mimic that found by RNA-sequencing, the primers were known to amplify both cDNA and gDNA. The presence of gDNA was highlighted by the no reverse transcriptase control and prevented conclusive verification of increased *Btg3* expression by CD4+ T cells from infected animals. New primers for *Btg3* could be designed to span an exon-exon junction, preventing gDNA contamination. Furthermore, even with the identification and confirmation of statistically significant gene expression, functional significance is not necessarily reflected. Owing to translational

regulation not all mRNA will be translated to protein. MicroRNAs are non-coding RNAs that post-transcriptionally regulate gene expression and prevent protein synthesis upon base-pairing to 3' untranslated regions of mRNA (Fabian et al., 2010). Translation of mRNA to protein in samples could be confirmed by flow cytometry and IHC.

Whilst the data from the RNA-seq experiment described in this chapter did not highlight a particularly exciting role for CD4+ T cells in experimental PD, it did provide an oral mucosal CD4+ T cell transciptome signature. There are a plethora of studies describing the immune cell basis of the gut mucosa, hence the gut mucosa is better understood than the oral mucosa (Wu et al., 2014). Therefore, the transcriptome profile of CD4+ T cells will help to build a basic understanding of oral mucosa's immune system, an understanding that at present remains somewhat elusive (Cutler and Jotwani, 2006). This study has described for the first time the direct comparsion of CD4+ T cells from gingivae and dLNs at the level of transcription. This is important as the immune response is highly compartmentalised based on anatomical locations (Horav 2014, Crabbe et al., 1965). It may be possible to identify publically available T cell transcriptomes from other mucosal barrier sites and mine these data to investgiate the differences between T cell in the oral mucosal compared with other sites.

In conclusion, very few genes were identified as being differentially expressed by CD4+ T cells of gingvae or dLN in experimental PD. Unlike human RNA-sequencing studies of whole tissue that idenfited numerous inflammatory pathway-associated genes to be increased in gingival biopsies, no inflammatory genes were increased or decreased in the mouse model of PD, which highlighted that CD4+ T cells may not play a predominant role in this disease. However, the RNA-sequencing data demonstrated that the gene expression profile of gingival CD4+ T cells differs from that of cervical CD4+ T cells.

Key findings from this chapter:

- *Btg3*, *Gm20634* and *Gm20633* expression was increased by CD4+ T cells from gingivae of *P. gingivalis*-infected mice.
- *Gm5451* expression was decreased by CD4+ T cells from dLNs of *P. gingivalis*-infected mice.
- CD4+ T cells did not play a key role in the orchestration of inflammation in experimental PD at 28 days post infection.
- CD4+ T cells from gingivae upregulated cytokine-cytokine receptor interaction, osteoclast differentiation, MAPK signaling, TNF signaling and apoptosis pathways compared to CD4+ T cells from dLN.
- CD4+ T cells from dLN upregulated ribosome and oxidative phosphorylation pathways compared to CD4+ T cells from gingivae.

6 Tracking the antigen specific T cell response in PD

6.1 Introduction

Thus far, the phenotype of T cells in oral mucosal tissues, in the presence and absence of *P. gingivalis* infection, has been described. What is lacking, however, is the nature and function of T cells specific for *P. gingivalis* antigens. It is likely that the *P. gingivalis*-specific cells orchestrate inflammation within the oral cavity in at least the early stages of *P. gingivalis* infection.

T cells specific for a particular antigen lack antigen-specific identifying markers and are present in low frequencies, making the study of specific T cell responses challenging. T cells specific for the relevant antigen can be investigated *in vivo* by adoptive transfer of antigen specific cells. T cells can be specific for epitopes on the antigen of interest, or heterologous antigens that are not typically expressed by the pathogen of interest. This system increases the number of antigen-specific T cells within the circulation of a recipient mouse (Jenkins et al., 2001). Initial studies exploiting this immunological tool determined the host-pathogen interaction in *Salmonella typhimurium* (*S. typhimurium*) infection. OVA-specific DO11.10 CD4+ T cells were assessed upon subcutaneous infection with *S. typhimurium* that was genetically manipulated to express heterologous OVA – thereby the antigen-specific T cell response. Antigen-specific CD4+ T cells were found to proliferate and increase IFN-γ secretion, validating the adoptive transfer model (Chen and Jenkins, 1999).

This technique is not exclusive to *Salmonella* species. OVA-expressing *E. coli* have been developed to aid in the study of antigen-specific CD4+ T cells in the induction of colitis *in vivo* (Yoshida et al., 2001, Feng et al., 2010) and to determine whether the presentation of gram-negative and gram-positive antigens differentially influence immunogenicity *in vitro* (Martner et al., 2013). Furthermore, *E. coli* expressing listeriolysin O and OVA have been shown to promote the presentation of a specific OVA epitope in MHC-I that enables OVA-specific CD8+ T cells to lyse OVA-expressing melanoma cell-lines both *in vitro* and *in vivo,* through genetic

modifications of bacteria and tumour cell lines and the use of OVA specific T cells (Radford et al., 2002).

Whilst OVA expressing bacteria are useful approaches to the study of specific immune responses, a major caveat is that the antigen is not naturally expressed. Therefore, such studies may not accurately represent T cell responses to bacterial antigen. To determine the immune response to natural antigens expressed by *Salmonella*, a system to adoptively transfer TCR transgenic CD4+ T cells specific for *Salmonella* flagellin was established. TCR transgenic mice with specificity to flagellin peptide (427-441)-I-A^b were generated by amplification of rearranged specific receptor sequences and insertion into TCR vectors. The vectors were then injected into fertilized eggs (McSorley et al., 2002). This novel technique mimicked the findings of oral infection with OVA-expressing *Salmonella* in which specific T cell activation occurred in Peyer's patches. However, it also provided evidence that antigen processing and presentation can be conducted in 3 hours in response to natural *Salmonella* antigen.

To evaluate the specific immune response generated in *P. gingivalis* infection, one study identified thiol peroxidase as a *P. gingivalis* antigen that potentially exacerbated PD. Identification of the antigen was through repeated co-culture of CD4+ T cells isolated from spleens of mice infected with *P. gingivalis*, to initially generate *P. gingivalis*-specific CD4+ T cells. APCs pulsed with transformed *E. coli* expressing *P. gingivalis* DNA libraries were then cultured with *P. gingivalis*-specific CD4+ T cells to identify antigens that stimulated proliferation. However, the specific CD4+ T cells were not exploited to assess the *in vitro* or *in vivo* responses to *P. gingivalis*. Rather, following oral infection with *P. gingivalis,* the Th immune response generated specifically to thiol peroxidase was determined by IgG2a and IgG1 antibodies in serum. Whilst the greater abundance of IgG2a specific for thiol peroxidase implied a Th1 response, the phenotype of specific cells was not investigated (Gonçalves et al., 2006).

Furthermore, human *P. gingivalis* specific-CD4+ T cells were generated by a similar manner to that described above for murine cells, whereby *P. gingivalis*-pulsed DCs

were co-cultured repeatedly with CD4+ T cells obtained from peripheral blood. The supernatants from specific CD4+ T cell and *P. gingivalis*-pulsed DC co-cultures were found to contain elevated levels of IFN-γ compared to specific CD4+ T cells co-cultured with unpulsed DCs. The phenotype of *P. gingivalis*-specific CD4+ T cells was not explored (Aroonrerk et al., 2003).

Although CD4+ T cells specific to natural *P. gingivalis* antigens are likely to better address the immune response in infection, a limitation is that generation of specific cells requires repeated stimulation of T cells with *P. gingivalis*-pulsed APCS. Repeated stimulation has been found to cause inefficient effector CD4+ T cell expansion, impaired cytokine production and altered migration (Jelley-Gibbs et al., 2005) and could therefore interfere with the natural functioning of the T cell. To date, the genetic manipulation of *P. gingivalis* to express a heterologous antigen as a means to assess T cell specificity has not been described in the literature.

Due to the lack of studies tracking *P. gingivalis*-specific T responses in the context of PD, *P. gingivalis* W83 was genetically manipulated to express OVA peptide to gauge an idea of the specific bacterial antigen response using OVA-specific T cells.

The aims of this chapter were:

- To investigate whether OVA-expressing *P. gingivalis* could stimulate an immune response *in vitro*.
- To investigate whether OVA-expressing *P. gingivalis* could stimulate an immune response *in vivo*.
- Pending the outcome of the above, to investigate the antigen specific T cell response in a murine model of PD.

6.2 Results

Bacteria can be genetically manipulated to enable tracking within *in vitro* or *in vivo* model systems. A technique previously described to track the induction and maintenance of specific T cell responses to bacteria uses the expression of OVA peptide by bacteria. OVA-specific T cells from an OTII or DO11.10 mouse can be adoptively transferred to a recipient mouse of non-transgenic background to allow tracking of the immune response to OVA-expressing bacteria. *P. gingivalis* W83 was modified to express OVA by Jan Potempa and integration of the OVA expressing construct confirmed by PCR. This strain – known as RgpbOVA-A – was modified to introduce OVA peptide (323-339) into arginine-specific gingipain B (RgpB). The insertion of OVA peptide into RgpB did not interfere with its activity; therefore RgpbOVA-A mimicked WT *P. gingivalis* W83.

To determine the position of OVA peptide 323-339 within RgpB, a 3D model structure of RgpbOVA-A was generated. The amino acid sequence of conventional RgpB was inserted into SWISS-MODEL ExPASy online tool to model RgpB pro- and mature domains (**figure 6.1**). The insertion site LNE/SIA was found within an apparently highly exposed region of the mature domain of RgpB. A model structure of RgpbOVA-A was next generated (**figure 6.2A-B**) and illustrated that OVA peptide forms a protruding loop at the side of the mature domain. Therefore, it doesn't appear likely that APCs would have difficulty accessing OVA peptide within the gingipain. Furthermore, APCs readily present OVA peptide 323-339 despite this peptide being found in the middle of OVA protein and having no amino acids extending out-with the structure of OVA (**figure 6.2C**).

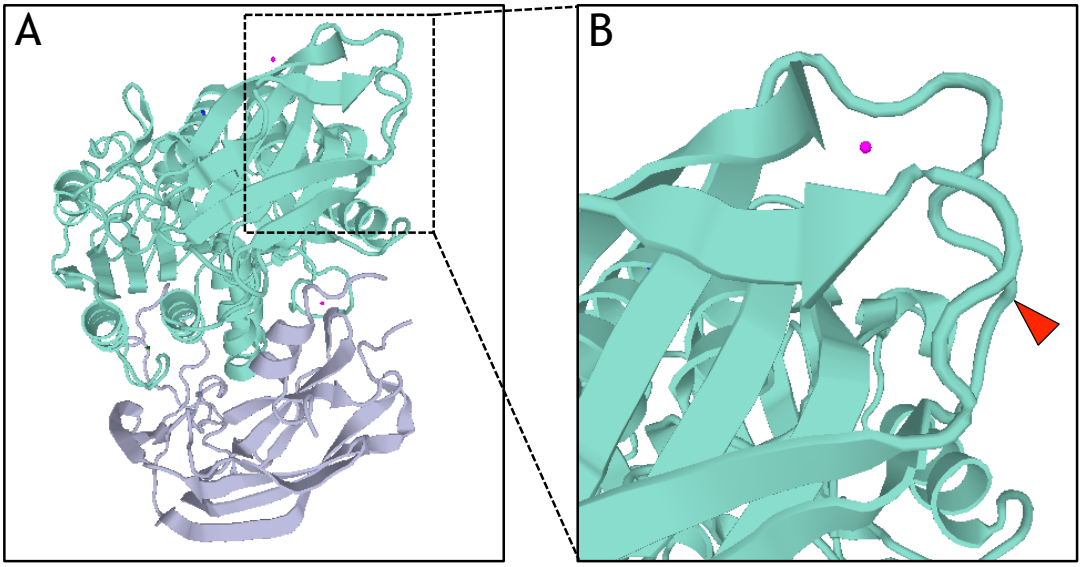

Figure 6.1. Model structure of RgpB pro- and mature domains.
The representative structure of *P. gingivalis* W83 RgpB pro- and mature domains was generated by inserting the amino acid sequence into SWISS-MODEL, ExPASy online tool. (A) Structure of pro- and mature domains of the gingipain RgpB. The blue structures represent the gingipain R2 mature domain and purple structures represent the gingipain R2 pro-domain. (B) Enlarged image of boxed area in (A). The red arrow indicates the region where the OVA peptide sequence has been inserted, between LNE and SIA sequence sites.

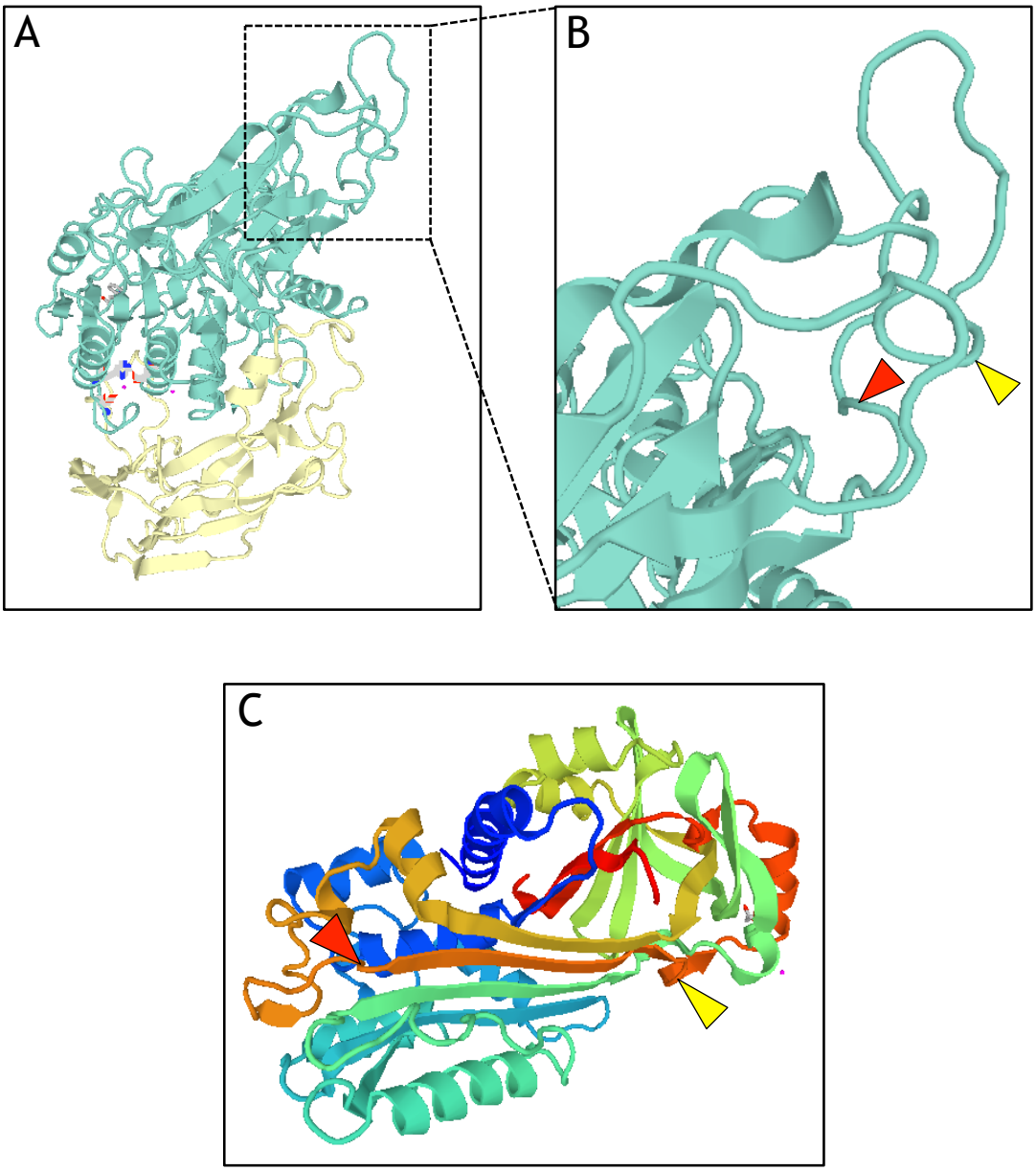

Figure 6.2. Model structure of RgpB pro- and mature domains with ovalbumin peptide insertion and ovalbumin peptide within ovalbumin protein.
Representative structures of *P. gingivalis* W83 RgpB pro- and mature domains with insertion of OVA peptide and OVA protein were generated by inserting the amino acid sequences into SWISS-MODEL, ExPASy online tool. (A) Structure of pro- and mature domains of RgpBOVA. The blue structures represent the gingipain R2 mature domain and yellow structures represent the gingipain R2 pro-domain. (B) Enlarged image of boxed area in (A). The red arrow indicates the start of the OVA peptide sequence at LNE sequence site and the yellow arrow indicates the end of the OVA peptide sequence at SIA sequence site. (C) Structure of OVA protein. Rainbow colour scheme has been used for clearer identification of OVA peptide. The red arrow indicates the start of OVA peptide sequence and the yellow arrow indicates the end of the OVA peptide sequence.

As the OVA peptide was inserted into the middle of RgpB, studies by Jan Potempa's group confirmed expression of RgpB by western blot and it was therefore plausible that OVA peptide was co-expressed (data not shown). Further western blots were conducted to determine whether the OVA peptide was expressed, using anti-OVA peptide 323-339 antibody. **Figure 6.3A** suggests that OVA peptide was expressed by RgpbOVA-A but not by WT *P. gingivalis*. The mass of OVA peptide is approximately 1.77 kDa therefore only the 2kDa protein standard was marked on the blot as a reference for the expected distance migrated by OVA peptide from RgpbOVA-A. The peptide did not migrate as far down the gel as expected, perhaps due to its position within RgpB that may have prevented complete isolation of OVA peptide. OVA peptide alone, at concentrations of 0.5 µg and 0.1 µg could not be visualized. Ponceau S staining of the blot demonstrated protein bands in all of the lanes except those containing OVA peptide, which suggests that the peptide may have run off the gel during electrophoresis (ponceau S data not shown). OVA protein was used as a positive control for the next blot. OVA protein could clearly be identified at 10 µg, 5 µg and 1 µg, whilst faint bands of OVA peptide could be visualized from lanes containing RgpbOVA-A, by the anti-OVA peptide antibody. There was no staining of the WT *P.* gingivalis using this antibody. The actual size of whole OVA protein is 45 kDa, suggesting that the blot was successful (**figure 6.3B**). Finally, to determine that WT *P. gingivalis* was loaded correctly into the well of the gel, the expression of GroEL by both strains of *P. gingivalis* was evaluated. GroEL is a chaperonin found in many bacteria and aids in the folding of proteins (Frieden and Clark, 1997) and was expressed by both WT and transgenic *P. gingivalis* (**figure 6.3C**). Although each of the OVA peptide western blots had caveats, taken together with the PCR data, it appeared likely that RgpbOVA-A expressed OVA.

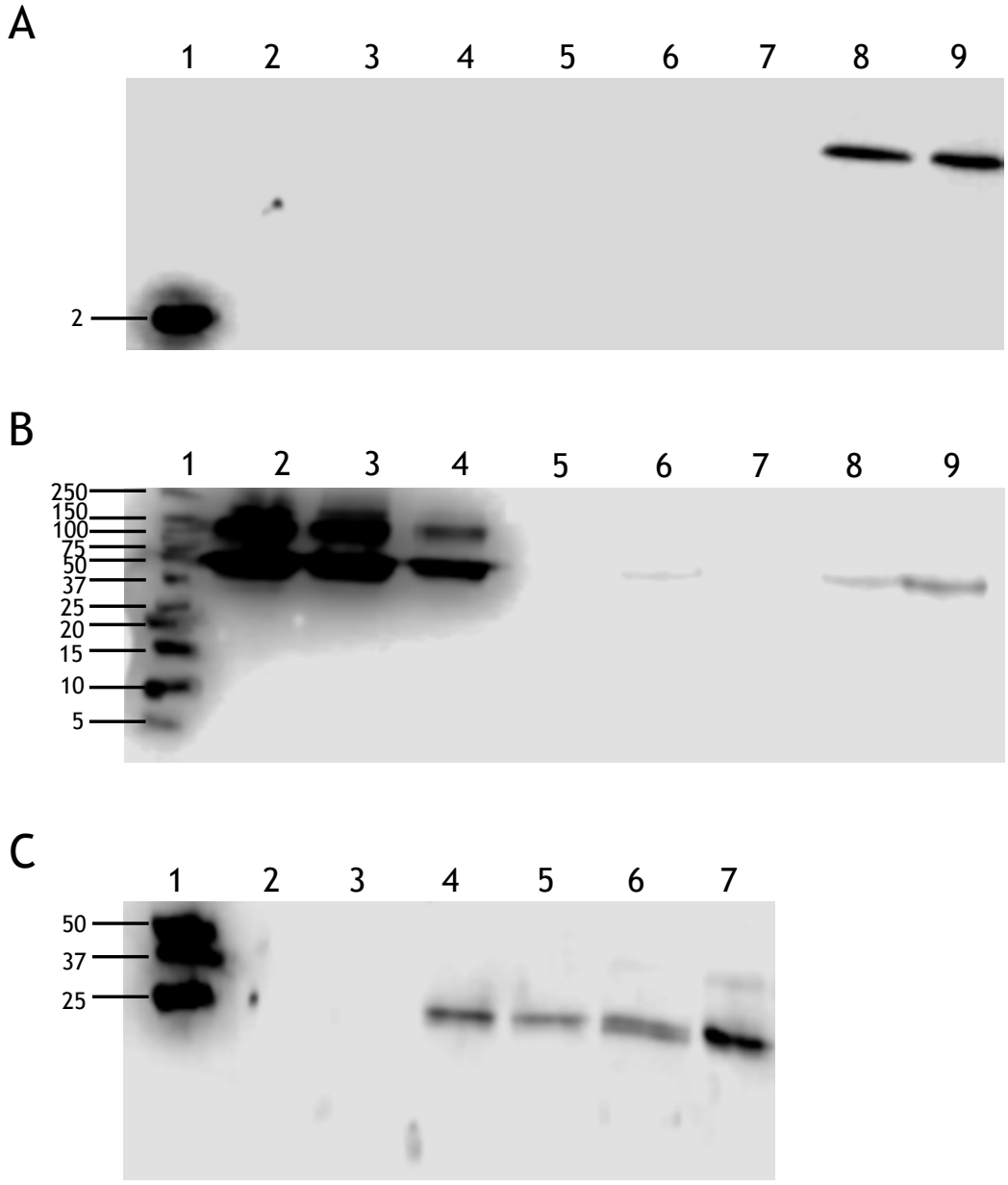

Figure 6.3. Western blot analysis of expression of ovalbumin peptide by *P. gingivalis* and RgpbOVA-A.
Expression of ovalbumin (OVA) peptide by RgpbOVA-A was determined by western blot using an OVA peptide-specific antibody. (A) OVA peptide expression. Lane 1, 2 and 3 – ladder; lane 4 – OVA peptide, 0.5 µg; lane 5 - OVA peptide 0.1 µg; lanes 6 and 7 – WT *P. gingivalis;* lanes 8 and 9 RgpbOVA-A (B) OVA peptide expression. Lane 1 – ladder; lane 2 – OVA protein 10 µg; lane 3 – OVA protein 5 µg; in lane 4 – OVA protein 1 µ; lanes 5 and 7 - WT *P. gingivalis;* lanes 6, 8 and 9 – RgpbOVA-A. (C) GroEL expression. Lane 1 – ladder; lane 2 – OVA peptide 0.5 µg; lane 3 – OVA peptide 0.1 µg; lanes 4 and 5 - WT *P. gingivalis*; lanes 6 and 7 – RgpbOVA-A. Various kDAs have been marked at the appropriate fraction of the ladders.

The data described above suggest that the RgpbOVA-A seemed likely to express OVA peptide. The capacity for RgpbOVA-A to stimulate OVA-specific T cells *in vitro* was then investigated. Splenocytes from a DO11.10 mouse were incubated with OVA protein, WT *P. gingivalis*, OVA protein + WT *P. gingivalis*, RgpbOVA-A, anti-CD3 or media only for 2 hours at 37^{o}C. Unbound antigen and non-adherent cells were then washed off, leaving the adherent APCs. Lymphocytes from DO11.10 mice were then incubated with the APCs described above and assessed for markers of proliferation (Ki67) and activation (CD69) (**figure 6.4**). As expected, in the media control, only a small percentage of OVA-specific (KJ1.26) CD4+ T cells proliferated (mean 2.47 +/- 0.06% Ki67+) or became activated (mean 11.21 +/- 1.36% CD69+). This was also true of cells stimulated with WT *P. gingivalis* (mean 1.40 +/- 0.60% Ki67+; mean 12.34 +/- 2.28% CD69+). On the other hand, KJ1.26+ T cells stimulated with anti-CD3 (mean 12.93 +/- 1.00% Ki67+; mean 74.67 +/- 0.88% CD69+), OVA protein (mean 14.31 +/- 1.05% Ki67+; mean 47.73 +/- 0.45 CD69+) and OVA protein + WT *P. gingivalis* (mean 21.36 +/- 1.01% Ki67+; mean 60.02 +/- 0.42% CD69+) both proliferated and became activated. Interestingly, despite the expression of OVA peptide by RgpbOVA-A, the cells stimulated with this transgenic strain of *P. gingivalis* expressed Ki67 and CD69 at levels similar to the media control (mean 1.52 +/- 0.94% Ki67+; mean 9.00 +/- 4.19% CD69+). To determine whether the *in vitro* culture conditions were unfavorable for presentation of OVA peptide from RgpbOVA-A, the ability of RgpbOVA-A to induce activation of KJ1.26+ cells in an *in vivo* mouse model was next assessed.

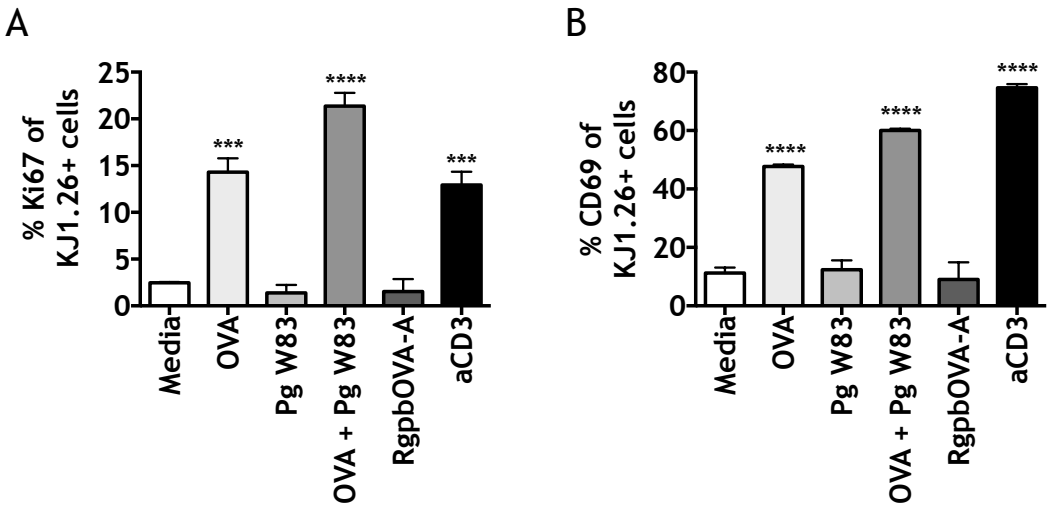

Figure 6.4. Stimulation of ovalbumin-specific T cells by RgpbOVA-A, *in vitro*. Splenocytes and cervical lymph nodes were removed from a DO11.10 mouse and cells isolated. As a source of antigen presenting cells, 2 x 10^5 splenocytes were incubated with OVA protein (1 mg/ml); anti-CD3 (1 µg/ml); 1 x 10^7 WT *P. gingivalis* W83 (Pg W83); 1 x 10^7 WT *P. gingivalis* W83 along with OVA protein (1 mg/ml) (OVA + PgW83); 1 x 10^7 RgpbOVA-A or media only for 2 hours. Unbound antigen and non-adherent cells were washed off, leaving adherent APCs. Pulsed APCs were then incubated with 2 x 10^5 cervical LN cells for 72 hours. The OVA-specific T cells (CD4+ KJ1.26+) were analysed by flow cytometry for proliferation and activation. (A) Percentage of proliferating Ki67+ KJ1.26+ cells. (B) Percentage of activated CD69+ KJ1.26+. Data are mean + SEM, from 2 replicates (the cells from one mouse were used for all stimulations and each stimulation was conducted in duplicate). Statistical significance was determined by a multiple comparison one way ANOVA, comparing each stimulus with the media control, as indicated on the graph (***P < 0.001 and ****P < 0.0001).

For the *in vivo* test of RgpbOVA-A, CD4+ KJ1.26+ T cells were adoptively transferred from a DO11.10 mouse to BALB/c mice to increase the frequency of specific cells in the recipients. The mice were split into four groups as described in **table 6.1** and received scruff injections of WT *P. gingivalis*, RgpbOVA-A, WT *P. gingivalis* + OVA protein all in combination with CFA or CFA only. Ten days later, the mice received footpad injections of the same antigen, without CFA. Seventy-two hours post injection, the cells of popliteal LNs were isolated and the proportion of OVA-specific, KJ1.26+ T cells in the dLN analysed by flow cytometry (**figure 6.5A-B**). The rationale behind the experimental design was that antigen emulsified in CFA induced antigen processing and presenting to T cells. After re-exposure to antigen in the footpad and therefore the secondary antigen response, OVA-specific T cells

would further expand and the response would be amplified (Allen, 2013). The footpad is an ideal site for antigen re-exposure as it provides a dLN to focus on – popliteal LN.

Table 6.1. Experimental setup for stimulating ovalbumin-specific T cells by RgpbOVA-A, *in vivo*.

Group (n=3)	DO11.10 transfer	Scruff injection	Footpad injections
1	✔	*P. gingivalis* W83 + CFA	*P. gingivalis* W83
2	✔	RgpbOVA-A + CFA	RgpbOVA-A
3	✔	*P. gingivalis* W83 + OVA + CFA	*P. gingivalis* W83 + OVA
4	✔	CFA	PBS

Abbreviations: CFA, complete freud's adjuvant; OVA, ovalbumin protein.

The *in vivo* model demonstrated that compared to the PBS control group, RgpbOVA-A footpad injection recruited a similar percentage of KJ1.26+ T cells to the dLN, as did footpad injections of WT *P. gingivalis* (mean 0.127 +/- 0.024% PBS vs. mean 0.046 +/- 0.020% RgpbOVA-A vs. mean 0.019 +/- 0.004% WT *P. gingivalis*, NS). Although not statistically significant, WT *P. gingivalis* + OVA protein appeared to recruit more KJ1.26+ T cells (mean 0.402 +/- 0.220% WT *P. gingivalis* + OVA). With regard to proliferation, only WT *P. gingivalis* + OVA protein caused a significant increase in Ki67 expression of OVA specific T cells in the dLN (mean 3.760 +/- 2.168% PBS vs. mean 8.167 +/- 1.878% RgpbOVA-A vs. mean 5.047 +/- 2.536%, NS; mean 3.760 +/- 2.168% PBS vs. mean 93.300 +/- 3.099% WT *P. gingivalis*, $P < 0.0001$). Therefore only administration of exogenous OVA protein alongside *P. gingivalis* induced the proliferation of OVA-specific T cells in this model. As a further measure of the OVA specific immune response, serum antibody titres were determined (**figure 6.5C**). Once again, the only mice that mounted anti-OVA IgG titres were those of group 3, which received WT *P. gingivalis* + OVA protein (mean 52.2 +/- 13.9 PBS vs. mean 2773.0 +/- 254.8 WT *P. gingivalis* + OVA, $P < 0.0001$). The other groups mirrored the anti-OVA response of PBS (mean 52.2 +/- 13.9 PBS vs. mean 43.3 +/- 9.4 RgpbOVA-A vs. mean 34.9 +/- 11.9 WT *P. gingivalis*, NS). To determine whether RgpbOVA-A itself induced an immune response, serum anti-*P.*

gingivalis IgG titres were measured (**figure 6.5D**). All groups which received *P. gingivalis*, either transgenic or WT, produced antibody titres significantly greater than PBS control mice (mean 13.8 +/- 8.0 EU PBS vs. mean 728.6 +/- 47.8 EU RgpbOVA-A vs. mean 816.0 +/- 129.8 EU WT *P. gingivalis* vs. 938.8 +/- 324.3 EU WT *P. gingivalis* + OVA, $P < 0.05$). The ELISA data highlighted that RgpbOVA-A acted similarly to WT *P. gingivalis* and was able to stimulate the immune response to generate antibodies specific for *P. gingivalis*. It can therefore be concluded that whilst RgpbOVA-A seems to express OVA peptide, it failed to induce an OVA-specific immune response *in vitro* or *in vivo*.

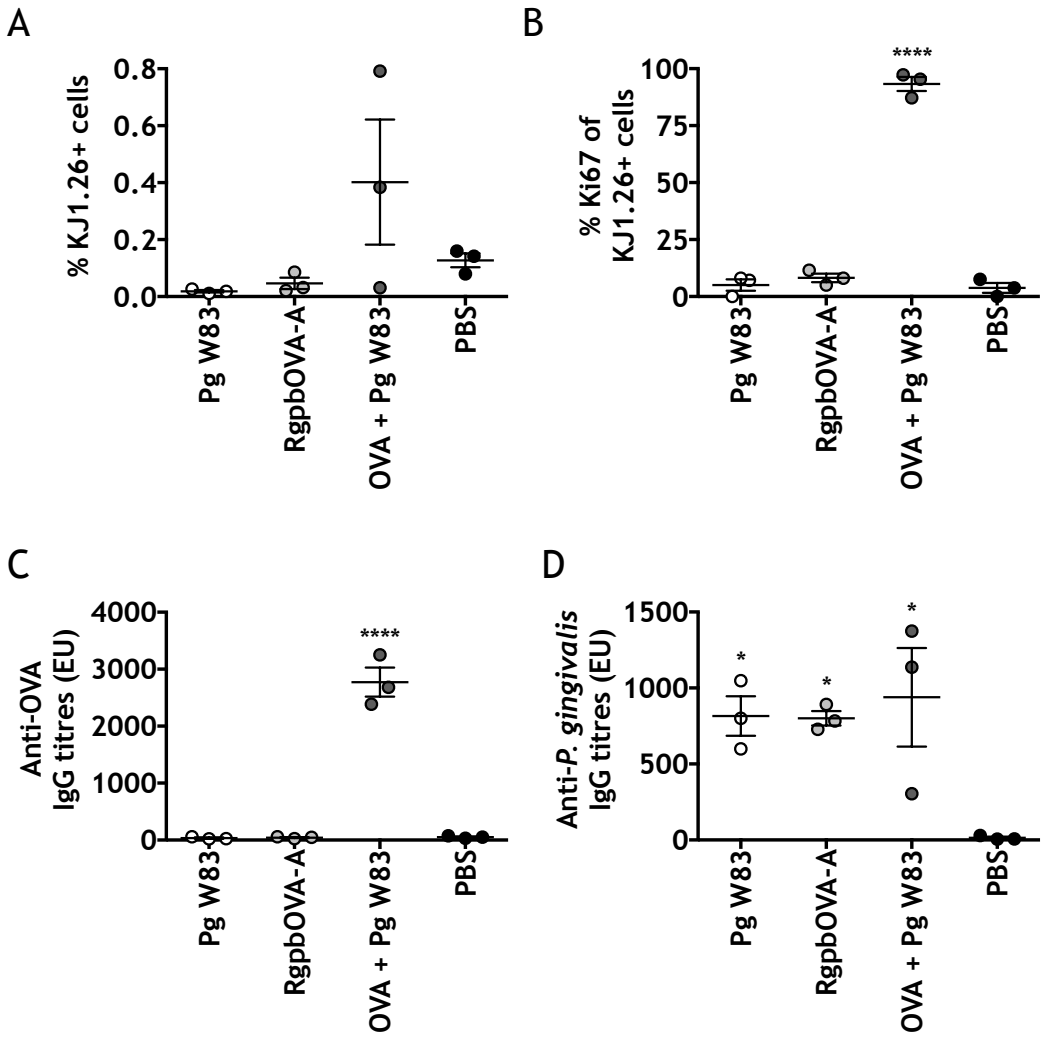

Figure 6.5. Stimulation of ovalbumin-specific T cells by RgpbOVA-A, *in vivo*.
Three million CD4+ KJ1.26+ T cells, from DO11.10 mice, were transferred intravenously to BALB/c mice. Twenty-four hours post adoptive transfer, mice received scruff injections and 10 days later received footpad injections as described in **table 6.1**. Mice were culled 72 hours post footpad injection, and popliteal lymph nodes and serum collected. Cells from popliteal lymph nodes were analysed by flow cytometry and serum antibodies were analysed by ELISA. (A) Percentage of CD4+ KJ1.26+ cells of the total viable cell population from popliteal lymph nodes. (B) Percentage of proliferating Ki67+ CD4+ KJ1.26+ cells from popliteal lymph nodes. Data are shown as mean + SEM, from 1 experiment, n = 3 mice/group. (C) Anti-OVA IgG titres in serum. (D) Anti-*P. gingivalis* IgG titres in serum. Data are ELISA Units (EU) shown as individual mice (symbols) with mean +/- SEM for each group (lines), from 1 experiment, n = 3 mice/group. Statistical significance was determined by a Dunnett's multiple comparison one way ANOVA, comparing each stimulus with the PBS control group, as indicated on the graph (*P < 0.05, ****P < 0.0001).

6.3 Discussion

Previous chapters demonstrated very subtle changes in CD4+ T cell phenotype in experimental PD. However, these studies investigated the entire CD4+ population and the phenotype of antigen-specific T cells was not addressed. In an attempt to understand antigen-specific T cell responses to *P. gingivalis*, RgpbOVA-A was obtained. Despite seemingly expressing OVA peptide, RgpbOVA-A was unable to activate DO11.10 cells *in vitro* and *in vivo*.

As a means to determine the antigen specific CD4+ and CD8+ T cell responses to *E. coli* and *P. gingivalis* LPS *in vivo*, LPS was co-injected with soluble OVA intraperitoneally or into the footpad of mice previously receiving OTII or OTI cells. Cytokine profiles of OVA-specific T cells were assessed and highlighted that LPS from different bacterial strains elicited unique immune responses. *E.coli* LPS was found to induce Th1 responses demonstrated by CD4+ T cell IFN-γ and CD8+ T cell IL-12 production. *P. gingivalis* LPS stimulated Th2 responses characterized by increased production of IL-5, IL-13 and IL-10 (Pulendran et al., 2001). In this model, it assumed that LPS was taken up and presented by APCs along with OVA, meaning that OVA-specific T cells are representative of LPS-specific T cells. However, OVA may drain independently of co-injected LPS. To overcome this caveat, *P. gingivalis* was genetically manipulated to express OVA peptide to identify the immune response mounted by OVA-specific T cells, in this chapter.

Whilst RgpbOVA-A seemingly expressed OVA peptide and its location within RgpB seemed hypothetically optimal for identification by APCs, RgpbOVA-A lacked the capacity to activate OVA-specific T cells both *in vitro* and *in vivo*. As illustrated by the OVA protein 3D model, the position of the OVA peptide does not seem crucial for appropriate presentation by APCs to T cells. Therefore, the position of OVA peptide in RgpbOVA-A may not have been an important factor for activating APCs to prime T cells. To improve the efficiency of APCs to present OVA from RgpbOVA-A, the incubation time of the APC: RgpbOVA-A co-culture could have been increased. In other OVA-specific T cell *in vitro* investigations, APCs were pulsed with antigen for 18 hours (Martner et al., 2013) and were activated through administration of IL-

2 (Gonçalves et al., 2006). As DCs are the most efficient APCs, a pure population of these cells could have been pulsed with *P. gingivalis* for *in vitro* cultures.

For the *in vivo* studies, a control group receiving OVA protein emulsified in CFA in the scruff, followed by footpad injection of OVA protein only was missing. A shortage of donors for the adoptive transfer at the time of this experiment forced reduction in recipient numbers. It was decided that a minimum group size of three was preferable to a greater number of smaller groups. This control would have indicated the response of transgenic CD4+ T cells to their cognate antigen without the influence of *P. gingivalis*. Still, OVA-specific T cells from group 3 mice (WT *P. gingivalis* + OVA) increased proliferation and activation markers, demonstrating that the cells could efficiently respond to specific antigen, thereby essentially confirming a positive control.

Both WT and transgenic *P. gingivalis* used for the experiments in this chapter were heat-killed, therefore the host immunoregulatory properties of *P. gingivalis* would have been impaired (Stathopoulou et al., 2009b). Heat-killing of *P. gingivalis* reduces gingipain activity – the site of the bacterium in which OVA peptide had been inserted. However, RgpB is anchored into the cell surface of *P. gingivalis*, and whilst it can also be secreted, the heat-killed bacteria would have expressed surface gingipains. Despite the unlikeliness of heat-killing *P. gingivalis* to affect the surface expression of modified RgpB, it would have been appropriate to determine the capacity of live bacteria to induce specific CD4+ T cell responses. Due to time restrictions this was not possible.

Arginine gingipains (RgpA and RgpB) are arginine-specific cysteine proteinases that function to cleave arginine-Xaa peptide bonds (Guo et al., 2010). It is unlikely that the arginase activity of RgpB would have cleaved the arginine residue from OVA peptide, leaving it fragile to damage, as the pro-domains of RgpB prevent proteolytic activity prior to extracellular secretion (de Diego et al., 2013). To test this, RgpbOVA-A could be grown as it was for previous western blots. The supernatant containing secreted and potentially enzyme active RgpB could be collected and RgpbOVA-A bacteria containing membrane bound, non-active RgpB

could be collected separately. The bacteria could be lysed as before and then both bacterial lysates and gingipains could be assessed for OVA peptide expression by western blot. It would be assumed that OVA peptide would be expressed by RgpbOVA-A lysates and that secreted RgpB may have cleaved OVA peptide and therefore no or lower expression would be found.

Gingipains are key virulence factors of *P. gingivalis* and have been found at high concentrations at severe PD sites in gingival tissue. Therefore, inserting OVA peptide into a gingipain seems optimal for inducing specific immune responses. Kgp has been found to be fundamental for bone resorption in a *P. gingivalis*-induced model of murine PD. Furthermore, a chimera therapeutic vaccine comprising the active site sequence and A1 adhesion domain of Kgp used in a murine model of PD was found to protect against alveolar bone loss (O'Brien-Simpson et al., 2016). Owing to the findings that Kgp has a strong influence over immunity and bone resorption, perhaps Kgp would be a better site to insert OVA peptide into.

RgpbOVA-A is not the first genetically modified *P. gingivalis* strain to lack OVA-specific T cell stimulatory capacity (unpublished observations, personal communication with Dr John Butcher, University of the West of Scotland), which perhaps explains the absence of OVA-expressing transgenic *P. gingivalis* studies. Furthermore, transgenic *Leishmania mexicana* modified to express Eα-GFP is also incapable of inducing activation of specific T cells (TEa) (unpublished observations, personal communication with with Dr Owain Millington, University of Strathclyde); thereby *P. gingivalis* is not the only pathogen that when genetically modified does not stimulate appropriate cells.

This technique was unable to broaden the understanding of *P. gingivalis*-specific T cells and their role in PD. However, there are other methods with the potential to do so. As mentioned previously, *Salmonella* flagellin-specific CD4+ T cells were generated to address the activation and migration of *Salmonella*-specific T cells in response to oral infection (McSorley et al., 2002). A similar approach was taken with regard to *P. gingivalis*-specific CD4+ T cells; however the phenotype of specific T cells was not assessed (Gonçalves et al., 2006). With the development and

improvement of flow cytometers, the *P. gingivalis*-specific T cells generated by Gonçalves could be labeled (i.e. with CFSE) and adoptively transferred to recipient mice to assess the *in vivo* responses mounted by these cells in experimental PD. Cells from gingivae and dLNs could be isolated and phenotypic markers of interest stained for flow cytomtery. The specific CD4+ T cells would be identified by their pre-transfer labeling by flow cytometry and could be further analyzed. A limitation that can present with TCR transgenic mice is cell phenotypical abnormalities due to the initial non-physiologically high frequency of transgenic T cells (Marzo et al., 2005). Furthermore, typical functions of cells can be impaired due to the repeated stimulations required for generation of specific T cells (Jelley-Gibbs et al., 2005).

Antigen-specific T cells can also be tracked and quantified using MHC-I and MHC-II tetramers. Tetramers are recombinant peptide antigen-bound-to-MHC molecules that can interact and bind to specific T cells. The tetramers are usually biotinylated to enable coupling of fluorophore-labeled streptavidin, that makes identification of tetramer bound T cells possible by flow cytometry. This technique is thought to avoid the limitations regarding quantification and precision that other T cell tracking methodologies present (Kurtulus and Hildeman, 2013). Tetramers ($I\text{-}A^b$) displaying RgpA and/or Kgp peptides were used to investigate *P. gingivalis*-specific CD4+ T cell responses. RgpA and Kgp peptides were selected based on their ability to prime effector CD4+ T cells. Mice were orally infected with *P. gingivalis* and dLNs harvested at 21 days post infection. The cell suspensions from dLNs were pooled and 4×10^6 cells stained with PE-conjugated tetramers along with anti-B220, anti-CD3ε, anti-CD4, anti-CD8α and anti-CD44. Flow cytometry analysis illustrated that antigen experienced CD4+ T cells (CD3+ CD4+ CD44+) were found at elevated levels compared to CD4+ T cells from sham-infected mice, demonstrating clonal expansion had occurred *in vivo*. By contrast, there were few antigen inexperienced CD4+ T cells (CD3+ CD4+ CD44-) in dLNs (Bittner-Eddy et al., 2013). Still, R/Kgp peptide tetramers could be further exploited to determine the complete phenotype and function of *P. gingivalis*-specific T cells in experimental PD.

In conclusion, whilst RgpbOVA-A expressed OVA peptide that could be identified by western blot, the transgenic strain was unable to activate OVA-specific T cells.

Future studies could investigate alternative expression systems, alternative model antigens and perhaps other T cell tracking systems, such as MHC tetramers, in the context of experimental PD.

Key findings of this chapter were:

- Western blotting illustrated that RgpbOVA-A expressed OVA.
- RgpbOVA-A did not stimulate an OVA-specific T cell response *in vitro* or *in vivo*.

7 General Discussion

The studies described in this thesis were conducted with an overall aim of better understanding the adaptive immune response associated with PD. T cells are undoubtedly evident in PD and years of scrutiny have identified varied and dynamic roles of T cells in both human and experimental PD. Whilst CD4+ T cells have and continue to be a focus of PD studies, there is ambiguity regarding their specific functions and whether they contribute to the protection or immunopathogenesis of this disease. For this reason, the predominant aim of these studies was to characterize the phenotype of CD4+ T cells in a murine model of PD at various early stages post infection.

A key finding from the data presented in **Chapter 4** was the suggested association of IFN-γ with PD. Whilst the production of this cytokine by CD4+ T cells isolated from dLNs was not statistically significantly increased by comparison to their sham-infected counterparts, there was a clear trend by later stages of the PD model. Likewise, there was a trend in elevated IFN-γ expression by CD8+ T cells of dLNs and a significant increase in production by CD8+ T cells isolated from gingival tissues. Further suggestive of a link with IFN-γ and PD was the cytokine analysis of the supernatants from *P. gingivalis* re-stimulated splenocytes. Cells from *P. gingivalis*-infected mice were found to increase production of IFN-γ, at concentrations greater than that produced by splenocytes from sham-infected mice. IFN-γ is a cytokine characteristic of a Th1 immune response, and therefore the systemic production of the cytokine was hinted at through a predominance of *P. gingivalis*-specific IgG2a antibodies in serum of infected mice. Altogether, it could be speculated that IFN-γ is involved in early orchestration of the immune response upon microbial dysbiosis.

As aforementioned, previous studies have regarded IFN-γ as a PD-associated cytokine (Seymour et al., 1993, Gamonal et al., 2001, Taubman and Kawai, 2001, Baker et al., 1999a). Longitudinal studies found that IFN-γ concentrations and T-bet (Th1 transcription factor) were upregulated in GCF of active lesions from chronic PD patients and therefore the presence of this cytokine in GCF was deemed a risk

factor for PD progression (Dutzan et al., 2008, Alpagot et al., 2003). It has also been postulated that a decrease in levels of IFN-γ in GCF from PD patients can verify improvement of disease following treatment (Tsai et al., 2007). Therefore, IFN-γ in GCF is a significant risk for progression of established PD. However, to date, there are no longitudinal studies evaluating GCF cytokine composition in gingivitis patients that would inform whether cytokine expression in gingivitis is predictive of progression to periodontitis. Perhaps GCF IFN-γ in gingivitis could be a risk biomarker for the development of PD. It would be advantageous to identify a gingivitis patient at risk of developing PD, as gingivitis is reversible through implementation of sufficient cleaning of teeth and is more easily treatable than chronic PD. The 'at risk' patient may be more motivated to comply with OHI and the dentist could employ extra prevention plans. Therefore, a longitudinal study evaluating GCF cytokines in patients with gingivitis at regular intervals could potentially identify risk biomarkers and through implementation of appropriate treatments, prevent the incidence of PD. There are ethical barriers with such a study – as it would essentially involve supervising a patient's progression to periodontitis. Moreover, sampling of GCF can prove quite difficult. The washing method is useful for identification of cytokines, microbes and also gingipains, the latter of which is not possible by other methods (Guentsch et al., 2011). The technique is difficult to perform and can often result in blood contamination due to gingival irritation; therefore it is not typically used. Microcapillary pipetting is also used to sample GCF but again requires greater technical skills (Alpagot et al., 2003). The absorption method, and in particular paper strips, are most commonly employed for sampling GCF for cytokines (Alpagot et al., 2003) and would be sufficient for the purposes of a longitudinal gingivitis study.

For patients displaying established and progressing PD, perhaps local, topical anti-IFN-γ therapies could be employed as adjuncts to mechanical debridement of dental plaque. Anti-cytokine therapy is used to restore the balance between pro- and anti-inflammatory mediators and is currently used to treat numerous chronic inflammatory diseases including RA, ulcerative colitis, Crohn's disease, ankylosing spondyloarthritis, juvenile idiopathic arthritis, psoriatic arthritis and psoriasis (Astrakhantseva et al., 2014). Anti-cytokine therapy is currently used as an adjunct

to disease-modifying anti-rheumatic drugs (DMARDs) in treatment of RA patients whom fail to respond to conventional DMARDs. The anti-cytokine therapies offered by NHS target TNF-α and IL-6 and are described in **table 7.1**. In clinical trials, anti-IFN-γ therapy has proven to be well tolerated and reduce disease activity in severe RA patients whom fail to respond to conventional DMARD treatment (Sigidin et al., 2001). In a more recent clinical study, anti-IFN-γ was found to mimic the results achieved by existing anti-TNF-α therapy, and in some patients the outcome of therapy was actually superior (Skurkovich et al., 2015). Furthermore, patients with pediatric primary Hemophagocytic Lymphohistiocytosis refractory to conventional therapies were treated with anti-IFN-γ, which resulted in promising outcomes in a clinical trial (Prof et al., 2015).

Table 7.1. Anti-cytokine drugs currently used to treat rheumatoid arthritis - available on NHS.

Drug	Drug type	Target
Etanercept	Soluble TNFR2	TNF-α
Infliximab	Chimeric monoclonal antibody	TNF-α
Adalimumab	Fully humanized monoclonal antibody	TNF-α
Certolizumab	PEGylated Fab fragment	TNF-α
Golimumab	Fully humanized monoclonal antibody	TNF-α
Tocilizumab	Humanized anti-IL-6R monoclonal antibody	IL-6

Abbreviations: Fab, antibody binding fragment; IL, interleukin; IL-6Rα, interleukin-6 receptor alpha; PEG, polyethylene glycol;TNF-α, tumour necrosis factor alpha; TNFR, tumour necrosis factor receptor. (Culshaw et al., 2011).
(http://www.nhs.uk/Conditions/Rheumatoid-arthritis/Pages/Treatment.aspx accessed on 14/03/17)

Whilst the potential use of anti-cytokine therapy for treatment of PD has been discussed for several years (Waykole et al., 2009), there have been no studies conducted to evaluate the efficacy of inhibitors of any inflammatory cytokine in the context of human PD. As mentioned above, IFN-γ could potentially be used as a biomarker of progression towards PD, yet for patients with established chronic PD; anti-IFN-γ could be the immune-targeted treatment that is required for amelioration of disease (**figure 7.1**). Both of these hypotheses require substantial

future research. A major disadvantage of cytokine therapies is the gateway for opportunistic infection that occurs as a result of the down-regulated immune response. However, screening of patients for latent disease prior to prescribing of the drug should limit the number of opportunistic infections (Keane et al., 2001). Furthermore, the nature of PD would likely require much lower doses than administered for systemic autoimmune disease, and therapy could be administered topically.

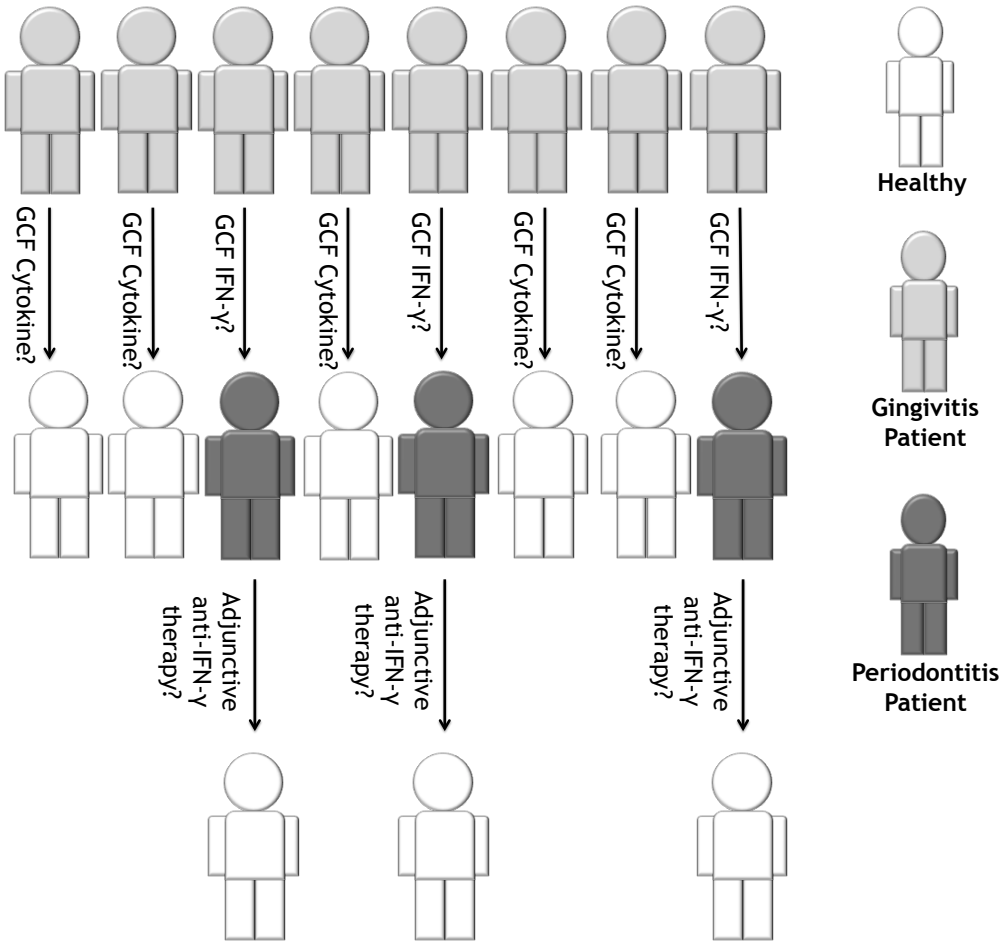

Figure 7.1. Working hypothesis of the role of IFN-γ in the development and treatment of PD.
Patients attending the dental clinic will present with gingivitis and whilst some will revert back to health, some will develop periodontitis. IFN-γ in gingival crevicular fluid (GCF) could indicate whether the gingivitis patient will develop periodontitis and other as yet undefined cytokines could indicate a gingivitis patient that will remain stable with gingivitis or revert back to health. Periodontitis patients could be treated with anti-IFN-γ therapy to ameliorate disease and revert patient back to health, alternatively anti-IFN-γ treatment could be used to supplement routine treatment for patients whose disease persists.

The studies conducted in this thesis did not portray an incredibly exciting role for CD4+ T cells in PD. The RNA-sequencing data, in particular, revealed differences between CD4+ T cells of different tissues rather than differences between infection statuses, with the down-regulation of only a single gene in dLN CD4+ T cells and upregulation of only three genes in gingival CD4+ T cells following *P. gingivalis* infection (**chapter 5**). Notably, the greatest trend in IFN-γ production was observed in CD8+ T cells isolated from dLNs of infected mice. The only statistically significant T cell-attributed change to occur in gingival cells was elevated IFN-γ production by CD8+ T cells. Previously, activated CD8+ T cells were found in greater abundances in PD compared to healthy controls, both systemically and locally (Cifcibasi et al., 2015a). To date, a comparison of the detailed phenotype of CD8+ T cells in health and PD remains elusive. Therefore, comprehensive characterization of CD8+ T is required and the data from our studies implies that future investigations may point to a role for CD8+ T cells in PD. The apparent lack of differences in the transcriptome of the T cells from infected compared with healthy mice suggests that either the T cell response is not in action at the time of sampling, or that the T cells are activated elsewhere. Investigation of peripheral blood from patients with PD had identified an increase in myeloid DCs (mDCs) and it was demonstrated that mDCs carried *P. gingivalis* (Miles et al., 2014). Therefore, it is possible that circulating T cells may alter their phenotype and function upon *P. gingivalis*-infection. T cells could be investigated through blood collection and harvesting of spleens from mice.

Throughout these studies, it has been assumed that the class switched antibody responses to *P. gingivalis* indicated a preceding CD4+ T cell response. However, B cells are capable of T cell-independent class switching. Numerous antigens can cause B cell activation independently of T cells and are described as T-independent type 1 (TI-1) or type 2 (TI-2) antigens. Whilst TI-2 antigens require non-specific T cell help, TI-1 antigens stimulate B cells in the absence of a second signal and require no T cell help. TI-1 antigens include LPS and several viruses. Introduction of TI-1 antigens into T cell deficient mice was shown to induce IgG class switching (Fehr et al., 1998). To investigate whether *P. gingivalis* can stimulate T cell-independent IgG production, the PD model could be conducted using αß T cell

deficient mice (*Tcra*^{tm1Mom}). To further investigate whether *P. gingivalis* antigens act as TI-1 or TI-2 antigens, CBA/*Nxid* mice could be employed. CBA/*Nxid* mice have a mutation in Bruton's tyrosine kinase gene and subsequently lack the capacity to generate antibody responses to TI-2 antigens (https://www.jax.org/strain/001011 - accessed 02/04/17).

By comparison to other barrier sites, including the gut and skin, little is known about the mechanisms that orchestrate oral mucosal T cell responses. However, it has very recently been demonstrated that instructions for oral effector CD4+ T cell differentiation are unique from that at other barrier tissues. For example, commensal bacteria mediate Th17 cell expansion in the gut but Th17 cells are found within gingival tissues of germ-free mice. Further still, within different sites of the oral cavity the requirements for CD4+ T cell differentiation differ (Dutzan et al., 2017). Th17 cells within the tongue are dependent upon the presence of commensal bacteria (Conti et al., 2014); therefore the oral cavity is not a single immune entity. The oral mucosal studies in this thesis have focused on gingival and palatal tissue. It would be of interest to identify markers that promote tissue tropism and residence within distinct mucosal compartments to understand the basic immunology within the oral cavity and to identify site-specific targets as novel therapies for oral disease. For example, lichen planus is a chronic mucocutaneous disorder that typically manifests in the oral cavity prior to development systemically. CD8+ T cells mediate this autoimmune disorder through inducing apoptosis of basal cells of the oral epithelium. Lichen planus does not affect a specific location within the oral cavity but presents anywhere; most commonly the lips, tongue, floor of the mouth, buccal mucosa, gingiva and palate are affected (Gupta and Jawanda, 2015). Therefore, topical oral cavity site-specific drugs directed at CD8+ T cells may be useful for treatment of different manifestations of lichen planus.

The RNA-sequencing data highlighted an oral mucosal CD4+ T cell transcriptome profile. To validate these findings, the protein expression of the molecules of interest (**figure 7.2**) should be investigated – ideally by IHC to localize the CD4+ T cells within the mucosa, or by flow cytometry to determine whether the changes in

gene expression are reflected by changes in protein expression. Ideally, if protein expression is confirmed, then function would be investigated by inhibition of the protein of interest for example using blocking antibodies or using siRNA. Unfortunately time constraints limited these studies in the current work. Whilst the gene expression of CD4+ T cells from dLNs differed from that of CD4+ T cells from gingivae, the data does not provide an insight as to which CD4+ T cells were resident in the gingivae or which had migrated from other sites. To understand the migratory capacity of cells between dLN and oral mucosa, the Kaede mouse model could be employed. Kaede is a photoconvertible GFP that changes from green to red fluorescence upon exposure to UV light. Transgenic mice expressing Kaede can permit monitoring of the movement of cells *in vivo* from and to any site of interest. With regard to the migratory dLN and gingival cells in the PD model, the cells of the dLNs could be photoconverted to assess the types of cells that migrate to the oral cavity and the time after infection in which this happens. Likewise the migration of gingival cells to dLNs to induce an adaptive immune response after *P. gingivalis*-infection could be evaluated through photoconversion of cells of the gingivae (Tomura et al., 2008).

It was hypothesized that CD4+ T cells in the oral cavity had a unique phenotype and that that would alter with functional consequence in response to oral *P. gingivalis*-infection and inflammation. Confirming the initial part of the hypothesis, the CD4+ T cells isolated from gingival tissue differentially expressed thousands of genes, and therefore a variety of pathways comparing to CD4+ T cells from dLNs. However, there was minimal change in phenotype of gingival CD4+ T cells upon *P. gingivalis*-infection.

In conclusion, the studies in this thesis have provided an insight into the possible nature of oral mucosal CD4+ T cells in gingival tissue (**figure 7.2**) and the PD-associated phenotype of T cells in a murine model of PD. Subtle differences in CD4+ T cells occur upon *P. gingivalis* infection, most notably a suggested increase in IFN-γ. This inflammatory cytokine was upregulated by *P. gingivalis* infected gingival and dLN CD8+ T cells, and splenocytes, and therefore was the result of both local and systemic immune responses. This advocates a possible role of CD8+ T cells in

experimental PD but also implicates a potential biological target for adjunctive PD treatment.

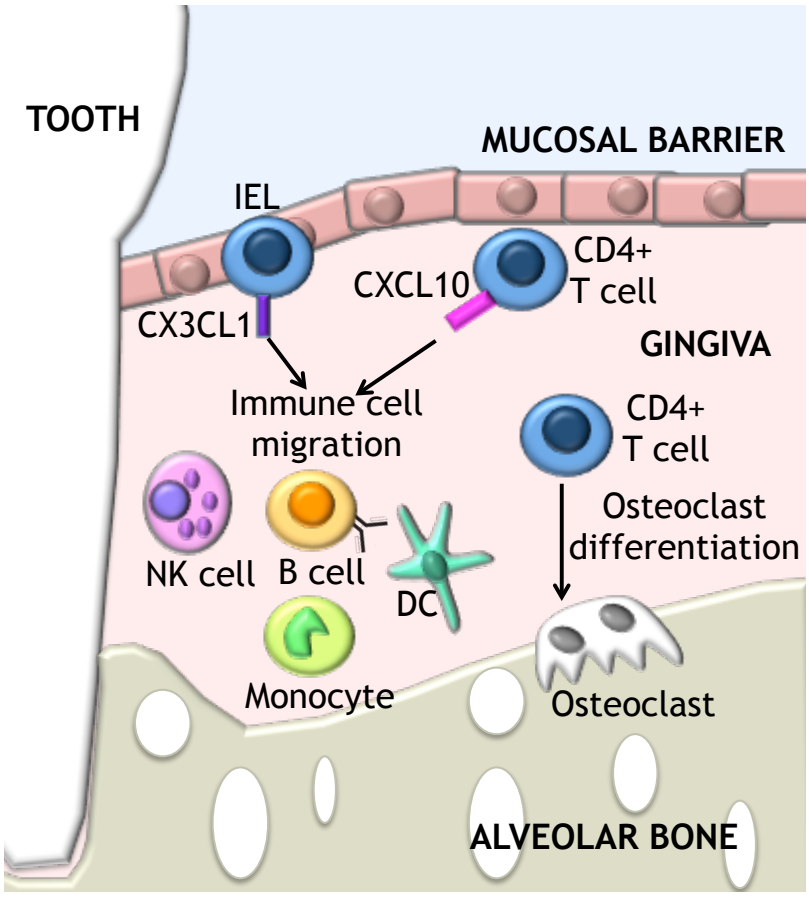

Figure 7.2. Schematic of the speculative potential roles of CD4+ T cells in gingival tissue.
CD4+ T cells within the gingiva upregulated the expression of a variety of genes by comparison to CD4+ T cells of the cervical (draining) lymph nodes (dLN). CD4+ T cells from gingival tissue upregulated osteoclast differentiation, MAPK and TNF signaling pathways, and showed elevated expression of CX3CL1 and CXCL10 compared to that of dLN CD4+ T cells. Therefore, it could by hypothesized that CD4+ T cells of the gingiva may influence local osteoclast activity and induce immune cell migration including dendritic cells (DC), natural killer (NK) cells, monocytes and B cells.

List of Publications

Campbell L, Millhouse E, Malcolm J, Culshaw S. 2016. T cells, teeth and tissue destruction - what do t cells do in periodontal disease? Molecular oral microbiology. 31(6):445-456.

Malcolm J, Millington O, Millhouse E, **Campbell L**, Adrados Planell A, Butcher JP, Lawrence C, Ross K, Ramage G, McInnes IB et al. 2016. Mast cells contribute to porphyromonas gingivalis-induced bone loss. Journal of dental research. 95(6):704-710.

Malcolm J, Awang RA, Oliver-Bell J, Butcher JP, **Campbell L**, Adrados Planell A, Lappin DF, Fukada SY, Nile CJ, Liew FY et al. 2015. Il-33 exacerbates periodontal disease through induction of rankl. Journal of dental research. 94(7):968-975.

Oliver-Bell J, Butcher JP, Malcolm J, MacLeod MK, Adrados Planell A, **Campbell L**, Nibbs RJ, Garside P, McInnes IB, Culshaw S. 2015. Periodontitis in the absence of b cells and specific anti-bacterial antibody. Molecular oral microbiology. 30(2):160-169.

References

ABBEY, J. L. & O'NEILL, H. C. 2007. Expression of T-cell receptor genes during early T-cell development. *Immunol Cell Biol,* 86**,** 166-174.

ABE, T. & HAJISHENGALLIS, G. 2013. Optimization of the ligature-induced periodontitis model in mice. *Journal of immunological methods,* 394**,** 49-54.

ADIBRAD, M., DEYHIMI, P., GANJALIKHANI HAKEMI, M., BEHFARNIA, P., SHAHABUEI, M. & RAFIEE, L. 2012. Signs of the presence of Th17 cells in chronic periodontal disease. *Journal of periodontal research,* 47**,** 525-531.

AGRAWAL, N., DASARADHI, P. V. N., MOHMMED, A., MALHOTRA, P., BHATNAGAR, R. K. & MUKHERJEE, S. K. 2003. RNA Interference: Biology, Mechanism, and Applications. *Microbiology and Molecular Biology Reviews,* 67**,** 657-685.

ALBANDAR, J. M. 2014. Aggressive periodontitis: case definition and diagnostic criteria. *Periodontology 2000,* 65**,** 13-26.

ALBANDAR, J. M. & KINGMAN, A. 1994. Gingival recession, gingival bleeding, and dental calculus in adults 30 years of age and older in the United States, 1988-1994. *Journal of Periodontology,* 70**,** 30-43.

ALJEHANI, Y. A. 2014. Risk Factors of Periodontal Disease: Review of the Literature. *International Journal of Dentistry,* 2014**,** 182513.

ALLAM, J.-P. P., DUAN, Y., HEINEMANN, F., WINTER, J., GÖTZ, W., DESCHNER, J., WENGHOEFER, M., BIEBER, T., JEPSEN, S. & NOVAK, N. 2011. IL-23-producing CD68(+) macrophage-like cells predominate within an IL-17-polarized infiltrate in chronic periodontitis lesions. *Journal of clinical periodontology,* 38**,** 879-886.

ALLAM, J. P., STOJANOVSKI, G., FRIEDRICHS, N., PENG, W., BIEBER, T., WENZEL, J. & NOVAK, N. 2008. Distribution of Langerhans cells and mast cells within the human oral mucosa: new application sites of allergens in sublingual immunotherapy? *Allergy,* 63**,** 720-727.

ALLEN, I. C. 2013. Delayed-Type Hypersensitivity Models in Mice. *In:* ALLEN, I. C. (ed.) *Mouse Models of Innate Immunity: Methods and Protocols.* Totowa, NJ: Humana Press.

ALPAGOT, T., FONT, K. & LEE, A. 2003. Longitudinal evaluation of GCF IFN-γ levels and periodontal status in HIV+ patients. *Journal of Clinical Periodontology,* 30**,** 944-948.

AMUNULLA, A., VENKATESAN, R., RAMAKRISHNAN, H., ARUN, K. V., SUDARSHAN, S. & TALWAR, A. 2008. Lymphocyte subpopulation in healthy and diseased gingival tissue. *Journal of Indian Society of Periodontology,* 12**,** 45-50.

ANDERSEN, M. H., SCHRAMA, D., THOR STRATEN, P. & BECKER, J. C. 2006. Cytotoxic T Cells. *Journal of Investigative Dermatology,* 126**,** 32-41.

ANDRIOPOULOS, B., CORRADINI, E., XIA, Y., FAASSE, S. A., CHEN, S., GRGUREVIC, L., KNUTSON, M. D., PIETRANGELO, A., VUKICEVIC, S., LIN, H. Y. & BABITT, J. L. 2009. BMP-6 is a key endogenous regulator of hepcidin expression and iron metabolism. *Nature genetics,* 41**,** 482-487.

ARCHANA, P. M., SALMAN, A. A., KUMAR, T. S. S., SARASWATHI, P. K., PANISHANKAR, K. H. & KUMARASAMY, P. 2012. Association between interleukin-1 gene polymorphism and severity of chronic periodontitis in a south Indian population group. *Journal of Indian Society of Periodontology,* 16**,** 174-178.

ARIZON, M., NUDEL, I., SEGEV, H., MIZRAJI, G., ELNEKAVE, M., FURMANOV, K., ELI-BERCHOER, L., CLAUSEN, B. E., SHAPIRA, L., WILENSKY, A. & HOVAV, A.-H. 2012. Langerhans cells down-regulate inflammation-driven alveolar bone loss. *Proceedings of the National Academy of Sciences,* 109**,** 7043-7048.

ARMITAGE, G. C. 2004. Periodontal diagnoses and classification of periodontal diseases. *Periodontology 2000,* 34**,** 9-21.

ARMITAGE, G. C. & CULLINAN, M. P. 2010. Comparison of the clinical features of chronic and aggressive periodontitis. *Periodontology 2000,* 53**,** 12-27.

AROONRERK, N., PICHYANGKUL, S., YONGVANITCHIT, K., WISETCHANG, M., SA-ARD-IAM, N., SIRISINHA, S. & MAHANONDA, R. 2003. Generation of gingival T cell lines/clones specific with Porphyromonas gingivalis pulsed dendritic cells from periodontitis patients. *Journal of Periodontal Research,* 38**,** 262-268.

ARORA, P. & PORCELLI, S. A. 2016. An Efficient and High Yield Method for Isolation of Mouse Dendritic Cell Subsets. *J Vis Exp,* 18**,** doi: 10.3791/53824.

ASHCROFT, G. S., MILLS, S. J. & ASHWORTH, J. J. 2002. Ageing and wound healing. *Biogerontology,* 3**,** 337-345.

ASTRAKHANTSEVA, I. V., EFIMOV, G. A., DRUTSKAYA, M. S., KRUGLOV, A. A. & NEDOSPASOV, S. A. 2014. Modern anti-cytokine therapy of autoimmune diseases. *Biochemistry (Mosc),* 79**,** 1308-1321.

AUTENGRUBER, A., GEREKE, M., HANSEN, G., HENNIG, C. & BRUDER, D. 2012. Impact of enzymatic tissue disintegration on the level of surface molecule

expression and immune cell function. *European Journal of Microbiology & Immunology,* 2**,** 112-120.

AWANG, R. A., LAPPIN, D. F., MACPHERSON, A., RIGGIO, M., ROBERTSON, D., HODGE, P., RAMAGE, G., CULSHAW, S., PRESHAW, P. M., TAYLOR, J. & NILE, C. 2014. Clinical associations between IL-17 family cytokines and periodontitis and potential differential roles for IL-17A and IL-17E in periodontal immunity. *Inflamm Res,* 63**,** 1001-12.

BACHMANN, M. F., BARNER, M., VIOLA, A. & KOPF, M. 1999. Distinct kinetics of cytokine production and cytolysis in effector and memory T cells after viral infection. *European Journal of Immunology,* 29**,** 291-299.

BAINBRIDGE, B., VERMA, R., EASTMAN, C., YEHIA, B., RIVERA, M., MOFFATT, C., BHATTACHARYYA, I., LAMONT, R. & KESAVALU, L. 2010. Role of Porphyromonas gingivalis phosphoserine phosphatase enzyme SerB in inflammation, immune response, and induction of alveolar bone resorption in rats. *Infection and immunity,* 78**,** 4560-4569.

BAKER, P., DIXON, M., EVANS, R., DUFOUR, L., JOHNSON, E. & ROOPENIAN, D. 1999a. CD4(+) T cells and the proinflammatory cytokines gamma interferon and interleukin-6 contribute to alveolar bone loss in mice. *Infection and immunity,* 67**,** 2804-2809.

BAKER, P., EVANS, R. & ROOPENIAN, D. 1994a. Oral infection with Porphyromonas gingivalis and induced alveolar bone loss in immunocompetent and severe combined immunodeficient mice. *Archives of oral biology,* 39**,** 1035-1040.

BAKER, P. J., CARTER S FAU - DIXON, M., DIXON M FAU - EVANS, R. T., EVANS RT FAU - ROOPENIAN, D. C. & ROOPENIAN, D. C. 1999b. Serum antibody response to oral infection precedes but does not prevent Porphyromonas gingivalis-induced alveolar bone loss in mice. *Oral Microbiol Immunol,* 14**,** 194-196.

BAKER, P. J., EVANS, R. T. & ROOPENIAN, D. C. 1994b. Oral infection with Porphyromonas gingivalis and induced alveolar bone loss in immunocompetent and severe combined immunodeficient mice. *Arch Oral Biol,* 39**,** 1035-1040.

BAKER, P. J., HOWE, L., GARNEAU, J. & ROOPENIAN, D. C. 2002. T cell knockout mice have diminished alveolar bone loss after oral infection with Porphyromonas gingivalis. *FEMS Immunology & Medical Microbiology,* 34**,** 45-50.

BANCHEREAU, J., BRIERE, F., CAUX, C., DAVOUST, J., LEBECQUE, S., LIU, Y.-J., PULENDRAN, B. & PALUCKA, K. 2000. Immunobiology of Dendritic Cells. *Annual Review of Immunology,* 18**,** 767-811.

BANCHEREAU, J. & STEINMAN, R. M. 1998. Dendritic cells and the control of immunity. *Nature,* 392**,** 245-252.

BASU, S., CAMPBELL, H. M., DITTEL, B. N. & RAY, A. 2010. Purification of Specific Cell Population by Fluorescence Activated Cell Sorting (FACS). *Journal of Visualized Experiments : JoVE***,** 1546.

BAUMJOHANN, D. & ANSEL, K. M. 2013. Identification of T follicular helper (Tfh) cells by flow cytometry. *Protocol exchange***,** doi:10.1038/protex.2013.060.

BEKLEN, A., AINOLA, M., HUKKANEN, M., GÜRGAN, C., SORSA, T. & KONTTINEN, Y. T. 2007. MMPs, IL-1, and TNF are regulated by IL-17 in periodontitis. *Journal of dental research,* 86**,** 347-351.

BELIBASAKIS, G. N. & BOSTANCI, N. 2012. The RANKL-OPG system in clinical periodontology. *J Clin Periodontol,* 39**,** 239-48.

BELTON, C. M., IZUTSU KT FAU - GOODWIN, P. C., GOODWIN PC FAU - PARK, Y., PARK Y FAU - LAMONT, R. J. & LAMONT, R. J. 1999. Fluorescence image analysis of the association between Porphyromonas gingivalis and gingival epithelial cells. *Cell Microbiol,* 1**,** 215-223.

BENSON, R. A., MACLEOD, M. K. L., HALE, B. G., PATAKAS, A., GARSIDE, P. & BREWER, J. M. 2015. Antigen presentation kinetics control T cell/dendritic cell interactions and follicular helper T cell generation in vivo. *eLife,* 4**,** e06994.

BERGLUNDH, T. & DONATI, M. 2005. Aspects of adaptive host response in periodontitis. *Journal of Clinical Periodontology,* 32**,** 87-107.

BERGLUNDH, T., LILJENBERG B FAU - LINDHE, J. & LINDHE, J. 2002. Some cytokine profiles of T-helper cells in lesions of advanced periodontitis.

BEZERRA, M. M., LIMA, V. D., ALENCAR, V. B. M., VIEIRA, I. B., BRITO, G. A. C., RIBEIRO, R. A. & ROCHA, F. A. C. 2000. Selective Cyclooxygenase-2 Inhibition Prevents Alveolar Bone Loss in Experimental Periodontitis in Rats. *Journal of Periodontology,* 71**,** 1009-1014.

BITTNER-EDDY, P. D., FISCHER, L. A. & COSTALONGA, M. 2013. Identification of gingipain-specific I-Ab-restricted CD4+T cells following mucosal colonization with Porphyromonas gingivalis in C57BL/6 mice. *Molecular Oral Microbiology,* 28**,** 452-466.

BOYCE, B. F., AUFDEMORTE, T. B., GARRETT, I. R., YATES, A. J. P. & MUNDY, G. R. 1989. Effects of Interleukin-1 on Bone Turnover in Normal Mice*. *Endocrinology,* 125**,** 1142-1150.

BRANCO, P., WEIDLICH, P., OPPERMANN, R. V. & ROSING, C. K. 2015. Early supra- and subgingival plaque formation in experimental gingivitis in smokers and never-smokers. *Oral Health Prev Dent,* 13**,** 13-20.

BRISTOW, M. R. & LONG, C. S. 2002. Cardiotrophin-1 in Heart Failure. *Circulation,* 106**,** 1430.

BRUNNER, J., SCHERES, N., EL IDRISSI, N., DENG, D., LAINE, M., VAN WINKELHOFF, A. & CRIELAARD, W. 2010. The capsule of Porphyromonas gingivalis reduces the immune response of human gingival fibroblasts. *BMC microbiology,* 10**,** 5.

CALANDRA, T. & ROGER, T. 2003. Macrophage migration inhibitory factor: a regulator of innate immunity. *Nat Rev Immunol,* 3**,** 791-800.

CARCUAC, O., ABRAHAMSSON, I., ALBOUY, J.-P., LINDER, E., LARSSON, L. & BERGLUNDH, T. 2013. Experimental periodontitis and peri-implantitis in dogs. *Clinical Oral Implants Research,* 24**,** 363-371.

CARDOSO, C., GARLET, G., MOREIRA, A., JÚNIOR, W., ROSSI, M. & SILVA, J. 2008a. Characterization of CD4+CD25+ natural regulatory T cells in the inflammatory infiltrate of human chronic periodontitis. *Journal of leukocyte biology,* 84**,** 311-318.

CARDOSO, C., GARLET, G., MOREIRA, A., JÚNIOR, W., ROSSI, M. & SILVA, J. 2008b. Characterization of CD4+CD25+ natural regulatory T cells in the inflammatory infiltrate of human chronic periodontitis. *J Leukoc Biol,* 84**,** 311-318.

CARDOSO, C. R., GARLET, G. P., CRIPPA, G. E., ROSA, A. L., JÚNIOR, W. M., ROSSI, M. A. & SILVA, J. S. 2009. Evidence of the presence of T helper type 17 cells in chronic lesions of human periodontal disease. *Oral microbiology and immunology,* 24**,** 1-6.

CARLSEN, H. S., BAEKKEVOLD, E. S., JOHANSEN, F. E., HARALDSEN, G. & BRANDTZAEG, P. 2002. B cell attracting chemokine 1 (CXCL13) and its receptor CXCR5 are expressed in normal and aberrant gut associated lymphoid tissue. *Gut,* 51**,** 364-371.

CATO, M. H., YAU, I. W. & RICKERT, R. C. 2011. Magnetic-based purification of untouched mouse germinal center B cells for ex vivo manipulation and biochemical analysis. *Nature Protocols,* 6**,** 953-960.

CHANDRAMOULI, K. & QIAN, P.-Y. 2009. Proteomics: Challenges, Techniques and Possibilities to Overcome Biological Sample Complexity. *Human Genomics and Proteomics : HGP,* 2009**,** 239204.

CHAPPLE, I. L. 2014. Time to take periodontitis seriously. *BMJ (Clinical research ed.),* 348.

CHAPPLE, I. L. & GENCO, R. 2013. Diabetes and periodontal diseases: consensus report of the Joint EFP/AAP Workshop on Periodontitis and Systemic Diseases. *J Periodontol,* 84**,** S106-S112.

CHARBONNIER, L. M., JANSSEN, E., CHOU, J., OHSUMI, T. K., KELES, S., HSU, J. T., MASSAAD, M. J., GARCIA-LLORET, M., HANNA-WAKIM, R., DBAIBO, G., ALANGARI, A. A., ALSULTAN, A., AL-ZAHRANI, D., GEHA, R. S. & CHATILA, T. A. 2015. Regulatory T-cell deficiency and immune dysregulation, polyendocrinopathy, enteropathy, X-linked-like disorder caused by loss-of-function mutations in LRBA. *J Allergy Clin Immunol,* 135**,** 217-227.

CHEN, T., NAKAYAMA, K., BELLIVEAU, L. & DUNCAN, M. 2001. Porphyromonas gingivalis gingipains and adhesion to epithelial cells. *Infection and immunity,* 69**,** 3048-3056.

CHEN, Z.-M. & JENKINS, M. K. 1999. Clonal Expansion of Antigen-Specific CD4 T Cells following Infection with Salmonella typhimurium Is Similar in Susceptible (Ity(s)) and Resistant (Ity(r)) BALB/c Mice. *Infection and Immunity,* 67**,** 2025-2029.

CHU, Y. & COREY, D. R. 2012. RNA Sequencing: Platform Selection, Experimental Design, and Data Interpretation. *Nucleic Acid Therapeutics,* 22**,** 271-274.

CIFCIBASI, E., CIBLAK, M., KIRAN, B., BADUR, S., FIRATLI, E., ISSEVER, H. & CINTAN, S. 2015a. The Role of Activated Cytotoxic T Cells in Etiopathogenesis of Periodontal Disease: Does It Harm or Does It Heal? *Scientific Reports,* 5**,** 9262.

CIFCIBASI, E., CIBLAK, M., KIRAN, B., BADUR, S., FIRATLI, E., ISSEVER, H. & CINTAN, S. 2015b. The role of activated cytotoxic T cells in etiopathogenesis of periodontal disease: does it harm or does it heal? *Sci Rep,* 5**,** 9262.

COATS, S., JONES, J., DO, C., BRAHAM, P., BAINBRIDGE, B., TO, T., GOODLETT, D., ERNST, R. & DARVEAU, R. 2009. Human Toll-like receptor 4 responses to P. gingivalis are regulated by lipid A 1- and 4'-phosphatase activities. *Cellular microbiology,* 11**,** 1587-1599.

CONNOLLY, E., MILLHOUSE, E., DOYLE, R., CULSHAW, S., RAMAGE, G. & MORAN, G. P. 2017. The Porphyromonas gingivalis hemagglutinins HagB and HagC are

major mediators of adhesion and biofilm formation. *Molecular Oral Microbiology,* 32**,** 35-47.

CONTI, H. R., PETERSON, A. C., BRANE, L., HUPPLER, A. R., HERNÁNDEZ-SANTOS, N., WHIBLEY, N., GARG, A. V., SIMPSON-ABELSON, M. R., GIBSON, G. A., MAMO, A. J., OSBORNE, L. C., BISHU, S., GHILARDI, N., SIEBENLIST, U., WATKINS, S. C., ARTIS, D., MCGEACHY, M. J. & GAFFEN, S. L. 2014. Oral-resident natural Th17 cells and γδ T cells control opportunistic Candida albicans infections. *The Journal of Experimental Medicine,* 211**,** 2075-2084.

COPE, A. P. 2008. T cells in rheumatoid arthritis. *Arthritis Research & Therapy,* 10**,** S1-S1.

COSTALONGA, M. & HERZBERG, M. C. 2014. The oral microbiome and the immunobiology of periodontal disease and caries. *Immunology Letters,* 162**,** 22-38.

CRABBE, P. A., CARBONARA, A. O. & HEREMANS, J. F. 1965. THE NORMAL HUMAN INTESTINAL MUCOSA AS A MAJOR SOURCE OF PLASMA CELLS CONTAINING GAMMA-A-IMMUNOGLOBULIN. *Lab Invest,* 14**,** 235-248.

CRAWFORD, J. M., KRISKO, J. M., MORRIS, G. A. & CHAMBERS, D. A. 1989. The distribution of Langerhans cells and CD1a antigen in healthy and diseased human gingiva. *Reg Immnol,* 2**,** 91-97.

CROTTY, S. 2011. Follicular helper CD4 T cells (TFH). *Annual review of immunology,* 29**,** 621-663.

CROTTY, S. 2014. T Follicular Helper Cell Differentiation, Function, and Roles in Disease. *Immunity,* 41**,** 529-542.

CUI, D., ZHANG, L., CHEN, J., ZHU, M., HOU, L., CHEN, B. & SHEN, B. 2015. Changes in regulatory B cells and their relationship with rheumatoid arthritis disease activity. *Clinical and Experimental Medicine,* 15**,** 285-292.

CULSHAW, S., MCINNES, I. B. & LIEW, F. Y. 2011. What can the periodontal community learn from the pathophysiology of rheumatoid arthritis? *Journal of Clinical Periodontology,* 38**,** 106-113.

CURTSINGER, J. M., LINS, D. C. & MESCHER, M. F. 2003. Signal 3 Determines Tolerance versus Full Activation of Naive CD8 T Cells: Dissociating Proliferation and Development of Effector Function. *The Journal of Experimental Medicine,* 197**,** 1141-1151.

CURTSINGER, J. M., SCHMIDT CS FAU - MONDINO, A., MONDINO A FAU - LINS, D. C., LINS DC FAU - KEDL, R. M., KEDL RM FAU - JENKINS, M. K., JENKINS MK FAU -

MESCHER, M. F. & MESCHER, M. F. 1999. Inflammatory cytokines provide a third signal for activation of naive CD4+ and CD8+ T cells. *J Immunol,* 162**,** 3256-3262.

CURY, P. R., FURUSE, C., RODRIGUES, A. E. A., BARBUTO, J. A., ARAÚJO, C. D. & ARAÚJO, N. S. D. 2008. Interstitial and Langerhans' dendritic cells in chronic periodontitis and gingivitis. *Brazilian Oral Research,* 22**,** 258-263.

CUTLER, C. W. & JOTWANI, R. 2006. Dendritic Cells at the Oral Mucosal Interface. *Journal of dental research,* 85**,** 678-689.

DAHLÉN, G., CHARALAMPAKIS, G., ABRAHAMSSON, I., BENGTSSON, L. & FALSEN, E. 2012. Predominant bacterial species in subgingival plaque in dogs. *Journal of Periodontal Research,* 47**,** 354-364.

DARVEAU, R., BELTON, C., REIFE, R. & LAMONT, R. 1998. Local chemokine paralysis, a novel pathogenic mechanism for Porphyromonas gingivalis. *Infection and immunity,* 66**,** 1660-1665.

DARVEAU, R. P., HAJISHENGALLIS, G. & CURTIS, M. A. 2012. Porphyromonas gingivalis as a Potential Community Activist for Disease. *Journal of Dental Research,* 91**,** 816-820.

DAVANIAN, H., STRANNEHEIM, H., BÅGE, T., LAGERVALL, M., JANSSON, L., LUNDEBERG, J. & YUCEL-LINDBERG, T. 2012. Gene Expression Profiles in Paired Gingival Biopsies from Periodontitis-Affected and Healthy Tissues Revealed by Massively Parallel Sequencing. *PLoS ONE,* 7**,** e46440.

DAVIES, E. G. 2013. Immunodeficiency in DiGeorge Syndrome and Options for Treating Cases with Complete Athymia. *Frontiers in Immunology,* 4**,** 322.

DE DIEGO, I., VEILLARD, F. T., GUEVARA, T., POTEMPA, B., SZTUKOWSKA, M., POTEMPA, J. & GOMIS-RÜTH, F. X. 2013. Porphyromonas gingivalis Virulence Factor Gingipain RgpB Shows a Unique Zymogenic Mechanism for Cysteine Peptidases. *The Journal of Biological Chemistry,* 288**,** 14287-14296.

DE MOLON, R. S., MASCARENHAS, V. I., DE AVILA, E. D., FINOTI, L. S., TOFFOLI, G. B., SPOLIDORIO, D. M. P., SCAREL-CAMINAGA, R. M., TETRADIS, S. & CIRELLI, J. A. 2016. Long-term evaluation of oral gavage with periodontopathogens or ligature induction of experimental periodontal disease in mice. *Clinical Oral Investigations,* 20**,** 1203-1216.

DE PABLO, P., CHAPPLE, I. L. C., BUCKLEY, C. D. & DIETRICH, T. 2009. Periodontitis in systemic rheumatic diseases. *Nat Rev Rheumatol,* 5**,** 218-224.

DE SILVA, N. S. & KLEIN, U. 2015. Dynamics of B cells in germinal centres. *Nat Rev Immunol,* 15**,** 137-148.

DEMMER, R., BEHLE, J. H., WOLF, D. L., HANDFIELD, M., KEBSCHULL, M., CELENTI, R., PAVLIDIS, P. & PAPAPANOU, P. N. 2008. Transcriptomes in Healthy and Diseased Gingival Tissues. *Journal of periodontology,* 79**,** 2112-2124.

DEREKA, X. E., TOSIOS, K. I., CHRYSOMALI, E. & ANGELOPOULOU, E. 2004. Factor XIIIa+ dendritic cells and S-100 protein+ Langerhans' cells in adult periodontitis. *Journal of Periodontal Research,* 39**,** 447-452.

DEWHIRST, F. E., CHEN, T., IZARD, J., PASTER, B. J., TANNER, A. C. R., YU, W.-H., LAKSHMANAN, A. & WADE, W. G. 2010. The Human Oral Microbiome. *Journal of Bacteriology,* 192**,** 5002-5017.

DI PAOLO, N. C. & SHAYAKHMETOV, D. M. 2016. Interleukin 1[alpha] and the inflammatory process. *Nat Immunol,* 17**,** 906-913.

DI SABATINO, A., CALAROTA, S. A., VIDALI, F., MACDONALD, T. T. & CORAZZA, G. R. 2011. Role of IL-15 in immune-mediated and infectious diseases. *Cytokine & Growth Factor Reviews,* 22**,** 19-33.

DIETRICH, T., SHARMA, P., WALTER, C., WESTON, P. & BECK, J. 2013. The epidemiological evidence behind the association between periodontitis and incident atherosclerotic cardiovascular disease. *Journal of Clinical Periodontology,* 40**,** S70-S84.

DIVARIS, K., MONDA, K. L., NORTH, K. E., OLSHAN, A. F., REYNOLDS, L. M., HSUEH, W. C., LANGE, E. M., MOSS, K., BARROS, S. P., WEYANT, R. J., LIU, Y., NEWMAN, A. B., BECK, J. D. & OFFENBACHER, S. 2013. Exploring the genetic basis of chronic periodontitis: a genome-wide association study. *Human Molecular Genetics,* 22**,** 2312-2324.

DOMMISCH, H., STAUFENBIEL, I., SCHULZE, K., STIESCH, M., WINKEL, A., FIMMERS, R., DOMMISCH, J., JEPSEN, S., MIOSGE, N., ADAM, K. & EBERHARD, J. 2015. Expression of antimicrobial peptides and interleukin-8 during early stages of inflammation: An experimental gingivitis study. *Journal of Periodontal Research,* 50**,** 836-845.

DU, Y., HASHIZUME, T., KURITA-OCHIAI, T., YUZAWA, S., ABIKO, Y. & YAMAMOTO, M. 2011. Nasal immunization with a fusion protein consisting of the hemagglutinin A antigenic region and the maltose-binding protein elicits CD11c(+) CD8(+) dendritic cells for induced long-term protective immunity. *Infection and immunity,* 79**,** 895-904.

DU, Y., LIU P FAU - ZANG, W., ZANG W FAU - WANG, Y., WANG Y FAU - CHEN, X., CHEN X FAU - LI, M., LI M FAU - ZHAO, G. & ZHAO, G. 2015. BTG3 upregulation induces cell apoptosis and suppresses invasion in esophageal adenocarcinoma. *Mol Cell Biochem,* 404**,** 31-38.

DUAN, X., GLEASON, R. C., LI, F., HOSUR, K. B., DUAN, X., HUANG, D., WANG, H., HAJISHENGALLIS, G. & LIANG, S. 2016. Sex dimorphism in periodontitis in animal models. *Journal of Periodontal Research,* 51**,** 196-202.

DUDLEY, E. C., PETRIE, H. T., SHAH, L. M., OWEN, M. J. & HAYDAY, A. C. 1994. T cell receptor beta chain gene rearrangement and selection during thymocyte development in adult mice. *Immunity,* 1**,** 83-93.

DUNCAN, L., YOSHIOKA, M., CHANDAD, F. & GRENIER, D. 2004. Loss of lipopolysaccharide receptor CD14 from the surface of human macrophage-like cells mediated by Porphyromonas gingivalis outer membrane vesicles. *Microbial pathogenesis,* 36**,** 319-325.

DUTZAN, N., ABUSLEME, L., BRIDGEMAN, H., GREENWELL-WILD, T., ZANGERLE-MURRAY, T., FIFE, M. E., BOULADOUX, N., LINLEY, H., BRENCHLEY, L., WEMYSS, K., CALDERON, G., HONG, B.-Y., BREAK, T. J., BOWDISH, D. M. E., LIONAKIS, M. S., JONES, S. A., TRINCHIERI, G., DIAZ, P. I., BELKAID, Y., KONKEL, J. E. & MOUTSOPOULOS, N. M. 2017. On-going Mechanical Damage from Mastication Drives Homeostatic Th17 Cell Responses at the Oral Barrier. *Immunity,* 46**,** 133-147.

DUTZAN, N., GAMONAL, J., SILVA, A., SANZ, M. & VERNAL, R. 2009. Over-expression of forkhead box P3 and its association with receptor activator of nuclear factor-κ B ligand, interleukin (IL) -17, IL-10 and transforming growth factor-β during the progression of chronic periodontitis. *J Clin Periodontol,* 36**,** 396-403.

DUTZAN, N., KONKEL, J. E., GREENWELL-WILD, T. & MOUTSOPOULOS, N. M. 2016. Characterization of the human immune cell network at the gingival barrier. *Mucosal immunology,* 9**,** 1163-1172.

DUTZAN, N., VERNAL R FAU - VAQUE, J. P., VAQUE JP FAU - GARCIA-SESNICH, J., GARCIA-SESNICH J FAU - HERNANDEZ, M., HERNANDEZ M FAU - ABUSLEME, L., ABUSLEME L FAU - DEZEREGA, A., DEZEREGA A FAU - GUTKIND, J. S., GUTKIND JS FAU - GAMONAL, J. & GAMONAL, J. 2012a. Interleukin-21 expression and its association with proinflammatory cytokines in untreated chronic periodontitis patients. *J Periodontol,* 83**,** 948-954.

DUTZAN, N., VERNAL, R., HERNANDEZ, M., DEZEREGA, A., RIVERA, O., SILVA, N., AGUILLON, J. C., PUENTE, J., POZO, P. & GAMONAL, J. 2008. Levels of Interferon-Gamma and Transcription Factor T-Bet in Progressive Periodontal

Lesions in Patients With Chronic Periodontitis. *Journal of Periodontology,* 80**,** 290-296.

DUTZAN, N., VERNAL, R., VAQUE, J. P., GARCÍA-SESNICH, J., HERNANDEZ, M., ABUSLEME, L., DEZEREGA, A., GUTKIND, J. S. & GAMONAL, J. 2012b. Interleukin-21 expression and its association with proinflammatory cytokines in untreated chronic periodontitis patients. *Journal of periodontology,* 83**,** 948-954.

EASTCOTT, J., YAMASHITA, K., TAUBMAN, M., HARADA, Y. & SMITH, D. 1994. Adoptive transfer of cloned T helper cells ameliorates periodontal disease in nude rats. *Oral microbiology and immunology,* 9**,** 284-289.

EBERHARD, J., GROTE, K., LUCHTEFELD, M., HEUER, W., SCHUETT, H., DIVCHEV, D., SCHERER, R., SCHMITZ-STREIT, R., LANGFELDT, D., STUMPP, N., STAUFENBIEL, I., SCHIEFFER, B. & STIESCH, M. 2013. Experimental Gingivitis Induces Systemic Inflammatory Markers in Young Healthy Individuals: A Single-Subject Interventional Study. *PLoS ONE,* 8**,** e55265.

EDWARDS, J. C. W., SEDGWICK, A. D. & WILLOUGHBY, D. A. 1981. The formation of a structure with the features of synovial lining by subcutaneous injection of air: An in vivo tissue culture system. *The Journal of Pathology,* 134**,** 147-156.

ESKAN, M., JOTWANI, R., ABE, T., CHMELAR, J., LIM, J.-H., LIANG, S., CIERO, P., KRAUSS, J., LI, F., RAUNER, M., HOFBAUER, L., CHOI, E., CHUNG, K.-J., HASHIM, A., CURTIS, M., CHAVAKIS, T. & HAJISHENGALLIS, G. 2012. The leukocyte integrin antagonist Del-1 inhibits IL-17-mediated inflammatory bone loss. *Nature immunology,* 13**,** 465-473.

FABIAN, M. R., SONENBERG, N. & FILIPOWICZ, W. 2010. Regulation of mRNA Translation and Stability by microRNAs. *Annual Review of Biochemistry,* 79**,** 351-379.

FEHR, T., SKRASTINA, D., PUMPENS, P. & ZINKERNAGEL, R. M. 1998. T cell-independent type I antibody response against B cell epitopes expressed repetitively on recombinant virus particles. *Proceedings of the National Academy of Sciences of the United States of America,* 95**,** 9477-9481.

FENG, T., WANG, L., SCHOEB, T. R., ELSON, C. O. & CONG, Y. 2010. Microbiota innate stimulation is a prerequisite for T cell spontaneous proliferation and induction of experimental colitis. *The Journal of Experimental Medicine,* 207**,** 1321.

FERRETTI, E., PISTOIA, V. & CORCIONE, A. 2014. Role of Fractalkine/CX3CL1 and Its Receptor in the Pathogenesis of Inflammatory and Malignant Diseases with Emphasis on B Cell Malignancies. *Mediators of Inflammation,* 2014**,** 480941.

FORD, A. L., FOULCHER, E., GOODSALL, A. L. & SEDGWICK, J. D. 1996. Tissue digestion with dispase substantially reduces lymphocyte and macrophage cell-surface antigen expression. *Journal of Immunological Methods,* 194**,** 71-75.

FOX, S. W. & CHAMBERS, T. J. 2000. Interferon-γ Directly Inhibits TRANCE-Induced Osteoclastogenesis. *Biochemical and Biophysical Research Communications,* 276**,** 868-872.

FRIEDEN, C. & CLARK, A. C. 1997. Protein folding: how the mechanism of GroEL action is defined by kinetics. *Proceedings of the National Academy of Sciences of the United States of America,* 94**,** 5535-5538.

GADDIS, D. E., MAYNARD, C. L., WEAVER, C. T., MICHALEK, S. M. & KATZ, J. 2013. Role of TLR2-dependent IL-10 production in the inhibition of the initial IFN-γ T cell response to Porphyromonas gingivalis. *Journal of Leukocyte Biology,* 93**,** 21-31.

GAFFEN, S. & HAJISHENGALLIS, G. 2008. A new inflammatory cytokine on the block: re-thinking periodontal disease and the Th1/Th2 paradigm in the context of Th17 cells and IL-17. *Journal of dental research,* 87**,** 817-828.

GALINDO, R., LEVI, P., LAROCCA, A. P. & NART, J. 2015. Periodontal Re-treatment in Patients on Maintenance Following Pocket Reduction Surgery. *Journal of oral Health and Dental Management,* 14**,** 58-63.

GAMONAL, J., ACEVEDO, A., BASCONES, A., JORGE, O. & SILVA, A. 2001. Characterization of cellular infiltrate, detection of chemokine receptor CCR5 and interleukin-8 and RANTES chemokines in adult periodontitis. *J Periodontal Res,* 36**,** 194-203.

GAO, Y., GRASSI, F., RYAN, M. R., TERAUCHI, M., PAGE, K., YANG, X., WEITZMANN, M. N. & PACIFICI, R. 2007. IFN-γ stimulates osteoclast formation and bone loss in vivo via antigen-driven T cell activation. *Journal of Clinical Investigation,* 117**,** 122-132.

GARLET, G., CARDOSO, C., CAMPANELLI, A., GARLET, T., AVILA-CAMPOS, M., CUNHA, F. & SILVA, J. 2008. The essential role of IFN-gamma in the control of lethal Aggregatibacter actinomycetemcomitans infection in mice. *Microbes and infection / Institut Pasteur,* 10**,** 489-496.

GARLET, G. P., CARDOSO, C. R., MARIANO, F. S., CLAUDINO, M., DE ASSIS, G. F., CAMPANELLI, A. P., AVILA-CAMPOS, M. J. & SILVA, J. S. S. 2010a. Regulatory T cells attenuate experimental periodontitis progression in mice. *Journal of clinical periodontology,* 37**,** 591-600.

GARLET, G. P., CARDOSO, C. R., MARIANO, F. S., CLAUDINO, M., DE ASSIS, G. F., CAMPANELLI, A. P., AVILA-CAMPOS, M. J. & SILVA, J. S. S. 2010b. Regulatory T cells attenuate experimental periodontitis progression in mice. *J Clin Periodontol,* 37**,** 591-600.

GEMMELL, E., CARTER, C. L., HART, D. N. J., DRYSDALE, K. E. & SEYMOUR, G. J. 2002. Antigen-presenting cells in human periodontal disease tissues. *Oral Microbiology and Immunology,* 17**,** 388-393.

GEMMELL, E., FELDNER, B. & SEYMOUR, G. J. 1992. CD45RA and CD45RO positive CD4 cells in human peripheral blood and periodontal disease tissue before and after stimulation with periodontopathic bacteria. *Oral Microbiol Immunol,* 7**,** 84-8.

GENCO, C. A., CUTLER, C. W., KAPCZYNSKI, D., MALONEY, K. & ARNOLD, R. R. 1991. A novel mouse model to study the virulence of and host response to Porphyromonas (Bacteroides) gingivalis. *Infection and Immunity,* 59**,** 1255-1263.

GERMAIN, R. N. 2002. T-cell development and the CD4-CD8 lineage decision. *Nat Rev Immunol,* 2**,** 309-322.

GHORESCHI, K., LAURENCE, A., YANG, X. P., TATO, C. M., MCGEACHY, M. J., KONKEL, J. E., RAMOS, H. L., WEI, L., DAVIDSON, T. S., BOULADOUX, N., GRAINGER, J. R., CHEN, Q., KANNO, Y., WATFORD, W. T., SUN, H. W., EBERL, G., SHEVACH, E. M., BELKAID, Y., CUA, D. J., CHEN, W. & O'SHEA, J. J. 2010. Generation of pathogenic T(H)17 cells in the absence of TGF-beta signalling. *Nature,* 467**,** 967-71.

GLENN, T. C. 2011. Field Guide to Next Generation DNA Sequencers. *Molecular Ecology Resources*, doi: 10.1111/j.1755-0998.2011.03024.

GMÜR, R., HRODEK, K., SAXER, U. P. & GUGGENHEIM, B. 1986. Double-blind analysis of the relation between adult periodontitis and systemic host response to suspected periodontal pathogens. *Infection and immunity,* 52**,** 768-776.

GODFREY, D. I., KENNEDY J FAU - SUDA, T., SUDA T FAU - ZLOTNIK, A. & ZLOTNIK, A. 1993. A developmental pathway involving four phenotypically and functionally distinct subsets of CD3-CD4-CD8- triple-negative adult mouse thymocytes defined by CD44 and CD25 expression. *J Immunol,* 150**,** 4244-4252.

GONÇALVES, R. B., LESHEM, O., BERNARDS, K., WEBB, J. R., STASHENKO, P. P. & CAMPOS-NETO, A. 2006. T-Cell Expression Cloning of Porphyromonas gingivalis Genes Coding for T Helper-Biased Immune Responses during Infection. *Infection and Immunity,* 74**,** 3958-3966.

GOOD-JACOBSON, K. L., SZUMILAS, C. G., CHEN, L., SHARPE, A. H., TOMAYKO, M. M. & SHLOMCHIK, M. J. 2010. PD-1 regulates germinal center B cell survival and the formation and affinity of long-lived plasma cells. *Nat Immunol,* 11**,** 535-542.

GOODYEAR, A. W., KUMAR, A., DOW, S. & RYAN, E. P. 2014. Optimization of murine small intestine leukocyte isolation for global immune phenotype analysis. *Journal of Immunological Methods,* 405**,** 97-108.

GRASWINCKEL, J. E. M., VAN DER VELDEN, U., VAN WINKELHOFF, A. J., HOEK, F. J. & LOOS, B. G. 2004. Plasma antibody levels in periodontitis patients and controls. *Journal of Clinical Periodontology,* 31**,** 562-568.

GRAVES, D. T., FINE, D., TENG, Y.-T. A., VAN DYKE, T. E. & HAJISHENGALLIS, G. 2008. The Use of Rodent Models to Investigate Host-Bacteria Interactions Related to Periodontal Diseases. *Journal of clinical periodontology,* 35**,** 89-105.

GRAVES, D. T., OSKOUI, M., VOLEINIKOVA, S., NAGUIB, G., CAI, S., DESTA, T., KAKOURAS, A. & JIANG, Y. 2001. Tumor Necrosis Factor Modulates Fibroblast Apoptosis, PMN Recruitment, and Osteoclast Formation in Response to P. gingivalis Infection. *Journal of Dental Research,* 80**,** 1875-1879.

GRENIER, D. & MAYRAND, D. 1987. Selected characteristics of pathogenic and nonpathogenic strains of Bacteroides gingivalis. *Journal of clinical microbiology,* 25**,** 738-740.

GRIFFEN, A. L., BEALL, C. J., CAMPBELL, J. H., FIRESTONE, N. D., KUMAR, P. S., YANG, Z. K., PODAR, M. & LEYS, E. J. 2012. Distinct and complex bacterial profiles in human periodontitis and health revealed by 16S pyrosequencing. *The ISME Journal,* 6**,** 1176-1185.

GRIFFEN, A. L., BECKER, M. R., LYONS, S. R., MOESCHBERGER, M. L. & LEYS, E. J. 1998. Prevalence of Porphyromonas gingivalis and Periodontal Health Status. *Journal of Clinical Microbiology,* 36**,** 3239-3242.

GUENTSCH, A., KRAMESBERGER, M., SROKA, A., PFISTER, W., POTEMPA, J. & EICK, S. 2011. Comparison of Gingival Crevicular Fluid Sampling Methods in Patients with Severe Chronic Periodontitis. *Journal of periodontology,* 82**,** 1051-1060.

GUO, Y., NGUYEN, K.-A. & POTEMPA, J. 2010. Dichotomy of gingipains action as virulence factors: from cleaving substrates with the precision of a surgeon's knife to a meat chopper-like brutal degradation of proteins. *Periodontology 2000,* 54**,** 15-44.

GUPTA, A. K. & GUPTA, U. D. 2014. Chapter 19 - Next Generation Sequencing and Its Applications A2 - Verma, Ashish S. *In:* SINGH, A. (ed.) *Animal Biotechnology*. San Diego: Academic Press.

GUPTA, S. & JAWANDA, M. K. 2015. Oral Lichen Planus: An Update on Etiology, Pathogenesis, Clinical Presentation, Diagnosis and Management. *Indian Journal of Dermatology,* 60**,** 222-229.

HAFFAJEE, A. D., SOCRANSKY SS FAU - GUNSOLLEY, J. C. & GUNSOLLEY, J. C. 2003. Systemic anti-infective periodontal therapy. A systematic review. *Ann Periodontol,* 8**,** 115-181.

HAJISHENGALLIS, G., LIANG, S., PAYNE, M., HASHIM, A., JOTWANI, R., ESKAN, M., MCINTOSH, M., ALSAM, A., KIRKWOOD, K., LAMBRIS, J., DARVEAU, R. & CURTIS, M. 2011a. Low-abundance biofilm species orchestrates inflammatory periodontal disease through the commensal microbiota and complement. *Cell host & microbe,* 10**,** 497-506.

HAJISHENGALLIS, G., LIANG, S., PAYNE, MARK A., HASHIM, A., JOTWANI, R., ESKAN, MEHMET A., MCINTOSH, MEGAN L., ALSAM, A., KIRKWOOD, KEITH L., LAMBRIS, JOHN D., DARVEAU, RICHARD P. & CURTIS, MICHAEL A. 2011b. Low-Abundance Biofilm Species Orchestrates Inflammatory Periodontal Disease through the Commensal Microbiota and Complement. *Cell Host & Microbe,* 10**,** 497-506.

HAJISHENGALLIS, G., LIANG, S., PAYNE, M. A., HASHIM, A., JOTWANI, R., ESKAN, M. A., MCINTOSH, M. L., ALSAM, A., KIRKWOOD, K. L., LAMBRIS, J. D., DARVEAU, R. P. & CURTIS, M. A. 2011c. A Low-Abundance Biofilm Species Orchestrates Inflammatory Periodontal Disease through the Commensal Microbiota and the Complement Pathway. *Cell host & microbe,* 10**,** 497-506.

HAMEL, K. M., CAO, Y., WANG, Y., RODEGHERO, R., KOBEZDA, T., CHEN, L. & FINNEGAN, A. 2010. B7-H1 expression on non-B and non-T cells promotes distinct effects on T- and B-cell responses in autoimmune arthritis. *European Journal of Immunology,* 40**,** 3117-3127.

HAN, X., KAWAI, T., EASTCOTT, J. W. & TAUBMAN, M. A. 2006. Bacterial-Responsive B Lymphocytes Induce Periodontal Bone Resorption. *The Journal of Immunology,* 176**,** 625-631.

HAN, X., LIN, X., SELIGER, A. R., EASTCOTT, J., KAWAI, T. & TAUBMAN, M. A. 2009. Expression of receptor activator of nuclear factor-kappaB ligand by B cells in response to oral bacteria. *Oral Microbiol Immunol,* 24**,** 190-6.

HASEGAWA, Y., TRIBBLE, G., BAKER, H., MANS, J., HANDFIELD, M. & LAMONT, R. 2008. Role of Porphyromonas gingivalis SerB in gingival epithelial cell

cytoskeletal remodeling and cytokine production. *Infection and immunity,* 76**,** 2420-2427.

HASENBERG, M., KÖHLER, A., BONIFATIUS, S., BORUCKI, K., RIEK-BURCHARDT, M., ACHILLES, J., MÄNN, L., BAUMGART, K., SCHRAVEN, B. & GUNZER, M. 2011. Rapid Immunomagnetic Negative Enrichment of Neutrophil Granulocytes from Murine Bone Marrow for Functional Studies In Vitro and In Vivo. *PLoS ONE,* 6**,** e17314.

HAWLISCH, H., BELKAID, Y., BAELDER, R., HILDEMAN, D., GERARD, C. & KÖHL, J. 2005. C5a negatively regulates toll-like receptor 4-induced immune responses. *Immunity,* 22**,** 415-426.

HAYES, S. M., LI, L. & LOVE, P. E. 2005. TCR Signal Strength Influences αß/γδ Lineage Fate. *Immunity,* 22**,** 583-593.

HAYNES, N. M., ALLEN CD FAU - LESLEY, R., LESLEY R FAU - ANSEL, K. M., ANSEL KM FAU - KILLEEN, N., KILLEEN N FAU - CYSTER, J. G. & CYSTER, J. G. 2007. Role of CXCR5 and CCR7 in follicular Th cell positioning and appearance of a programmed cell death gene-1high germinal center-associated subpopulation. *J Immunol,* 179**,** 5099-5108.

HEASMAN, P. A., COLLINS, J. G. & OFFENBACHER, S. 1993. Changes in crevicular fluid levels of interleukin-1 beta, leukotriene B4, prostaglandin E2, thromboxane B2 and tumour necrosis factor alpha in experimental gingivitis in humans. *J Periodontal Res,* 28**,** 241-247.

HENDERSON, L. A., KING, S. L., AMERI, S., MARTIN, S. D., SIMMONS, B. P., NIGROVIC, P. A. & FUHLBRIGGE, R. C. 2014. A161: Novel 3-Dimensional Explant Method Facilitates the Study of Lymphocyte Populations in the Synovium and Reveals a Large Population of Resident Memory T cells in Rheumatoid Arthritis. *Arthritis & Rheumatology,* 66**,** S209-S209.

HERRERA, D., SANZ, M., JEPSEN, S., NEEDLEMAN, I. & ROLDÁN, S. 2002. A systematic review on the effect of systemic antimicrobials as an adjunct to scaling and root planing in periodontitis patients. *Journal of Clinical Periodontology,* 29**,** 136-159.

HO, S., CLIPSTONE, N., TIMMERMANN, L., NORTHROP, J., GRAEF, I., FIORENTINO, D., NOURSE, J. & CRABTREE, G. R. 1996. The mechanism of action of cyclosporin A and FK506. *Clinical immunology and immunopathology,* 80**,** 5.

HOENNSCHEIDT, C., MAX D FAU - RICHTER, N., RICHTER N FAU - STAEGE, M. S. & STAEGE, M. S. 2009. Expression of CD4 on Epstein-Barr virus-immortalized B cells. *Scandinavian journal of immunology,* 70**,** 216-225.

HOFFMAN, E. S., PASSONI, L., CROMPTON, T., LEU, T. M., SCHATZ, D. G., KOFF, A., OWEN, M. J. & HAYDAY, A. C. 1996. Productive T-cell receptor beta-chain gene rearrangement: coincident regulation of cell cycle and clonality during development in vivo. *Genes & Development,* 10**,** 948-962.

HOLT, S. & EBERSOLE, J. 2005. Porphyromonas gingivalis, Treponema denticola, and Tannerella forsythia: the "red complex", a prototype polybacterial pathogenic consortium in periodontitis. *Periodontology 2000,* 38**,** 72-122.

HOLT, S., KESAVALU, L., WALKER, S. & GENCO, C. 1999. Virulence factors of Porphyromonas gingivalis. *Periodontology 2000,* 20**,** 168-238.

HONDA, T., AOKI, Y., TAKAHASHI, N., MAEKAWA, T., NAKAJIMA, T., ITO, H., TABETA, K., OKUI, T., KAJITA, K., DOMON, H. & YAMAZAKI, K. 2008. Elevated expression of IL-17 and IL-12 genes in chronic inflammatory periodontal disease. *Clinica chimica acta; international journal of clinical chemistry,* 395**,** 137-141.

HORAV , A. H. 2014. Dendritic cells of the oral mucosa. *Mucosal immunology,* 7**,** 27-37.

HOVAV, A. H. 2014. Dendritic cells of the oral mucosa. *Mucosal Immunol,* 7**,** 27-37.

HUANG, J., WU, C., TIAN, B., ZHOU, X., MA, N. & QIAN, Y. 2016. Myricetin Prevents Alveolar Bone Loss in an Experimental Ovariectomized Mouse Model of Periodontitis. *International Journal of Molecular Sciences,* 17.

IWASAKI, A. & MEDZHITOV, R. 2015. Control of adaptive immunity by the innate immune system. *Nat Immunol,* 16**,** 343-353.

JAIN, R., WALDVOGEL-THURLOW, S., DARVEAU, R. & DOUGLAS, R. 2016. Differences in the paranasal sinuses between germ-free and pathogen-free mice. *International Forum of Allergy & Rhinology,* 6**,** 631-637.

JAMUR, M. C., GRODZKI, A. C. G., MORENO, A. N., DE MELLO, L. D. F. C., PASTOR, M. V. D., BERENSTEIN, E. H., SIRAGANIAN, R. P. & OLIVER, C. 2001. Identification and Isolation of Rat Bone Marrow-derived Mast Cells Using the Mast Cell-specific Monoclonal Antibody AA4. *Journal of Histochemistry & Cytochemistry,* 49**,** 219-228.

JELLEY-GIBBS, D. M., DIBBLE, J. P., FILIPSON, S., HAYNES, L., KEMP, R. A. & SWAIN, S. L. 2005. Repeated stimulation of CD4 effector T cells can limit their protective function. *The Journal of Experimental Medicine,* 201**,** 1101-1112.

JENKINS, M. K., KHORUTS A FAU - INGULLI, E., INGULLI E FAU - MUELLER, D. L., MUELLER DL FAU - MCSORLEY, S. J., MCSORLEY SJ FAU - REINHARDT, R. L.,

REINHARDT RL FAU - ITANO, A., ITANO A FAU - PAPE, K. A. & PAPE, K. A. 2001. In vivo activation of antigen-specific CD4 T cells. *Annual review of immunology,* 19**,** 23-45.

JEPSEN, K. & JEPSEN, S. 2016. Antibiotics/antimicrobials: systemic and local administration in the therapy of mild to moderately advanced periodontitis. *Periodontology 2000,* 71**,** 82-112.

JOHNSON, L. A. & JACKSON, D. G. 2013. The chemokine CX3CL1 promotes trafficking of dendritic cells through inflamed lymphatics. *Journal of Cell Science,* 126**,** 5259-5270.

JÖNSSON, D., RAMBERG, P., DEMMER, R. T., KEBSCHULL, M., DAHLÉN, G. & PAPAPANOU, P. N. 2011. Gingival tissue transcriptomes in experimental gingivitis. *Journal of clinical periodontology,* 38**,** 599-611.

JOTWANI, R., PALUCKA, A. K., AL-QUOTUB, M., NOURI-SHIRAZI, M., KIM, J., BELL, D., BANCHEREAU, J. & CUTLER, C. W. 2001. Mature Dendritic Cells Infiltrate the T Cell-Rich Region of Oral Mucosa in Chronic Periodontitis: In Situ, In Vivo, and In Vitro Studies(). *Journal of immunology (Baltimore, Md. : 1950),* 167**,** 4693-4700.

JUNGBLUT, M., OELTZE, K., ZEHNTER, I., HASSELMANN, D. & BOSIO, A. 2009. Standardized Preparation of Single-Cell Suspensions from Mouse Lung Tissue using the gentleMACS Dissociator. *Journal of Visualized Experiments : JoVE***,** 1266.

KAECH, S. M., TAN JT FAU - WHERRY, E. J., WHERRY EJ FAU - KONIECZNY, B. T., KONIECZNY BT FAU - SURH, C. D., SURH CD FAU - AHMED, R. & AHMED, R. 2003. Selective expression of the interleukin 7 receptor identifies effector CD8 T cells that give rise to long-lived memory cells. *Nat Immunol,* 4**,** 1191-1198.

KAECH, S. M., WHERRY, E. J. & AHMED, R. 2002. Effector and memory T-cell differentiation: implications for vaccine development. *Nat Rev Immunol,* 2**,** 251-262.

KAWAI, T., MATSUYAMA, T., HOSOKAWA, Y., MAKIHIRA, S., SEKI, M., KARIMBUX, N., GONCALVES, R., VALVERDE, P., DIBART, S., LI, Y.-P., MIRANDA, L., ERNST, C., IZUMI, Y. & TAUBMAN, M. 2006. B and T lymphocytes are the primary sources of RANKL in the bone resorptive lesion of periodontal disease. *The American journal of pathology,* 169**,** 987-998.

KE, Y., LI, Y. & KAPP, J. A. 1995. Ovalbumin injected with complete Freund's adjuvant stimulates cytolytic responses. *European Journal of Immunology,* 25**,** 549-553.

KEANE, J., GERSHON S FAU - WISE, R. P., WISE RP FAU - MIRABILE-LEVENS, E., MIRABILE-LEVENS E FAU - KASZNICA, J., KASZNICA J FAU - SCHWIETERMAN, W. D., SCHWIETERMAN WD FAU - SIEGEL, J. N., SIEGEL JN FAU - BRAUN, M. M. & BRAUN, M. M. 2001. Tuberculosis associated with infliximab, a tumor necrosis factor alpha-neutralizing agent. *N Engl J Med,* 345**,** 1098-1104.

KEESTRA, J. A. J., GROSJEAN, I., COUCKE, W., QUIRYNEN, M. & TEUGHELS, W. 2015a. Non-surgical periodontal therapy with systemic antibiotics in patients with untreated aggressive periodontitis: a systematic review and meta-analysis. *Journal of Periodontal Research,* 50**,** 689-706.

KEESTRA, J. A. J., GROSJEAN, I., COUCKE, W., QUIRYNEN, M. & TEUGHELS, W. 2015b. Non-surgical periodontal therapy with systemic antibiotics in patients with untreated chronic periodontitis: a systematic review and meta-analysis. *Journal of Periodontal Research,* 50**,** 294-314.

KHALAF, H. & BENGTSSON, T. 2012. Altered T-Cell Responses by the Periodontal Pathogen Porphyromonas gingivalis. *PLoS ONE,* 7**,** e45192.

KILIAN, M., CHAPPLE, I. L. C., HANNIG, M., MARSH, P. D., MEURIC, V., PEDERSEN, A. M. L., TONETTI, M. S., WADE, W. G. & ZAURA, E. 2016. The oral microbiome - an update for oral healthcare professionals. *Br Dent J,* 221**,** 657-666.

KIM, P. D., XIA-JUAN, X., CRUMP, K. E., ABE, T., HAJISHENGALLIS, G. & SAHINGUR, S. E. 2015. Toll-Like Receptor 9-Mediated Inflammation Triggers Alveolar Bone Loss in Experimental Murine Periodontitis. *Infection and Immunity,* 83**,** 2992-3002.

KIM, Y.-G., KIM, M., KANG, J. H., KIM, H. J., PARK, J.-W., LEE, J.-M., SUH, J.-Y., KIM, J.-Y., LEE, J.-H. & LEE, Y. 2016. Transcriptome sequencing of gingival biopsies from chronic periodontitis patients reveals novel gene expression and splicing patterns. *Human Genomics,* 10**,** 28.

KISTLER, J. O., BOOTH, V., BRADSHAW, D. J. & WADE, W. G. 2013. Bacterial Community Development in Experimental Gingivitis. *PLOS ONE,* 8**,** e71227.

KITTIPATARIN, C. & KHALED, A. R. 2007. INTERLINKING INTERLEUKIN-7. *Cytokine,* 39**,** 75-83.

KLEINSCHEK, M. A., BONIFACE, K., SADEKOVA, S., GREIN, J., MURPHY, E. E., TURNER, S. P., RASKIN, L., DESAI, B., FAUBION, W. A., DE WAAL MALEFYT, R., PIERCE, R. H., MCCLANAHAN, T. & KASTELEIN, R. A. 2009. Circulating and gut-resident human Th17 cells express CD161 and promote intestinal inflammation. *The Journal of Experimental Medicine,* 206**,** 525-534.

KOLENBRANDER, P. 2000. Oral microbial communities: biofilms, interactions, and genetic systems. *Annual review of microbiology,* 54**,** 413-437.

KONDRACK, R. M., HARBERTSON J FAU - TAN, J. T., TAN JT FAU - MCBREEN, M. E., MCBREEN ME FAU - SURH, C. D., SURH CD FAU - BRADLEY, L. M. & BRADLEY, L. M. 2003. Interleukin 7 regulates the survival and generation of memory CD4 cells. *J Exp Med,* 198.

KROEMER, G., CUENDE E FAU - MARTINEZ, C. & MARTINEZ, C. 1993. Compartmentalization of the peripheral immune system. *Adv Immunol,* 53**,** 157-216.

KUPER, C. F., HAMELEERS, D. M., BRUIJNTJES, J. P., VAN DER VEN, I., BIEWENGA, J. & SMINIA, T. 1990. Lymphoid and non-lymphoid cells in nasal-associated lymphoid tissue (NALT) in the rat. An immuno- and enzyme-histochemical study. *Cell Tissue Res,* 259**,** 371-377.

KURTULUS, S. & HILDEMAN, D. 2013. Assessment of CD4(+) and CD8(+) T Cell Responses Using MHC Class I and II Tetramers. *Methods in molecular biology (Clifton, N.J.),* 979**,** 71-79.

LAPPIN, D. F., KOULOURI, O., RADVAR, M., HODGE, P. & KINANE, D. F. 1999. Relative proportions of mononuclear cell types in periodontal lesions analyzed by immunohistochemistry. *Journal of Clinical Periodontology,* 26**,** 183-189.

LAPPIN, D. F., MACLEOD, C. P., KERR, A., MITCHELL, T. & KINANE, D. F. 2001. Anti-inflammatory cytokine IL-10 and T cell cytokine profile in periodontitis granulation tissue. *Clinical and experimental immunology,* 123**,** 294-300.

LAURELL, L., RYLANDER H FAU - SUNDIN, Y. & SUNDIN, Y. 1987. Histologic characteristics of clinically healthy gingiva in adolescents. *Scand J Dent Res,* 95**,** 456-462.

LI, C. H. & AMAR, S. 2007. Morphometric, Histomorphometric, and Microcomputed Tomographic Analysis of Periodontal Inflammatory Lesions in a Murine Model. *Journal of Periodontology,* 78**,** 1120-1128.

LIANG, S., KRAUSS, J. L., DOMON, H., MCINTOSH, M. L., HOSUR, K. B., QU, H., LI, F., TZEKOU, A., LAMBRIS, J. D. & HAJISHENGALLIS, G. 2011. The C5a receptor impairs IL-12–dependent clearance of Porphyromonas gingivalis and is required for induction of periodontal bone loss. *Journal of immunology (Baltimore, Md. : 1950),* 186**,** 869-877.

LIOU, Y.-R., WANG, Y.-H., LEE, C.-Y. & LI, P.-C. 2015. Buoyancy-Activated Cell Sorting Using Targeted Biotinylated Albumin Microbubbles. *PLoS ONE,* 10**,** e0125036.

LISTGARTEN, M. A., SCHIFTER, C. C. & LASTER, L. 1985. 3-year longitudinal study of the periodontal status of an adult population with gingivitis. *Journal of Clinical Periodontology,* 12**,** 225-238.

LISTL, S., GALLOWAY, J., MOSSEY, P. A. & MARCENES, W. 2015. Global Economic Impact of Dental Diseases. *Journal of Dental Research,* 94**,** 1355-1361.

LIU, M., GUO, S. & STILES, J. K. 2011. The emerging role of CXCL10 in cancer (Review). *Oncology Letters,* 2**,** 583-589.

LIU, Y.-Z., MANEY, P., PURI, J., ZHOU, Y., BADDOO, M., STRONG, M., WANG, Y.-P., FLEMINGTON, E. & DENG, H.-W. 2016. RNA-sequencing study of peripheral blood monocytes in chronic periodontitis. *Gene,* 581**,** 152-160.

LÖE, H., ANERUD, A., BOYSEN, H. & MORRISON, E. 1986. Natural history of periodontal disease in man. Rapid, moderate and no loss of attachment in Sri Lankan laborers 14 to 46 years of age. *Journal of clinical periodontology,* 13**,** 431-445.

LÖE, H., THEILADE, E. & JENSEN, S. B. 1965. EXPERIMENTAL GINGIVITIS IN MAN. *J Periodontol,* 36**,** 177-187.

LONDON, C. A., LODGE MP FAU - ABBAS, A. K. & ABBAS, A. K. 2000. Functional responses and costimulator dependence of memory CD4+ T cells. *J Immunol,* 64**,** 265-272.

LOOS, B. G., DYER, D. W., WHITTAM, T. S. & SELANDER, R. K. 1993. Genetic structure of populations of Porphyromonas gingivalis associated with periodontitis and other oral infections. *Infection and Immunity,* 61**,** 204-212.

LORD, M. S., CHENG, B., FARRUGIA, B. L., MCCARTHY, S. & WHITELOCK, J. M. 2017. Platelet factor 4 binds to vascular proteoglycans and controls both growth factor activities and platelet activation. *Journal of Biological Chemistry.*

LU, Y.-C., YEH, W.-C. & OHASHI, P. 2008. LPS/TLR4 signal transduction pathway. *Cytokine,* 42**,** 145-151.

LUNDMARK, A., DAVANIAN, H., BÅGE, T., JOHANNSEN, G., KORO, C., LUNDEBERG, J. & YUCEL-LINDBERG, T. 2015. Transcriptome analysis reveals mucin 4 to be highly associated with periodontitis and identifies pleckstrin as a link to systemic diseases. *Scientific Reports,* 5**,** 18475.

MACKAY, F. & BROWNING, J. L. 2002. BAFF: A fundamental survival factor for B cells. *Nat Rev Immunol,* 2**,** 465-475.

MACKAY, L. K., RAHIMPOUR, A., MA, J. Z., COLLINS, N., STOCK, A. T., HAFON, M.-L., VEGA-RAMOS, J., LAUZURICA, P., MUELLER, S. N., STEFANOVIC, T., TSCHARKE, D. C., HEATH, W. R., INOUYE, M., CARBONE, F. R. & GEBHARDT, T. 2013. The developmental pathway for CD103+CD8+ tissue-resident memory T cells of skin. *Nat Immunol,* 14**,** 1294-1301.

MACLEOD, M. K. L., KAPPLER, J. W. & MARRACK, P. 2010. Memory CD4 T cells: generation, reactivation and re-assignment. *Immunology,* 130**,** 10-15.

MACLEOD, M. K. L., MCKEE, A., CRAWFORD, F., WHITE, J., KAPPLER, J. & MARRACK, P. 2008. CD4 memory T cells divide poorly in response to antigen because of their cytokine profile. *Proceedings of the National Academy of Sciences of the United States of America,* 105**,** 14521-14526.

MADIANOS, P., PAPAPANOU, P. & SANDROS, J. 1997. Porphyromonas gingivalis infection of oral epithelium inhibits neutrophil transepithelial migration. *Infection and immunity,* 65**,** 3983-3990.

MAGGI, L., CAPONE M FAU - GIUDICI, F., GIUDICI F FAU - SANTARLASCI, V., SANTARLASCI V FAU - QUERCI, V., QUERCI V FAU - LIOTTA, F., LIOTTA F FAU - FICARI, F., FICARI F FAU - MAGGI, E., MAGGI E FAU - TONELLI, F., TONELLI F FAU - ANNUNZIATO, F., ANNUNZIATO F FAU - COSMI, L. & COSMI, L. 2013. CD4+CD161+ T lymphocytes infiltrate Crohn's disease-associated perianal fistulas and are reduced by anti-TNF-alpha local therapy.

MAHANONDA, R., SA-ARD-IAM, N., YONGVANITCHIT, K., WISETCHANG, M., ISHIKAWA, I., NAGASAWA, T., WALSH, D. S. & PICHYANGKUL, S. 2002. Upregulation of co-stimulatory molecule expression and dendritic cell marker (CD83) on B cells in periodontal disease. *J Periodontal Res,* 37**,** 177-183.

MALCOLM, J., AWANG, R. A., OLIVER-BELL, J., BUTCHER, J. P., CAMPBELL, L., ADRADOS PLANELL, A., LAPPIN, D. F., FUKADA, S. Y., NILE, C. J., LIEW, F. Y. & CULSHAW, S. 2015a. IL-33 Exacerbates Periodontal Disease through Induction of RANKL. *J Dent Res,* 94**,** 968-975.

MALCOLM, J., AWANG, R. A., OLIVER-BELL, J., BUTCHER, J. P., CAMPBELL, L., ADRADOS PLANELL, A., LAPPIN, D. F., FUKADA, S. Y., NILE, C. J., LIEW, F. Y. & CULSHAW, S. 2015b. IL-33 Exacerbates Periodontal Disease through Induction of RANKL. *Journal of Dental Research*.

MALCOLM, J., MILLINGTON, O., MILLHOUSE, E., CAMPBELL, L., ADRADOS PLANELL, A., BUTCHER, J. P., LAWRENCE, C., ROSS, K., RAMAGE, G., MCINNES, I. B. &

CULSHAW, S. 2016. Mast Cells Contribute to Porphyromonas gingivalis–induced Bone Loss. *Journal of Dental Research,* 95**,** 704-710.

MALEK, R., FISHER, J., CALECA, A., STINSON, M., VAN OSS, C., LEE, J., CHO, M., GENCO, R., EVANS, R. & DYER, D. 1994. Inactivation of the Porphyromonas gingivalis fimA gene blocks periodontal damage in gnotobiotic rats. *Journal of bacteriology,* 176**,** 1052-1059.

MALISSEN, M., GILLET, A., ARDOUIN, L., BOUVIER, G., TRUCY, J., FERRIER, P., VIVIER, E. & MALISSEN, B. 1995. Altered T cell development in mice with a targeted mutation of the CD3-epsilon gene. *The EMBO Journal,* 14**,** 4641-4653.

MALOY, K. J. & POWRIE, F. 2001. Regulatory T cells in the control of immune pathology. *Nat Immunol,* 2**,** 816-822.

MANHART, S. S., REINHARDT, R. A., PAYNE, J. B., SEYMOUR, G. J., GEMMELL, E., DYER, J. K. & PETRO, T. M. 1994. Gingival cell IL-2 and IL-4 in early-onset periodontitis. *Journal of periodontology,* 65**,** 807-813.

MARCOTTE, H. & LAVOIE, M. C. 1998. Oral Microbial Ecology and the Role of Salivary Immunoglobulin A. *Microbiology and Molecular Biology Reviews,* 62**,** 71-109.

MARTNER, A., ÖSTMAN, S., LUNDIN, S., RASK, C., BJÖRNSSON, V., TELEMO, E., COLLINS, L. V., AXELSSON, L. & WOLD, A. E. 2013. Stronger T Cell Immunogenicity of Ovalbumin Expressed Intracellularly in Gram-Negative than in Gram-Positive Bacteria. *PLoS ONE,* 8**,** e65124.

MARZO, A. L., KLONOWSKI, K. D., LE BON, A., BORROW, P., TOUGH, D. F. & LEFRANÇOIS, L. 2005. Initial T cell frequency dictates memory CD8(+) T cell lineage commitment. *Nature immunology,* 6**,** 793-799.

MATSUDA, K., IWAKI, K. K., GARCIA-GOMEZ, J., HOFFMAN, J., INDERLIED, C. B., MASON, W. H. & IWAKI, Y. 2011. Bacterial Identification by 16S rRNA Gene PCR-Hybridization as a Supplement to Negative Culture Results. *Journal of Clinical Microbiology,* 49**,** 2031-2034.

MAURI, C., GRAY, D., MUSHTAQ, N. & LONDEI, M. 2003. Prevention of Arthritis by Interleukin 10–producing B Cells. *The Journal of Experimental Medicine,* 197**,** 489-501.

MCINTOSH, M. L. & HAJISHENGALLIS, G. 2012. Inhibition of Porphyromonas gingivalis-induced periodontal bone loss by CXCR4 antagonist treatment. *Molecular oral microbiology,* 27**,** 449-457.

MCMANUS, M. M. & GRILL, R. J. 2011. Longitudinal Evaluation of Mouse Hind Limb Bone Loss After Spinal Cord Injury using Novel, in vivo, Methodology. *Journal of Visualized Experiments : JoVE*, 3246.

MCSORLEY, S. J., ASCH, S., COSTALONGA, M., REINHARDT, R. L. & JENKINS, M. K. 2002. Tracking Salmonella-Specific CD4 T Cells In Vivo Reveals a Local Mucosal Response to a Disseminated Infection. *Immunity,* 16, 365-377.

MDALA, I., OLSEN, I., HAFFAJEE, A. D., SOCRANSKY, S. S., DE BLASIO, B. F. & THORESEN, M. 2013. Multilevel analysis of bacterial counts from chronic periodontitis after root planing/scaling, surgery, and systemic and local antibiotics: 2-year results. *Journal of Oral Microbiology,* 5, 10.3402/jom.v5i0.20939.

MICHALOWICZ, B. S., DIEHL, S. R., GUNSOLLEY, J. C., SPARKS, B. S., BROOKS, C. N., KOERTGE, T. E., CALIFANO, J. V., BURMEISTER, J. A. & SCHENKEIN, H. A. 2000. Evidence of a Substantial Genetic Basis for Risk of Adult Periodontitis. *Journal of Periodontology,* 71, 1699-1707.

MILES, A. A., MISRA, S. S. & IRWIN, J. O. 1938. The estimation of the bactericidal power of the blood. *The Journal of Hygiene,* 38, 732-749.

MILES, B., ABDEL-GHAFFAR, K. A., GAMAL, A. Y., BABAN, B. & CUTLER, C. W. 2014. Blood dendritic cells: “canary in the coal mine” to predict chronic inflammatory disease? *Frontiers in Microbiology,* 5, 6.

MILLER, J. 1961. Immunological function of the thymus. *Lancet,* ii, 748-749.

MILLER, J. 1962. Effect of neonatal thymectomy on the immunological responsiveness of the mouse. *Proc Roy Soc London,* 156B, 410-428.

MITANI, A., NIEDBALA, W., FUJIMURA, T., MOGI, M., MIYAMAE, S., HIGUCHI, N., ABE, A., HISHIKAWA, T., MIZUTANI, M., ISHIHARA, Y., NAKAMURA, H., KURITA, K., OHNO, N., TANAKA, Y., HATTORI, M. & NOGUCHI, T. 2015. Increased expression of interleukin (IL)-35 and IL-17, but not IL-27, in gingival tissues with chronic periodontitis. *Journal of periodontology,* 86, 301-309.

MIZRAJI, G., SEGEV, H., WILENSKY, A. & HOVAV, A.-H. 2013. Isolation, processing and analysis of murine gingival cells. *Journal of visualized experiments : JoVE*.

MKONYI, L. E., BLETSA, A., BOLSTAD, A. I., BAKKEN, V., WIIG, H. & BERGGREEN, E. 2012. Gingival Lymphatic Drainage Protects Against Porphyromonas gingivalis–Induced Bone Loss in Mice. *The American Journal of Pathology,* 181, 907-916.

MOSER, B., CLARK-LEWIS, I., ZWAHLEN, R. & BAGGIOLINI, M. 1990. Neutrophil-activating properties of the melanoma growth-stimulatory activity. *The Journal of Experimental Medicine,* 171**,** 1797-1802.

MOUGHAL, N. A., ADONOGIANAKI E FAU - KINANE, D. F. & KINANE, D. F. 1992. Langerhans cell dynamics in human gingiva during experimentally induced inflammation. *J Biol Buccale,* 20**,** 163-167.

MOUTSOPOULOS, N. M., KLING, H. M., ANGELOV, N., JIN, W., PALMER, R. J., NARES, S., OSORIO, M. & WAHL, S. M. 2012. Porphyromonas gingivalis promotes Th17 inducing pathways in chronic periodontitis. *Journal of autoimmunity,* 39**,** 294-303.

MYERS, L. A., PATEL, D. D., PUCK, J. M. & BUCKLEY, R. H. 2002. Hematopoietic stem cell transplantation for severe combined immunodeficiency in the neonatal period leads to superior thymic output and improved survival. *Blood,* 99**,** 872-878.

MYNENI, S., SETTEM, R., CONNELL, T., KEEGAN, A., GAFFEN, S. & SHARMA, A. 2011. TLR2 signaling and Th2 responses drive Tannerella forsythia-induced periodontal bone loss. *Journal of immunology (Baltimore, Md. : 1950),* 187**,** 501-509.

NACER, A., CARAPAU, D., MITCHELL, R., MELTZER, A., SHAW, A., FREVERT, U. & NARDIN, E. H. 2014. Imaging murine NALT following intranasal immunization with flagellin-modified circumsporozoite protein malaria vaccines. *Mucosal immunology,* 7**,** 304-314.

NAKAJIMA, T., UEKI-MARUYAMA K FAU - ODA, T., ODA T FAU - OHSAWA, Y., OHSAWA Y FAU - ITO, H., ITO H FAU - SEYMOUR, G. J., SEYMOUR GJ FAU - YAMAZAKI, K. & YAMAZAKI, K. 2005. Regulatory T-cells infiltrate periodontal disease tissues. *J Dent Res,* 84**,** 639-643.

NEEDLEMAN, I., SUVAN, J., MOLES, D. R. & PIMLOTT, J. 2005. A systematic review of professional mechanical plaque removal for prevention of periodontal diseases. *Journal of Clinical Periodontology,* 32**,** 229-282.

NEGISHI, I., MOTOYAMA, N., NAKAYAMA, K.-I., NAKAYAMA, K., SENJU, S., HATAKEYAMA, S., ZHANG, Q., CHAN, A. C. & LOH, D. Y. 1995. Essential role for ZAP-70 in both positive and negative selection of thymocytes. *Nature,* 376**,** 435-438.

NISTALA, K., ADAMS, S., CAMBROOK, H., URSU, S., OLIVITO, B., DE JAGER, W., EVANS, J. G., CIMAZ, R., BAJAJ-ELLIOTT, M. & WEDDERBURN, L. R. 2010. Th17 plasticity in human autoimmune arthritis is driven by the inflammatory

environment. *Proceedings of the National Academy of Sciences of the United States of America,* 107**,** 14751-14756.

NORDERYD, O. & HUGOSON, A. 1998. Risk of severe periodontal disease in a Swedish adult population. *Journal of Clinical Periodontology,* 25**,** 1022-1028.

NORDERYD, O., HUGOSON, A. & GRUSOVIN, G. 1999. Risk of severe periodontal disease in a Swedish adult population. *Journal of Clinical Periodontology,* 26**,** 608-615.

NORDLAND, P., GARRETT, S., KIGER, R., VANOOTEGHEM, R., HUTCHENS, L. H. & EGELBERG, J. 1987. The effect of plaque control and root debridement in molar teeth. *Journal of Clinical Periodontology,* 14**,** 231-236.

NOVAK, N., HABERSTOK, J., BIEBER, T. & ALLAM, J.-P. 2008. The immune privilege of the oral mucosa. *Trends in Molecular Medicine,* 14**,** 191-198.

O'GRADY, N. P., TROPEA, M., PREAS, I. I. H. L., REDA, D., VANDIVIER, R. W., BANKS, S. M. & SUFFREDINI, A. F. 1999. Detection of Macrophage Inflammatory Protein (MIP)-1α and MIP-ß during Experimental Endotoxemia and Human Sepsis. *The Journal of Infectious Diseases,* 179**,** 136-141.

O'BRIEN-SIMPSON, N. M., HOLDEN, J. A., LENZO, J. C., TAN, Y., BRAMMAR, G. C., WALSH, K. A., SINGLETON, W., ORTH, R. K. H., SLAKESKI, N., CROSS, K. J., DARBY, I. B., BECHER, D., ROWE, T., MORELLI, A. B., HAMMET, A., NASH, A., BROWN, A., MA, B., VINGADASSALOM, D., MCCLUSKEY, J., KLEANTHOUS, H. & REYNOLDS, E. C. 2016. A therapeutic Porphyromonas gingivalis gingipain vaccine induces neutralising IgG1 antibodies that protect against experimental periodontitis. *Npj Vaccines,* 1**,** 16022.

OFFENBACHER, S., BARROS, S. P., PAQUETTE, D. W., WINSTON, J. L., BIESBROCK, A. R., THOMASON, R. G., GIBB, R. D., FULMER, A. W., TIESMAN, J. P., JUHLIN, K. D., WANG, S. L., REICHLING, T. D., CHEN, K.-S. & HO, B. 2009. Gingival Transcriptome Patterns During Induction and Resolution of Experimental Gingivitis in Humans. *Journal of Periodontology,* 80**,** 1963-1982.

OFFENBACHER, S., DIVARIS, K., BARROS, S. P., MOSS, K. L., MARCHESAN, J. T., MORELLI, T., ZHANG, S., KIM, S., SUN, L., BECK, J. D., LAUDES, M., MUNZ, M., SCHAEFER, A. S. & NORTH, K. E. 2016. Genome-wide association study of biologically informed periodontal complex traits offers novel insights into the genetic basis of periodontal disease. *Human Molecular Genetics,* 25**,** 2113-2129.

OGAWA, T., TARKOWSKI, A., MCGHEE, M. L., MOLDOVEANU, Z., MESTECKY, J., HIRSCH, H. Z., KOOPMAN, W. J., HAMADA, S., MCGHEE, J. R. & KIYONO, H.

1989. Analysis of human IgG and IgA subclass antibody-secreting cells from localized chronic inflammatory tissue. *The Journal of Immunology,* 142**,** 1150.

OKADA, H., KIDA, T. & YAMAGAMI, H. 1983. Identification and distribution of immunocompetent cells in inflamed gingiva of human chronic periodontitis. *Infection and Immunity,* 41**,** 365-374.

OLDENHOVE, G., DE HEUSCH M FAU - URBAIN-VANSANTEN, G., URBAIN-VANSANTEN G FAU - URBAIN, J., URBAIN J FAU - MALISZEWSKI, C., MALISZEWSKI C FAU - LEO, O., LEO O FAU - MOSER, M. & MOSER, M. 2003. CD4+ CD25+ regulatory T cells control T helper cell type 1 responses to foreign antigens induced by mature dendritic cells in vivo. *J Exp Med,* 198**,** 259-266.

OLIVEIRA, M., TAVARES, M., GOMES, D., TOURET, T., SÃO BRAZ, B., TAVARES, L. & SEMEDO-LEMSADDEK, T. 2016. Virulence traits and antibiotic resistance among enterococci isolated from dogs with periodontal disease. *Comparative Immunology, Microbiology and Infectious Diseases,* 46**,** 27-31.

OLIVER-BELL, J., BUTCHER, J. P., MALCOLM, J., MACLEOD, M. K. L., ADRADOS PLANELL, A., CAMPBELL, L., NIBBS, R. J. B., GARSIDE, P., MCINNES, I. B. & CULSHAW, S. 2015. Periodontitis in the absence of B cells and specific anti-bacterial antibody. *Molecular Oral Microbiology,* 30**,** 160-169.

OZ, H. S. & PULEO, D. A. 2011. Animal Models for Periodontal Disease. *Journal of Biomedicine and Biotechnology,* 2011**,** 754857.

PAPAPANOU, P. N., ABRON, A., VERBITSKY, M., PICOLOS, D., YANG, J., QIN, J., FINE, J. B. & PAVLIDIS, P. 2004. Gene expression signatures in chronic and aggressive periodontitis: a pilot study. *European Journal of Oral Sciences,* 112**,** 216-223.

PAPAPANOU, P. N., NEIDERUD, A.-M., SANDROS, J. & DAHLÉN, G. 2001. Interleukin-1 gene polymorphism and periodontal status
Interleukin-1 Gen Polymorphismus und parodontaler Status: Eine Fall-kontrollierte Studie
Polymorphisme du gène Interleukine-1 et état parodontal: une étude d'un cas. *Journal of Clinical Periodontology,* 28**,** 389-396.

PAPE, K. A., KHORUTS A FAU - MONDINO, A., MONDINO A FAU - JENKINS, M. K. & JENKINS, M. K. 1997. Inflammatory cytokines enhance the in vivo clonal expansion and differentiation of antigen-activated CD4+ T cells. *J Immunol,* 159**,** 591-598.

PARK, C. & KUPPER, T. S. 2015. The emerging role of resident memory T cells in protective immunity and inflammatory disease *Nature medicine,* 21**,** 688-697.

PARK, C. H., ABRAMSON, Z. R., TABA, M., JIN, Q., CHANG, J., KREIDER, J. M., GOLDSTEIN, S. A. & GIANNOBILE, W. V. 2007. Three-Dimensional Micro-Computed Tomographic Imaging of Alveolar Bone in Experimental Bone Loss or Repair. *Journal of periodontology,* 78**,** 273-281.

PARK, S.-N., PARK, J.-Y. & KOOK, J.-K. 2011. Development of Porphyromonas gingivalis-specific quantitative real-time PCR primers based on the nucleotide sequence of rpoB. *The Journal of Microbiology,* 49**,** 315.

PARRY, G. & MACKMAN, N. 1997. Role of cyclic AMP response element-binding protein in cyclic AMP inhibition of NF-kappaB-mediated transcription. *Journal of immunology (Baltimore, Md. : 1950),* 159**,** 5450-5456.

PASTER, B. J., OLSEN, I., AAS, J. A. & DEWHIRST, F. E. 2006. The breadth of bacterial diversity in the human periodontal pocket and other oral sites. *Periodontology 2000,* 42**,** 80-87.

PAVLICA, Z., PETELIN, M., NEMEC, A., ERZEN, D. & SKALERIC, U. 2004. Measurement of total antioxidant capacity in gingival crevicular fluid and serum in dogs with periodontal disease. *Am J Vet Res,* 65**,** 1584-1588.

PEJCIC, A., DJORDJEVIC V FAU - KOJOVIC, D., KOJOVIC D FAU - ZIVKOVIC, V., ZIVKOVIC V FAU - MINIC, I., MINIC I FAU - MIRKOVIC, D., MIRKOVIC D FAU - STOJANOVIC, M. & STOJANOVIC, M. 2014. Effect of periodontal treatment in renal transplant recipients.

PELLEGRINO, M., SCIAMBI, A., YATES, J. L., MAST, J. D., SILVER, C. & EASTBURN, D. J. 2016. RNA-Seq following PCR-based sorting reveals rare cell transcriptional signatures. *BMC Genomics,* 17**,** 361.

PERRIER, S., DARAKHSHAN, F. & HAJDUCH, E. 2006. IL-1 receptor antagonist in metabolic diseases: Dr Jekyll or Mr Hyde? *FEBS Lett,* 580**,** 6289-6294.

PERUZZO, D. C., GIMENES, J. H., TAIETE, T., CASARIN, R. C. V., FERES, M., SALLUM, E. A., CASATI, M. Z., KANTOVITZ, K. R. & NOCITI, F. H. 2016. Impact of smoking on experimental gingivitis. A clinical, microbiological and immunological prospective study. *Journal of Periodontal Research,* 51**,** 800-811.

PETIT, M. D., HOVENKAMP E FAU - HAMANN, D., HAMANN D FAU - ROOS, M. T., ROOS MT FAU - VAN DER VELDEN, U., VAN DER VELDEN U FAU - MIEDEMA, F.,

MIEDEMA F FAU - LOOS, B. G. & LOOS, B. G. 2001. Phenotypical and functional analysis of T cells in periodontitis. *J Periodontal Res,* 36**,** 214-220.

POPADIAK, K., POTEMPA, J., RIESBECK, K. & BLOM, A. 2007. Biphasic effect of gingipains from Porphyromonas gingivalis on the human complement system. *Journal of immunology (Baltimore, Md. : 1950),* 178**,** 7242-7250.

POULIOT, M., CLISH, C. B., PETASIS, N. A., VAN DYKE, T. E. & SERHAN, C. N. 2000. Lipoxin A4 Analogues Inhibit Leukocyte Recruitment to Porphyromonas gingivalis: A Role for Cyclooxygenase-2 and Lipoxins in Periodontal Disease. *Biochemistry,* 39**,** 4761-4768.

PROF, F. L., ALLEN, C., DE BENEDETTI, F., GROM, A. A., BALLABIO, M., FERLIN, W. G. & DE MIN, C. 2015. A Novel Targeted Approach to the Treatment of Hemophagocytic Lymphohistiocytosis (HLH) with an Anti-Interferon Gamma (IFNγ) Monoclonal Antibody (mAb), NI-0501: First Results from a Pilot Phase 2 Study in Children with Primary HLH. *Blood,* 126**,** LBA-3.

PULENDRAN, B., KUMAR, P., CUTLER, C. W., MOHAMADZADEH, M., VAN DYKE, T. & BANCHEREAU, J. 2001. Lipopolysaccharides from Distinct Pathogens Induce Different Classes of Immune Responses In Vivo. *Journal of immunology (Baltimore, Md. : 1950),* 167**,** 5067-5076.

PUNKOSDY, G. A., BLAIN, M., GLASS, D. D., LOZANO, M. M., O'MARA, L., DUDLEY, J. P., AHMED, R. & SHEVACH, E. M. 2011. Regulatory T-cell expansion during chronic viral infection is dependent on endogenous retroviral superantigens. *Proceedings of the National Academy of Sciences of the United States of America,* 108**,** 3677-3682.

RADFORD, K. J., HIGGINS DE FAU - PASQUINI, S., PASQUINI S FAU - CHEADLE, E. J., CHEADLE EJ FAU - CARTA, L., CARTA L FAU - JACKSON, A. M., JACKSON AM FAU - LEMOINE, N. R., LEMOINE NR FAU - VASSAUX, G. & VASSAUX, G. 2002. A recombinant E. coli vaccine to promote MHC class I-dependent antigen presentation: application to cancer immunotherapy. *Gene Therapy,* 9**,** 1455-1463.

RAJESH, N., ARUN, K. V., KUMAR, T. S. S., REDDY, K. K. M., ALAMELU, S. & REDDY, B. R. 2015. Evaluation of mRNA expression of the transcription factors of Th1 and Th2 subsets (T-bet and GATA-3) in periodontal health and disease - A pilot study in south Indian population. *Journal of Indian Society of Periodontology,* 19**,** 624-627.

RENVERT, S., PERSSON, R. E. & PERSSON, G. R. 2013. Tooth Loss and Periodontitis in Older Individuals: Results From the Swedish National Study on Aging and Care. *Journal of Periodontology,* 84**,** 1134-1144.

RETTENMIER, C. W., ROUSSEL, M. F. & SHERR, C. J. 1988. The colony-stimulating factor 1 (CSF-1) receptor (c-fms proto-oncogene product) and its ligand. *J Cell Sci Suppl,* 9**,** 27-44.

ROBEY, E. & FOWLKES, B. J. 1994. Selective Events in T Cell Development. *Annual Review of Immunology,* 12**,** 675-705.

RODRIGUE, L. & LAVOIE, M. C. 1996. Comparison of the proportions of oral bacterial species in BALB/c mice from different suppliers. *Lab Anim,* 30**,** 108-113.

ROSSER, ELIZABETH C. & MAURI, C. 2015. Regulatory B Cells: Origin, Phenotype, and Function. *Immunity,* 42**,** 607-612.

RYDER, M. I., NITTAYANANTA, W., COOGAN, M., GREENSPAN, D. & GREENSPAN, J. S. 2012. Periodontal disease in HIV/AIDS. *Periodontology 2000,* 60**,** 78-97.

SÁNCHEZ-MARTÍN, L., ESTECHA, A., SAMANIEGO, R., SÁNCHEZ-RAMÓN, S., VEGA, M. Á. & SÁNCHEZ-MATEOS, P. 2011. The chemokine CXCL12 regulates monocyte-macrophage differentiation and RUNX3 expression. *Blood,* 117**,** 88.

SANZ, M., TEUGHELS, W. & ON BEHALF OF GROUP, A. O. T. E. W. O. P. 2008. Innovations in non-surgical periodontal therapy: Consensus Report of the Sixth European Workshop on Periodontology. *Journal of Clinical Periodontology,* 35**,** 3-7.

SATTLER, S., LING, G.-S., XU, D., HUSSAARTS, L., ROMAINE, A., ZHAO, H., FOSSATI-JIMACK, L., MALIK, T., COOK, H. T., BOTTO, M., LAU, Y.-L., SMITS, H. H., LIEW, F. Y. & HUANG, F.-P. 2014. IL-10-producing regulatory B cells induced by IL-33 (Breg(IL-33)) effectively attenuate mucosal inflammatory responses in the gut(). *Journal of Autoimmunity,* 50**,** 107-122.

SCHIFFERLE, R., WILSON, M., LEVINE, M. & GENCO, R. 1993a. Activation of serum complement by polysaccharide-containing antigens of Porphyromonas gingivalis. *Journal of Periodontal Research,* 28.

SCHIFFERLE, R. E., CHEN, P. B., DAVERN, L. B., AGUIRRE, A., GENCO, R. J. & LEVINE, M. J. 1993b. Modification of experimental Porphyromonas gingivalis murine infection by immunization with a polysaccharide-protein conjugate. *Oral Microbiology and Immunology,* 8.

SCHLAPBACH, C., GEHAD, A., YANG, C., WATANABE, R., GUENOVA, E., TEAGUE, J. E., CAMPBELL, L., YAWALKAR, N., KUPPER, T. S. & CLARK, R. A. 2014. Human T(H)9 cells are skin-tropic and have autocrine and paracrine pro-inflammatory capacity. *Science translational medicine,* 6**,** 219ra8-219ra8.

SÉGUIER, S., GODEAU, G., LEBORGNE, M., PIVERT, G. & BROUSSE, N. 2000. Quantitative morphological analysis of Langerhans cells in healthy and diseased human gingiva. *Archives of Oral Biology,* 45**,** 1073-1081.

SEYMOUR, G. J., GEMMELL E FAU - REINHARDT, R. A., REINHARDT RA FAU - EASTCOTT, J., EASTCOTT J FAU - TAUBMAN, M. A. & TAUBMAN, M. A. 1993. Immunopathogenesis of chronic inflammatory periodontal disease: cellular and molecular mechanisms.

SHARMA, A., INAGAKI, S., HONMA, K., SFINTESCU, C., BAKER, P. J. & EVANS, R. T. 2005. Tannerella forsythia-induced Alveolar Bone Loss in Mice Involves Leucine-rich-repeat BspA Protein. *Journal of Dental Research,* 84**,** 462-467.

SHEETS, S., POTEMPA, J., TRAVIS, J., FLETCHER, H. & CASIANO, C. 2006. Gingipains from Porphyromonas gingivalis W83 synergistically disrupt endothelial cell adhesion and can induce caspase-independent apoptosis. *Infection and immunity,* 74**,** 5667-5678.

SIGIDIN, Y. A., LOUKINA GV FAU - SKURKOVICH, B., SKURKOVICH B FAU - SKURKOVICH, S. & SKURKOVICH, S. 2001. Randomized, double-blind trial of anti-interferon-gamma antibodies in rheumatoid arthritis. *Scand J Rheumatol,* 30**,** 203-207.

SIMON, V., HO, D. D. & KARIM, Q. A. 2006. HIV/AIDS epidemiology, pathogenesis, prevention, and treatment. *Lancet,* 368**,** 489-504.

SINGH, A., WYANT, T., ANAYA-BERGMAN, C., ADUSE-OPOKU, J., BRUNNER, J., LAINE, M., CURTIS, M. & LEWIS, J. 2011. The capsule of Porphyromonas gingivalis leads to a reduction in the host inflammatory response, evasion of phagocytosis, and increase in virulence. *Infection and immunity,* 79**,** 4533-4542.

SKURKOVICH, S., LUKINA, G., SIGIDIN, Y. A., PUSHKOVA, O., MACH, E. & SKURKOVICH, B. 2015. Comparative Clinical Trial of Antibodies to Interferon-Gamma (IFN-γ) and Tumor Necrosis Factor-Alpha (TNF-α) in the Treatment of Rheumatoid Arthritis. *Journal of Immune Based Therapies, Vaccines and Antimicrobials,* 4**,** 1-8.

SLADE, G. D. & SPENCER, A. J. 1995. Periodontal attachment loss among adults aged 60+ in South Australia. *Community Dentistry and Oral Epidemiology,* 23**,** 237-242.

SOCRANSKY, S. S., HAFFAJEE, A. D., CUGINI, M. A., SMITH, C. & KENT, R. L. 1998. Microbial complexes in subgingival plaque. *Journal of Clinical Periodontology,* 25**,** 134-144.

SONG, W.-C. 2012. Crosstalk between complement and toll-like receptors. *Toxicologic pathology,* 40**,** 174-182.

STARR, T. K., JAMESON, S. C. & HOGQUIST, K. A. 2003. Positive and Negative Selection of T cells. *Annual Review of Immunology,* 21**,** 139-176.

STATHOPOULOU, P., BENAKANAKERE, M., GALICIA, J. & KINANE, D. 2009a. The host cytokine response to Porphyromonas gingivalis is modified by gingipains. *Oral microbiology and immunology,* 24**,** 11-17.

STATHOPOULOU, P. G., BENAKANAKERE, M. R., GALICIA, J. C. & KINANE, D. F. 2009b. The host cytokine response to Porphyromonas gingivalis is modified by gingipains. *Oral microbiology and immunology,* 24**,** 11-17.

STELIN, S., RAMAKRISHAN, H., TALWAR, A., ARUN, K. & KUMAR, T. S. S. 2009. Immunohistological analysis of CD1a+ langerhans cells and CD57+ natural killer cells in healthy and diseased human gingival tissue: A comparative study. *Journal of Indian Society of Periodontology,* 13**,** 150-154.

STRUILLOU, X., BOUTIGNY, H., SOUEIDAN, A. & LAYROLLE, P. 2010. Experimental Animal Models in Periodontology: A Review. *The Open Dentistry Journal,* 4**,** 37-47.

SUÁREZ-FARIÑAS, M., FUENTES-DUCULAN, J., LOWES, M. A. & KRUEGER, J. G. 2011. Resolved psoriasis lesions retain expression of a subset of disease-related genes. *The Journal of investigative dermatology,* 131**,** 391-400.

SZAFRAŃSKI, S. P., DENG, Z.-L., TOMASCH, J., JAREK, M., BHUJU, S., MEISINGER, C., KÜHNISCH, J., SZTAJER, H. & WAGNER-DÖBLER, I. 2015. Functional biomarkers for chronic periodontitis and insights into the roles of Prevotella nigrescens and Fusobacterium nucleatum; a metatranscriptome analysis. *Npj Biofilms And Microbiomes,* 1**,** 15017.

TAKEICHI, O., HABER, J., KAWAI, T., SMITH, D., MORO, I. & TAUBMAN, M. 2000. Cytokine profiles of T-lymphocytes from gingival tissues with pathological pocketing. *Journal of dental research,* 79**,** 1548-1555.

TAUBMAN, M. A. & KAWAI, T. 2001. Involvement of T-lymphocytes in periodontal disease and in direct and indirect induction of bone resorption. *Crit Rev Oral Biol Med,* 12**,** 125-35.

THORBERT-MROS, S., LARSSON, L. & BERGLUNDH, T. 2015. Cellular composition of long-standing gingivitis and periodontitis lesions. *Journal of Periodontal Research,* 50**,** 535-543.

TOHYAMA, M., SAYAMA, K., KOMATSUZAWA, H., HANAKAWA, Y., SHIRAKATA, Y., DAI, X., YANG, L., TOKUMARU, S., NAGAI, H., HIRAKAWA, S., SUGAI, M. & HASHIMOTO, K. 2007. CXCL16 is a novel mediator of the innate immunity of epidermal keratinocytes. *International Immunology,* 19**,** 1095-1102.

TOMASI, C., KOUTOUZIS T FAU - WENNSTROM, J. L. & WENNSTROM, J. L. 2008. Locally delivered doxycycline as an adjunct to mechanical debridement at retreatment of periodontal pockets. *J Periodontol,* 79**,** 431-439.

TOMURA, M., YOSHIDA, N., TANAKA, J., KARASAWA, S., MIWA, Y., MIYAWAKI, A. & KANAGAWA, O. 2008. Monitoring cellular movement in vivo with photoconvertible fluorescence protein "Kaede" transgenic mice. *Proceedings of the National Academy of Sciences of the United States of America,* 105**,** 10871-10876.

TORRES DE HEENS, G. L., LOOS, B. G. & VAN DER VELDEN, U. 2010. Monozygotic twins are discordant for chronic periodontitis: clinical and bacteriological findings. *Journal of Clinical Periodontology,* 37**,** 120-128.

TRIBBLE, G. & LAMONT, R. 2010. Bacterial invasion of epithelial cells and spreading in periodontal tissue. *Periodontology 2000,* 52**,** 68-83.

TSAI, C.-C., KU, C.-H., HO, Y.-P., HO, K.-Y., WU, Y.-M. & HUNG, C.-C. 2007. Changes in Gingival Crevicular Fluid Interleukin-4 and Interferon-gamma in Patients with Chronic Periodontitis Before and After Periodontal Initial Therapy. *The Kaohsiung Journal of Medical Sciences,* 23**,** 1-7.

TZANKOV, A., BOURGAU C FAU - KAISER, A., KAISER A FAU - ZIMPFER, A., ZIMPFER A FAU - MAURER, R., MAURER R FAU - PILERI, S. A., PILERI SA FAU - WENT, P., WENT P FAU - DIRNHOFER, S. & DIRNHOFER, S. 2005. Rare expression of T-cell markers in classical Hodgkin's lymphoma. *Mod Pathol,* 18**,** 1542-1549.

UNSOELD, H. & PIRCHER, H. 2005. Complex Memory T-Cell Phenotypes Revealed by Coexpression of CD62L and CCR7. *Journal of Virology,* 79**,** 4510-4513.

VAN 'T VEER, L. J., DAI, H., VAN DE VIJVER, M. J., HE, Y. D., HART, A. A. M., MAO, M., PETERSE, H. L., VAN DER KOOY, K., MARTON, M. J., WITTEVEEN, A. T., SCHREIBER, G. J., KERKHOVEN, R. M., ROBERTS, C., LINSLEY, P. S., BERNARDS, R. & FRIEND, S. H. 2002. Gene expression profiling predicts clinical outcome of breast cancer. *Nature,* 415**,** 530-536.

VAN HOUTE, J. 1982. Bacterial adherence and dental plaque formation. *Infection,* 10**,** 252-260.

VAN OERS, N. S., VON BOEHMER, H. & WEISS, A. 1995. The pre-T cell receptor (TCR) complex is functionally coupled to the TCR-zeta subunit. *The Journal of Experimental Medicine,* 182**,** 1585.

VAN OERS, N. S. C., LOWIN-KROPF, B., FINLAY, D., CONNOLLY, K. & WEISS, A. 1996. T Cell Development Is Abolished in Mice Lacking Both Lck and Fyn Protein Tyrosine Kinases. *Immunity,* 5**,** 429-436.

VERNAL, R., DIAZ-GUERRA, E., SILVA, A., SANZ, M. & GARCIA-SANZ, J. 2014. Distinct human T-lymphocyte responses triggered by Porphyromonas gingivalis capsular serotypes. *Journal of clinical periodontology,* 41**,** 19-30.

VERNAL, R., DUTZAN, N., HERNANDEZ, M., CHANDIA, S., PUENTE, J., LEON, R., GARCIA, L., DEL VALLE, I., SILVA, A. & GAMONAL, J. 2006. High expression levels of receptor activator of nuclear factor-kappa B ligand associated with human chronic periodontitis are mainly secreted by CD4+ T lymphocytes. *J Periodontol,* 77**,** 1772-80.

VERNAL, R., LEÓN, R., SILVA, A., VAN WINKELHOFF, A., GARCIA-SANZ, J. & SANZ, M. 2009. Differential cytokine expression by human dendritic cells in response to different Porphyromonas gingivalis capsular serotypes. *Journal of clinical periodontology,* 36**,** 823-829.

VOGEL, C. & MARCOTTE, E. M. 2012. Insights into the regulation of protein abundance from proteomic and transcriptomic analyses. *Nature reviews. Genetics,* 13**,** 227-232.

VON BOEHMER, H. & FEHLING, H. J. 1997. Structure and function of the pre-T cell receptor. *Annual Review of Immunology,* 15**,** 433-452.

VON BOEHMER, H., TEH, H. S. & KISIELOW, P. 1989. The thymus selects the useful, neglects the useless and destroys the harmful. *Immunology Today,* 10**,** 57-61.

WALK, E. L., MCLAUGHLIN, S. L. & WEED, S. A. 2015. High-frequency Ultrasound Imaging of Mouse Cervical Lymph Nodes. *Journal of Visualized Experiments : JoVE*, 52718.

WANG, H.-L. & GREENWELL, H. 2001. Surgical periodontal therapy. *Periodontology 2000,* 25**,** 89-99.

WANG, M., KRAUSS, J., DOMON, H., HOSUR, K., LIANG, S., MAGOTTI, P., TRIANTAFILOU, M., TRIANTAFILOU, K., LAMBRIS, J. & HAJISHENGALLIS, G. 2010a. Microbial hijacking of complement-toll-like receptor crosstalk. *Science signaling,* 3.

WANG, R. N., GREEN, J., WANG, Z., DENG, Y., QIAO, M., PEABODY, M., ZHANG, Q., YE, J., YAN, Z., DENDULURI, S., IDOWU, O., LI, M., SHEN, C., HU, A., HAYDON, R. C., KANG, R., MOK, J., LEE, M. J., LUU, H. L. & SHI, L. L. 2014. Bone Morphogenetic Protein (BMP) signaling in development and human diseases. *Genes & Diseases,* 1**,** 87-105.

WANG, Y.-H. H., VOO, K. S., LIU, B., CHEN, C.-Y. Y., UYGUNGIL, B., SPOEDE, W., BERNSTEIN, J. A., HUSTON, D. P. & LIU, Y.-J. J. 2010b. A novel subset of CD4(+) T(H)2 memory/effector cells that produce inflammatory IL-17 cytokine and promote the exacerbation of chronic allergic asthma. *The Journal of experimental medicine,* 207**,** 2479-2491.

WANG, Z., GERSTEIN, M. & SNYDER, M. 2009. RNA-Seq: a revolutionary tool for transcriptomics. *Nature reviews. Genetics,* 10**,** 57-63.

WARRINGTON, R., WATSON, W., KIM, H. L. & ANTONETTI, F. R. 2011. An introduction to immunology and immunopathology. *Allergy Asthma Clin Immunol,* 7**,** doi: 10.1186/1710-1492-7S1-S1.

WAYKOLE, Y. P., DOIPHODE, S. S., RAKHEWAR, P. S. & MHASKE, M. 2009. Anticytokine therapy for periodontal diseases: Where are we now? *Journal of Indian Society of Periodontology,* 13**,** 64-68.

WESTHOVENS, R. & VERSCHUEREN, P. 2010. The Efficacy and Safety of Abatacept in Rheumatoid Arthritis. *Therapeutic Advances in Musculoskeletal Disease,* 2**,** 89-94.

WHITE, D. A., TSAKOS, G., PITTS, N. B., FULLER, E., DOUGLAS, G. V. A., MURRAY, J. J. & STEELE, J. G. 2012. Adult Dental Health Survey 2009: common oral health conditions and their impact on the population. *Br Dent J,* 213**,** 567-572.

WILENSKY, A., POLAK, D., HOURI-HADDAD, Y. & SHAPIRA, L. 2013. The role of RgpA in the pathogenicity of Porphyromonas gingivalis in the murine periodontitis model. *Journal of clinical periodontology,* 40**,** 924-932.

WILENSKY, A., SEGEV, H., MIZRAJI, G., SHAUL, Y., CAPUCHA, T., SHACHAM, M. & HOVAV, A. H. 2014. Dendritic cells and their role in periodontal disease. *Oral Diseases,* 20**,** 119-126.

WILENSKY, A., TZACH-NAHMAN, R., POTEMPA, J., SHAPIRA, L. & NUSSBAUM, G. 2015. Porphyromonas gingivalis gingipains selectively reduce CD14 expression, leading to macrophage hypo-responsiveness to bacterial infection. *Journal of innate immunity,* 7**,** 127-135.

WISHART, D. S. 2016. Emerging applications of metabolomics in drug discovery and precision medicine. *Nat Rev Drug Discov,* 15**,** 473-484.

WOLF, D. L., NEIDERUD, A. M., HINCKLEY, K., DAHLÉN, G., VAN DE WINKEL, J. G. J. & PAPAPANOU, P. N. 2006. Fcγ receptor polymorphisms and periodontal status: a prospective follow-up study. *Journal of Clinical Periodontology,* 33**,** 691-698.

WU, H. Y., NGUYEN, H. H. & RUSSELL, M. W. 1997. Nasal lymphoid tissue (NALT) as a mucosal immune inductive site. *Scandinavian journal of immunology,* 46**,** 506-513.

WU, R.-Q., ZHANG, D.-F., TU, E., CHEN, Q.-M. & CHEN, W. 2014. The mucosal immune system in the oral cavity—an orchestra of T cell diversity. *International Journal of Oral Science,* 6**,** 125-132.

WYATT, A. W., OSBORNE, R. J., STEWART, H. & RAGGE, N. K. 2010. Bone morphogenetic protein 7 (BMP7) mutations are associated with variable ocular, brain, ear, palate, and skeletal anomalies. *Human Mutation,* 31**,** 781-787.

XU, X., HE, J., XUE, J., WANG, Y., LI, K., ZHANG, K., GUO, Q., LIU, X., ZHOU, Y., CHENG, L., LI, M., LI, Y., LI, Y., SHI, W. & ZHOU, X. 2015. Oral cavity contains distinct niches with dynamic microbial communities. *Environmental Microbiology,* 17**,** 699-710.

XU, X.-C., CHEN, H., ZHANG, X., ZHAI, Z.-J., LIU, X.-Q., QIN, A. & LU, E.-Y. 2014. Simvastatin prevents alveolar bone loss in an experimental rat model of periodontitis after ovariectomy. *Journal of Translational Medicine,* 12**,** 284.

YAMAZAKI, S., MARUYAMA A FAU - OKADA, K., OKADA K FAU - MATSUMOTO, M., MATSUMOTO M FAU - MORITA, A., MORITA A FAU - SEYA, T. & SEYA, T. 2012. Dendritic cells from oral cavity induce Foxp3(+) regulatory T cells upon antigen stimulation. *PLoS ONE,* 7**,** e51665.

YAO, Y., LIU, R., SHIN, M. S., TRENTALANGE, M., ALLORE, H., NASSAR, A., KANG, I., POBER, J. & MONTGOMERY, R. R. 2014. CyTOF supports efficient detection of immune cell subsets from small samples. *Journal of immunological methods,* 415**,** 1-5.

YOSHIDA, M., WATANABE, T., USUI, T., MATSUNAGA, Y., SHIRAI, Y., YAMORI, M., ITOH, T., HABU, S., CHIBA, T., KITA, T. & WAKATSUKI, Y. 2001. CD4 T cells monospecific to ovalbumin produced by Escherichia coli can induce colitis upon transfer to BALB/c and SCID mice. *International Immunology,* 13**,** 1561-1570.

YU, J., RUDDY, M., WONG, G., SFINTESCU, C., BAKER, P., SMITH, J., EVANS, R. & GAFFEN, S. 2007. An essential role for IL-17 in preventing pathogen-initiated bone destruction: recruitment of neutrophils to inflamed bone requires IL-17 receptor-dependent signals. *Blood,* 109**,** 3794-3802.

YU, P., HU, Y., LIU, Z., KAWAI, T., TAUBMAN, M. A., LI, W. & HAN, X. 2016. Local Induction of B Cell Interleukin-10 Competency Alleviates Inflammation and Bone Loss in Ligature-Induced Experimental Periodontitis in Mice. . *Infect Immun,* 85**,** doi:10.1128/IAI.00645-16.

YUN, P., DECARLO, A., CHAPPLE, C., COLLYER, C. & HUNTER, N. 2005. Binding of Porphyromonas gingivalis gingipains to human CD4(+) T cells preferentially down-regulates surface CD2 and CD4 with little affect on co-stimulatory molecule expression. *Microbial pathogenesis,* 38**,** 85-96.

ZHANG, W., JU, J., RIGNEY, T. & TRIBBLE, G. 2014. Porphyromonas gingivalis infection increases osteoclastic bone resorption and osteoblastic bone formation in a periodontitis mouse model. *BMC Oral Health,* 14**,** 89.

ZHANG, X., KIMURA, Y., FANG, C., ZHOU, L., SFYROERA, G., LAMBRIS, J., WETSEL, R., MIWA, T. & SONG, W.-C. 2007. Regulation of Toll-like receptor-mediated inflammatory response by complement in vivo. *Blood,* 110**,** 228-236.

ZHANG, Y., WANG, T., CHEN, W., YILMAZ, O., PARK, Y., JUNG, I.-Y., HACKETT, M. & LAMONT, R. 2005. Differential protein expression by Porphyromonas gingivalis in response to secreted epithelial cell components. *Proteomics,* 5**,** 198-211.

ZINKERNAGEL, R. M. 1997. The Nobel Lectures in Immunology. The Nobel Prize for Physiology or Medicine, 1996. Cellular immune recognition and the biological role of major transplantation antigens. *Scandinavian journal of immunology,* 46**,** 421-436.